NAM

Liquefaction Hazard Pilot Study for the Groningen Region of the Netherlands due to Induced Seismicity

R.A. Green, J.J. Bommer, P.J. Stafford, B.W. Maurer, B. Edwards, P.P. Kruiver, A. Rodriguez-Marek, G. de Lange, S.J. Oates, T. Storck, P. Omidi, S.J. Bourne, and J. van Elk

Datum August 2018

Editors Jan van Elk & Dirk Doornhof

General Introduction

The soils in Groningen contain deposits of saturated sands. Therefore, the possibility of earthquake-induced liquefaction needs to be considered. Potentially, liquefaction could be important for critical infra-structure like dikes and levees (Ref. 1).

Existing methods for the evaluation of liquefaction triggering were developed using liquefaction observations for large magnitude earthquakes. While most of the recently proposed liquefaction triggering evaluation procedures yield similar results for scenarios that are well represented in the liquefaction case history databases, their predictions deviate for other scenarios (e.g., low magnitude events, very shallow and very deep liquefiable layers, high fines content, medium dense to dense soils). These deviations can be sufficiently significant for these methods for evaluating liquefaction triggering to be not appropriate for use in the Groningen conditions (Ref. 2). Extending the database with the New Zealand liquefaction case histories, which are very relevant to the Groningen situation, and re-analyzing the case histories in the already existing database, allowed development of a methodology for evaluation of liquefaction triggering more appropriate for the Groningen region.

A pilot study area for the liquefaction hazard assessment was chosen such that the area with largest shaking hazard (Ref. 3), thick shallow young loose sands (Ref. 4) and multiple site response zones (Ref. 5) was included. Building on the probabilistic hazard model, a probabilistic assessment was prepared for the liquefaction hazard in this pilot area.

For grounding, an investigation based on the international literature was prepared into the smallest earthquake magnitude that can trigger liquefaction (Ref. 6). To provide an indication of the impact liquefaction could have on the foundations of buildings a modelling study was carried out (Ref. 7).

References

1. Code calibration for coupled, effective stress FEM-assessments of the primary flood defenses at Eemshaven-Delfzijl, RMC & Fugro, R. Jongejans, A. Giannakou, V. Drosos and P. Tasiopoulou, February 2017
2. Unbiased Cyclic Resistance Ratio Relationships for Evaluating Liquefaction Potential in Groningen, Russell Green, Adrian Rodriguez-Marek, Peter Stafford, Julian Bommer, April 2016.
3. Hazard, Building Damage and |Risk Assessment – November 2017, NAM, Jan van Elk and Dirk Doornhof, November 2017.
4. Liquefaction sensitivity of the shallow subsurface of Groningen, Deltares, November 2016
5. Geological schematisation of the shallow subsurface of Groningen (For site response to earthquakes for the Groningen gas field) – Parts I, II & III, Deltares, Pauline Kruiver, Ger de Lange, Ane Wiersma, Piet Meijers, Mandy Korff, Jan Peeters, Jan Stafleu, Ronald Harting, Roula Dambrink, Freek Busschers, Jan Gunnink
6. Smallest Earthquake Magnitude that Can Trigger Liquefaction, Russell Green, Julian Bommer, June 2018
7. Evaluation of Liquefaction-Induced Settlement of Typical Residential Buildings on Shallow Foundations Groningen, The Netherlands, Fugro, August 2018

NAM

Title	**Liquefaction Hazard Pilot Study for the Groningen Region of the Netherlands due to Induced Seismicity**		**Date**	August 2018
			Initiator	NAM
Author(s)	R.A. Green, J.J. Bommer, P.J. Stafford, B.W. Maurer, B. Edwards, P.P. Kruiver, A. Rodriguez-Marek, G. de Lange, S.J. Oates, T. Storck, P. Omidi, S.J. Bourne, and J. van Elk	**Editor**	Jan van Elk Dirk Doornhof	
Organisation	Team of Academic Experts	**Organisation**	NAM	
Place in the Study and Data Acquisition Plan	Study Theme: Liquefaction Comment: The soils in Groningen contain deposits of saturated sands. Therefore, the possibility of earthquake-induced liquefaction needs to be considered. Potentially, liquefaction could be important for critical infra-structure like dikes and levees. Existing methods for the evaluation of liquefaction triggering were developed using liquefaction observations for large magnitude earthquakes. While most of the recently proposed liquefaction triggering evaluation procedures yield similar results for scenarios that are well represented in the liquefaction case history databases, their predictions deviate for other scenarios (e.g., low magnitude events, very shallow and very deep liquefiable layers, high fines content, medium dense to dense soils). These deviations can be sufficiently significant for these methods for evaluating liquefaction triggering to be not appropriate for use in the Groningen conditions. Extending the database with the New Zealand liquefaction case histories, which are very relevant to the Groningen situation, and re-analyzing the case histories in the already existing database, allowed development of a methodology for evaluation of liquefaction triggering more appropriate for the Groningen region. A pilot study area for the liquefaction hazard assessment was chosen such that the area with largest shaking hazard, thick shallow young loose sands and multiple site response zones was included. Building on the probabilistic hazard model, a probabilistic assessment was prepared for the liquefaction hazard in this pilot area. For grounding, an investigation based on the international literature was prepared into the smallest earthquake magnitude that can trigger liquefaction. To provide an indication of the impact liquefaction could have on the foundations of buildings a modelling study was carried out.			

Directly linked research	1. Site Response of shallow subsurface and soils. 2. Ground Motion Prediction.
Used data	liquefaction case history databases extended with liquefaction case histories from recent earthquakes near Canterbury, New Zealand.
Associated organisation	Department of Civil and Environmental Engineering at Virginia Tech, Virginia, USA.
Assurance	This research has been published in peer-reviewed papers.

Liquefaction Hazard Pilot Study for the Groningen Region of the Netherlands due to Induced Seismicity

R.A. Green[1], J.J. Bommer[2], P.J. Stafford[3], B.W. Maurer[4], B. Edwards[5], P.P. Kruiver[6], A. Rodriguez-Marek[7], G. de Lange[8], S.J. Oates[9], T. Storck[10], P. Omidi[11], S.J. Bourne[12], and J. van Elk[13]

Executive Summary:

This report details a pilot study that assessed the liquefaction hazard in the Groningen region of northern Netherlands due to induced seismicity, resulting from natural gas production. In response to concerns about the induced earthquakes, the field operator Nederlandse Aardolie Maatschappij (NAM) is leading an effort to quantify the seismic hazard and risk resulting from the gas production operations (van Elk et al. 2017). Although an almost negligible contributor to earthquake fatalities, liquefaction triggering is an important threat to the built environment and in particular to infrastructure and lifelines (e.g., Bird and Bommer 2004) and is thus being included as part of the seismic hazard and risk study. Towards this end, the liquefaction hazard pilot study detailed in this report was performed, wherein the study area was selected to simultaneously satisfy three criteria: (a) proximity to the region of highest shaking hazard; (b) sampling of areas with thick, shallow young loose sand deposits; and (c) sampling of multiple site response zones used in developing application-specific ground motion predictive equations (GMPEs) (Rodriguez-Marek et al. 2017).

[1]Professor, Dept. of Civil and Environmental Engineering, Virginia Tech, Blacksburg, VA, USA (email: rugreen@vt.edu)
[2]Director, Bommer Consulting Ltd., Hampton TW12 2NG, U.K. Sorry
[3]Reader, Dept. of Civil and Environmental Engineering, Imperial College London, London, UK
[4]Assistant Professor, Dept. of Civil and Environmental Engineering, University of Washington, Seattle, WA, USA
[5]Senior Lecturer, School of Environmental Sciences, University of Liverpool, Liverpool, UK
[6]Senior Geophysicist, Deltares, Delft, the Netherlands
[7]Professor, Dept. of Civil and Environmental Engineering, Virginia Tech, Blacksburg, VA, USA
[8]Senior Engineering Geologist, Deltares, Delft, the Netherlands
[9]Shell Global Solutions International B.V., Rijswijk, the Netherlands
[10]Alten, Capelle ann den Ijssel, the Netherlands
[11]Alten, Capelle ann den Ijssel, the Netherlands
[12]Shell Global Solutions International B.V., Rijswijk, the Netherlands
[13]Development Lead Groningen Asset, Nederlandse Aardolie Maatschappij B.V., Assen, the Netherlands

Due to the unique characteristics of both the seismic hazard and the geologic profiles/soil deposits in Groningen, direct application of existing liquefaction evaluation procedures in the study was deemed inappropriate. Accordingly, efforts were first focused on reanalyzing the liquefaction case histories that were compiled for natural earthquakes to remove bias in their interpretation. Towards this end, new a depth-stress reduction factor (r_d) and number of equivalent cycles (n_{eq})/magnitude scaling factor (MSF) relationships for shallow crustal active tectonic regimes were developed and used in the reanalysis of the cone penetration test (CPT) liquefaction case histories compiled by Boulanger and Idriss (2014). These case histories were then used to regress a new liquefaction triggering curve (or cyclic resistance ratio curve: CRR). Next, using similar approaches to those employed to develop the new r_d and MSF relationships for natural earthquakes occurring in shallow crustal active tectonic regimes, Groningen-specific relationships were developed for evaluating liquefaction triggering due to induced seismicity in Groningen for magnitudes ranging from M_w3.5 to 7.0. These efforts significantly benefited from the broader efforts to assess the regional seismic hazard in Groningen, to include the development of a regional geologic model (Kruiver et al. 2017a, b), stochastic source model Bommer et al. (2017a), site response model (Rodriguez-Marek et al. 2017), and GMPE (Bommer et al. 2017b).

The liquefaction hazard was calculated using a Monte Carlo method wherein probability distributions for activity rates (Bourne and Oates 2017), event locations and magnitudes, and resulting ground motions are sampled such that the simulated future seismic hazard is consistent with historical seismic and reservoir compaction datasets (Bourne et al. 2015) up to a maximum event, the size of which is defined by a logic-tree (Bommer and van Elk 2017). For each event scenario, the developed Groningen-specific relationships were used to compute the factor of safety against liquefaction triggering (FS_{liq}) as a function of depth for 95 profiles across the pilot study area and corresponding Ishihara Inspired Liquefaction Potential Index (LPI_{ish}) (Maurer et al. 2015) hazard curves were computed for each profile. Consistent with the requirements of NPR 9998-2017 (NPR 9998 2017), LPI_{ish} values corresponding to an annual frequency of exceedance (AFE) of ~4×10^{-4} (or a 2475-year return period) are of particular interest. The LPI_{ish} values corresponding to 2475-year return period for the vast majority of the sites across the study area are less than 5, indicating that "No to Minor Surficial Liquefaction Manifestations." The only sites within the pilot study area that had LPI_{ish} values greater than 5, which is the threshold between "No to Minor

Surficial Liquefaction Manifestations" and "Moderate Surficial Liquefaction Manifestations," were in Zandeweer, with only some of the sites in Zandeweer exceeding this threshold value. No sites across the pilot study are were predicted to have "Severe Surficial Liquefaction Manifestations."

1 Introduction

The Groningen gas field is located in the northeastern region of the Netherlands and is one of the largest in the world. It has produced over 2000 billon m^3 of natural gas since the start of production in 1963. The first earthquakes linked to the gas production in the Groningen field occurred in 1991, although earthquakes were linked to production at other gas fields in the region since 1986. To date the largest induced earthquake due to production at the Groningen field is the 2012 local magnitude (M_L) 3.6 Huizinge event, and the largest recorded peak ground acceleration (PGA) is 0.11 g which was recorded during a more recent, slightly smaller magnitude event. In response to concerns about the induced earthquakes, the field operator Nederlandse Aardolie Maatschappij (NAM) is leading an effort to quantify the seismic hazard and risk resulting from the gas production operations (van Elk et al. 2017). Because of the widespread deposits of saturated sands in the region, the risk due to earthquake-induced liquefaction is being evaluated as part of this effort. Although an almost negligible contributor to earthquake fatalities, liquefaction triggering is an important threat to the built environment and in particular to infrastructure and lifelines (e.g., Bird and Bommer 2004). The workflow followed for the liquefaction hazard assessment of the Groningen field is shown in Figure 1.

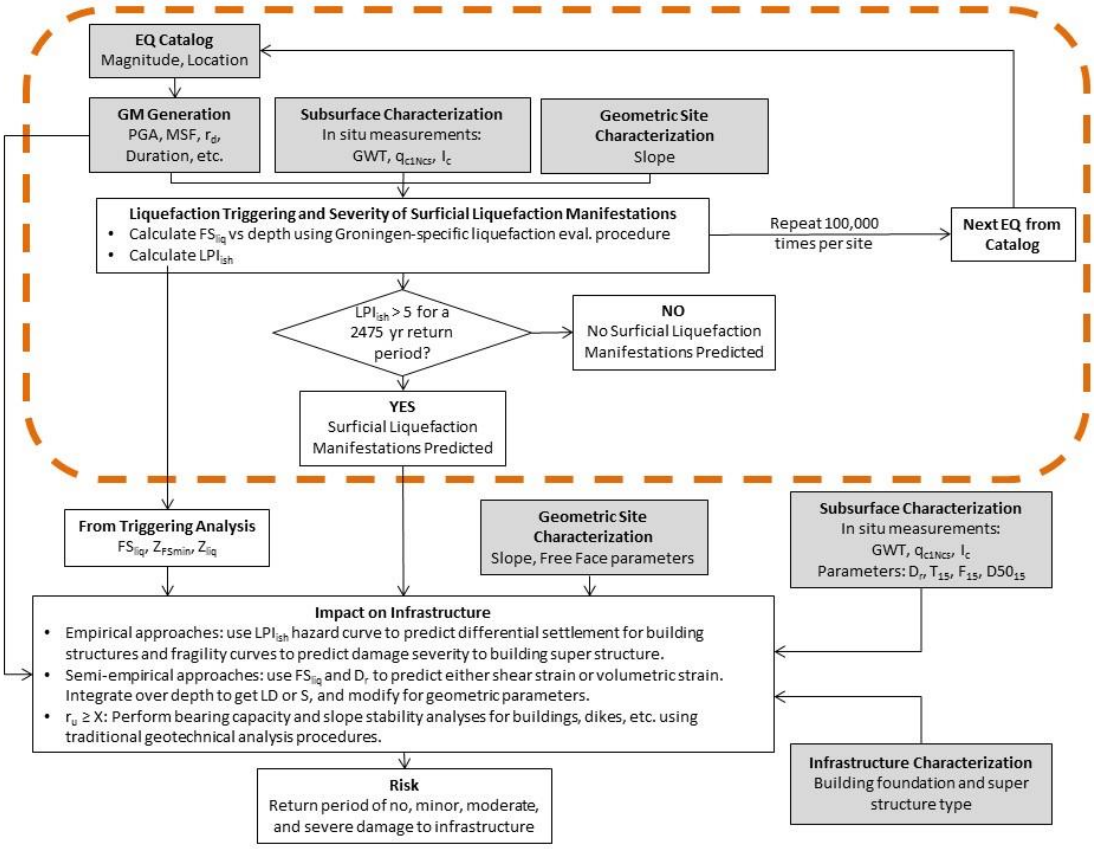

EQ: earthquake
GM: ground motion
PGA: peak ground acceleration
MSF: Magnitude Scaling Factor
r_d: depth-stress reduction factor
GWT: depth to the ground water table
q_{c1ncs}: normalized Cone Penetration Test tip resistance
I_c: Soil Behavior Type Index
FS_{liq}: factor of safety against liquefaction triggering
LPI_{ish}: Ishihara inspired liquefaction damage potential index
Z_{FSmin}: depth to the minimum value of FS_{liq}
Z_{liq}: depth to the center of the liquefied stratum
D_r: relative density
T_{15}: cumulative thickness (m) of saturated cohesionless sediment with a corrected Standard Penetration Test blow count ≤ 15 blows/30c m
F_{15}: average fines content (%) of strata include in T_{15}
$D50_{15}$: mean grain size (mm) of strata included in T_{15}
LD: lateral displacement
S: vertical settlement
r_u: excess pore pressure ratio
X: threshold value of ru for acceptable performance for bearing capacity of soil

Fig. 1 Workflow followed for the liquefaction hazard assessment of the Groningen field. The elements within the dashed area constitute the core components of the approach to calculating the severity/damage potential of liquefaction given the characteristics of the subsurface and the earthquake-induced ground shaking within the framework of the Monte Carlo-based probabilistic hazard calculations. The lower part of the figure relates to the extension of the calculations from the likelihood of liquefaction occurring to estimates of the risk associate with liquefaction triggering.

Central to the liquefaction hazard/risk assessment of the Groningen field is the stress-based "simplified" liquefaction evaluation procedure, which is the most widely used approach to evaluate liquefaction potential worldwide. While most of the recently proposed variants of this procedure yield similar results for scenarios that are well represented in the liquefaction case history databases (e.g., Green et al. 2014), their predictions deviate for other scenarios (e.g., small and large magnitude events, very shallow and very deep liquefiable layers, high fines content, medium dense to dense soils). These deviations can be significant enough that the results from one evaluation procedure may indicate that the hazard due to liquefaction is low, while another procedure may indicate that the hazard is high. Analysis of fifty well-documented liquefaction case histories from the 2010-2011 Canterbury, New Zealand, earthquake sequence showed that of the three commonly used Cone Penetration Test (CPT)-based simplified liquefaction evaluation procedures (i.e., Robertson and Wride 1998; Moss et al. 2006; Idriss and Boulanger 2008), Idriss and Boulanger (2008) performed better than the others. The same conclusion was obtained from the analysis of several thousand case studies from the Canterbury earthquake sequence, wherein the procedures were used in conjunction with the Liquefaction Potential Index (LPI: Iwasaki et al. 1978) framework, and other liquefaction damage potential frameworks, to evaluate the severity of surficial liquefaction manifestations (Green et al. 2015; Maurer et al. 2015a).

Despite the conclusions from the comparative studies using the New Zealand data, the suitability of the Idriss and Boulanger (2008) (or any other existing variant of this procedure) for direct use to evaluate liquefaction in Groningen is questionable. This is because the simplified procedure is semi-empirical, with the empirical aspects of it derived from data from tectonic earthquakes in active shallow-crustal tectonic regimes (e.g., California, Japan, and New Zealand). Additionally, the seismic hazard and the geologic profiles/soil deposits in Groningen differ significantly from those used to develop the empirical aspects of the simplified procedure. Specifically, and as detailed in subsequent sections of this report, the suitability of the depth-stress reduction factor (r_d) and magnitude scaling factor (MSF) relationships inherent to existing variants of the simplified liquefaction evaluation procedure for use in evaluating the liquefaction potential in Groningen is uncertain. Accordingly, prior to the implementation of the workflow for the liquefaction hazard assessment depicted in Figure 1, efforts were first focused on developing a framework for

evaluating liquefaction potential in the region. This actually required an additional step backwards to develop an "unbiased" liquefaction triggering procedure for tectonic earthquakes, due to biases in the r_d and MSF relationships inherent to existing variants of the simplified procedure (e.g., Boulanger and Idriss 2014). Then moving forward, Groningen-specific r_d and MSF relationships were developed using the same approaches as for the "unbiased" worldwide relationships, thus allowing the Groningen-specific relationships to be used in place of the worldwide relationships for evaluating liquefaction potential in Groningen.

In the following sections, an overview of the shortcomings in current variants of the simplified procedures for use in Groningen is detailed, with focus on issues with the r_d and MSF relationships inherent to Boulanger and Idriss (2014) procedure. Then, the efforts to develop new "unbiased" r_d and MSF relationships and an "unbiased" liquefaction triggering curve (or cyclic resistance ratio curve: $CRR_{M7.5}$) are detailed. This is followed by a presentation on the development of the Groningen-specific r_d and MSF relationships. Details of the liquefaction hazard pilot study, to include the results for ~100 sites across the pilot study area, are then presented.

2 Shortcoming in existing variants of the simplified liquefaction evaluation procedure for use in Groningen

2.1 Overview of the simplified procedure

As mentioned in the Introduction, the stress-based simplified liquefaction evaluation procedure is central to the workflow for the liquefaction hazard assessment for the Groningen region. Per this procedure the seismic demand is quantified in terms of Cyclic Stress Ratio (CSR), which is the cyclic shear stress (τ_c) imposed on the soil at a given depth in the profile normalized by the initial vertical effective stress (σ'_{vo}) at that same depth. The word "simplified" in the procedure's title originated from the proposed use of a form of Newton's Second Law to compute τ_c at a given depth in the profile, in lieu of performing numerical site response analyses (Whitman 1971; Seed and Idriss 1971). The resulting "simplified" expression for CSR is given by Eq. 1:

$$CSR = \frac{\tau_c}{\sigma'_{vo}} = 0.65(\frac{a_{max}}{g})(\frac{\sigma_v}{\sigma'_{vo}})r_d \quad (1)$$

where: a_{max} = maximum horizontal acceleration at the ground surface (equivalent to PGA at the surface of a soil profile); g = acceleration due to gravity; σ_v and σ'_{vo} = total and initial effective vertical stresses, respectively; and r_d = depth-stress reduction factor that accounts for the non-rigid response of the soil profile.

Additional factors are applied to Eq. 1, the needs for which were largely based on results from laboratory studies, to account for the effects of the shaking duration (MSF: Magnitude Scaling Factor, where the reference motion duration is for a moment magnitude, **M**, 7.5 earthquake), initial effective overburden stress (K_σ, where the reference initial effective overburden stress is 1 atm), and initial static shear stress (K_α, where the initial static shear stress is zero, e.g., level ground conditions). The resulting expression for the normalized CSR (i.e., CSR*: CSR normalized for motion duration for a **M** 7.5 event, 1 atm initial effective overburden stress, and level ground conditions) is given by Eq. 2:

$$CSR^* = \frac{CSR}{MSF \cdot K_\sigma \cdot K_\alpha} = 0.65(\frac{a_{max}}{g})(\frac{\sigma_v}{\sigma'_{vo}})r_d \frac{1}{MSF \cdot K_\sigma \cdot K_\alpha} \quad (2)$$

Case histories compiled from post-earthquake investigations were categorized as either "liquefaction" or "no liquefaction" based on whether evidence of liquefaction was or was not observed. The seismic demand (or normalized Cyclic Stress Ratio: CSR*) for each of the case histories is plotted as a function of the corresponding normalized in situ test metric, e.g., Standard Penetration Test (SPT): $N_{1,60cs}$; Cone Penetration Test (CPT): q_{c1Ncs}; or small strain shear-wave velocity (V_S): V_{S1}. In this plot, the "liquefaction" and "no liquefaction" cases tend to lie in two different regions of the graph. The "boundary" separating these two sets of case histories is referred to as the Cyclic Resistance Ratio ($CRR_{M7.5}$) and represents the capacity of the soil to resist liquefaction during an **M** 7.5 event. This boundary can be expressed as a function of the normalized in situ test metrics.

Consistent with the conventional definition for factor of safety (FS), the FS against liquefaction

(FS_{liq}) is defined as the capacity of the soil to resist liquefaction divided by the seismic demand:

$$FS_{liq} = \frac{CRR_{M7.5}}{CSR^*} \quad (3)$$

$CRR_{M7.5}$ is an inherent property of the soil, and is independent of earthquake shaking characteristics. In contrast, CSR* is directly a function of the characteristics of the earthquake shaking that impacts a site. Accordingly, $CRR_{M7.5}$ developed from case histories from tectonic earthquakes can be used to compute FS_{liq}. This is not necessarily the case for CSR* due to potential differences in tectonic vs. induced earthquake ground motions characteristics and potential differences in the site response characteristics of the tectonic earthquake case history profiles vs. those in the region impacted by the induced seismicity. These potential differences would manifest in the r_d and MSF relationships used to compute CSR* (Eq. 2).

2.2 Depth-stress reduction factor: r_d

As stated above, r_d is an empirical factor that accounts for the non-rigid response of the soil profile. Both the Idriss and Boulanger (2008) and the Boulanger and Idriss (2014) simplified liquefaction evaluation procedures use an r_d relationship that was developed by Idriss (1999). As shown in Figure 2, the Idriss (1999) r_d relationship is a function of earthquake magnitude and depth, with r_d being closer to one for larger magnitude events (note that $r_d = 1$ for all depths corresponds to the rigid response of the profile). This is because larger magnitude events have longer characteristic periods (e.g., Green et al. 2011) and, hence, longer wavelengths. As a result, even a soft profile will tend to respond as a rigid body if the characteristic wavelength of the ground motions is significantly longer than the height of the profile. Accordingly, the correlation between earthquake magnitude and the frequency content of the earthquake motions significantly influences the r_d relationship. This raises questions regarding the appropriateness of the Idriss (1999) relationship, which was developed using motions recorded during moderate to major tectonic events ($5 < \mathbf{M} < 8$), for evaluating liquefaction potential in Groningen where the seismic hazard is dominated by small magnitude induced earthquakes ($\mathbf{M} < 5$).

Another issue with the Idriss (1999) r_d relationship is that it tends to predict overly high CSR*

values at depth in a soil profile for tectonic events. This bias is also illustrated in Figure 2 and is pronounced for depths between ~3 to 20 m below the ground surface. This over-prediction may have initially been intentional under the premise that when the procedures were used in forward analyses to evaluate a site's liquefaction potential, they will yield "conservative" results (i.e., an over estimation of the CSR*). However, when used to evaluate case histories to develop the $CRR_{M7.5}$ curves that are central to the procedure, the biased r_d relationship actually results in an "unconservative" positioning of the $CRR_{M7.5}$ curve (i.e., the $CRR_{M7.5}$ curve yields a higher estimated liquefaction resistance of the soil than is warranted). The significance of this issue is mitigated to some extent when the same r_d relationship used to develop the $CRR_{M7.5}$ curve is also used in forward analyses (i.e., the bias cancels out). However, this will not be the case if site/region-specific r_d relationships (e.g., Groningen-specific r_d relationship) are developed and used in conjunction with a $CRR_{M7.5}$ curve that was developed using a "biased" r_d relationship.

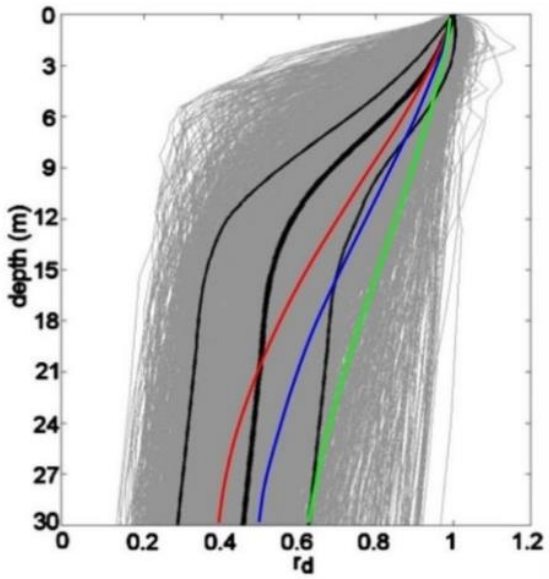

Fig. 2 r_d factor used to account for the non-rigid response of the soil column. The red, blue, and green lines were computed using the Idriss (1999) r_d relationship for **M** 5.5, **M** 6.5, and **M** 7.5 events, respectively. The grey lines were computed by Cetin (2000) from equivalent linear site response analyses performed using a matrix of 50 soil profiles and 40 recorded and scaled ground motions and two synthetic motions for **M** 8 strike slip and reverse events. The black lines are the median (thick line) and median plus/minus one standard deviation (thinner lines) for the Cetin (2000) analyses.

2.3 Magnitude Scaling Factors: MSF

As stated above, MSF account for the influence of the strong motion duration on liquefaction triggering. For historical reasons, MSF is normalized to **M** 7.5. MSF have traditionally been computed as the ratio of the number of equivalent cycles for an **M** 7.5 event to that of a magnitude **M** event, raised to the power *b* [i.e., MSF = $(n_{eq\ M7.5}/n_{eq\ M})^b$]. Both the Idriss and Boulanger (2008) and Boulanger and Idriss (2014) used the Seed et al. (1975) variant of the Palmgren-Miner (P-M) fatigue theory to compute $n_{eq\ M7.5}$ and $n_{eq\ M}$ from earthquake motions recorded at the surface of soil profiles. Furthermore, they obtained the value of *b* from laboratory test data. *b* is the negative slope of a plot of log(CSR) vs. log(N_{liq}), as shown in Figure 3; N_{liq} is the number of cycles required to trigger liquefaction in a soil specimen subjected to sinusoidal loading having an amplitude of CSR, typically determined using cyclic triaxial or cyclic simple shear tests.

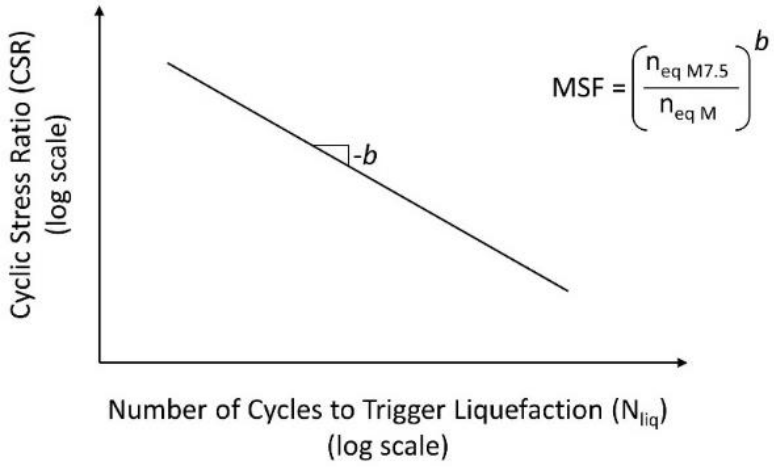

Fig. 3 For liquefaction evaluations, the Seed et al. (1975) variant of the P-M fatigue theory has most commonly been used to compute the equivalent number of cycles (n_{eq}). Per this approach, the negative of the slope of a CSR vs. N_{liq} curve (or *b* value) developed from laboratory tests is used to relate the "damage" induced in a soil sample from a pulse having one amplitude to that having a different amplitude. The *b* value is also used to relate n_{eq} and MSF.

There are several shortcomings inherent to the approach used by Idriss and Boulanger (2008) and Boulanger and Idriss (2014) to compute the number of equivalent cycles and MSF. These include:

- Both the magnitude and uncertainty of n_{eq}, and hence MSF, are assumed to be constant with depth. However, Green and Terri (2005) have shown that n_{eq} can vary with depth in a given profile and Lasley et al. (2017) showed that while the median value for n_{eq} computed for a large number of soil profiles and ground motions remains relatively constant with depth, the uncertainty in n_{eq} varies with depth.
- Pulses in the acceleration time history having an amplitude less than $0.3 \cdot a_{max}$ are assumed not to contribute to the triggering of liquefaction, and thus are not considered in the computation of n_{eq}. Using a relative amplitude criterion to exclude pulses is contrary to the known nonlinear response of soil which is governed by the absolute amplitude of the imposed load, among other factors. The use of a relative amplitude exclusion criterion with tectonic earthquake motions may inherently bias the resulting MSF, limiting its validity for use with motions having different characteristics (e.g., motions from induced earthquakes).
- Each of the two horizontal components of ground motion is treated separately, inherently assuming that both components have similar characteristics. However, analysis of recorded motions has shown this is not always the case, particularly for motions in the near fault region of tectonic events (e.g., Green et al. 2008; Carter et al. 2014, 2016) and for the Groningen motions, the horizontal components of which have been shown to exhibit very strong polarization (Bommer et al. 2017a).
- The *b* values used by Boulanger and Idriss (2014) were derived from several laboratory studies performed on various soils and it is uncertain whether all these studies used a consistent definition of liquefaction in interpreting the test data. As a result, the *b* values proposed by Boulanger and Idriss (2014) entail a considerable amount of uncertainty (Ulmer et al. 2018), with the proposed values not being in accord with those inherent to the shear modulus and damping degradation curves used in the equivalent linear site response analyses to develop the r_d correlations (elaborated on subsequently).
- Recent studies have shown that the amplitude and duration of earthquake ground motions are negatively correlated (e.g., Bradley 2011); preliminary models confirm this observation for Groningen field ground motions (e.g., Bommer et al. 2016). None of the MSF correlations developed to date, to include the one proposed by Boulanger and Idriss (2014), have considered this.

Some of the above listed shortcomings will be more significant to the Groningen liquefaction hazard assessment than others, but it is difficult to state *a priori* which ones these are. Furthermore, even for tectonic earthquakes the validation of MSF is hindered by the limited magnitude range of case histories in the field liquefaction databases, with the majority of the cases being for events having magnitudes ranging from **M** 6.25 to **M** 7.75 (NRC 2016). Specific to the Groningen liquefaction hazard assessment, MSF for small magnitude events is very important, particularly given that published MSF values vary by a factor of 3 for **M** 5.5 (Youd et al. 2001), with this factor increasing if the proposed MSF relations are extrapolated to lower magnitudes.

3 Removing bias from the simplified liquefaction evaluation procedure for tectonic earthquakes

3.1 Depth-stress reduction factor: r_d

A new relationship for r_d was developed by Lasley et al. (2016) using an approach similar to that used by Cetin (2000). Equivalent linear site response analyses were performed on 50 soil profiles compiled by Cetin (2000) that are representative of those in the liquefaction case history databases. However, Lasley et al. (2016) used a larger set of recorded input motions in their analyses than were available at the time Cetin (2000) performed his study. Several functional forms for r_d were examined by Lasley et al. (2016) in regressing the results from the site response analyses, with the following form selected because of its simplicity and shape (i.e., relatively low standard deviation of the regressed data):

$$r_d = (1-\alpha)exp\left(\frac{-z}{\beta}\right) + \alpha + \varepsilon_{r_d}; \qquad 0 \leq r_d \leq 1 \tag{4}$$

where α is the limiting value of r_d at large depths and can range from 0 to 1. The variable β controls the curvature of the function at shallow depths, z is the depth in meters, and ε_{r_d} is a zero-mean random variable with standard deviation σ_{r_d}. The term (1-α) scales the exponential so that r_d is equal to one at the ground surface.

Two different sets of expressions for α and β were developed, one set being a function of **M** and

the small-strain shear-wave velocity (V_S) averaged over the upper 12 m of the profile (V_{S12}) and the other being solely a function of **M**. This allows the use of the r_d relationship for profiles having varying levels of characterization. The first set of expressions for α and β is:

$$\alpha_1 = exp(b_1 + b_2\boldsymbol{M} + b_3 V_{S12}) \quad (5a)$$

$$\beta_1 = exp(b_4 + b_5\boldsymbol{M} + b_6 V_{S12}) \quad (5b)$$

and the second set is:

$$\alpha_2 = exp(b_1 + b_2\boldsymbol{M}) \quad (6a)$$

$$\beta_2 = b_3 + b_4\boldsymbol{M} \quad (6b)$$

where b_1-b_6 are regression coefficients. The standard deviation associated with Eq. 4, σ_{r_d}, is defined as:

$$\sigma_{r_d} = \frac{b_7}{[1+exp(b_8 * z)]} \quad (7)$$

where b_7 and b_8 are additional regression coefficients, and *z* is as defined for Eq. 4. Table 1 lists the mean values of the regression coefficients b_1 – b_8. As with any empirical relationship, care should be used when applying these equations for conditions outside the ranges from which they were regressed (i.e., **M**: 5.3 to 7.6 and V_{S12}: 130 to 220 m/s). In particular, erroneous values will result when β is less than or equal to zero.

Table 1 Regression coefficients for the r_d relationships

Form	b_1	b_2	b_3	b_4	b_5	b_6	b_7	b_8
1	-3.793	0.4016	-0.001405	-1.380	0.3276	0.01332	0.1473	-0.4111
2	-4.373	0.4491	-20.11	6.247	-	-	0.1506	-0.4975

Figure 4 shows the proposed r_d relationship (using Eq. 6 for α and β) for magnitudes of 5.5 and 7.5, along with the r_d values predicted by a few commonly used relationships. The Liao and Whitman (1986) relationship is solely a function of depth and was adopted for use in the Youd et

al. (2001) liquefaction evaluation procedures, which are widely used in practice. Cetin (2000) proposed two variants of an r_d relationship, one being a function of **M**, a_{max}, V_{S12}, and depth (i.e., Cetin with V_{S12}) and the other being a function of **M**, a_{max}, and depth (i.e., Cetin without V_{S12}). These relationships were adopted for use in the Cetin et al. (2004), Moss et al. (2006), and Kayen et al. (2013) simplified liquefaction evaluation procedures. As mentioned previously, the Idriss (1999) r_d relationship is a function of **M** and depth and was adopted for use in the Idriss and Boulanger (2008) and Boulanger and Idriss (2014) liquefaction evaluation procedures. Relative to the other relationships shown in Figure 4, Lasley et al. (2016) was developed using more site response data and more rigorous regression analyses. So while all relationships inherently have some bias, a strong argument can be made that Lasley et al. (2016) has the least amount of bias of commonly used relationships and was therefore adopted for use herein.

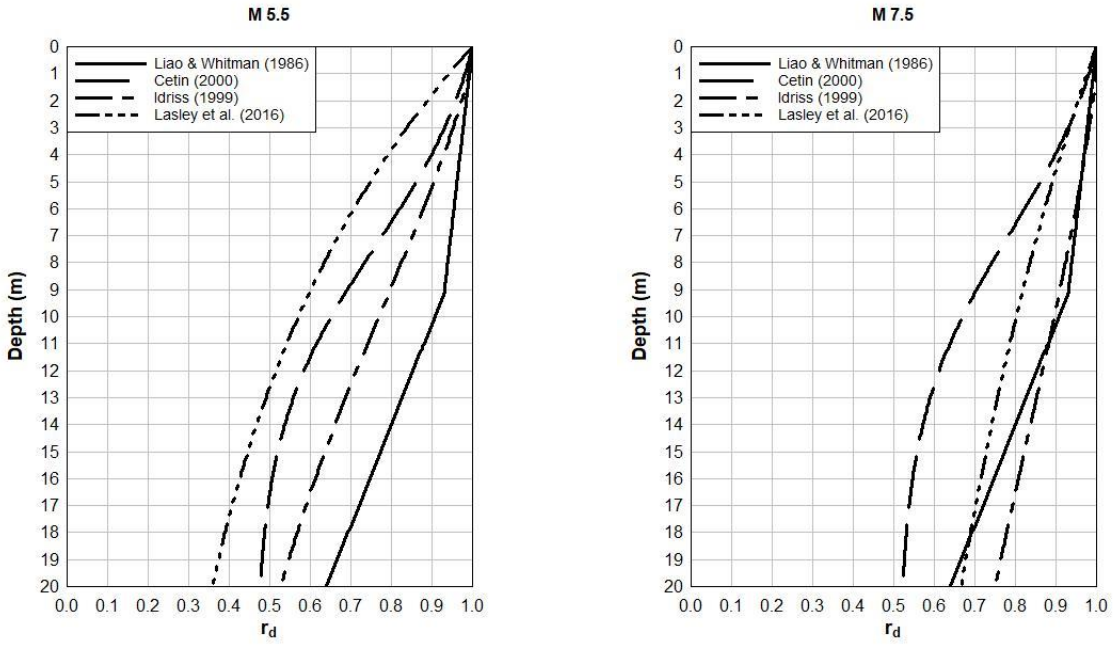

Fig. 4 Comparison of commonly used r_d relationships proposed by Liao and Whitman (1986), Cetin (2000), Idriss (2000), and Lasley et al. (2016) (Eqs. 4 and 6) for two different earthquake scenarios: (a) **M** 5.5 and a_{max} = 0.1g, and (b) **M** 7.5 and a_{max} = 0.3g. Note: Liao and Whitman (1986) relationship is only a function of depth; Idriss (1999) and Eqs. 4 and 6 are only dependent on **M** and depth; and Cetin (2000) is dependent on **M**, a_{max}, and depth.

3.2 Magnitude Scaling Factor: MSF

Development of a MSF relationship that overcomes all the shortcomings listed above for the Idriss and Boulanger (2008) and Boulanger and Idriss (2014) relationships is not as straightforward as developing the new r_d relationships. The reason for this is that there are many more issues with existing MSF than there are with the r_d relationships. As a result, a new approach needed to be used to compute the MSF, as opposed to implementing an existing approach using a more comprehensive dataset and a more rigorous regression analysis.

As mentioned previously and shown in Figure 3, MSF are computed from equivalent number of cycles, n_{eq}. Well-established fatigue theories have been proposed for computing n_{eq} for materials having varying phenomenological behavior; reviews of different approaches for computing n_{eq} are provided in Green and Terri (2005), Hancock and Bommer (2005), and Green and Lee (2006), among others. Developed specifically for use in evaluating liquefaction potential, the approach proposed by Green and Terri (2005) was selected for developing an n_{eq} relationship for the Groningen project. This approach is an alternative implementation of the P-M fatigue theory that better accounts for the nonlinear behavior of the soil than the Seed et al. (1975) variant. In this approach, dissipated energy is explicitly used as the damage metric. n_{eq} is determined by equating the energy dissipated in a soil element subjected to an earthquake motion to the energy dissipated in the same soil element subjected to a sinusoidal motion of a given amplitude and a duration of n_{eq}. Dissipated energy was selected as the damage metric because it has been shown to correlate with excess pore pressure generation in saturated cohesionless soil samples subjected to undrained cyclic loading (e.g., Green et al. 2000; Polito et al. 2008). Furthermore, from a microscopic perspective, the energy is thought to be predominantly dissipated by the friction between sand grains as they move relative to each other as the soil skeleton breaks down, which is requisite for liquefaction triggering.

Conceptually, the Green and Terri (2005) approach for computing n_{eq} is shown in Figure 5. Stress and strain time histories at various depths in the soil profile are obtained from a site response analysis. By integrating the variation of shear stress over shear strain, the cumulative dissipated energy per unit volume of soil can be computed (i.e., the cumulative area bounded by the shear

stress-shear strain hysteresis loops). n_{eq} is then determined by dividing the cumulative dissipated energy for the entire earthquake motion by the energy dissipated in one equivalent cycle. For historical reasons, the shear stress amplitude of the equivalent cycle (τ_{avg}) is taken as $0.65 \cdot \tau_{max}$ (where τ_{max} is the maximum induced cyclic shear stress, τ_c, at a given depth), and the dissipated energy associated with the equivalent cycle is determined from the constitutive model used in the site response analysis.

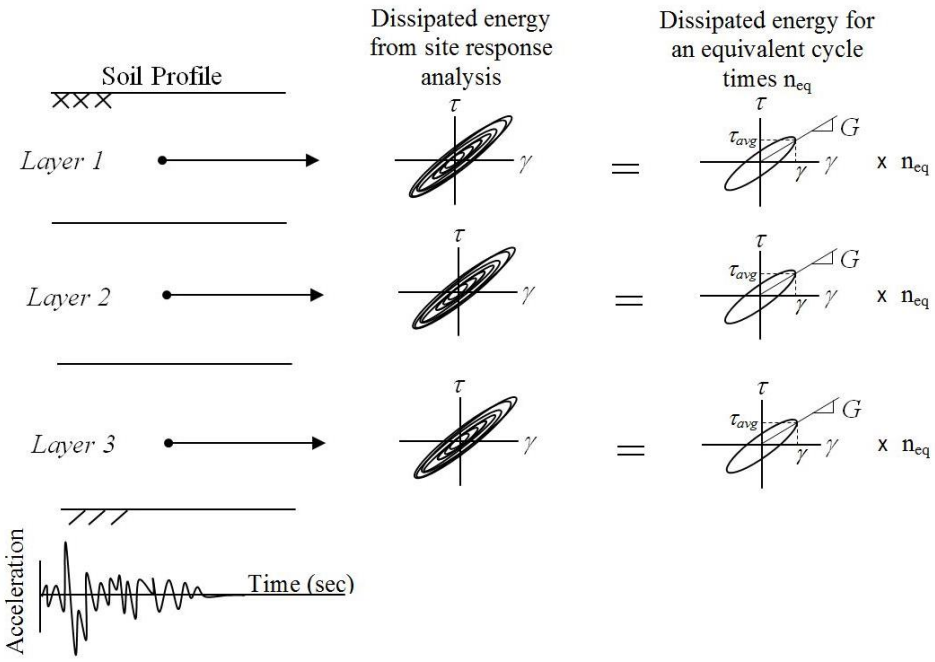

Fig. 5 Illustration of the proposed procedure to compute n_{eq}. In this procedure, the dissipated in a layer of soil, as computed from a site response analysis, is equated to the energy dissipated in an equivalent cycle of loading multiplied by n_{eq}.

As noted above, one of the shortcomings of the Seed et al. (1975) variant of the P-M fatigue theory is the way in which multi-directional shaking is taken into to account. Specifically, each of the two horizontal components of ground motion is treated separately, inherently assuming that both components have similar characteristics. However, analysis of recorded motions has shown this is not always the case, particularly for motions in the near fault region (e.g., Green et al. 2008; Carter et al. 2014, 2016) and for the Groningen motions, the horizontal components of which have been shown to exhibit very strong polarization (Bommer et al. 2017a). In contrast, Green and Terri

(2005) accounted for multi-directional shaking by performing separate site response analyses for each horizontal component in a pair of motions, adding the energy dissipated at the respective depths for each component of motion, and setting the amplitude of the equivalent cycle as the 0.65 times the geometric mean of the maximum shear stresses experienced at a given depth. This approach is referred to as "Approach 2" in Lasley et al. (2017) and is used herein because it is better accounts for differences in the characteristics in the two horizontal components of motion.

Lasley et al. (2017) implemented the Green and Terri (2005) approach for computing n_{eq} using the same motions and profiles used by Lasley et al. (2016) to develop their r_d relationship. Their proposed n_{eq} relationship is:

$$\ln(n_{eq}) = a_1 + a_2 \ln\left(\frac{a_{max}}{g}\right) + a_3 \boldsymbol{M} + \delta_{event} + \delta_{profile} + \delta_0 \quad (8)$$

where a_{max} is in units of g; a_1-a_3 are regression coefficients; δ_{event} and $\delta_{profile}$ are random effects terms that correspond to an average event residual and the average-profile residuals, respectively; and δ_0 is the residual term. The random effect terms and the residual term are assumed to be zero-mean normally-distributed random variables with standard deviations given by τ_{event}, $\tau_{profile}$, and τ_0 for the event, profile, and residual terms, respectively. Assuming that the random effect terms and the residual term are uncorrelated, the total standard deviation (σ_{Total}) is given by:

$$\sigma_{Total} = \sqrt{\tau_{event}^2 + \tau_{profile}^2 + \sigma_0^2} \quad (9)$$

The dependency of n_{eq} on a_{max} in Eq. 8 was chosen because of the observed negative correlation of strong ground motion duration with a_{max} (e.g., Bradley 2011; Bommer et al. 2016). Also, the functional form of this correlation is not an impediment to implementation because the simplified liquefaction evaluation procedures require both the magnitude (for MSFs and r_d) and a_{max} as input variables.

The mean values and the standard error of the regression coefficients for Eq. 8 are given in Table 2. The standard error of the regression coefficients is a measure of whether the coefficients are

well constrained by the data. The low values of these standard errors indicate that both the **M** and a_{max} scaling are well constrained by the data. The standard deviations of the residual components (Eq. 9) are given in Table 3 (in column labelled *Depth-Independent Model*). Analysis of total residuals indicated that the total standard deviation is depth-dependent, with higher standard deviations near the surface. Since most liquefaction cases occur near the surface, it was deemed important to capture this dependence. Residuals from Eq. 8 were used to constrain a depth-dependent total standard deviation model (σ_{Total}) using a boot-strapping technique. Only the total residuals were fitted in this way. The proposed model is a bilinear relationship given by:

$$\sigma_{Total}(z) = \max\left[\sigma_{surf} - \frac{z}{z_o}\left(\sigma_{surf} - \sigma_{depth}\right),\ \sigma_{depth}\right] \tag{10}$$

where z is depth in meters, σ_{surf} is the standard deviations at the surface, σ_{depth} is the standard deviation at depth, and z_o is the depth at which the standard deviation becomes constant. These parameters are given in Table 3. The depth-dependent standard deviation model is the recommended model to use in applications of Eq. 8.

Table 2 Regression coefficients and standard errors for n_{eq} correlation (Eq. 8)

a_1	σ_{a_1}	a_2	σ_{a_2}	a_3	σ_{a_3}
0.4605	0.08616	-0.4082	0.009325	0.2332	0.011800

Table 3 Inter-event, intra-event, and total errors for n_{eq} correlation (Eq. 8)

Depth-Independent Model (Eq. 9)				Depth-Dependent Model (Eq. 10)		
τ_{event}	$\tau_{profile}$	σ_0	σ_{Total}	σ_{surf}	σ_{depth}	z_o (m)
0.4051	0.1856	0.3851	0.5889	0.5399	0.4626	26.4

The *b* value that is needed to relate n_{eq} to MSF (e.g., Figure 3) can also be determined from the constitutive model used in the site response analysis, by assuming that the CSR vs. N_{liq} curve shown in Figure 3 is a contour of constant dissipated energy (Figure 6). In Figure 6, $\Delta W_{M7.5}$ is computed using Eq. 11. This equation is based on the assumption that the soil can be modelled as a visco-elastic material, consistent with the assumption inherent to the equivalent linear site response algorithm. For liquefaction evaluations, τ_{avg} used to compute $\Delta W_{M7.5}$ can be determined

from the $CRR_{M7.5}$ curve from the simplified liquefaction evaluation procedure (e.g., Boulanger and Idriss 2014). Accordingly, the computed CSR vs. N_{liq} curve corresponds to a soil having a given penetration resistance and confined at an initial effective overburden stress (σ'_{vo}) (i.e., $\tau_{avg} = CRR_{M7.5} \times \sigma'_{vo}$); the small strain shear modulus (G_{max}) for the soil should be consistent with the penetration resistance used to determine $CRR_{M7.5}$.

$$\Delta W_{M7.5} = \frac{2\pi \cdot D_\gamma \cdot \tau_{avg}^2}{G_{max} \cdot \left(\frac{G}{G_{max}}\right)_\gamma} \times n_{eq\ M7.5} \tag{11}$$

The damping (D_γ) and the degraded secant shear modulus, $G_{max} \cdot (G/G_{max})_\gamma$, values in Eq. 11 are commensurate with the induced shear strain (γ) in the soil and can be determined iteratively from the shear modulus and damping degradation curves used to model the soil response (e.g., Darendeli and Stokoe 2001). Once the value of $\Delta W_{M7.5}$ is determined, a contour of constant dissipated energy can be computed for different amplitudes of loading by simply computing the number of cycles for the assumed loading amplitude required for the dissipated energy to equal $\Delta W_{M7.5}$. The parameter *b*, which is the negative of the slope of the contour of constant dissipated energy, can now be computed.

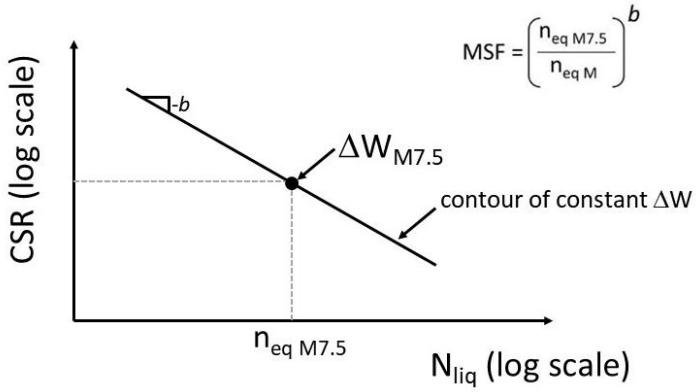

Fig. 6 A CSR vs. N_{liq} curve can be computed from shear modulus and damping degradation curves assuming the curve is a contour of constant dissipated energy. $\Delta W_{M7.5}$ can be computed using Eq. 11 and the remaining portions of the curve can be computed for different amplitudes of loading by simply computing the number of cycles for the assumed loading amplitude required for the dissipated energy to equal $\Delta W_{M7.5}$.

The assumption that the CSR vs. N_{liq} curve is a contour of constant dissipated energy inherently implies that the energy dissipated in a given element of soil at the point of liquefaction triggering is unique and independent of the imposed loading characteristics. Several studies have shown that this is a reasonable assumption (e.g., Polito et al. 2013; Kokusho and Kaneko 2014).

The degradation curves proposed Darendeli and Stokoe (2001) were used in this study to determine the *b* values following the procedure illustrated in Figure 6 for a range of effective confining stresses and soil densities, with the resulting values ranging from 0.33 to 0.35. However, $b = 0.34$ for the vast majority of the confining stress-density combinations considered and was thus used to compute MSF from n_{eq}. Additionally, $b = 0.34$ is consistent with laboratory curves developed from high-quality undisturbed samples obtained by freezing (Yoshimi et al. 1984). Accordingly, MSF is computed as:

$$MSF = \left(\frac{n_{eq\,M7.5}}{n_{eq\,M}}\right)^{b} = \left(\frac{14}{n_{eq\,M}}\right)^{0.34} \leq 2.02 \qquad (12)$$

where $n_{eq\,M}$ and $n_{eq\,M7.5}$ are computed using Eq. 8. To compute $n_{eq\,M7.5}$ using Eq. 8, **M** is set to 7.5 and a corresponding value for a_{max} needs to be assumed (i.e., $a_{max7.5}$). $a_{max7.5}$ was determined by computing the average a_{max} for the case histories in the Boulanger and Idriss (2014) SPT and CPT liquefaction case history databases ranging in magnitude from **M** 7.4 to 7.6. The average a_{max} for the 116 case histories that fell within this magnitude range was ~0.35 g. Using this value for $a_{max7.5}$, $n_{eq\,M7.5}$ was computed to be ~14. This value is similar to that determined by Seed et al. (1975), i.e., $n_{eq\,M7.5} = 15$. However, the value reported by Seed et al. (1975) represents the average for two horizontal components of motion, while the value computed herein represents the combined influence of both components of motion (Approach 2, Lasley et al. 2017). As a result, the value computed herein is approximately half of that computed by Seed et al. (1975). This difference is due both to the significantly larger ground motion database used by Lasley et al. (2017) to develop the Eq. 8, compared to that used by Seed et al. (1975), and to the differences in the approaches used to compute n_{eq}. However, both of these differences also influence the denominator in Eq. 12, which minimizes their influence on the resulting MSF.

The upper limit on the MSF (i.e., 2.02) corresponds to a scenario where the earthquake motions

consist of a single, low amplitude shear stress pulse in one of the horizontal components of motion. A plot of Eq. 12 is shown in Figure 7 for magnitudes ranging from **M** 5.0 to 8.5 and a_{max} ranging from 0.1 to 1.0 g.

A first order approximation for the standard deviation of the natural log of the MSF is:

$$\sigma_{\ln(MSF)} = b \cdot \sqrt{\sigma^2_{\ln(n_{eq\,M7.5})} + \sigma^2_{\ln(n_{eq\,M})} - 2 \cdot \rho \cdot \sigma_{\ln(n_{eq\,M7.5})} \sigma_{\ln(n_{eq\,M})}} \tag{13}$$

where $\sigma_{\ln(n_{eq\,M7.5})}$ and $\sigma_{\ln(n_{eq\,M})}$ are the standard deviations of the $\ln(n_{eq\ M7.5})$ and $\ln(n_{eqM})$, respectively, and ρ is the correlation coefficient of the residuals of $\ln(n_{eq\ M7.5})$ and $\ln(n_{eq\ M})$. However, because $n_{eq\,M7.5}$ is simply a normalization parameter for a reference scenario, $\sigma_{\ln(n_{eq\,M7.5})}$ = 0, and the correlation between the residuals of $\ln(n_{eqM7.5})$ and $\ln(n_{eq\ M})$ is also zero (i.e., ρ = 0). Accordingly, the standard deviation of the natural log of the MSF reduces to:

$$\sigma_{\ln(MSF)} = b \cdot \sigma_{\ln(n_{eq\,M})} = 0.34 \cdot \sigma_{\ln(n_{eq\,M})} \tag{14}$$

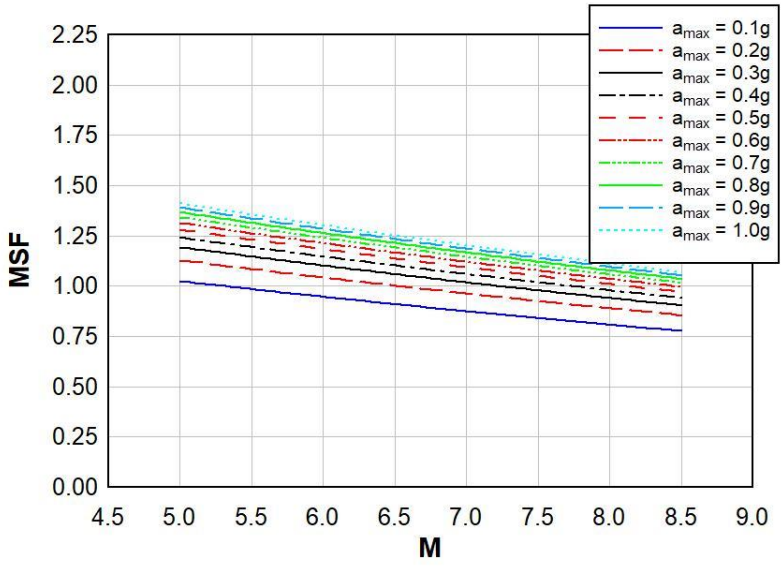

Fig. 7 MSF developed herein. For a given magnitude earthquake, MSF increases as a_{max} increases.

Figure 8 shows a comparison of the MSF developed in this study with those proposed by Idriss and Boulanger (2008) and Boulanger and Idriss (2014), where the latter is shown for q_{c1Ncs} = 84,

133, and 175 atm. As may be observed from this figure, for a given value of a_{max} the MSF developed in this study has about the same dependency on magnitude as the MSF proposed by Boulanger and Idriss (2014) for q_{c1Ncs} = 84 atm (i.e., medium dense sand). However, the difference between the two is that the former is a function of a_{max}, with MSF for a given magnitude increasing as a_{max} increases.

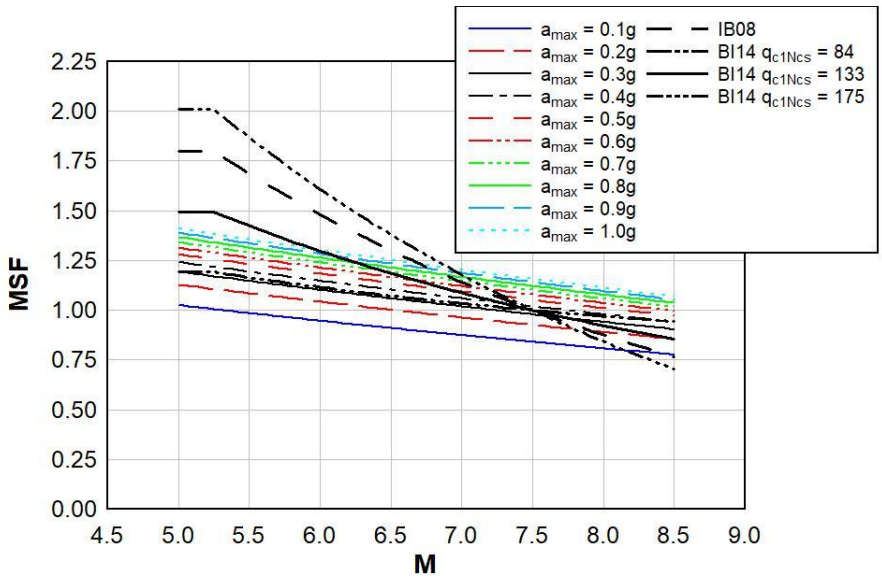

Fig. 8 Comparison of the MSF developed herein and those proposed by Idriss and Boulanger (2008) and Boulanger and Idriss (2014).

3.3 "Unbiased" $CRR_{M7.5}$ curve

The Lasley et al. (2016) r_d relationship and the MSF relationship developed in this study were used to re-analyze the CPT liquefaction case history database compiled by Boulanger and Idriss (2014); all other parameters/relationships used to analyze the case history data were the same as those used by Boulanger and Idriss (2014). These case histories were then used to regress a new "unbiased" deterministic liquefaction triggering curve (i.e., $CRR_{M7.5}$ curve), which is shown in Figure 9. This curve approximately corresponds to a probability of liquefaction [P(liq)] of 35% (total uncertainty) and is given by:

$$CRR_{M7.5} = exp\left\{\left(\frac{q_{c1Ncs}}{113}\right) + \left(\frac{q_{c1Ncs}}{1000}\right)^2 - \left(\frac{q_{c1Ncs}}{140}\right)^3 + \left(\frac{q_{c1Ncs}}{137}\right)^4 - 2.812\right\} \leq 0.6 \qquad (15)$$

where q_{c1Ncs} is computed using the procedure outlined in Boulanger and Idriss (2014).

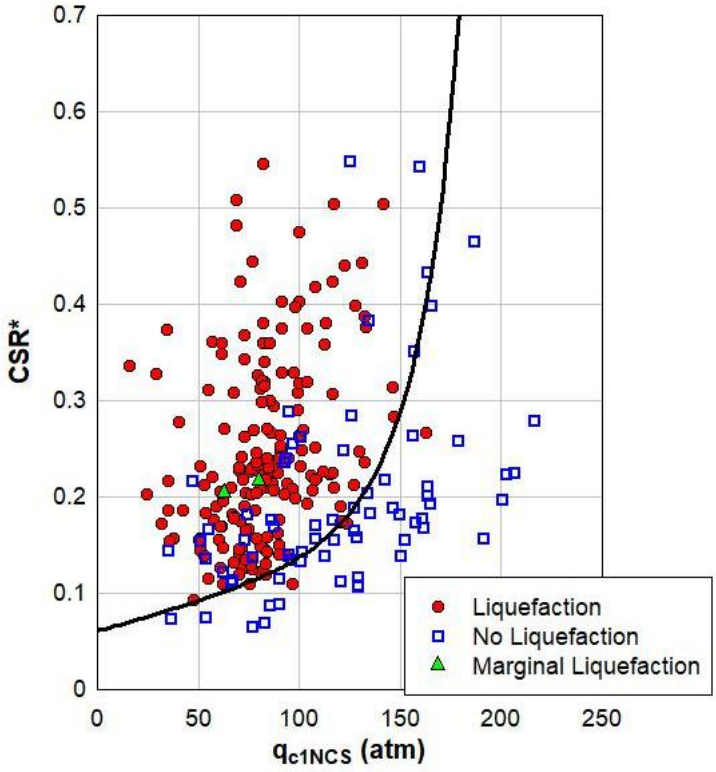

Fig. 9 "Unbiased" $CRR_{M7.5}$ curve regressed from liquefaction case history data from Boulanger and Idriss (2014) that were reanalysed using Lasley et al. (2016) r_d relationship and MSF developed herein.

To evaluate the relative efficacy of the "unbiased" simplified liquefaction evaluation procedure developed in this study versus the procedure proposed by Boulanger and Idriss (2014), 280 liquefaction/no liquefaction case histories from worldwide tectonic earthquakes were analyzed using the "Ishihara-inspired LPI" (LPI_{ish}) framework combined with the Receiver Operating Characteristic (ROC) framework (e.g., Maurer et al. 2015a, b). LPI_{ish} is a dimensionless index that correlates to the severity of surficial liquefaction manifestations resulting from the cumulative liquefaction response of a profile down to a depth of 20 m (Maurer et al. 2015c). The computed LPI_{ish} values are proportional to the cumulative thickness of liquefied layers, the proximity of these layers to the ground surface, and the amount by which FS_{liq} in each layer is less than 1.0, where FS_{liq} is computed using a simplified liquefaction evaluation procedure. ROC analyses, or "ROC

curves," are used in this study to assess the efficacy simplified liquefaction evaluation procedures for predicting the severity of liquefaction manifestation within the LPI_{ish} framework.

In a ROC analysis of the liquefaction evaluation procedures, the distributions of the "liquefaction" case histories (i.e., "positives") and "no liquefaction" case histories (i.e., "negatives") are determined as a function of LPI_{ish}, where it is very likely that there will be some overlap of the two distributions. Next, the relative probabilities of true positives (i.e., liquefaction is observed, as predicted) and false positives (i.e., liquefaction is predicted, but is not observed) are computed for a range of assumed threshold LPI_{ish} values, where no liquefaction is predicted for case histories having LPI_{ish} values below an assumed threshold LPI_{ish} value and liquefaction is predicted for case histories having LPI_{ish} values above the assumed threshold. A ROC curve is simply a plot of the relative probabilities of true positives (i.e., "True Positive Rate") and false positive (i.e., "False Positive Rate") for the range of assumed threshold LPI_{ish} values. The ROC curves for the Boulanger and Idriss (2014) and the "unbiased" liquefaction evaluation procedures for 280 worldwide liquefaction case histories are shown in Figure 10.

The area under a ROC curve (AUC) can be used to assess the relative efficacy of competing procedures, where AUC is equivalent to the probability that sites with liquefaction manifestations have higher computed LPI_{ish} than sites without manifestations (e.g., Fawcett 2005). As such, increasing AUC indicates better model performance. The AUC corresponding to the "unbiased" procedure proposed herein is essentially the same as that for the Boulanger and Idriss (2014) procedure for the 280 case histories analyzed (Figure 10): 0.78 vs. 0.77. However, we contend that the procedure proposed herein offers advantages over the Boulanger and Idriss (2014) procedure. Specifically, we contend that the "unbiased" procedure will yield more reliable results when evaluating scenarios that extend beyond those of the case histories used to develop the $CRR_{M7.5}$ curve (e.g., depths greater than 15 m and magnitudes less than ~**M** 6.25 or greater than ~**M** 7.75). Additionally, and more importantly, the "unbiased" procedure can be readily adapted to evaluate liquefaction potential from induced earthquakes in Groningen. This can be achieved by using similar approaches to those employed to develop the new r_d and MSF relationships for tectonic earthquakes presented above to develop Groningen-specific relationships using motions and soil profiles characteristic to Groningen. This effort is discussed in the next section.

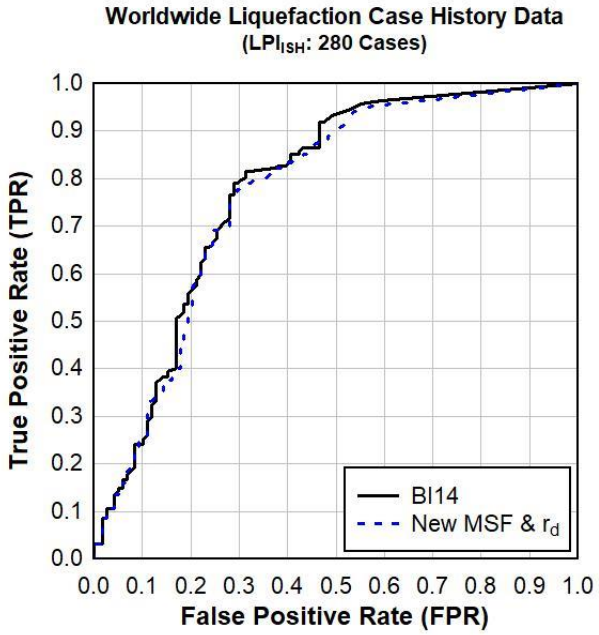

Fig. 10 Receiver Operator Characteristic (ROC) curves for 280 worldwide case histories categorized as either "liquefaction" or "no liquefaction." The areas under the ROC curves can be used to assess the relative efficacy of the "unbiased" liquefaction procedure proposed herein versus that proposed by Boulanger and Idriss (2014) in predicting liquefaction triggering.

4 Assessment of liquefaction hazard in Groningen

To determine whether a Groningen-wide liquefaction hazard assessment is warranted, a liquefaction hazard pilot study was performed first, wherein the study area was selected to simultaneously satisfy three criteria: (a) proximity to the region of highest shaking hazard; (b) sampling of areas with thick, shallow young loose sand deposits; and (c) sampling of multiple site response zones used in developing application-specific ground motion predictive equations (GMPEs) (Rodriguez-Marek et al. 2017). The location of pilot study area is shown in Figure 11, along with the cumulative thicknesses of the Holocene sand deposits that comprise the Naaldwijk formation which is considered to have the highest liquefaction potential in the region. However, before the liquefaction pilot study could be performed, Groningen-specific r_d and MSF relationships were developed following the approaches used by Lasley et al. (2016, 2017) and presented above. The consistency in the approaches used to develop the "unbiased" r_d and MSF for tectonic earthquakes and the Groningen-specific relationships allows the relationships to be

interchanged, otherwise these relationships would not be interchangeable (NRC 2016). The soil/geologic profiles and ground motions that used to develop the Groningen-specific relationships are detailed below.

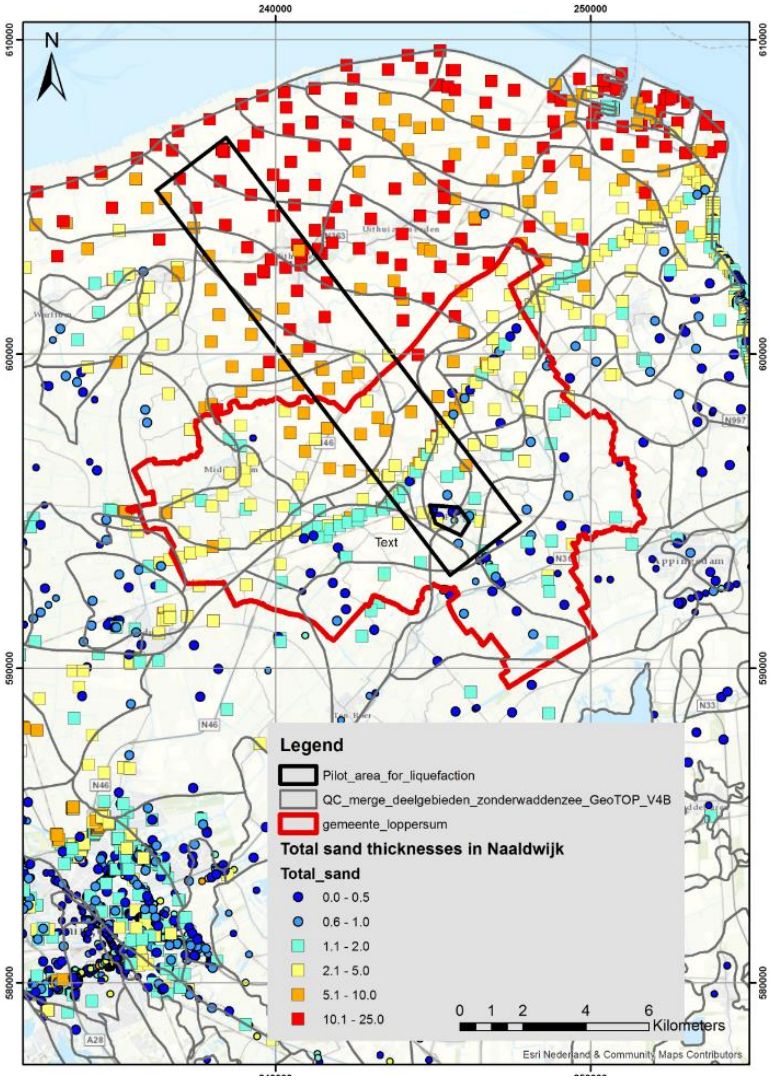

Fig. 11 Location of the liquefaction pilot study area across the Groningen gas field. Also shown are the cumulative thicknesses of the Holocene sand deposits that comprise the Naaldwijk formation.

4.1 Groningen-specific r_d, n_{eq}, and MSF relationships

A geologic cross section through the Groningen field is show in Figure 12. The gas reservoir exists within the Slochteren-Rotliegend sandstone at a depth of about 3 km; it is overlain by the Zechstein

salt layer and then a 1-km thick layer of chalk. A pronounced impedance contrast exists at the base of the North Sea Supergroup (designated henceforth as NS_B), which is at an average depth of ~800 m. This horizon has a V_S of ~1.5 km/s and a unit weight of 21 kN/m^3, and is chosen as the reference rock horizon that was treated as the top of the elastic half-space in the equivalent linear site response analyses that were performed (Rodriguez-Marek et al. 2017). The reason for selecting the NS_B to correspond to the elastic half-space is that it is the first elevation at which a strong and persistent velocity contrast is encountered. Although another velocity contrast is encountered at a depth of ~400 m at the Brussels Sands formation, a velocity reversal occurs at a depth of ~500 m which is inconsistent with the properties of an elastic half-space and thus prevents the top of the Brussels Sands formation from being used as the reference horizon. Moreover, the Brussels Sands formation is not consistently mapped across the entire field; in contrast, the NS_B is well defined over the entire study area.

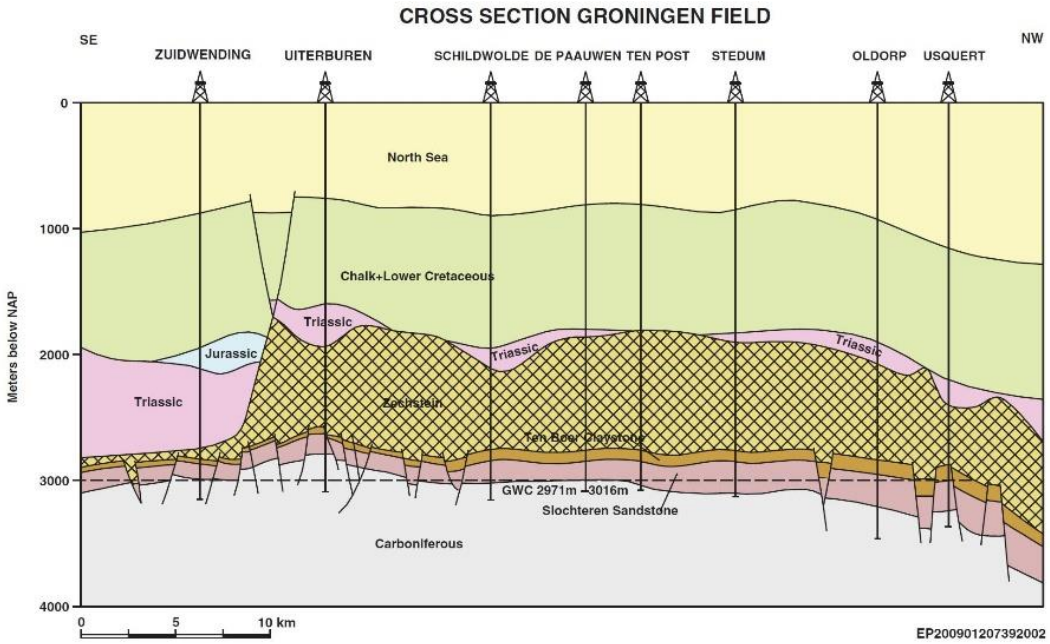

Fig. 12 Geologic cross section through the Groningen gas field (source: NAM). NAP, Dutch Ordnance Datum.

4.1.1 Geologic profiles used to develop Groningen-specific r_d and n_{eq} relationships

The velocity model from the ground surface down to the NS_B horizon is described in detail by

Kruiver et al. (2017a, b), and only a brief summary is presented herein. The velocity model from the ground surface to 50 m below the Dutch Ordnance Datum is based on a geo-statistical model, the GeoTOP model, with a 100 × 100 m spatial resolution that assigns a stratigraphic unit and a lithological class to 0.5-m thick voxels (Stafleu et al. 2011). The GeoTOP model includes a look-up table, which correlates each stratigraphic lithological unit to soil parameters (mean and standard deviation). These parameters include V_S, soil density, coefficients of uniformity, median grain-size diameter, measured CPT tip resistance (q_c), and undrained shear strength. When observed, depth dependency of V_S is included in these correlations. For depths greater than 50 m, velocities are assigned from the analysis of surface waves collected in field-wide seismic reflection surveys of Groningen gas reservoir. These measurements extend the V_S profile to a depth of about 120 m and are described in more detail in Kruiver et al. (2017a, b). Below this depth, measurements from sonic logs in the field are used to extend the profiles to the NS_B reference horizon (Kruiver et al. 2017a, b). The uncertainty in V_S for depths greater than about 50 m is ignored because these uncertainties have little impact on computed site response. An example of the resulting V_S profiles is shown in Figure 13. The assignment of unit weights for the various stratigraphic lithological units was based correlations with CPT from Lunne et al. (1997). For some of the deeper formations, the unit weight is assumed to be constant, consistent with the borehole logs from two deep boreholes (Kruiver et al. 2017a, b).

The GeoTOP model was used to develop profiles for use in the site response analyses to develop Groningen-specific r_d and n_{eq} relationships. The liquefaction pilot study area shown in Figure 11 crosses over several "zones" used to develop site amplification factors for the region (Rodriguez-Marek et al. 2017); for the most part the site amplification zones coincide with the geological zonation presented in Kruiver et al. (2017). The site amplification zones are shown in Figure 14, with the liquefaction pilot study area crossing over zones (from NW to SE) 821, 801, 603, 604, 1001, 602, 1032, and 2001. Given that r_d and n_{eq} relationships are functions of the response characteristics of a geologic profile, separate relationships were developed for each of the site amplification zones within the liquefaction pilot study area. Additionally, previous studies raised concerns about the liquefaction hazard in the "downtown" region of Zandeweer, which lies within the liquefaction pilot study area. As a result, this region was treated as a separate zone.

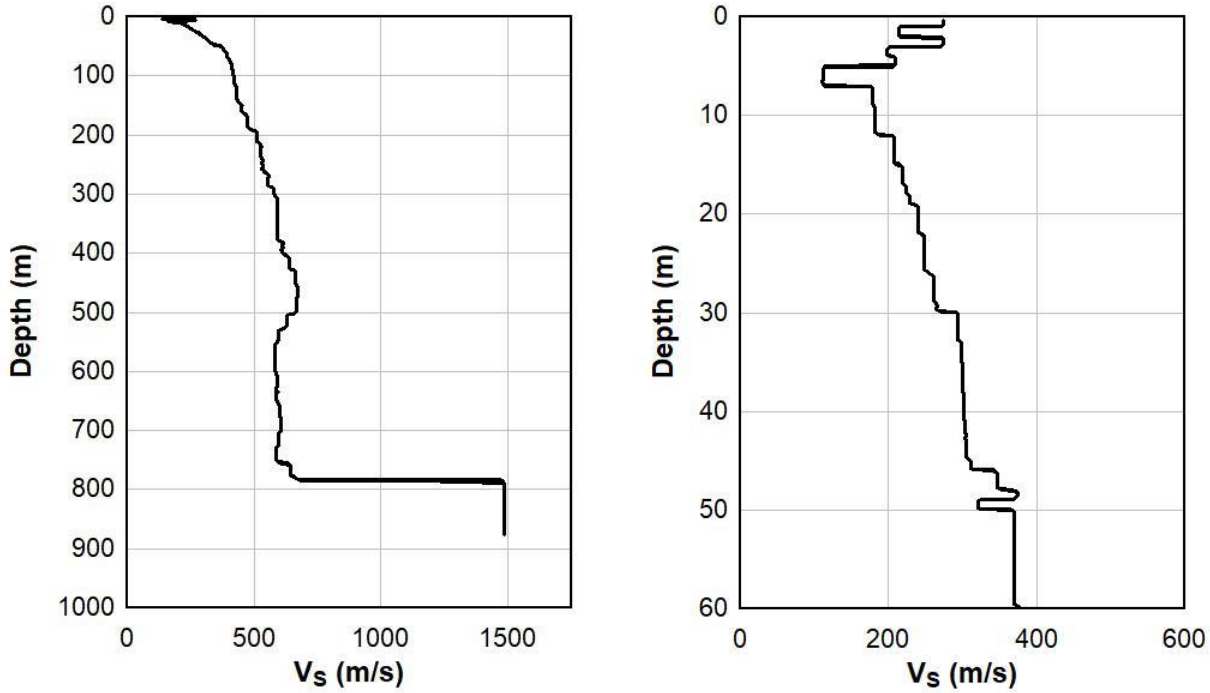

(a) (b)

Fig. 13 Sample V_S profile at the location of ground-motion recording station G09 (Bommer et al., 2017a): (a) full profile down to NS_B; and (b) enlarged view of the upper 60 m of the profile. (Rodriguez-Marek et al. 2017)

In selecting sites used to developed the Groningen-zone-specific r_d and n_{eq} relationships, preference was given to sites that were characterized by CPT; the locations of the CPT soundings within the pilot study area that were available at the start of this study are shown in Figure 14. For each CPT, the corresponding GeoTOP voxel stack in which the sounding was performed was identified. In several cases, two or more soundings were performed within the same 100 × 100 m GeoTOP voxel stack. If the number of unique GeoTOP voxel stacks in which the CPT soundings were performed in a zone was less than ten, then additional GeoTOP voxel stacks were chosen to obtain ten unique GeoTOP voxel stacks in that zone. The locations of these additional GeoTOP voxel stacks were selected to ensure a relatively uniform spatial distribution across a zone. Also, if the number of unique GeoTOP voxel stacks in which the CPT soundings were performed in a zone was at least ten but the spatial distribution of these stacks was not relatively uniform across the zone, three additional GeoTOP voxel stacks were chosen for that zone. The locations of the additional GeoTOP voxel stack profiles used in the site response analyses are shown in Figure 14

and listed as “random” and “random_extra” in the figure legend. The number of profiles per zone are listed in Table 4, with a total of 110 profiles across the liquefaction pilot study area used to develop the zone-specific r_d and n_{eq} relationships.

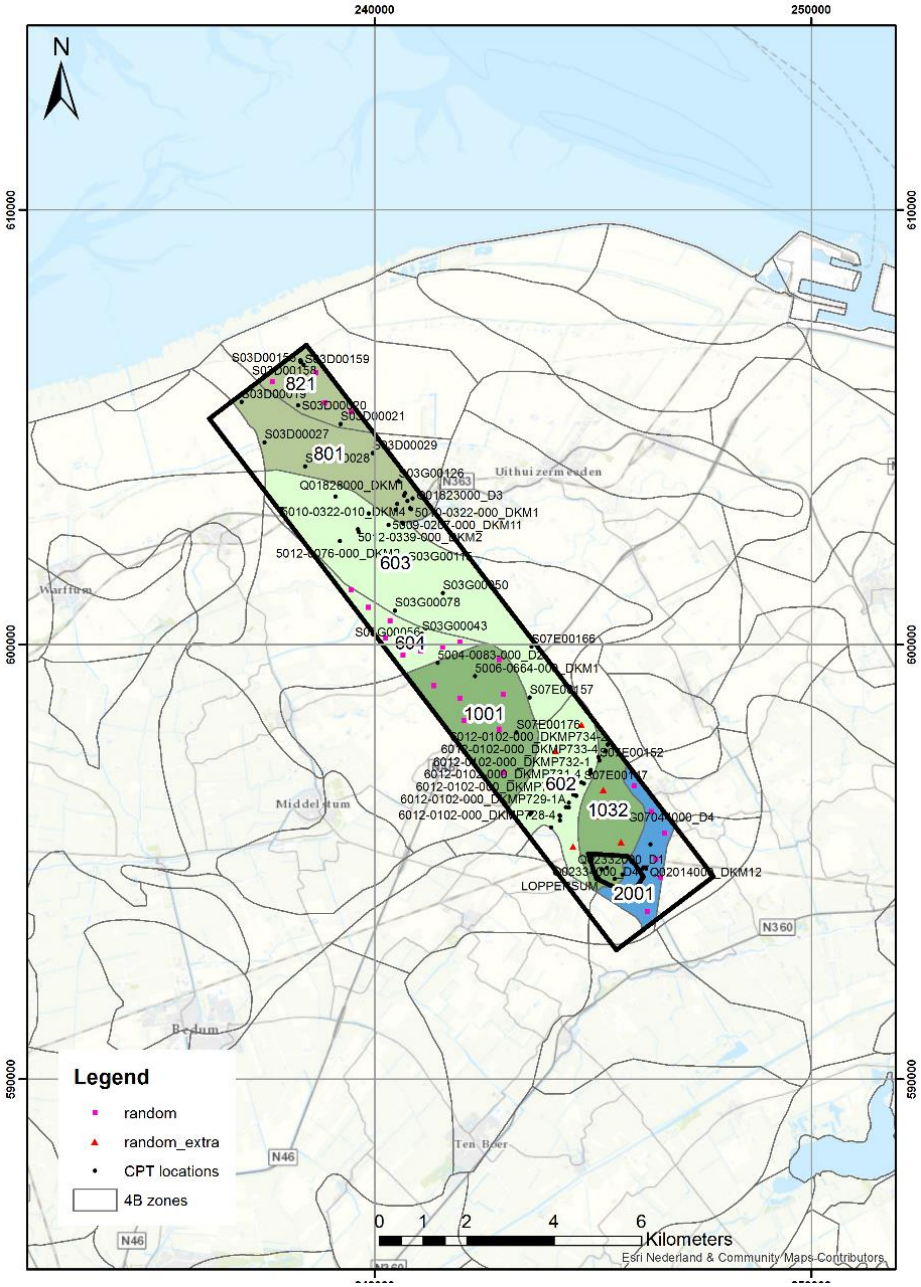

Fig. 14 Liquefaction pilot study area showing site amplification zones, locations of CPT soundings, and the locations of additional GeoTOP voxel stack profiles used in the site response analyses to generation Groningen-zone-specific r_d and n_{eq} relationships.

Table 4 Number of geologic profiles per zone used in the site response analyses to develop Groningen-zone-specific r_d and n_{eq} relationships.

Zone	No. of Profiles
602	16
603	12
604	10
801	11
821	10
1001	10
1032	15
2001	10
Zandeweer	16
Total	**110**

4.1.2 Ground motions used to develop Groningen-specific r_d and n_{eq} relationships

The ground motions at the NS_B reference horizon used in the site response analyses to develop the Groningen-zone-specific r_d and n_{eq} relationships were generated using finite-fault, stochastic simulation using the EXSIM code (Motazedian and Atkinson 2005; Boore 2009). Each of the distributed sub-faults in this technique is assumed to be a point source (effectively a small magnitude earthquake), and can be characterized using the seismological parameters observed in events recorded in the Groningen gas field. This process is illustrated in Figure 15 and described in detail by Bommer et al. (2017a), and briefly summarized below.

The first stage in calibrating the source model is to transform the surface recordings to the NS_B reference horizon, central to which is the velocity model from the NS_B horizon to the ground surface discussed above. The Fourier amplitude spectra (FAS) from the surface (B-stations in Figure 15) and from the 200-m boreholes (G-stations in Figure 15) were transformed to the NS_B horizon using a one-dimensional transfer function as implemented in the site response software STRATA (Kottke and Rathje 2008). Because the motions recorded to date are very weak (i.e., M_L 2.5 to 3.6 and distances from 0 to 20 km), the near-surface layers were assumed to have responded essentially linearly to the excitations, and therefore, the deconvolution was made assuming linear site response. Linear amplification factors were also calculated for the response spectra using the RVT procedure implemented in STRATA. The factors were calculated for the same V_S, damping,

and unit weight profiles, with input motions at the NS_B obtained from simulations, using an earlier version of the model. The amplification factors for the response spectra were found to be scenario-dependent (Stafford et al. 2017).

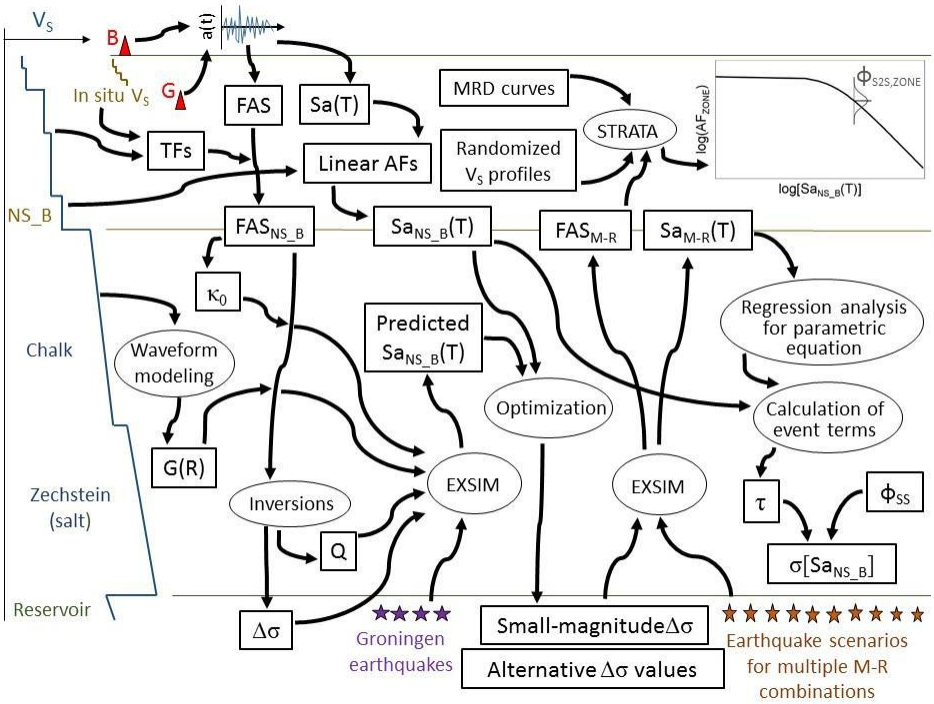

G and B: surface and borehole recording stations, respectively
NS_B: base of North Sea Supergroup (reference horizon)
TF: transfer function
AF: site amplification factor
Zone: field zonation for site amplification factors
FAS: Fourier amplitude spectra
Sa(T): response spectral acceleration at period T
G(R): shape of the geometric spreading function
EXSIM: software used for the stochastic simulations (Motazedian and Aktinson 2005; Boore 2009)
STRATA: 1D equivalent linear site response software (Kottke and Rathje 2008)
MRD: shear modulus reduction and damping used in STRATA
κ_o: site high frequency attenuation term
$\Delta\sigma$: stochastic model stress parameter
Q: quality factor
σ: total aleatory variability at rock horizon
τ: between event standard deviation
ϕ_{ss}: single-station within-event standard deviation
ϕ_{s2s}: site-to-site standard deviation

Fig. 15 Schematic illustration of the derivation of the Groningen-specific calibration parameters for the stochastic point source model, with quantities in rectangles and processes in ellipses. (Bommer et al. 2017a)

The FAS at the NS_B horizon were then inverted, following the approach of Edwards et al. (2011), for source, path, and site parameters (Figure 15). Three parameters were then fit to each FAS: the event-specific source corner-frequency (f_0) of a parametric source spectrum (e.g., Brune 1970, Boatwright 1978), the record-specific signal moment (long-period spectral displacement plateau), and high-frequency attenuation term, kappa (κ). As a result of the relatively small dataset of recorded motions available for these inversions, some elements were constrained independently. Firstly, κ was estimated from individual FAS plotted on log-linear axes following Anderson and Hough (1984). Secondly, the form of the geometric spreading was obtained from full waveform finite difference simulations performed using a 3D velocity model for the field. The inversions were then used to estimate the stress parameter ($\Delta\sigma$), the decay rates in each segment, the quality factor (Q) value, and the amplification factor at the NS_B (which was found to be close to 1). For the inversions, the use of both the Brune (1970) and Boatwright (1978) spectra was explored, with neither found to perform consistently better; hence, the former was used.

Based on the geometric spreading model and the results of the inversions of the FAS, many combinations of $\Delta\sigma$, Q, and site kappa (κ_0) were explored to identify the combination of parameters that best fit the response spectral ordinates at the NS_B horizon. The duration model used to link the FAS and response spectral ordinates was an empirically-based Groningen-specific model (Bommer et al 2016). The model that best fit the motions at the NS_B horizon in this case had a $\Delta\sigma$ of 60 bar, a frequency independent Q of 200, and a κ_0 of 0.015 s, which was then used in forward simulations.

The software EXSIM (Boore 2009, based on Motazedian and Atkinson 2005) was used in conjunction with the Groningen-specific stochastic point source model parameters to generate motions at the NS_B for magnitudes ranging from **M** 3.5 to 7.0, with Δ**M** = 0.5, and horizontal distances to the fault center (R) ranging from 0.1 to 60 km, with $\Delta\log(R) = 0.2$, resulting in a total of 120 magnitude-distance combinations. Each M-R scenario was recorded at 8 azimuths radially around the center of the strike of the finite fault, leading to 960 motions. Fault dimensions were based on Wells and Coppersmith (1994) for **M** > 5, otherwise Brune (1970), with each event sampling one realization of the distribution (with standard deviation of 0.15 log-units) of possible fault dimensions. Hypocenters were randomly located along strike, but always at Z = 3 km (the

reservoir depth), with propagation downwards (at 0.8β with 50% sub-fault pulsing) until the seismogenic depth of 13 km. For larger events, fault ruptures then grow horizontally, bounded by the reservoir and the seismogenic depth. Sub-fault durations were sampled from the Bommer et al. (2016) duration model, accounting for between- and within-event variability. The maximum magnitude of **M** 7.0 was determined by an expert panel using the SSHAC (Senior Seismic Hazard Analysis Committee) process (Bommer and van Elk 2017). In extrapolating to magnitudes so much larger than the largest recorded event (**M** 3.6), the inevitable epistemic uncertainty in the generated motions for larger magnitude events needed to be taken into account. This was done by both introducing magnitude-dependence of $\Delta\sigma$ into the model and also creating alternative (higher and lower) models, as had been done previously (Bommer et al. 2016). The weights assigned to these branches are 0.1 for the lower branch, since it is unclear whether low stress drop values would persist at larger magnitudes, and 0.3 each to the two central and upper models. In total 3840 motions were generated and used in the site response analyses to develop the Groningen-zone-specific r_d and n_{eq} relationships.

4.1.3 Groningen-zone-specific r_d, n_{eq}, and MSF relationships

In total 422,400 site response analyses were performed to develop Groningen-zone-specific r_d and n_{eq} relationships (110 profile × 3840 motions = 422,400 analyses). The site response analyses were performed using the equivalent linear code, ShakeVT2 (Lasley et al. 2014), which outputs r_d and n_{eq} values for the liquefiable layers, directly, for each analysis as a function of depth in the profile. The depth range considered for the regression analyses was restricted to 20 m and shallower. The reason for this was twofold. Firstly, the scaling of r_d was very stable over this depth range and including more data for deeper depths only acted to negatively influence the regression fit over the 0 – 20 m depth range. Secondly, and more importantly, liquefaction is a near surface phenomenon and none of the most recently compiled liquefaction case history databases (e.g., Cetin 2000; Moss et al. 2003; Kayen et al. 2013; Boulanger and Idriss 2014) include cases deeper than 20 m. The regression analyses were performed on well over 100,000 data points.

4.1.3.1 Groningen-zone-specific r_d relationships

For ease of model development, ease of implementation, and consistency with previous work, a relatively simple regression approach was used to develop the Groningen-zone-specific r_d relationships. Traditional nonlinear least-squares regression could not be used because of the complicated heteroscedastic standard deviation (i.e., the standard deviation is a function of the predictor variables: depth, z and magnitude, **M**). Therefore, maximum likelihood estimation was used directly and error estimates for each parameter were obtained from the Hessian matrix of the likelihood function.

A number of functional forms were considered during the model development, including the functional form adopted in the worldwide model developed by Lasley et al. (2016). The final functional form was based upon a sigmoid shape with the main variable being logarithmic depth. However, the location and scale parameters of the sigmoid are functions of **M**, V_S, and a_{max}. There is an apparent break in scaling for relatively large values of a_{max} and so this effect was modelled. The dependence upon V_{S12} that was included in the worldwide r_d relationship developed by Cetin (2000) was also observed in the Groningen data, and was thus included in the Groningen-zone-specific relationships developed herein. The same functional form of the regression equation was used for all zones, and the regression coefficients were found to be significant in all cases. The final functional form was selected on the basis of likelihood ratio tests performed on the alternative models considered.

The final functional form for $r_{d\text{-}Gron}$ is:

$$r_{d-Gron} = 1 - \frac{A_{rd}}{1+exp\left[-\frac{\ln(z)-(\beta_2+\beta_6\cdot\boldsymbol{M})}{(\beta_3+\beta_7\cdot\boldsymbol{M})}\right]};\ 0 \le r_d \le 1 \qquad (16)$$

where β_i are regression coefficients (Table 5), and A_{rd} is defined by Eq. 17 and represents the asymptotic level for $r_{d\text{-}Gron}$ at depth (that is, $r_{d\text{-}Gron} = 1\text{-}A_{rd}$ as $z \rightarrow \infty$).

$$A_{rd} = \beta_1 + \beta_4 \cdot \min[\boldsymbol{M}, 6.5] + \beta_5 \cdot \ln(a_{max}) + \beta_9 \cdot V_{s12};\ \text{for } a_{max} \le 0.3\ \text{g} \qquad (17a)$$

$$A_{rd} = \beta_1 + \beta_4 \cdot \min[\boldsymbol{M}, 6.5] + \beta_5 \cdot \ln(a_{max}) + \beta_8 \cdot \ln\left(\frac{a_{max}}{0.3}\right) + \beta_9 \cdot V_{s12};\ \text{for } a_{max} > 0.3 \text{ g} \quad (17b)$$

where a_{max} is in units of g and V_{S12} is in units of m/s.

The model also has a heteroscedastic standard deviation that is defined by:

$$\sigma_{r_d} = \frac{\beta_{10}}{1 + exp\left[-\frac{\ln(\max[z, 5]) - (\beta_2 + \beta_6 \cdot \boldsymbol{M})}{(\beta_3 + \beta_7 \cdot \boldsymbol{M})}\right]} \quad (18)$$

where z is in units of m, and β_i are regression coefficients (Table 5). Note that in Eq. 18 the depth is defined as the maximum of the actual depth, z, and 5 m in order to prevent the standard deviation becoming too small at very shallow depths.

Table 5 Regression coefficients for the $r_{d\text{-}Gron}$ model.

Zone	β_1	β_2	β_3	β_4	β_5	β_6	β_7	β_8	β_9	β_{10}
602	2.0845	1.1474	0.9709	-0.2080	0.0744	0.1148	-0.0882	0.2707	-0.0020	0.1520
603	2.1200	1.0467	0.6685	-0.2039	0.0800	0.1374	-0.0328	0.5033	-0.0024	0.1575
604	2.1687	1.2050	0.8968	-0.2205	0.0816	0.0629	-0.0738	0.4258	-0.0021	0.1443
801	2.5725	1.1450	0.4983	-0.2296	0.0734	0.1634	0.0437	0.7463	-0.0041	0.1908
821	2.7957	1.5813	0.9813	-0.2732	0.1003	0.0599	-0.0743	0.4674	-0.0039	0.1889
1001	2.1226	1.0583	0.7360	-0.2024	0.0722	0.1305	-0.0561	0.4349	-0.0032	0.1570
1032	1.7208	0.8872	0.4872	-0.1697	0.0638	0.1247	-0.0189	0.4720	-0.0017	0.1465
2001	2.2369	1.1288	0.8699	-0.2019	0.0772	0.1322	-0.0285	0.4831	-0.0030	0.1629
Zandeweer	2.4832	1.1972	0.8834	-0.2194	0.0772	0.1472	-0.0662	0.4002	-0.0037	0.1405

The residual plots against the predictor variables used in Eqs. 16 and 17 are shown in Figure 16 for Zone 602, as an example. The very large number of residuals for each analysis case poses challenges because small deviations are statistically significant and can lead to over-fitting. Therefore, in fitting the model we have focused upon the main trends that were observed. The binned residuals are shown in Figure 16 to better illustrate the center and the variance of the data. For example, in Figure 16a there is an apparently larger deviation of the data from the center near $\log(a_{max}) = -1$ from the residuals, but the binned residuals show that there is not really significantly more variance here, but rather, it is just that we have such a large sample that we see more points in the tails of the distribution. Additionally, it is important to note that the residual plots do not show any clear trends against the variables shown, and thus, the model appears to capture the location-specific scaling of r_d well.

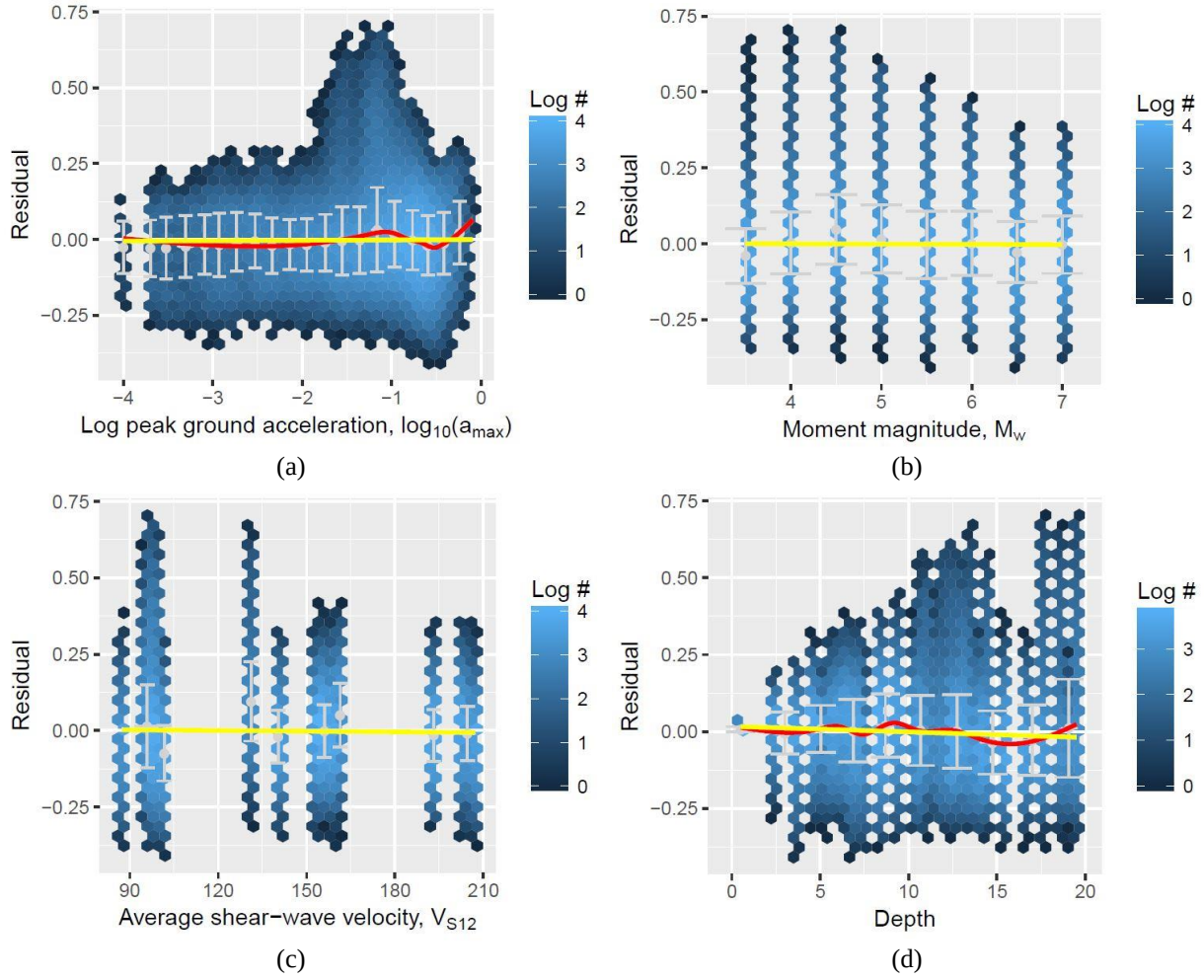

Fig. 16 Residuals of the $r_{d\text{-}Gron}$ model for predictor variables for Zone 602 used in Eqs. 16 and 17: (a) logarithm of a_{max}; (b) moment magnitude; (c) average small strain shear wave of the upper 12 m of a profile, V_{S12}; and (d) depth. Red lines show loess fits to the residuals, yellow lines show linear trends fitted to the residuals, and the light grey error bars show the means and standard deviations of residuals grouped into bins. Residuals are represented by color-coded hexagonal cells, with the color scaling in proportion to the logarithmic count of residuals in each hexagonal cell.

Figure 17 shows a comparison of the Groningen-specific r_d relationship for Zone 602, as an example, and the worldwide r_d relationships proposed by Idriss (1999) and Lasley et al. (2016). As may be observed from this figure, for low magnitude events (e.g., **M** 3.5) the Idriss (1999) and Lasley et al. (2016) relationships significantly over- and under-predict, respectively, r_d for the Groningen liquefaction pilot study area. However, the lack of accuracy of these relationships for

M 3.5 is not altogether surprising because their intended use was for **M** ~5.0 and greater. For moderate sized events (e.g., **M** 5.25), there is still a general trend for the Idriss (1999) and Lasley et al. (2016) relationship to over- and under-predict, respectively, r_d, albeit not significantly so, with the Lasley et al. (2016) relationship providing more accurate predictions for the Groningen region than the Idriss (1999) relationship. For large magnitude events (e.g., **M** 7.0), the three r_d relationships predict similar values, with the general trend for the Idriss (1999) and Lasley et al. (2016) relationship to over- and under-predict, respectively, r_d for the Groningen still persisting at a much less significant level.

4.1.3.2 Groningen-zone-specific n_{eq} and MSF relationships

The functional form for the Groningen-zone-specific n_{eq} relationship is a slight modification of the worldwide model developed by Lasley et al. (2017), with the modifications made to reflect a clear break in scaling at large values of a_{max} and to include the observed dependence on V_{S12}. The functional form for the Groningen-zone-specific n_{eq} relationship is:

$$ln\left[n_{eqM-Gron}(\boldsymbol{M}, a_{max}, V_{s12})\right] = \alpha_1 + \alpha_2 \cdot \ln(a_{max}) + \alpha_4 \cdot \boldsymbol{M} + \alpha_5 \cdot V_{s12}; \text{ for } a_{max} \leq 0.3 \text{ g} \quad (19a)$$

$$ln\left[n_{eqM-Gron}(\boldsymbol{M}, a_{max}, V_{s12})\right] = \alpha_1 + \alpha_2 \cdot \ln(a_{max}) + \alpha_3 \cdot \ln\left(\frac{a_{max}}{0.3}\right) + \alpha_4 \cdot \boldsymbol{M} + \alpha_5 \cdot V_{s12}; \text{ for } a_{max} > 0.3 \text{ g} \quad (19b)$$

where a_{max} is in units of g, V_{S12} is in units of m/s, α_i are the regression coefficients (Table 6), and $\sigma_{ln(neqM)}$ for each zone is listed in the last column of Table 6. This model was developed under the (visually-tested) assumption of log-normality of the equivalent number of cycles.

Figure 18 shows the residuals against the predictor variables used in Eq. 19 for Zone 602, as an example. The same comments made above in regards to the residual plots for the $r_{d\text{-}Gron}$ model (Figure 16) also apply to the residual plots for the $n_{eqM\text{-}Gron}$ model shown in Figure 18. In interpreting the residual plots shown in both Figures 16 and 18 it needs to be realized that any of

the small biases that may be observed are small in comparison with the standard deviations of the binned residuals.

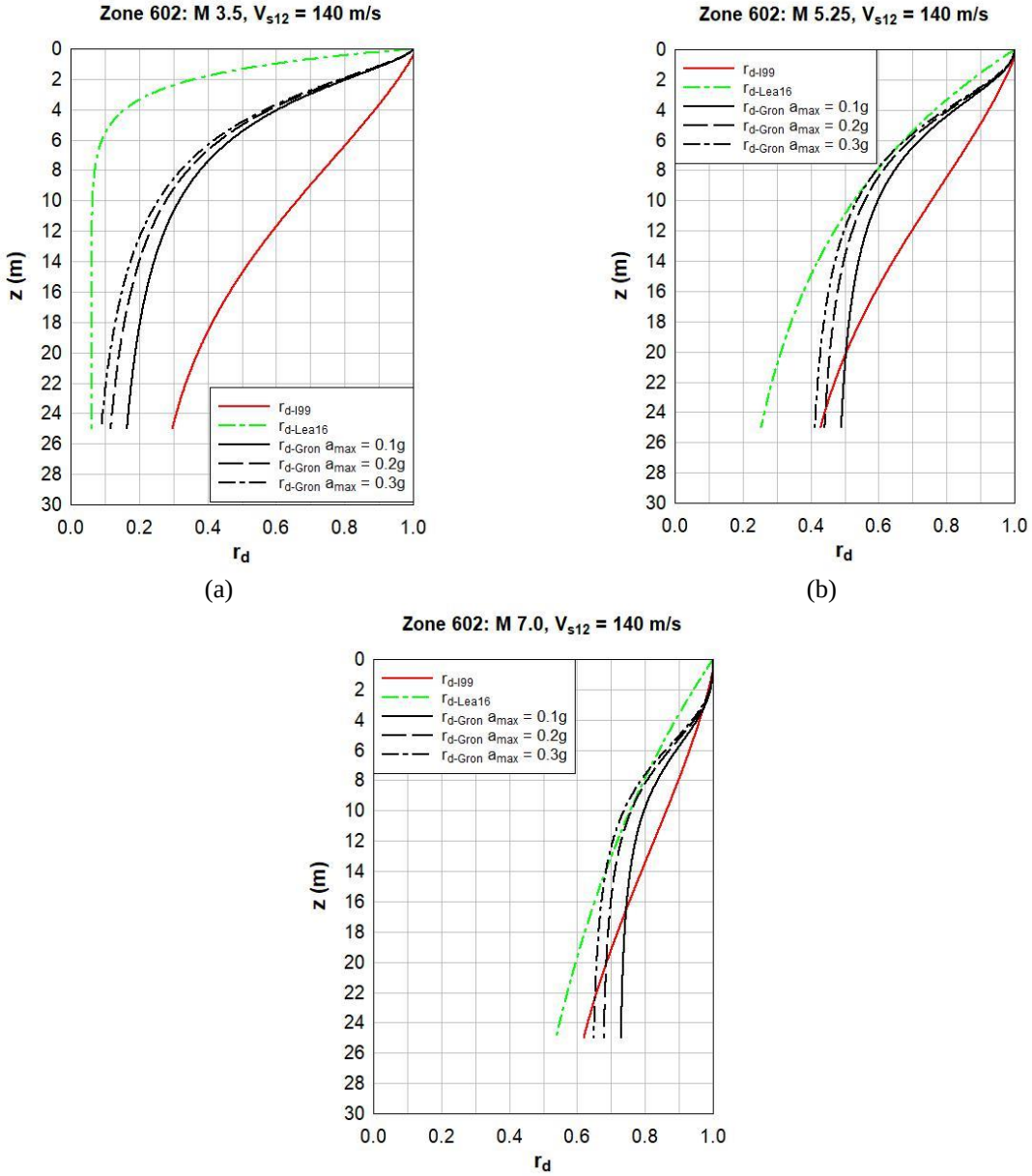

Fig. 17 Comparison of r_d relationships proposed by Idriss (1999) (I99), Lasley et al. (2016) (Lea16), and Groningen-specific relationship ($r_{d\text{-}Gron}$) for zone 602 for: (a) **M** 3.5; (b) **M** 5.25; and (c) **M** 7.0. Because $r_{d\text{-}Lea16}$ and $r_{d\text{-}Gron}$ are a function of V_{S12}, a representative value for the liquefaction pilot study area of 140 m/s was assumed for the plots. Additionally, because $r_{d\text{-}Gron}$ is also a function of a_{max}, a_{max} = 0.1, 0.2, and 0.3 g are shown in the plots.

Although the worldwide model for n_{eq} developed by Lasley et al. (2017) included a depth-dependence of the standard deviation, there is no compelling evidence of this effect in the Groningen datasets (Figure 18d). Accordingly, a homoscedastic standard deviation (i.e., independent of predictor variables) was adopted for the Groningen-zone-specific model.

Table 6 Regression coefficients for the $n_{eqM\text{-}Gron}$ model

Zone	α_1	α_2	α_3	α_4	α_5	$\sigma_{ln(neqM\text{-}Gron)}$
602	-0.2732	-0.3001	-0.8100	0.1996	0.0038	0.4373
603	-0.0097	-0.2721	-0.4491	0.1351	0.0037	0.4708
604	-0.1018	-0.2966	-0.0192	0.1612	0.0038	0.4662
801	0.3877	-0.3213	-0.0984	0.1620	-0.0007	0.4575
821	-0.3764	-0.3080	-0.2753	0.1634	0.0045	0.4571
1001	-0.1958	-0.3246	-0.6973	0.1583	0.0033	0.4314
1032	-0.2487	-0.3131	-0.4085	0.1766	0.0038	0.4446
2001	-0.4359	-0.2936	-0.0154	0.1934	0.0052	0.4498
Zandeweer	0.6419	-0.3025	-0.7874	0.1829	-0.0017	0.4453

Consistent with Figure 6 and Eq. 12, the Groningen-zone-specific MSF relationship is given by the following expression:

$$MSF_{Gron} = \left\{\frac{7.25}{n_{eqM-Gron}(\boldsymbol{M}, a_{max}, V_{s12})}\right\}^{0.34} \leq 2.04 \tag{20a}$$

and

$$\sigma_{\ln(MSF_{Gron})} = 0.34 \cdot \sigma_{\ln(n_{eqM-Gron})} \tag{20b}$$

where the denominator in Eq. 20a is computed using Eq. 19. Also, note that the numerator in Eq. 20a differs from that in Eq. 12 (i.e., 7.25 vs. 14). The reason for this is that Eq. 12 was derived using both horizontal components of motions recorded at a site during tectonic events and Eq. 20a was derived using single components motions generated using a seismic source model, as discussed above. Accordingly, 7.25 represents the reference number of equivalent cycles for one horizontal component of motion for **M** 7.5 event in active shallow tectonic seismic zones and is computed using the relationship given in Lasley et al. (2017), Approach 1, WUS: **M** = 7.5 and a_{max} = 0.35 g. The cap of 2.04 on MSF_{Gron} corresponds to a motion composed of one, low amplitude pulse in one of the horizontal components of motion.

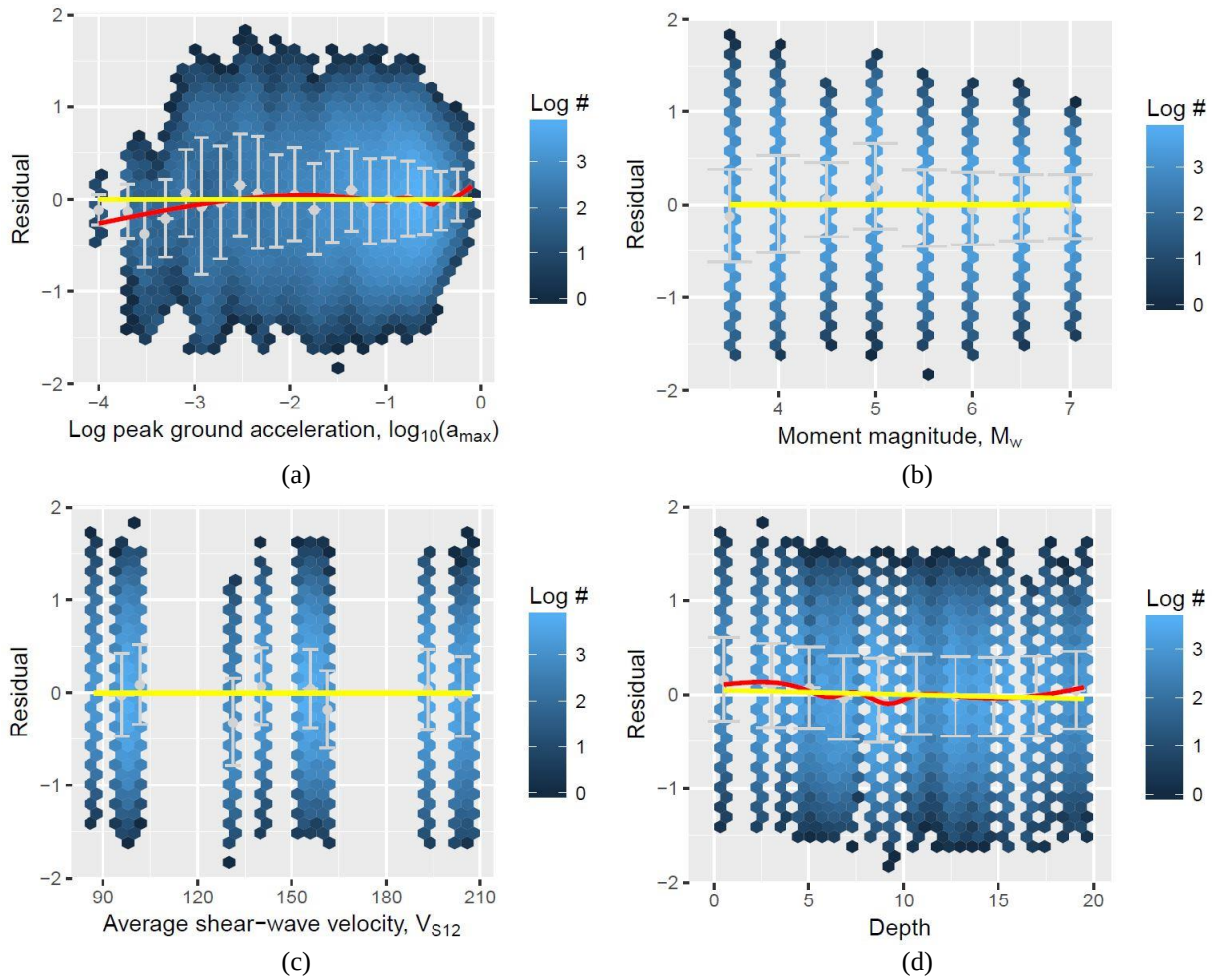

Fig. 18 Residuals of the n_{eqM} model for predictor variables for Zone 602 used in Eq. 19: (a) logarithm of a_{max}; (b) moment magnitude; (c) average small strain shear wave of the upper 12 m of a profile, V_{S12}; and (d) depth. Red lines show loess fits to the residuals, yellow lines show linear trends fitted to the residuals, and the light grey error bars show the means and standard deviations of residuals grouped into bins. Residuals are represented by color-coded hexagonal cells, with the color scaling in proportion to the logarithmic count of residuals in each hexagonal cell.

Figure 19 shows a comparison of the Groningen-specific MSF relationship for Zone 602, as an example, and the worldwide relationships proposed by Idriss and Boulanger (2008) (MSF_{IB08}) and developed herein (i.e., Eqs. 8 and 12: MSF_{WUS}). As shown in Figure 19, the MSF_{IB08} relationship predicts significantly larger values for magnitudes less than **M** ~7.0, with the over-prediction being more significant as magnitude decreases. However, the MSF_{WUS} and MSF_{Gron} do not differ significantly across all magnitudes, with the MSF_{Gron} showing a slightly less dependence on a_{max}.

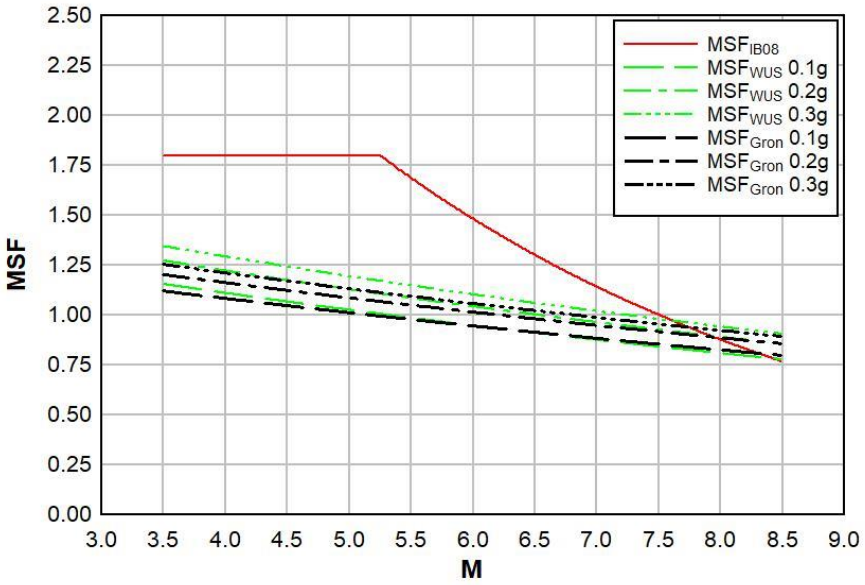

Fig. 19 Comparison of MSF relationships proposed by Idriss and Boulanger (2008) (MSF_{IB08}) and developed herein (i.e., Eqs. 8 and 12) (MSF_{wus}), and Groningen-specific relationship (MSF_{Gron}) for Zone 602. Because MSF_{wus} and MSF_{Gron} are functions of a_{max}, a_{max} = 0.1, 0.2, and 0.3g are shown in the plots.

4.1.3.3 Correlations between Groningen-zone-specific r_d and ln(n_{eq}) relationships

It was found that $r_{d\text{-}Gron}$ is correlated across depths and that ln($n_{eqM\text{-}Gron}$) and $r_{d\text{-}Gron}$ are negatively correlated at a given depth. The correlation coefficient of $r_{d\text{-}Gron}$ at depths z_i and z_j is given by the following expression,.

$$\rho\left[\varepsilon_{r_{d-Gron}}(z_i), \varepsilon_{r_{d-Gron}}(z_j)\right] = 1 + \alpha_{r_{d-Gron}} \cdot |z_i - z_j| \quad (21)$$

where $\varepsilon_{rd\text{-}Gron}$ is the number of standard deviations from the median $r_{d\text{-}Gron}$ value, $z_{i,j}$ are in m, and $\alpha_{rd\text{-}Gron}$ is dimensionless (Table 7). Also, the correlation coefficients for ln($n_{eqM\text{-}Gron}$) and $r_{d\text{-}Gron}$ (i.e., $\rho_{ln(neqM\text{-}Gron),rd\text{-}Gron}$) are listed in Table 7.

In the next section, the Groningen-specific relationships, $r_{d\text{-}Gron}$ and MSF_{Gron}, in conjunction with the "unbiased" $CRR_{M7.5}$ curve (Eq. 15 and Figure 9), are incorporated into the workflow for the liquefaction hazard assessment of the Groningen liquefaction pilot study area shown in Figure 1.

Table 7 Correlation coefficients for $r_{d\text{-}Gron}$ and $\ln(n_{eqM\_Gron})$ models.

Zone	$\alpha_{rd\text{-}Gron}$	$\rho_{\ln(neqM\text{-}Gron),rd\text{-}Gron}$
602	-0.0427	-0.2474
603	-0.0385	-0.3169
604	-0.0340	-0.3917
801	-0.0355	-0.3152
821	-0.0304	-0.3266
1001	-0.0486	-0.2627
1032	-0.0499	-0.2659
2001	-0.0495	-0.3881
Zandeweer	-0.0365	-0.3113

4.2 Liquefaction hazard curves

The liquefaction hazard was calculated for 95 sites across the liquefaction pilot study area using a Monte Carlo approach. The probability distributions for activity rates (Bourne and Oates 2017), event locations and magnitudes, and resulting ground motions were sampled such that the simulated future seismic hazard is consistent with historical seismic and reservoir compaction datasets (Bourne et al. 2015) up to a maximum event, the size of which is defined by a logic-tree (Bommer and van Elk 2017). The ground motions are predicted using the ground motion model described in Bommer et al. (2017b). The development of the ground motion model follows the scheme described in Figure 15 and is briefly summarized below. The ground-motion model described in Section 4.1.2 is used to generate ground motions for multiple scenarios (e.g., multiple magnitude and distance combinations) at the NS_B horizon. These motions are used to develop a parametric model for response spectral accelerations at this horizon. The ground-motion model is also used to generate input ground motions for equivalent linear site response analyses conducted using the RVT option in the STRATA software (Kottke and Rathje 2008). The results of the site response analyses are used to generate amplification factors (median values and standard deviations) for each of the zones in the Groningen region. These amplification factors are period-, intensity-, and scenario-dependent (Rodriguez-Marek et al. 2017; Stafford et al. 2017), and are used to convert the NS_B parametric model to surface ground motions.

For each event scenario, the Groningen-specific relationships, $r_{d\text{-}Gron}$ and MSF_{Gron}, in conjunction with the "unbiased" $CRR_{M7.5}$ curve (Eq. 15 and Figure 9), were used to compute the FS_{liq} as a

function of depth. All other relationships required to compute FS_{liq} were adopted from Boulanger and Idriss (2014), consistent with the development of the "unbiased" $CRR_{M7.5}$ curve. The LPI_{ish} framework was used to relate the computed FS_{liq} in strata at depth in a profile to the predicted severity of surficial liquefaction manifestations, which has been shown to correlate to the liquefaction damage potential for level ground sites (e.g., Iwasaki et al. 1978; Tonkin and Taylor 2013). As stated previously, the computed LPI_{ish} index values for a profile-earthquake scenario are proportional to the cumulative thickness of liquefied layers, the proximity of these layers to the ground surface, and the amount by which FS_{liq} in each layer is less than 1.0. The LPI_{ish} framework was proposed by Maurer et al. (2015c) and is a conceptual and mathematical merger of the Ishihara (1985) H_1-H_2 chart and LPI framework (Iwasaki et al., 1978), resulting in a framework that is relatively easy to implement for profiles having a varying stratigraphies (where the major limitation of the Ishihara H_1-H_2 chart is that it can only be applied to profiles having relatively simple stratigraphies, as discussed below) and better accounts for the thickness of the non-liquefiable crust on the severity of surficial liquefaction manifestations than the LPI framework. Background information on the LPI_{ish} framework is presented next.

4.2.1 Background of the LPI_{ish} framework

The significance of the non-liquefied crust on the severity of surficial liquefaction manifestations was initially identified by Ishihara and Ogawa (1978) using data compiled by Kishida (1969) from the 1891 Mino-Owari, 1944 Tohnankai, and 1948 Fukui earthquakes in Japan. Ishihara and Ogawa (1978) noticed that no sites having a non-liquefied crust of at least 3 m thick had surficial manifestations of liquefaction resulting from these earthquakes, regardless of the thickness of the underlying liquefied layer. Ishihara (1985) generalized the relationship between the thickness of the non-liquefied crust (H_1) and the thickness of the underlying liquefied layer (H_2) using data from the 1983, M_w7.7 Nihonkai-chubu and the 1976, M_w7.8 Tangshan earthquakes (Figure 20). The sites from the Nihonkai-chubu earthquake were estimated to have been subjected to motions having PGAs of ~0.2 g, while those from the Tangshan earthquake were estimated to have been subjected to motions having PGAs of ~0.4-0.5 g. The sizeable difference between these two curves led to the addition of an interpolated 0.3 g intermediary boundary curve between the two initial

curves. As shown in Figure 20, Ishihara (1985) defined H_1 and H_2 for three scenarios based on the depth of the ground water table and the presence and nature of the overlying non-liquefying soil.

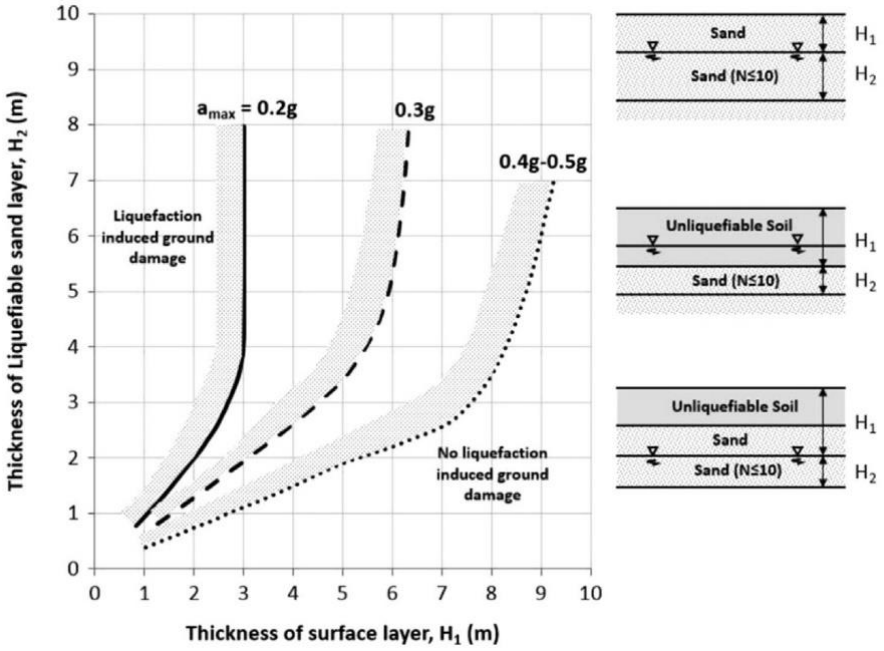

Fig. 20 Relationship between thickness of a liquefied layer (H_2) and thickness of the overlying non-liquefied crust (H_1) for level-ground sites for predicting when surficial liquefaction manifestations will and will not occur (from van Ballegooy et al., 2015; based on Ishihara, 1985).

Youd and Garris (1995) used a larger database of site observations from 13 other earthquakes and compared these with the Ishihara H_1-H_2 curves shown in Figure 20. They found that the curves were generally valid for surficial liquefaction manifestations other than either ground oscillation or lateral spread. Additionally, van Ballegooy et al. (2014, 2015) used data from the 2011, M_w6.2 Christchurch earthquake to examine the Ishihara boundary curves. However, the soil profiles in Christchurch are highly variable with many sites having multiple interbedded non-liquefying layers within liquefied deposits. As a result, a direct application of the Ishihara procedure was difficult. For these deposits, H_1 was taken as the thickness of the non-liquefying crust (consistent with Ishihara, 1985), but for practical purposes, H_2 was the taken as the cumulative thickness of the layers predicted to liquefy (CTL) within the top 10 m of the soil profile. For these cases, the Ishihara curves did not provide a clear separation of the sites with observed surficial liquefaction

manifestations from those without manifestations. Specifically, ~90% of sites with surface manifestation of liquefaction ejecta plotted to the left of the respective Ishihara boundary curves (i.e., true positives), with the remaining 10% having plotted to the right (i.e., false negatives). However, only ~30–40% of sites without surface manifestation of liquefaction ejecta plotted to the right of the respective Ishihara boundary curves (i.e., true negatives), with the remaining 60–70% having plotted to the left (i.e., false positives).

Despite issues with defining H_2 for all but the simplest of profiles, post-earthquake field observations have repeatedly shown that the trends of the Ishihara boundary curves are conceptually correct. For example, Tonkin and Taylor (2013) state: "*Visual observations of the land damage and dwelling foundation damage mapping over Canterbury [New Zealand] show that the majority of areas most severely affected by liquefaction coincide with low lying areas where the ground water table is shallow. Conversely, sites less affected by liquefaction are in areas of higher elevation where the depth to ground water is [high], indicating there is some correlation between liquefaction damage and the non-liquefying crust thickness.*" In an effort to quantitatively assess liquefaction damage potential that avoids the difficulties in implementing the Ishihara H_1-H_2 chart, Maurer et al. (2015c) developed the LPI_{ish} framework that conceptually and mathematically merges the Ishihara (1985) H_1-H_2 chart and LPI framework (Iwasaki et al. 1978).

Because LPI_{ish} framework builds on the LPI framework, an overview of the LPI framework is described first, followed an overview of the LPI_{ish} framework. The LPI index is computed as:

$$LPI = \int_0^{20\ m} F_{LPI}(FS_{liq}) \cdot w(z)dz \tag{22}$$

where $F_{LPI} = 1 - FS_{liq}$ for $FS_{liq} < 1.0$, $F_{LPI} = 0$ for $FS_{liq} \geq 1.0$; and w(z) is a depth weighting function given by $w(z) = 10 – 0.5z$, where z = depth in meters below the ground surface. Inherently, the LPI parameter assumes that each liquefying soil layer contributes to the damage potential at the ground surface. The shallower and/or thicker these layers are, the greater their potential contribution to damage, relative to deeper soil layers. Liquefied layers at depths greater than 20 m are assumed not to contribute to surficial liquefaction manifestations. In reviewing recent liquefaction case history databases (i.e., Cetin et al. 2000, Moss et al. 2003, Kayen et al. 2013, and Boulanger and

Idriss 2014), the maximum documented depth to liquefaction ranges from 15 to 20 m, with median depth for the liquefaction cases being ~5 m. Accordingly, the assumption that liquefied layers at depths greater than 20 m do not contribute to surficial liquefaction manifestations is considered reasonable. LPI can range from 0 for a site with no liquefaction potential to a maximum of 100 for a site where FS is zero over the entire 20 m depth. However, using SPT data from 45 liquefaction sites in Japan, Iwasaki et al. (1978) found that 80% of the sites had LPI > 5, while 50% had LPI > 15. Based on this data, the following severity criteria have been commonly used in practice: LPI < 5: No to Minor Surficial Liquefaction Manifestations; 5 ≤ LPI ≤ 15: Moderate Surficial Liquefaction Manifestations; LPI > 15: Severe Surficial Liquefaction Manifestations.

By making the following assumptions, Maurer et al. (2015c) derived the LPI_{ish} framework from both the Ishihara H_1-H_2 charts and the LPI framework:

1. The penetration resistance of the liquefiable strata corresponding to each of Ishihara's H_1-H_2 boundary curves is assumed to be the same. Maurer et al. (2015c) showed that this was a reasonable assumption and as a result, a_{max} surface is proportional to FS_{liq} in the liquefiable strata.
2. Each of Ishihara's H_1-H_2 boundary curves, which separate cases of liquefaction manifestation from no manifestation, is assumed to represent the same LPI value (i.e., the threshold LPI value for surficial liquefaction manifestation). LPI is thus constant along each boundary curve.
3. Each of Ishihara's H_1-H_2 boundary curves can be reasonably approximated by two straight lines having slopes m and ∞. As such, the thickness of the liquefiable strata, H_2, and the thickness of the non-liquefiable surface layer, H_1, may be related through the slope (m) of the lower portion of the boundary curves, where m is unique for each boundary curve.
4. The FS_{liq} for liquefied strata is assumed to be uniform with depth. As such, the F_{LPI} parameter in Eq. 22 (i.e., $F_{LPI} = 1 - FS_{liq}$) is constant.

LPI_{ish} is defined as:

$$LPI_{ish} = \int_{H_1}^{20\,m} F_{LPI_{ish}}(FS_{liq}) \cdot \frac{25.56}{z} dz \tag{23a}$$

$$F_{LPI_{ish}}(FS_{liq}) = 1 - FS_{liq} \quad if \quad FS_{liq} \leq 1 \;\; and \;\; H_1 \cdot m(FS) \leq 3 \tag{23b}$$

$$F_{LPI_{ish}}(FS_{liq}) = 0 \quad if \quad FS_{liq} > 1 \;\; or \; H_1 \cdot m(FS_{liq}) > 3 \tag{23c}$$

$$m(FS_{liq}) = exp\left\{\frac{5}{25.56 \cdot (1 - FS_{liq})}\right\} - 1 \quad if \quad FS_{liq} \leq 0.95 \tag{23d}$$

$$m(FS_{liq}) = 100 \quad if \quad FS_{liq} > 0.95 \tag{23e}$$

H_1 is taken as the depth from the ground surface to the first instance where $FS_{liq} < 1$ in the shallowest stratum that is susceptible to liquefaction (e.g., Green and Ziotopoulou 2015). The most notable differences between the original LPI and LPI_{ish} frameworks are that the latter explicitly accounts for the influence of the non-liquefiable crust on the severity of surficial liquefaction manifestations (Green et al. 2018, Green and Bommer 2018) and more appropriately weights the contribution of shallower liquefied layers to surficial manifestations (van Ballegooy et al. 2014). The LPI_{ish} framework was chosen for this study because it has been shown to yield more accurate predictions of the severity of surficial liquefaction manifestations than competing indices (Maurer et al. 2015c, d): LPI (Iwasaki et al. 1978) and LSN (van Ballegooy et al. 2014).

The optimal LPI_{ish} thresholds corresponding to different severities surficial liquefaction manifestations are dependent on the liquefaction triggering procedure used to compute FS_{liq} and the characteristics of the profile; the same is the case for LPI and LSN thresholds (Maurer et al., 2015b). However, without liquefaction case history data to develop Groningen-specific thresholds, the thresholds proposed by Iwasaki et al. (1978) were conservatively (Maurer et al. 2015b) used in the pilot study with the LPI_{ish} framework i.e.: $LPI_{ish} < 5$: No to Minor Surficial Liquefaction Manifestations; $5 \leq LPI_{ish} \leq 15$: Moderate Surficial Liquefaction Manifestations; $LPI_{ish} > 15$: Severe Surficial Liquefaction Manifestations.

4.2.2 Liquefaction Hazard across the Pilot Study Area

The output from the liquefaction pilot study is a set of liquefaction hazard curves for the 95 sites across the liquefaction pilot study area, where the hazard curves show the annual frequency of exceedance (AFE) for varying LPI_{ish} values for a site. Example curves computed for sites in Zones 602 and Zandeweer are shown in Figure 21; Zone 602 is representative of most of the zones across the liquefaction pilot study area, except for Zandeweer, which has the highest computed liquefaction hazard of all the zones. Consistent with the requirements of NPR 9998-2017 (NPR 9998 2017), LPI_{ish} values corresponding to an AFE of $\sim 4 \times 10^{-4}$ (or a 2475-year return period) are of most interest. However, the previous version of the NPR 9998 (NPR 9998 2015) specified an 800-year return period for evaluating liquefaction potential for CC1b type structures (i.e., 1, 2, or 3-story single family homes, agriculture buildings, greenhouses, and 1- or 2-story industrial buildings), which was used as the basis for a pervious liquefaction hazard study of Zandeweer (Kumar 2017). Also, both the 2015 and 2017 versions of the NPR 9998 reference the liquefaction evaluation procedure proposed by Idriss and Boulanger (2008) (IB08). As a result, Figure 21 also shows the AFE corresponding to an 800-year return period and the LPI_{ish} hazard curves computed using IB08. The liquefaction hazard curves for all 95 sites across the liquefaction pilot study area, grouped by zones, are included in the appendix.

As may be observed from Figure 21, the Groningen-specific liquefaction evaluation procedure results in a higher computed liquefaction hazard than using the IB08 procedure for a 2475-year return period; this was the case for all sites evaluated. Additionally, $LPI_{ish} < 5$: No to Minor Surficial Liquefaction Manifestations is predicted for an 800-year return period for both sites, when both the Groningen-specific and IB08 evaluation procedures are used; this again was the case for all sites evaluated. For a 2475-year return period, $LPI_{ish} < 5$: No to Minor Surficial Liquefaction Manifestations are predicted for both sites using IB08 liquefaction evaluation procedure (this was the case for all sites) and for the Zone 602 site using the Groningen-specific evaluation procedure. However, $LPI_{ish} \sim 8$ (i.e., Moderate Surficial Liquefaction Manifestations) is predicted for a 2475-year return period for the Zandeweer site using the Groningen-specific evaluation procedure. Moderate Surficial Liquefaction Manifestation is predicted for 21 of the 27

sites evaluated in Zandeweer for a 2475-year return period using the Groningen-specific evaluation procedure.

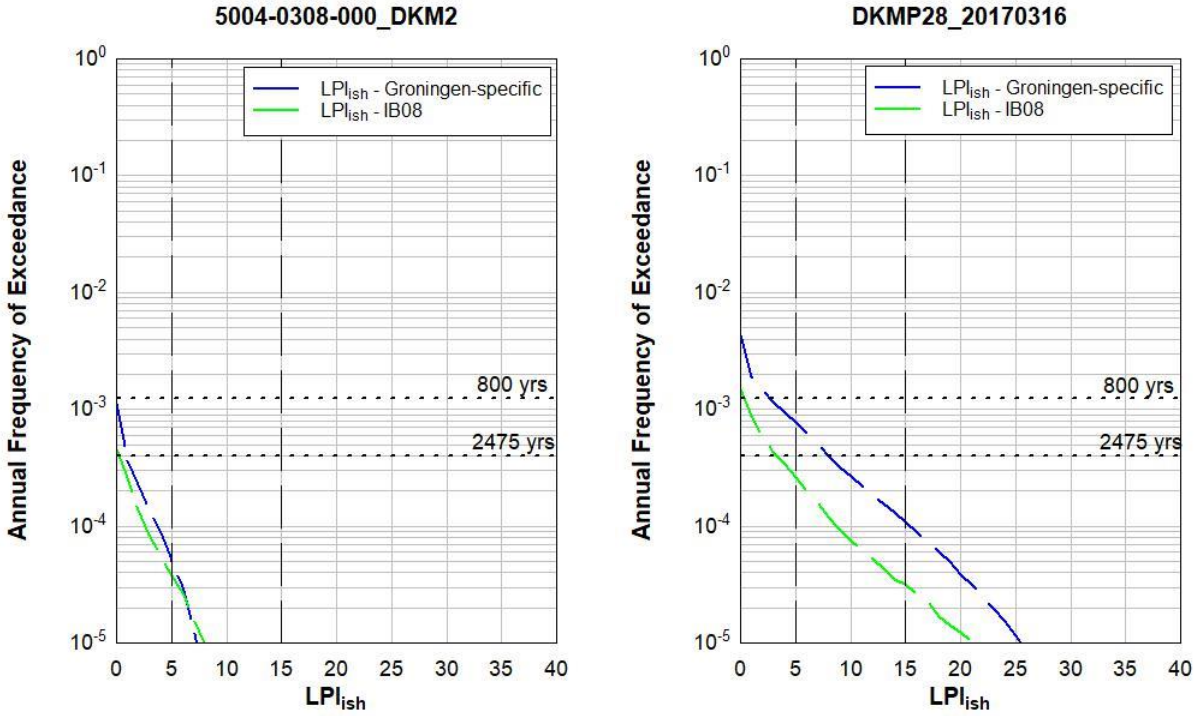

(a) (b)

Fig. 21 Liquefaction hazard curves computed for a sites in: (a) Zone 602; and (b) Zone Zandeweer. Zone 602 is representative of most of the zones of the across the liquefaction pilot study area, except for Zandeweer, which had the highest computed liquefaction hazard.

Figure 22 shows the liquefaction hazard maps for a 2475-year return period computed using the Groningen-specific liquefaction evaluation procedure for the entire liquefaction pilot study area and for Zandeweer. The only sites in the liquefaction pilot study area that are predicted to have Moderate Surficial Liquefaction Manifestations are all located in Zandeweer (Figure 22b); all other sites in across the study area have $LPI_{ish} < 5$.

5 Conclusions

Although an almost negligible contributor to earthquake fatalities, liquefaction triggering is an important threat to the built environment and in particular to infrastructure and lifelines (e.g., Bird

and Bommer 2004) and is thus being included as part of the seismic hazard and risk study being directed by NAM. Due to the unique characteristics of both the seismic hazard and the geologic profiles/soil deposits in Groningen, direct application of existing liquefaction evaluation procedures in the study was deemed inappropriate, and was shown to be so by comparing existing procedures with the Groningen-specific procedure developed as part of this study. The liquefaction hazard was calculated using a Monte Carlo method wherein probability distributions for activity rates (Bourne and Oates 2017), event locations and magnitudes, and resulting ground motions are sampled such that the simulated future seismic hazard is consistent with historical seismic and reservoir compaction datasets (Bourne et al. 2015) up to a maximum event, the size of which is defined by a logic-tree (Bommer and van Elk 2017). Consistent with the requirements of NPR 9998-2017 (NPR 9998 2017), LPI_{ish} values corresponding to an annual frequency of exceedance (AFE) of $\sim 4 \times 10^{-4}$ (or a 2475-year return period) were computed. The LPI_{ish} values for the vast majority of the sites across the study area are less than 5, indicating that "No to Minor Surficial Liquefaction Manifestations." The only sites within the pilot study area that had LPI_{ish} values greater than 5, which is the threshold between "No to Minor Surficial Liquefaction Manifestations" and "Moderate Surficial Liquefaction Manifestations," were in Zandeweer, with only some of the sites in Zandeweer exceeding this threshold value. No sites across the pilot study are were predicted to have "Severe Surficial Liquefaction Manifestations."

Finally, mention is needed regarding two phenomena that were not considered in the liquefaction pilot study presented in this report: the influence of sand age on liquefaction triggering resistance (i.e., aging effects) and the influence of thin layer effects on measured CPT tip resistance (i.e., thin layer effects). Investigations into both of these phenomena were being performed in parallel with the work presented in this report, with the efforts lead by colleagues at Deltares. The Deltares' studies were not far enough along to be incorporated into the analyses presented herein. However, it should be noted that ignoring both aging and thin layer effects will result in an over prediction of liquefaction hazard, but the extent of the over prediction is unknown at this time.

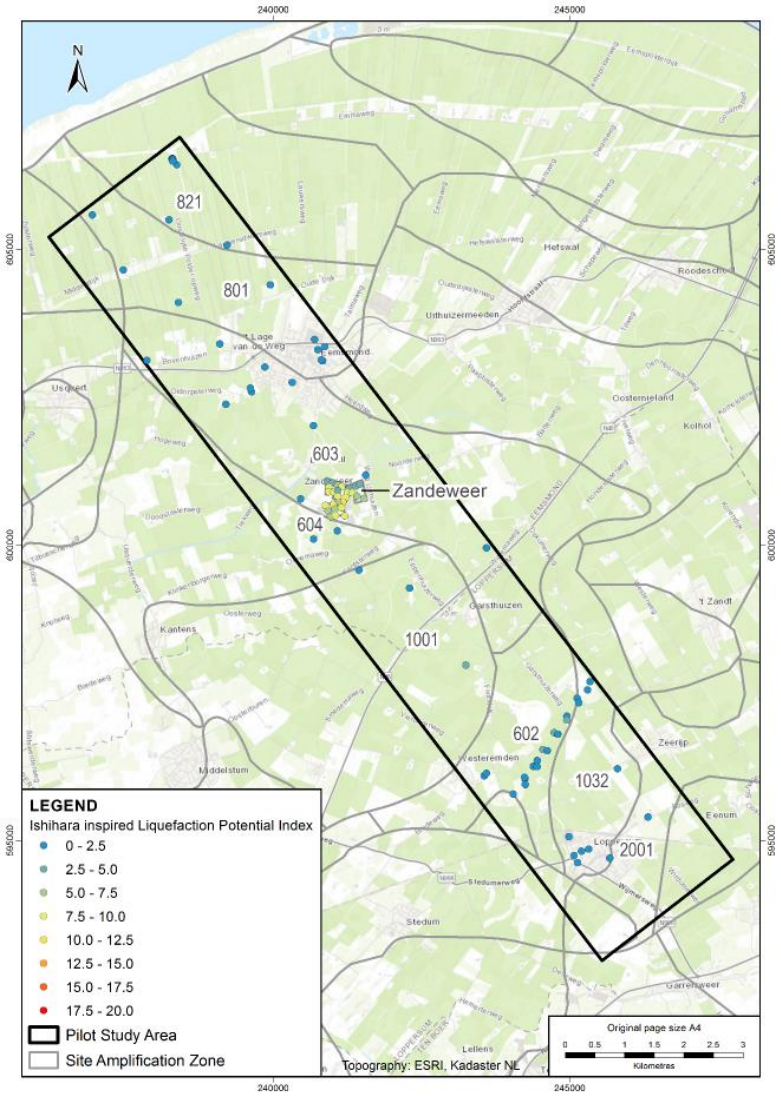

(a)

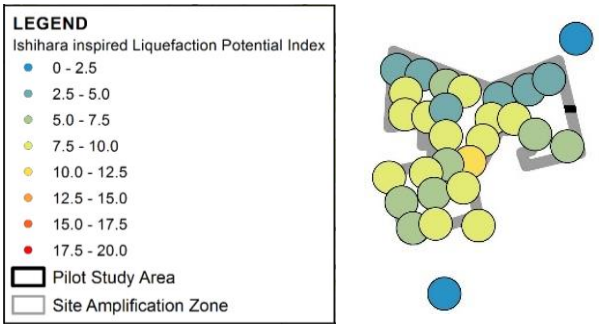

(b)

Fig. 22 Liquefaction hazard map for 2475-year return period computed using the Groningen-specific liquefaction evaluation procedure for: (a) the entire liquefaction pilot study area; and (b) for Zone Zandeweer.

Acknowledgments

This study has significantly benefited from enlightening discussions with colleagues at Shell, Deltares, Arup, Fugro, Beca, and on the NEN Liquefaction Task Force, which is coordinated by Dr. Mandy Korff. However, any opinions, findings, and conclusions or recommendations expressed in this report are those of the authors.

References

Anderson JG, Hough SE (1984) A model for the shape of the Fourier amplitude spectrum of acceleration at high frequencies. Bulletin of the Seismological Society of America 74:1969–1993.

Atkinson GM (2015) Ground-motion prediction equation for small-to-moderate events at short hypocentral distances, with applications to induced-seismicity hazard. Bulletin of the Seismological Society of America 105:981–992.

Bird JF, Bommer JJ (2004) Earthquake losses due to ground failure. Engineering Geology 75(2):147-179.

Boatwright J (1978) Detailed spectral analysis of two small New York state earthquakes. Bulletin of the Seismological Society of America 68:1117–1131.

Bommer JJ, van Elk J (2017) Comment on 'The maximum possible and the maximum expected earthquake magnitude for production-induced earthquakes at the gas field in Groningen, the Netherlands' by Gert Zöller and Matthias Holschneider. Bulletin of the Seismological Society of America 107(3):1564-1567.

Bommer JJ, Dost B, Edwards B, Stafford PJ, van Elk J, Doornhof D, Ntinalexis M (2016) Developing an application-specific ground-motion model for induced seismicity. Bulletin of the Seismological Society of America 106:158–173.

Bommer JJ, Stafford PJ, Edwards B, Dost B, v. Dedem E, Rodriguez-Marek A, Kruiver P, van Elk J, Doornhof D, Ntinalexis M (2017a) Framework for a ground-motion model for induced seismic hazard and risk analysis in the Groningen gas field, the Netherlands. Earthquake Spectra 33(2):481-498.

Bommer JJ, Dost B, Edwards B, Kruiver PP, Meijers P, Ntinalexis M, Rodriguez-Marek A, Ruigrok E, Spetzler J, Stafford PJ (2017b) V4 Ground-Motion Model (GMM) for Response Spectral Accelerations, Peak Ground Velocity, and Significant Durations in the Groningen Field. Version 2.1, 23 June 2017, 541 pp.

Boore DM (2009) Comparing stochastic point-source and finite-source ground-motion simulations: SMSIM and EXSIM. Bulletin of the Seismological Society of America 99:3202-3216.

Boulanger RW, Idriss IM (2014) CPT and SPT based liquefaction triggering procedures. Report No. UCD/CGM-14/01, University of California at Davis, Davis, CA.

Bourne SJ, Oates SJ (2017) Extreme threshold failures within a heterogeneous elastic thin-sheet account for the spatial-temporal development of induced seismicity within the Groningen gas field. Journal of Geophysical Research: Solid Earth 122. DOI: 10.1002/2017JB014356.

Bourne SJ, Oates SJ, Bommer JJ, Dost B, van Elk J, Doornhof D (2015) A Monte Carlo method for probabilistic seismic hazard assessment of induced seismicity due to conventional gas production. Bulletin of the Seismological Society of America 105:1721–1738.

Bradley BA (2011) Correlation of significant duration with amplitude and cumulative intensity measures and its use in ground motion selection. Journal of Earthquake Engineering 15:809–832.

Brune JN (1970) Tectonic stress and the spectra of seismic shear waves from earthquakes. Journal of Geophysical Research 75:4997–5009. 1971. Correction 76:5002.

Carter WL, Green RA, Bradley BA, Cubrinovski M (2014) The influence of near-fault motions on liquefaction triggering during the Canterbury earthquake sequence. Soil Liquefaction during Recent Large-Scale Earthquakes (R.P. Orense, I. Towhata, N. Chouw, eds.), CRC Press, Leiden, the Netherlands, 57-68.

Carter WL, Green RA, Bradley BA, Wotherspoon LM, Cubrinovski M (2016) Spatial variation of magnitude scaling factors during the 2010 Darfield and 2011 Christchurch, New Zealand, earthquakes. Soil Dynamics and Earthquake Engineering 91:175-186.

Cetin KO (2000) Reliability-based assessment of seismic soil liquefaction initiation hazard. Ph.D. Thesis, University of California at Berkeley, Berkeley, CA.

Cetin KO, Seed RB, Der Kiureghian A, Tokimatsu K, Harder LF, Kayen RE, Moss RES (2004) Standard penetration test-based probabilistic and deterministic assessment of seismic soil liquefaction potential. Journal of Geotechnical and Geoenvironmental Engineering 130(12):1314-1340.

Darendeli MB, Stokoe II KH (2001) Development of a new family of normalized modulus reduction and material damping curves. Geotechnical Engineering Report GD01-1, University of Texas at Austin, Austin, TX.

Edwards B, Fäh D, Giardini D (2011) Attenuation of seismic wave energy in Switzerland. Geophysical Journal International 185:967–984.

Fawcett T (2005) An introduction to ROC analysis. Pattern Recognition Letters 27:861-874.

Green RA, Bommer JJ (2018) What is the smallest earthquake magnitude that can trigger liquefaction?. Earthquake Spectra (*in review*)

Green RA, Lee J (2006) Computation of number of equivalent strain cycles: a theoretical framework. Geomechanics II: Testing, Modeling, and Simulation (P.V. Lade and T. Nakai, eds.)

ASCE Geotechnical Special Publication 156, 471-487.

Green RA, Terri GA (2005) Number of equivalent cycles concept for liquefaction evaluations - revisited. Journal of Geotechnical and Geoenvironmental Engineering 131(4):477-488.

Green RA, Ziotopoulou K (2015) Overview of screening criteria for liquefaction triggering susceptibility. Proc. 10th Pacific Conf. on Earthquake Engineering (10PCEE), Sydney, Australia, 6-8 November.

Green RA, Mitchell JK, Polito CP (2000). An energy-based excess pore pressure generation model for cohesionless soils. Proceedings of The John Booker Memorial Symposium – Developments in Theoretical Geomechanics (D.W. Smith and J.P. Carter, eds.), A.A. Balkema, Rotterdam, the Neatherlands, 383-390.

Green RA, Lee J, White TM, Baker JW (2008) The significance of near-fault effects on liquefaction. Proc. 14th World Conf. on Earthquake Engineering, Paper No. S26-019.

Green RA, Lee J, Cameron W, Arenas A (2011) Evaluation of various definitions of characteristic period of earthquake ground motions for site response analyses. Proc. 5th Intern. Conf. on Earthquake Geotechnical Engineering, Santiago, Chile, 10-13 January 2011.

Green RA, Cubrinovski M, Cox B, Wood C, Wotherspoon L, Bradley B, Maurer B (2014) Select liquefaction case histories from the 2010-2011 Canterbury earthquake sequence. Earthquake Spectra 30:131-153.

Green RA, Maurer BW, Cubrinovski M, Bradley BA (2015) Assessment of the relative predictive capabilities of CPT-based liquefaction evaluation procedures: Lessons learned from the 2010-2011 Canterbury Earthquake Sequence. Proc. 6th Intern. Conf. on Earthquake Geotechnical Engineering (6ICEGE), Christchurch, New Zealand, 2-4 November.

Green RA, Maurer BW, van Ballegooy S (2018) The influence of the non-liquefied crust on the

severity of surficial liquefaction manifestations: Case history from the 2016 Valentine's Day earthquake in New Zealand. Proc. Geotechnical Earthquake Engineering and Soil Dynamics V (GEESD V), Liquefaction Triggering, Consequences, and Mitigation (S.J. Brandenberg and M.T. Manzari, eds.), ASCE Geotechnical Special Publication (GSP) 290:21-32

Hancock J, Bommer JJ (2005) The effective number of cycles of earthquake ground motion. Earthquake Engineering and Structural Dynamics 34:637-664.

Idriss IM (1999) An update to the Seed-Idriss simplified procedure for evaluating liquefaction potential. Proc., TRB Workshop on New Approaches to Liquefaction, Publication No. FHWA-RD-99- 165, Federal Highway Administration.

Idriss IM, Boulanger RW (2008) Soil liquefaction during earthquakes. Monograph MNO-12, Earthquake Engineering Research Institute, Oakland, CA, 261 pp.

Ishihara K (1985) Stability of natural deposits during earthquakes. Proc. 11th Intern. Conf. on Soil Mechanics and Foundation Engineering, San Francisco, CA, USA, 1:321-376.

Ishihara K, Ogawa K (1978) Liquefaction susceptibility map of downtown Tokyo. Proc. 2nd Intern. Conf. Microzonation, Nov 26-Dec 1, San Francisco, CA, USA, 897–910.

Iwasaki T, Tatsuoka F, Tokida K, Yasuda S (1978) A practical method for assessing soil liquefaction potential based on case studies at various sites in Japan. Proc. 2nd Intern. Conf. on Microzonation, Nov 26-Dec 1, San Francisco, CA, USA.

Kayen R, Moss RES, Thompson EM, Seed RB, Cetin KO, Der Kiureghian A, Tanaka Y, Tokimatsu K (2013) Shear-wave velocity–based probabilistic and deterministic assessment of seismic soil liquefaction potential. Journal of Geotechnical and Geoenvironmental Engineering 139(3):407–419.

Kishida H (1969) Characteristics of liquefied sands during Mino-Owari, Tohnankai and Fukui

earthquakes. Soils and Foundations IX(1):75-92.

Kokusho T, Kaneko Y (2014) Dissipated & strain energies in undrained cyclic loading tests for liquefaction potential evaluations. Proc. Tenth US National Conf. on Earthquake Engineering, July 21-25, 2014, Anchorage, Alaska, DOI: 10.4231/D3DR2P89D

Korff M, Wiersma A, Meijers P, Kloosterman R, de Lange G (2017) Liquefaction mapping for induced seismicity based on geological and geotechnical features. Proc. 3rd Intern. Conf. on Performance-Based Design in Earthquake Geotechnical Engineering (PBDIII), Vancouver, Canada, 16-19 July, 2017.

Kottke AR, Rathje EM (2008) Technical manual for STRATA. PEER Report 2008/10, Pacific Earthquake Engineering Center, University of California at Berkeley.

Kruiver PP, van Dedem E, Romijn R, de Lange G, Korff M, Stafleu J, Gunnink JL, Rodriguez-Marek A, Bommer JJ, van Elk J, Doornhof D (2017a) An integrated shear-wave velocity model for the Groningen gas field, The Netherlands, Bulletin of Earthquake Engineering. doi: 10.1007/s10518-017-0105-y.

Kruiver PP, Wiersma A, Kloosterman FH, de Lange G, Korff M, Stafleu J, Busscher F, Harting R, Gunnink JL, Green RA, van Elk J, Doornhof D (2017b). Characterisation of the Groningen subsurface for seismic hazard and risk modelling. Netherlands Journal of Geosciences 96(5):s215-s233.

Kumar P (2017) Zandeweer areal approach ground models and liquefaction assessment. Report 229746_048.0_REP2064_Rev0.01, submitted to Centrum Veilig Wonen (CVW), Arup bv, Amsterdam, the Netherlands.

Lasley S, Green RA, Rodriguez-Marek A (2016). A new stress reduction coefficient relationship for liquefaction triggering analyses. Technical Note, Journal of Geotechnical and Geoenvironmental Engineering 142(11):06016013-1.

Lasley S, Green RA, Rodriguez-Marek A (2017) Number of equivalent stress cycles for liquefaction evaluations in active tectonic and stable continental regimes. Journal of Geotechnical and Geoenvironmental Engineering 143(4):04016116-1.

Liao SSC, Whitman RV (1986) Catalogue of liquefaction and non-liquefaction occurrences during earthquakes. Research Report Department of Civil Engineering, Massachusetts Institute of Technology, Cambridge, MA.

Lunne T, Robertson PK, Powell JJM (1997) Cone penetration testing in geotechnical practice. EF Spon/Blackie Academic, Routledge Publishers, London, United Kingdom, 312 pp.

Maurer BW, Green RA, Cubrinovski M, Bradley BA (2015a). Assessment of CPT-based methods for liquefaction evaluation in a Liquefaction Potential Index (LPI) framework. Geotechnique 65(5):328-336.

Maurer BW, Green RA, Cubrinovski M, Bradley BA (2015b) Fines-Content effects on liquefaction hazard evaluation for infrastructure in Christchurch, New Zealand. Soil Dynamics and Earthquake Engineering 76:58-68.

Maurer BW, Green RA, Taylor, O-DS (2015c) Moving towards an improved index for assessing liquefaction hazard: Lessons from historical data. Soils and Foundations 55(4):778-787.

Maurer BW, Green RA, Cubrinovski M, Bradley BA (2015d) Calibrating the Liquefaction Severity Number (LSN) for competing liquefaction evaluation procedures: A case study in Christchurch, New Zealand. Proc. 6th Intern. Conf. on Earthquake Geotechnical Engineering (6ICEGE), Christchurch, New Zealand, 2-4 November.

Motazedian D, Aktinson GM (2005) Stochastic finite-fault modelling based on a dynamic corner frequency. Bulletin of the Seismological Society of America 95:995-1010.

Moss RES, Seed RB, Kayen RE, Stewart JP, Youd TL, Tokimatsu K (2003) Field case histories for CPT-based in situ liquefaction potential evaluation. Geoengineering Research Report UCB/GE-2003/04, University of California, Berkeley, CA.

Moss RES, Seed RB, Kayen RE, Stewart JP, Der Kiureghian A, Cetin KO (2006) CPT-based probabilistic and deterministic assessment of in situ seismic soil liquefaction potential. Journal of Geotechnical and Geoenvironmental Engineering 132(8):1032-1051.

NPR 9998 (2015). Assessment of buildings in case of erection, reconstruction and disapproval – Basic rules for seismic actions: induced earthquakes: December 2015 version. NEN, Delft, Netherlands.

NPR 9998 (2017) Assessment of structural safety of buildings in case of erection, reconstruction and disapproval – Basis rules for seismic actions: induced earthquakes. NEN, Delft, Netherlands.

NRC (2016) State of the art and practice in the assessment of earthquake-induced soil liquefaction and consequences. Committee on Earthquake Induced Soil Liquefaction Assessment (Committee Members: Edward Kavazanjian, Jr., Chair, Jose E. Andrade, Kandian “Arul” Arulmoli, Brian F. Atwater, John T. Christian, Russell A. Green, Steven L. Kramer, Lelio Mejia, James K. Mitchell, Ellen Rathje, James R. Rice, and Yumie Wang) National Research Council, The National Academies Press, Washington, DC.

NZGS (2017) Module 5: Ground improvement of soils prone to liquefaction. New Zealand Geotechnical Society (NZGS) and Ministry of Business, Innovation & Employment (MBIE) Earthquake Geotechnical Engineering Practice in New Zealand, 60pp.

Polito CP, Green RA, Lee J (2008) Pore pressure generation models for sands and silty soils subjected to cyclic loading. Journal of Geotechnical and Geoenvironmental Engineering 134(10):1490-1500.

Polito C, Green RA, Dillon E, Sohn C (2013) The effect of load shape on the relationship between

dissipated energy and residual excess pore pressure generation in cyclic triaxial tests. Canadian Geotechnical Journal 50(9):1118-1128.

Robertson PK, Wride CE (1998) Evaluating cyclic liquefaction potential using cone penetration test. Canadian Geotechnical Journal 35(3):442-459.

Rodriguez-Marek A, Kruiver PP, Meijers P, Bommer JJ, Dost B, van Elk J, Doornhof D (2017) A regional site-response model for the Groningen gas field. Bulletin of the Seismological Society of America 107(5):2067-2077.

Seed HB, Idriss IM (1971) Simplified procedure for evaluating soil liquefaction potential. Journal of the Soil Mechanics and Foundations Division 97(SM9):1249–273.

Seed HB, Idriss IM, Makdisi F, Banerjee N (1975) Representation of irregular stress time histories by equivalent uniform stress series in liquefaction analysis. Report Number EERC 75-29, Earthquake Engineering Research Center, College of Engineering, University of California at Berkeley, Berkeley, CA.

Stafford PJ, Rodriguez-Marek A, Edwards B, Kruiver PP, Bommer JJ (2017) Scenario dependence of linear site effect factors for short-period response spectral ordinates. Bulletin of the Seismological Society of America 107(6):2859-2872.

Stafleu J, Maljers D, Gunnink JL, Menkovic A, Busschers FS (2011) 3D modelling of the shallow subsurface of Zeeland, the Netherlands. Netherlands Journal of Geoscience 90(4):293–310.

Tonkin and Taylor (2013). Liquefaction vulnerability study. Report prepared for the Earthquake Commission. Tonkin & Taylor LTD, New Zealand.

Ulmer KJ, Upadhyaya S, Green RA, Rodriguez-Marek A, Stafford PJ, Bommer JJ, van Elk J (2018) A Critique of b-values used for computing Magnitude Scaling Factors. Proc. Geotechnical Earthquake Engineering and Soil Dynamics V (GEESD V), Slope Stability and Landslides,

Laboratory Testing, and In Situ Testing (S.J. Brandenberg and M.T. Manzari, eds.), ASCE Geotechnical Special Publication (GSP) 293:112-121.

van Ballegooy S, Malan P, Lacrosse V, Jacka ME, Cubrinovski M, Bray JD, O'Rourke TD, Crawford SA, Cowan H (2014) Assessment of liquefaction-induced land damage for residential Christchurch. Earthquake Spectra 30(1):31–55.

van Ballegooy S, Green RA, Lees J, Wentz F, Maurer BW (2015) Assessment of various CPT based liquefaction severity index frameworks relative to the Ishihara (1985) H_1-H_2 boundary curves. Soil Dynamics and Earthquake Engineering 79(Part B):347–364.

van Elk J, Doornhof D, Bommer JJ, Bourne SJ, Oates SJ, Pinho R, Crowley H (2017) Hazard and risk assessments for induced seismicity in Groningen. Netherlands Journal of Geoscience 96(5): s259-s269.

Wells DL, Coppersmith KJ (1994) New empirical relationships among magnitude, rupture length, rupture width, rupture area, and surface displacement. Bulletin of the seismological Society of America 84(4):974-1002.

Whitman RV (1971) Resistance of soil to liquefaction and settlement. Soils and Foundations 11(4):59-68.

Yoshimi Y, Tokimatsu K, Kaneko O, Makihara Y (1984). Undrained cyclic shear strength of dense Niigata sand. Soils and Foundations, 24(4):131-145.

Youd TL, Garris CT (1995) Liquefaction-induced ground surface disruption. Journal of Geotechnical Engineering 121(11): 805-809.

Youd TL, Idriss IM, Andrus RD, Arango I, Castro G, Christian JT, Dobry R, Finn WDL, Harder LF, Hynes ME, Ishihara K, Koester JP, Liao SSC, Marcuson WF, Martin GR, Mitchell JK, Moriwaki Y, Power MS, Robertson PK, Seed RB, Stokoe KH (2001) Liquefaction resistance of

soils: Summary report from the 1996 NCEER and 1998 NCEER/NSF workshops on evaluation of liquefaction resistance of soils. Journal of Geotechnical and Geoenvironmental Engineering 127(4):297-313.

APPENDIX:

Liquefaction hazard curves for 95 sites in the Groningen liquefaction pilot study area

Liquefaction Pilot Study Area

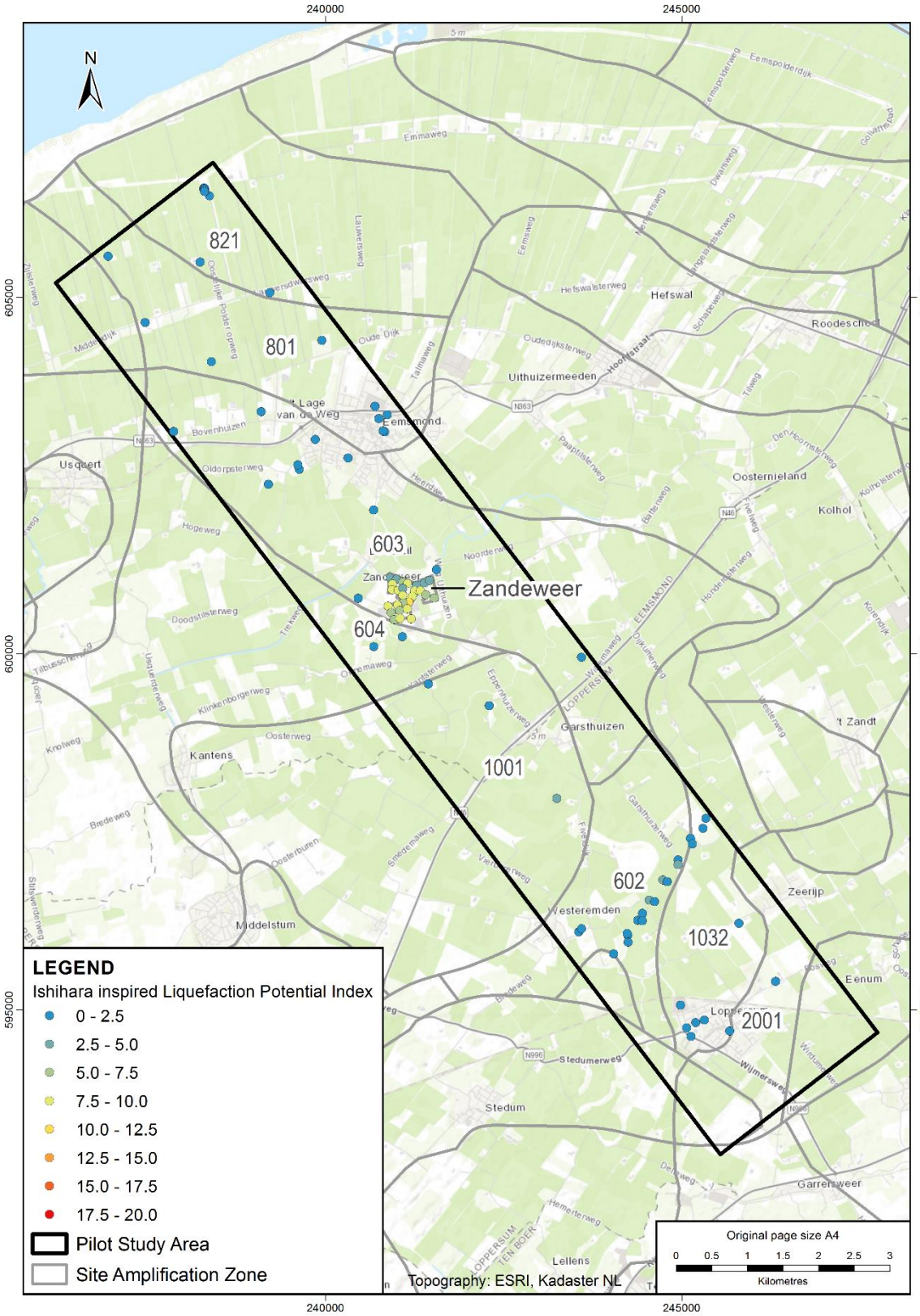

Zone 821

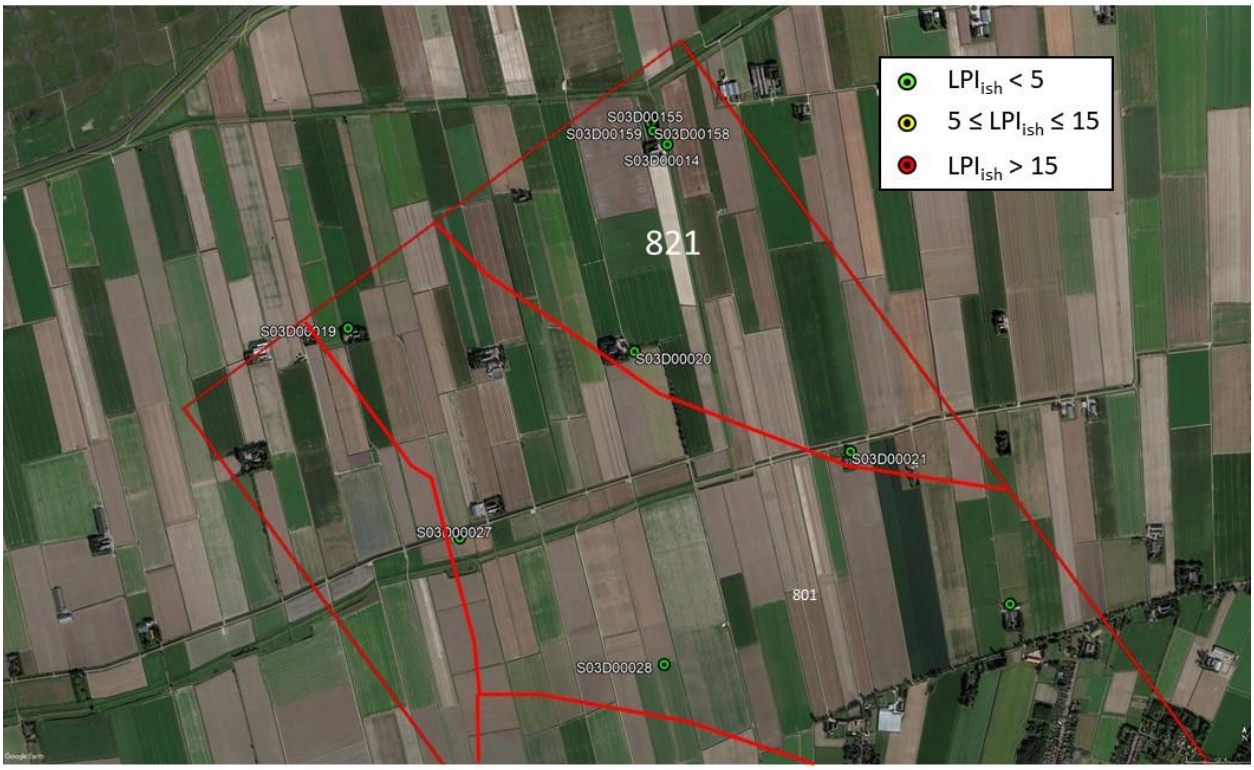
LPI$_{ish}$ < 5
5 ≤ LPI$_{ish}$ ≤ 15
LPI$_{ish}$ > 15
S03D00155
S03D00159
S03D00158
S03D00014
821
S03D00019
S03D00020
S03D00021
S03D00027
801
S03D00028

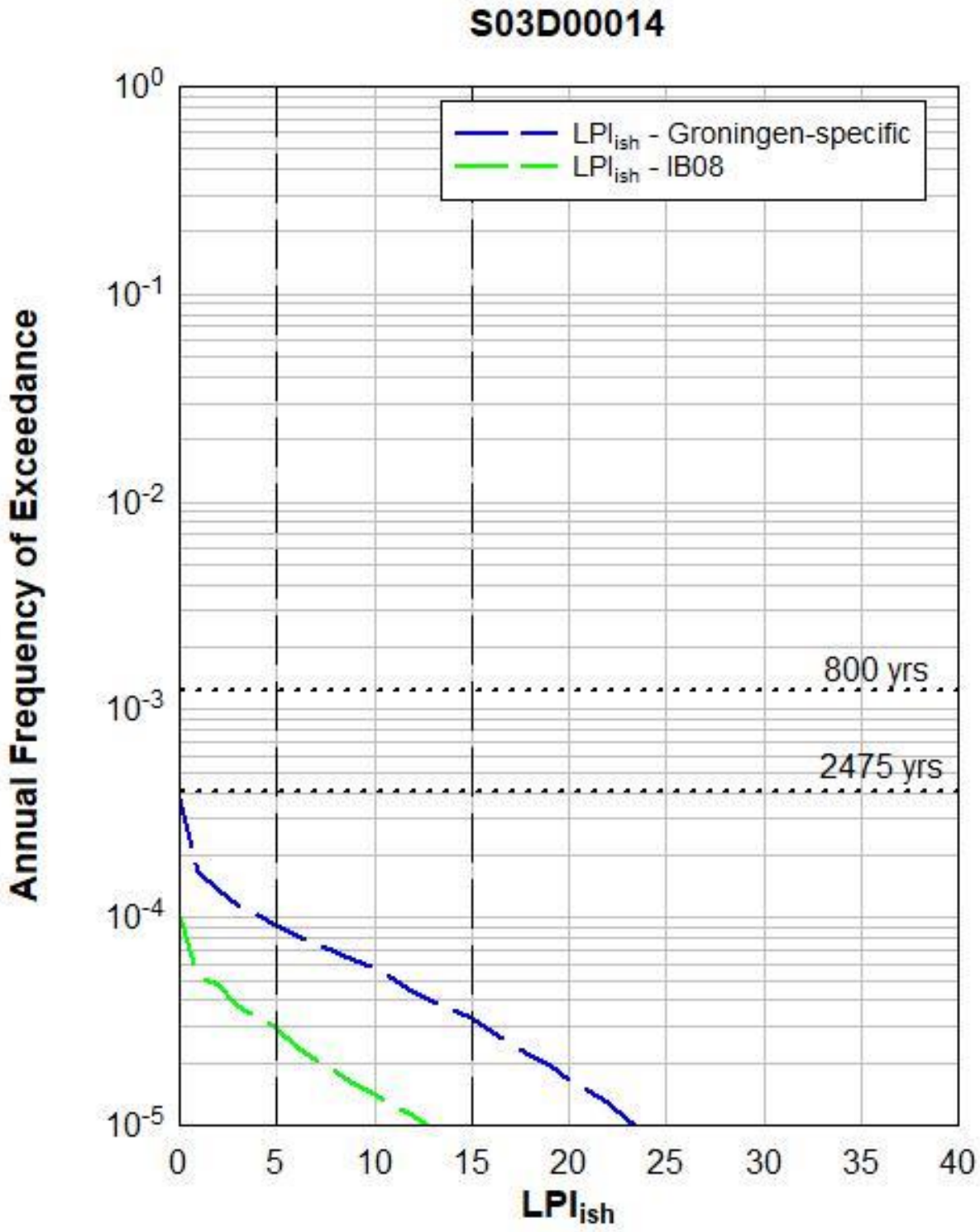
S03D00014
LPIish - Groningen-specific
LPIish - IB08
800 yrs
2475 yrs
Annual Frequency of Exceedance
LPIish
10^0
10^-1
10^-2
10^-3
10^-4
10^-5
0
5
10
15
20
25
30
35
40

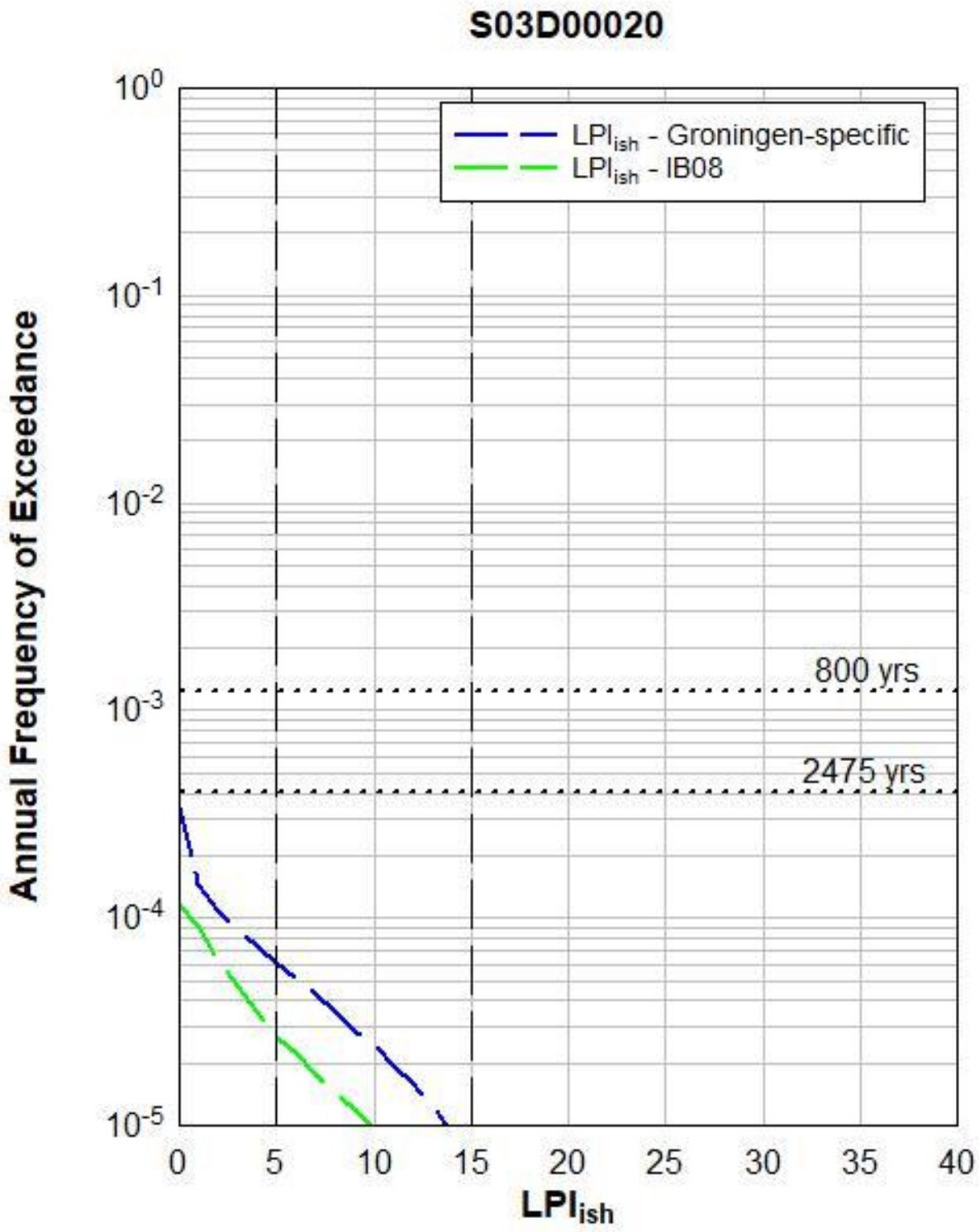
S03D00020
LPIish - Groningen-specific
LPIish - IB08
800 yrs
2475 yrs
Annual Frequency of Exceedance
LPIish
10^0
10^-1
10^-2
10^-3
10^-4
10^-5
0
5
10
15
20
25
30
35
40

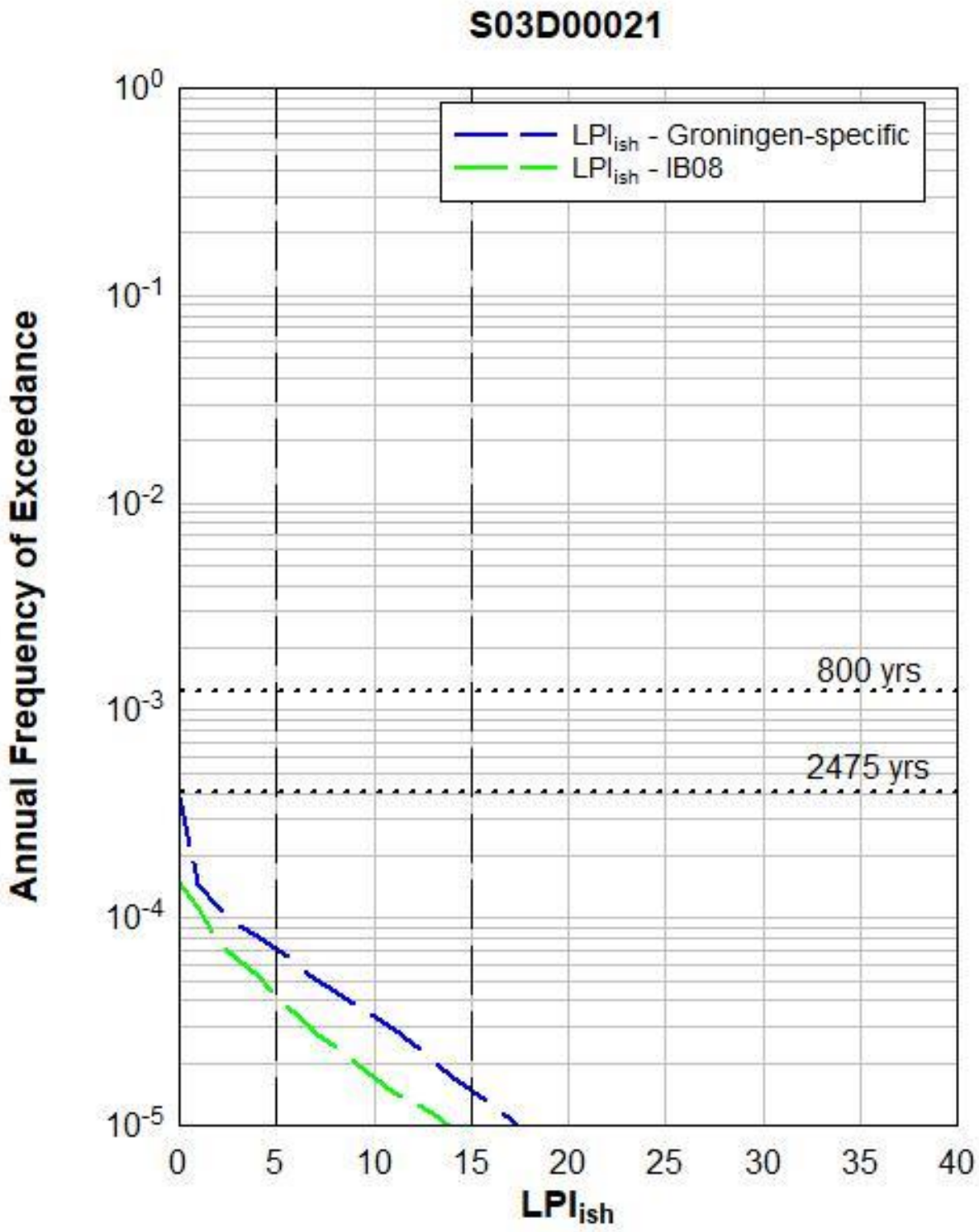
S03D00021
LPIish - Groningen-specific
LPIish - IB08
800 yrs
2475 yrs
Annual Frequency of Exceedance
LPIish
10^0
10^-1
10^-2
10^-3
10^-4
10^-5
0
5
10
15
20
25
30
35
40

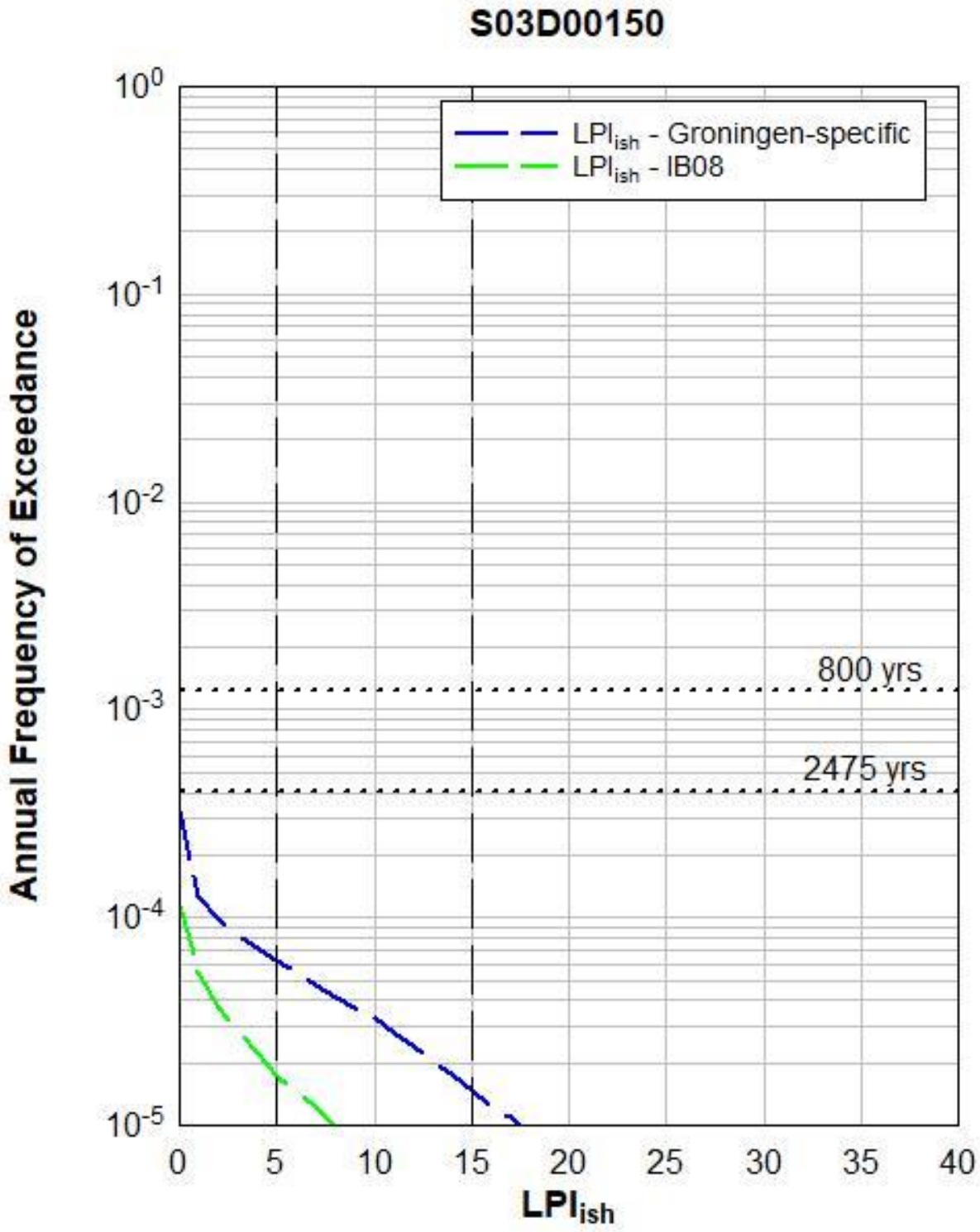
S03D00150
LPIish - Groningen-specific
LPIish - IB08
800 yrs
2475 yrs
Annual Frequency of Exceedance
LPIish
10^0
10^-1
10^-2
10^-3
10^-4
10^-5
0
5
10
15
20
25
30
35
40

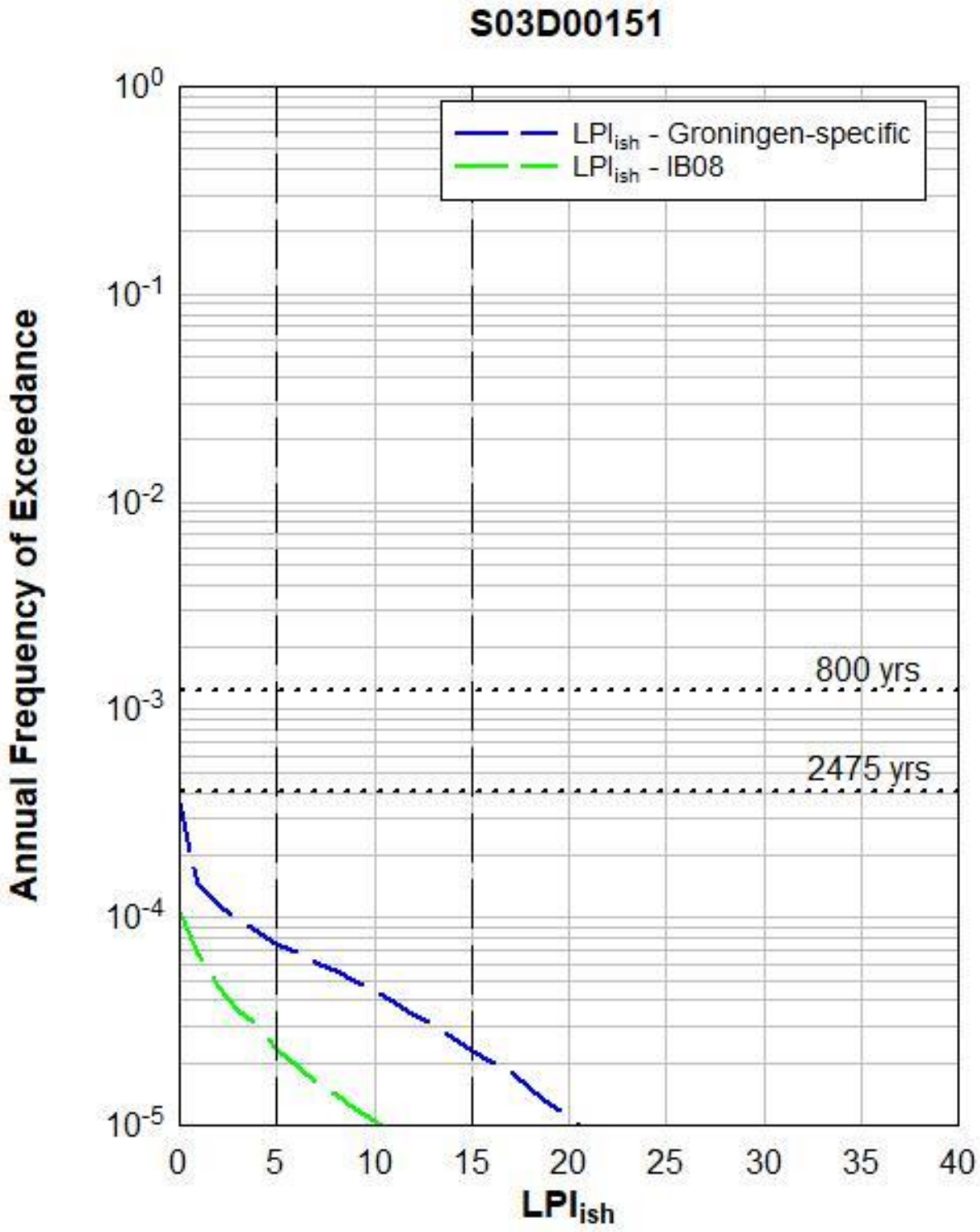
S03D00151
LPIish - Groningen-specific
LPIish - IB08
800 yrs
2475 yrs
Annual Frequency of Exceedance
LPIish
10^0
10^-1
10^-2
10^-3
10^-4
10^-5
0
5
10
15
20
25
30
35
40

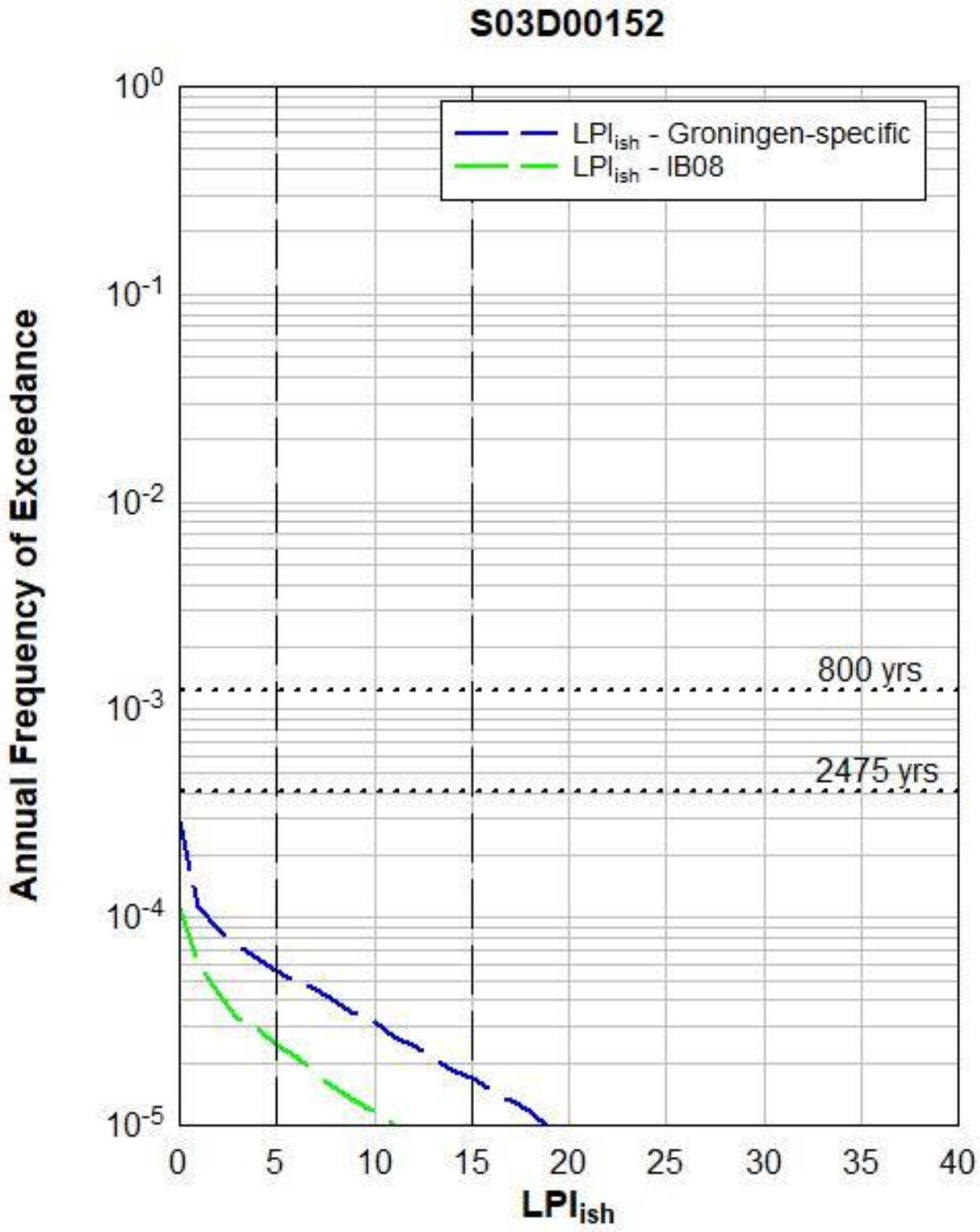
S03D00152
LPIish - Groningen-specific
LPIish - IB08
800 yrs
2475 yrs
Annual Frequency of Exceedance
LPIish
10^0
10^-1
10^-2
10^-3
10^-4
10^-5
0
5
10
15
20
25
30
35
40

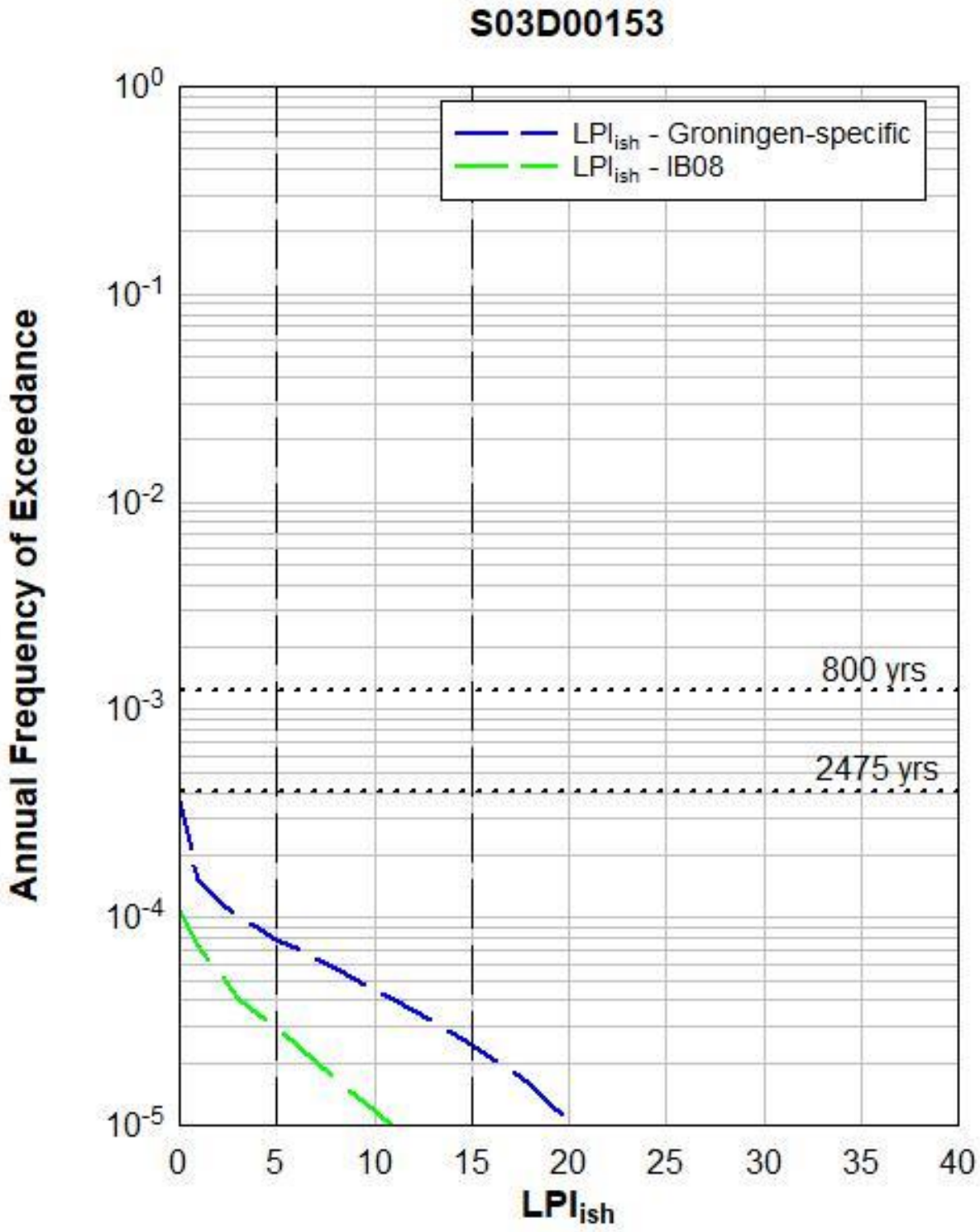
S03D00153
LPIish - Groningen-specific
LPIish - IB08
800 yrs
2475 yrs
Annual Frequency of Exceedance
LPIish
10^0
10^-1
10^-2
10^-3
10^-4
10^-5
0
5
10
15
20
25
30
35
40

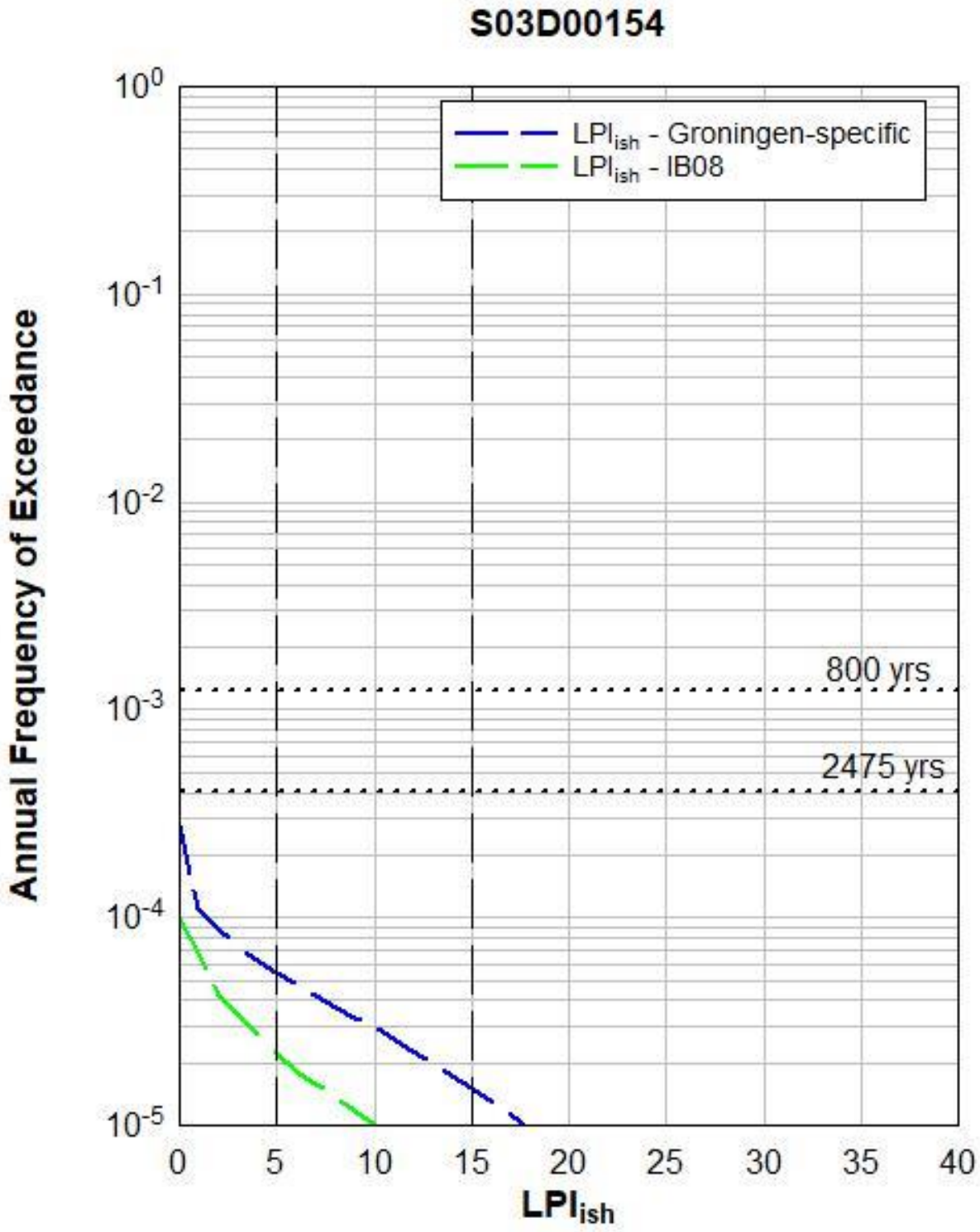
S03D00154
LPIish - Groningen-specific
LPIish - IB08
800 yrs
2475 yrs
Annual Frequency of Exceedance
LPIish
10^0
10^-1
10^-2
10^-3
10^-4
10^-5
0
5
10
15
20
25
30
35
40

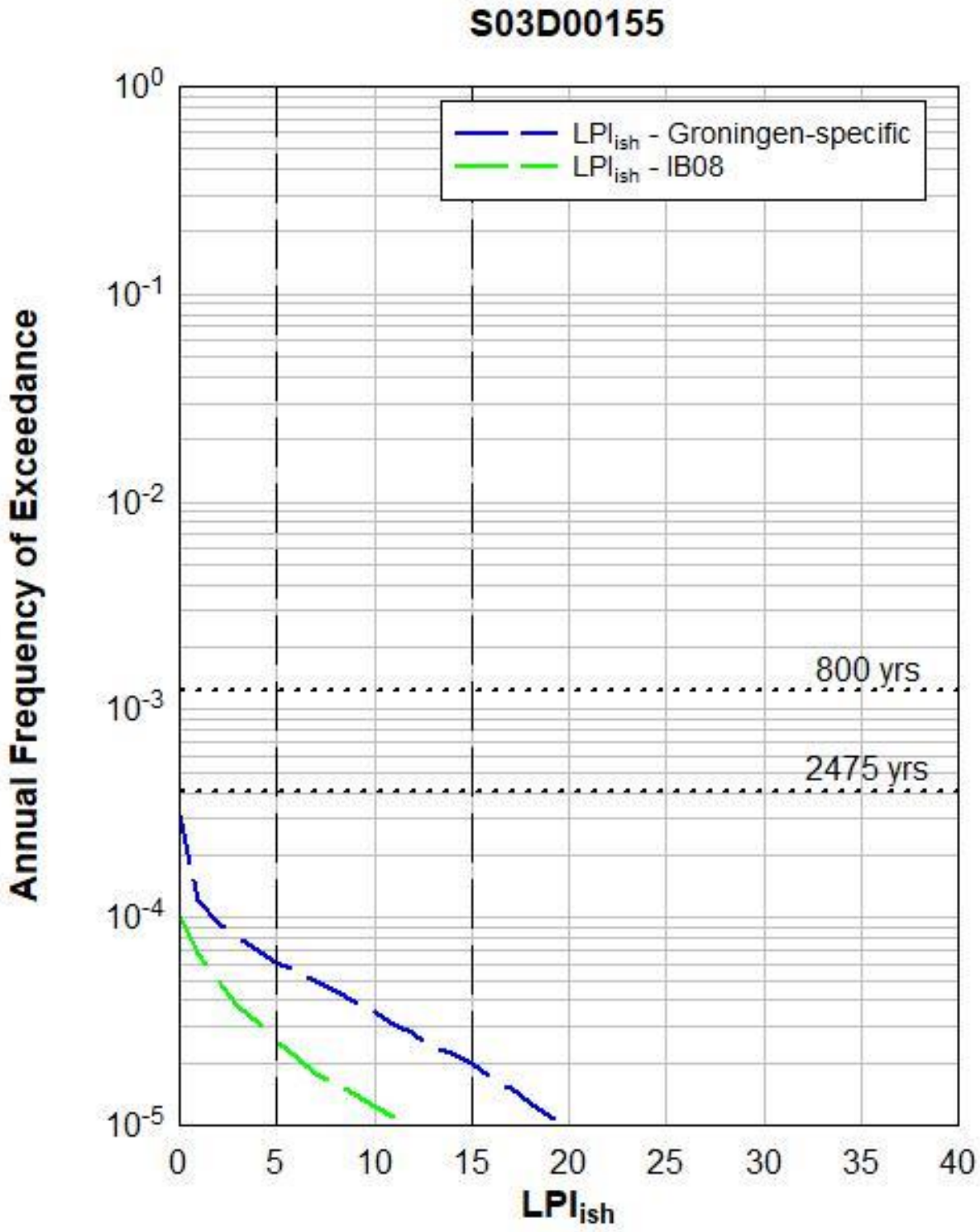
S03D00155
LPIish - Groningen-specific
LPIish - IB08
800 yrs
2475 yrs
Annual Frequency of Exceedance
LPIish
10^0
10^-1
10^-2
10^-3
10^-4
10^-5
0
5
10
15
20
25
30
35
40

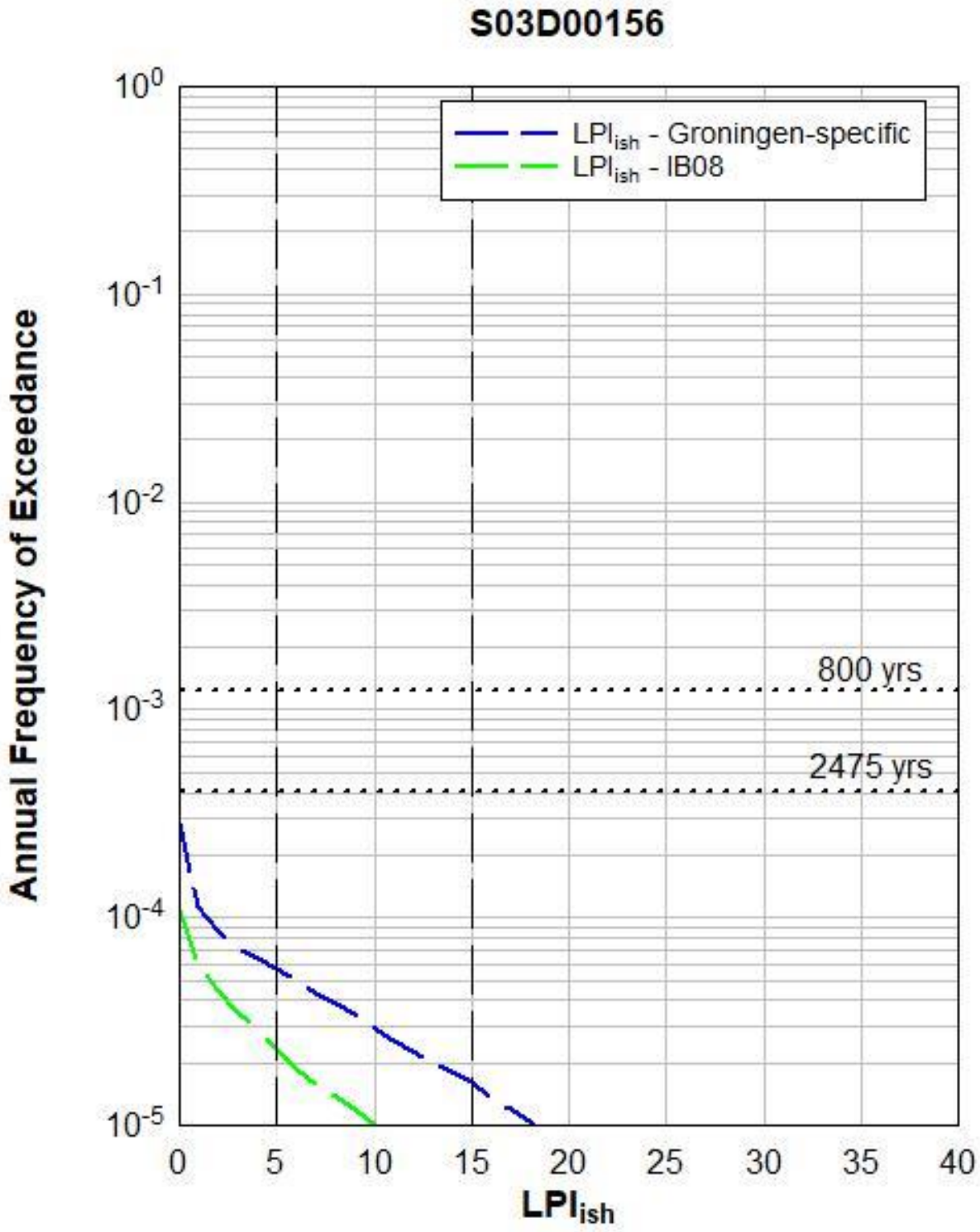
S03D00156
LPIish - Groningen-specific
LPIish - IB08
800 yrs
2475 yrs
Annual Frequency of Exceedance
LPIish
10^0
10^-1
10^-2
10^-3
10^-4
10^-5
0
5
10
15
20
25
30
35
40

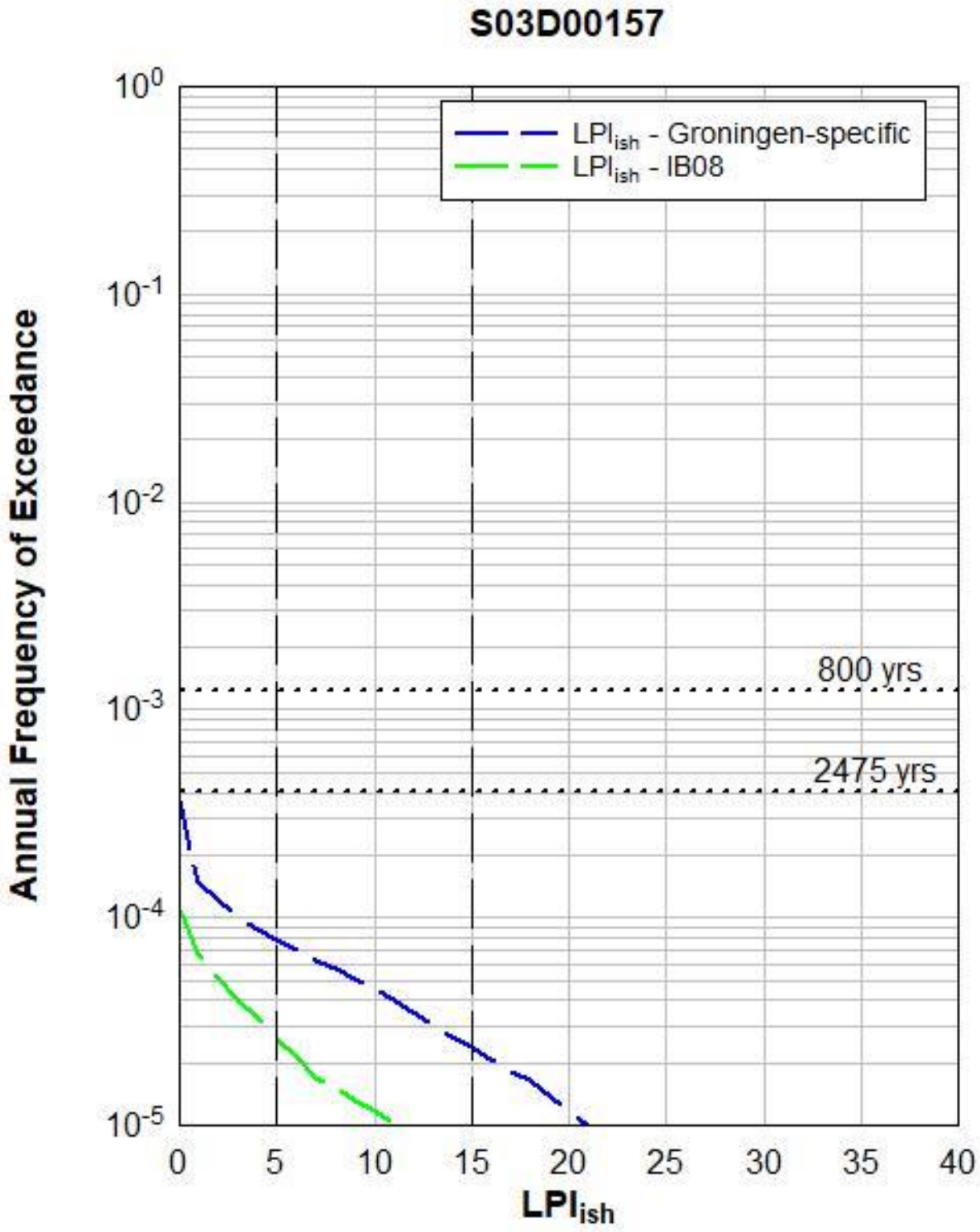
S03D00157
LPIish - Groningen-specific
LPIish - IB08
800 yrs
2475 yrs
Annual Frequency of Exceedance
LPIish
10^0
10^-1
10^-2
10^-3
10^-4
10^-5
0
5
10
15
20
25
30
35
40

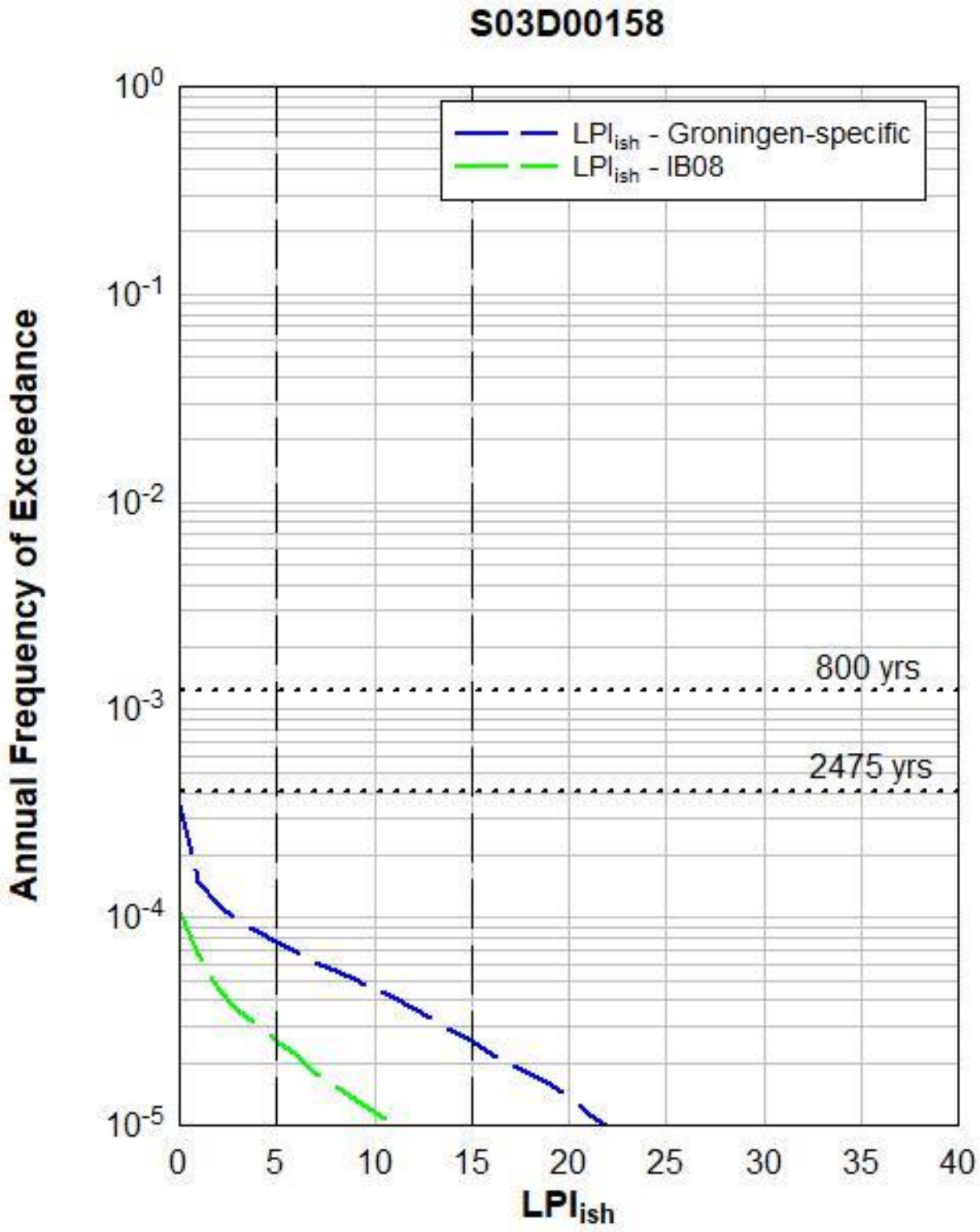
S03D00158
LPIish - Groningen-specific
LPIish - IB08
800 yrs
2475 yrs
Annual Frequency of Exceedance
LPIish
10^0
10^-1
10^-2
10^-3
10^-4
10^-5
0
5
10
15
20
25
30
35
40

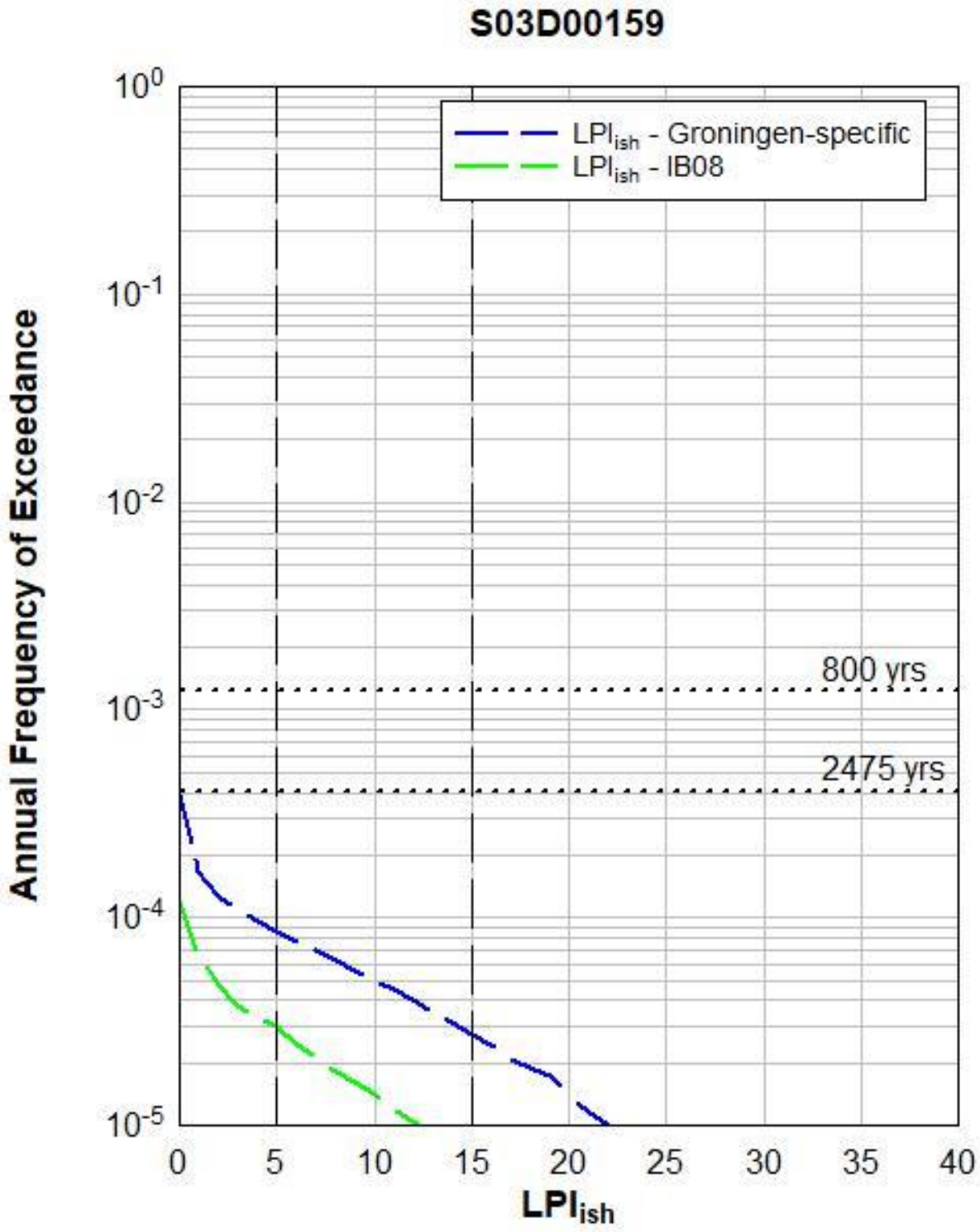
S03D00159
LPIish - Groningen-specific
LPIish - IB08
800 yrs
2475 yrs
Annual Frequency of Exceedance
LPIish
10^0
10^-1
10^-2
10^-3
10^-4
10^-5
0
5
10
15
20
25
30
35
40

Zone 801

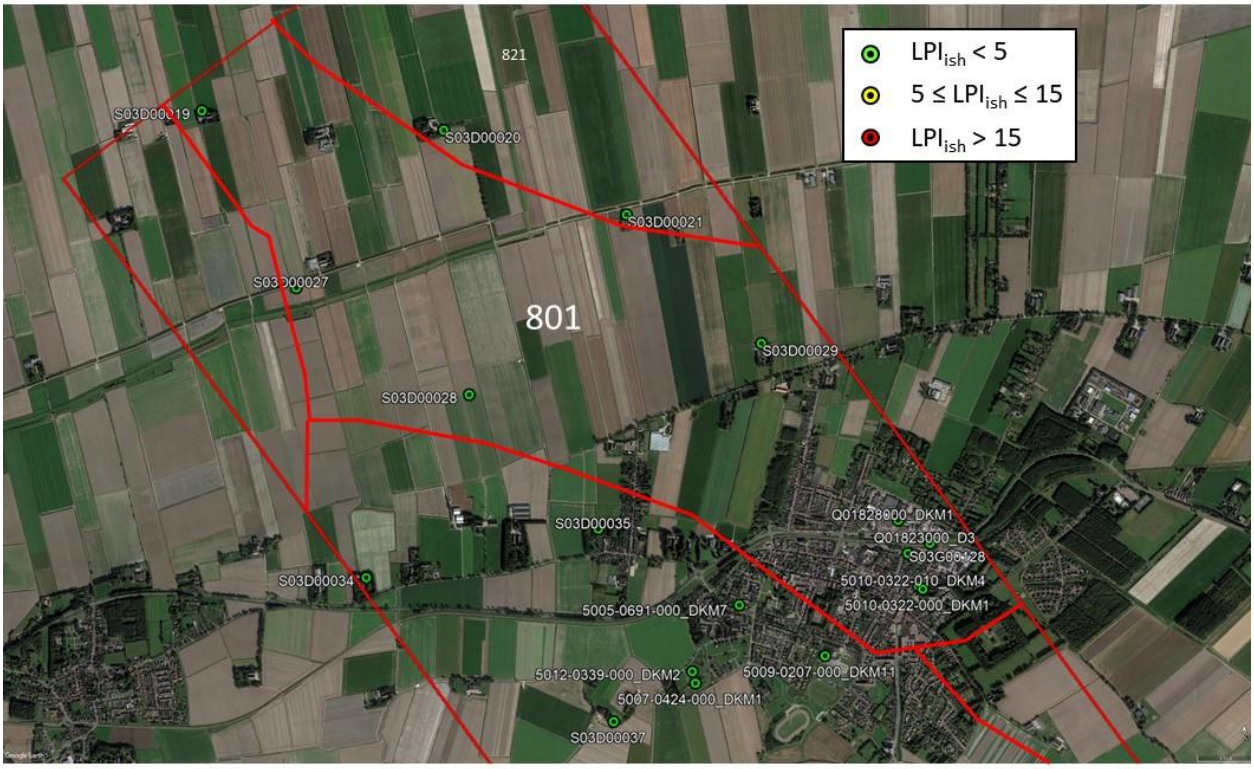
LPI$_{ish}$ < 5
5 ≤ LPI$_{ish}$ ≤ 15
LPI$_{ish}$ > 15
821
801
S03D00019
S03D00020
S03D00021
S03D00027
S03D00029
S03D00028
S03D00035
S03D00034
S03D00037
Q01828000_DKM1
Q01823000_D3
S03G00528
5010-0322-010_DKM4
5010-0322-000_DKM1
5005-0691-000_DKM7
5012-0339-000_DKM2
5009-0207-000_DKM11
5007-0424-000_DKM1

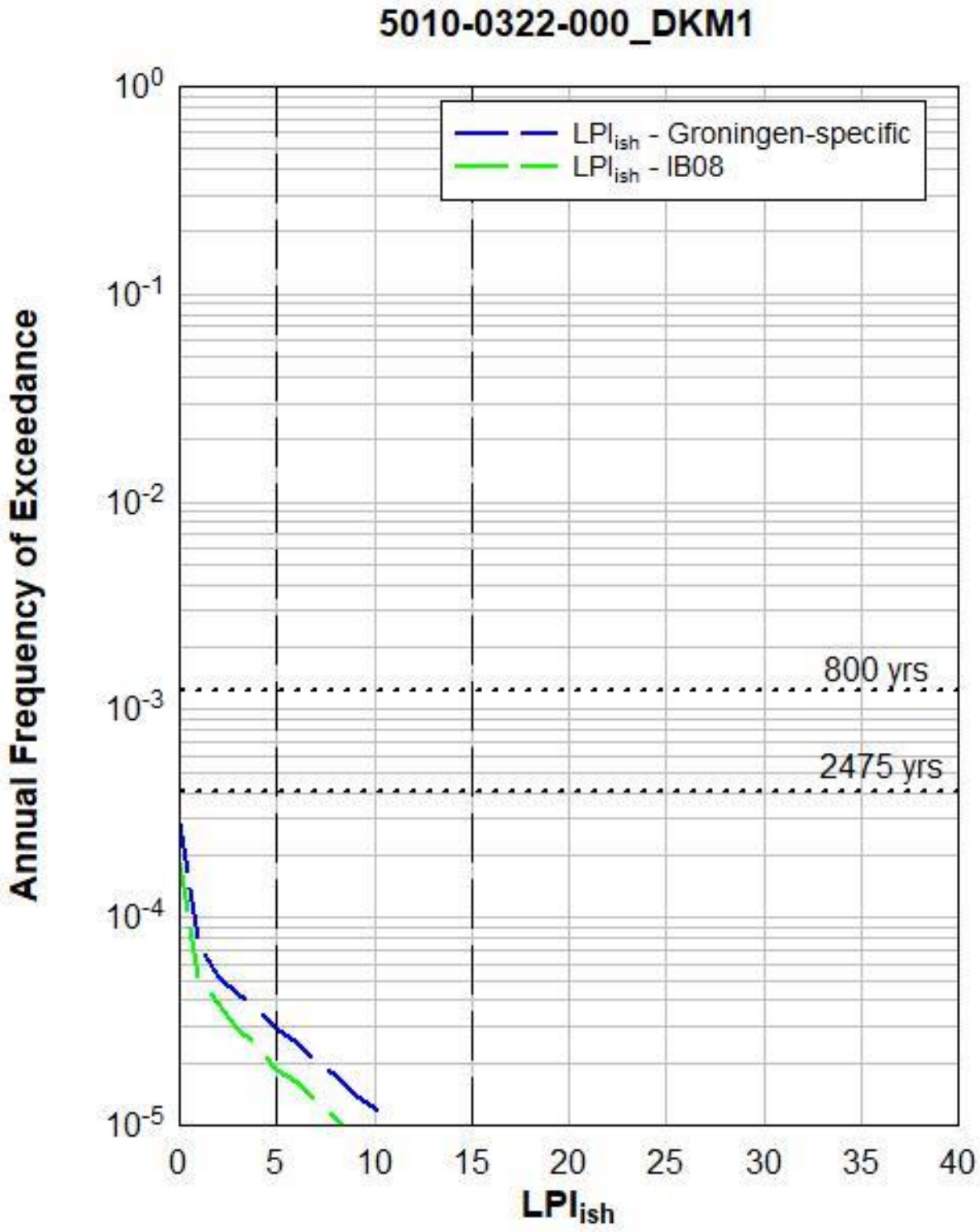
5010-0322-000_DKM1
LPIish - Groningen-specific
LPIish - IB08
800 yrs
2475 yrs
Annual Frequency of Exceedance
LPIish
10^0
10^-1
10^-2
10^-3
10^-4
10^-5
0
5
10
15
20
25
30
35
40

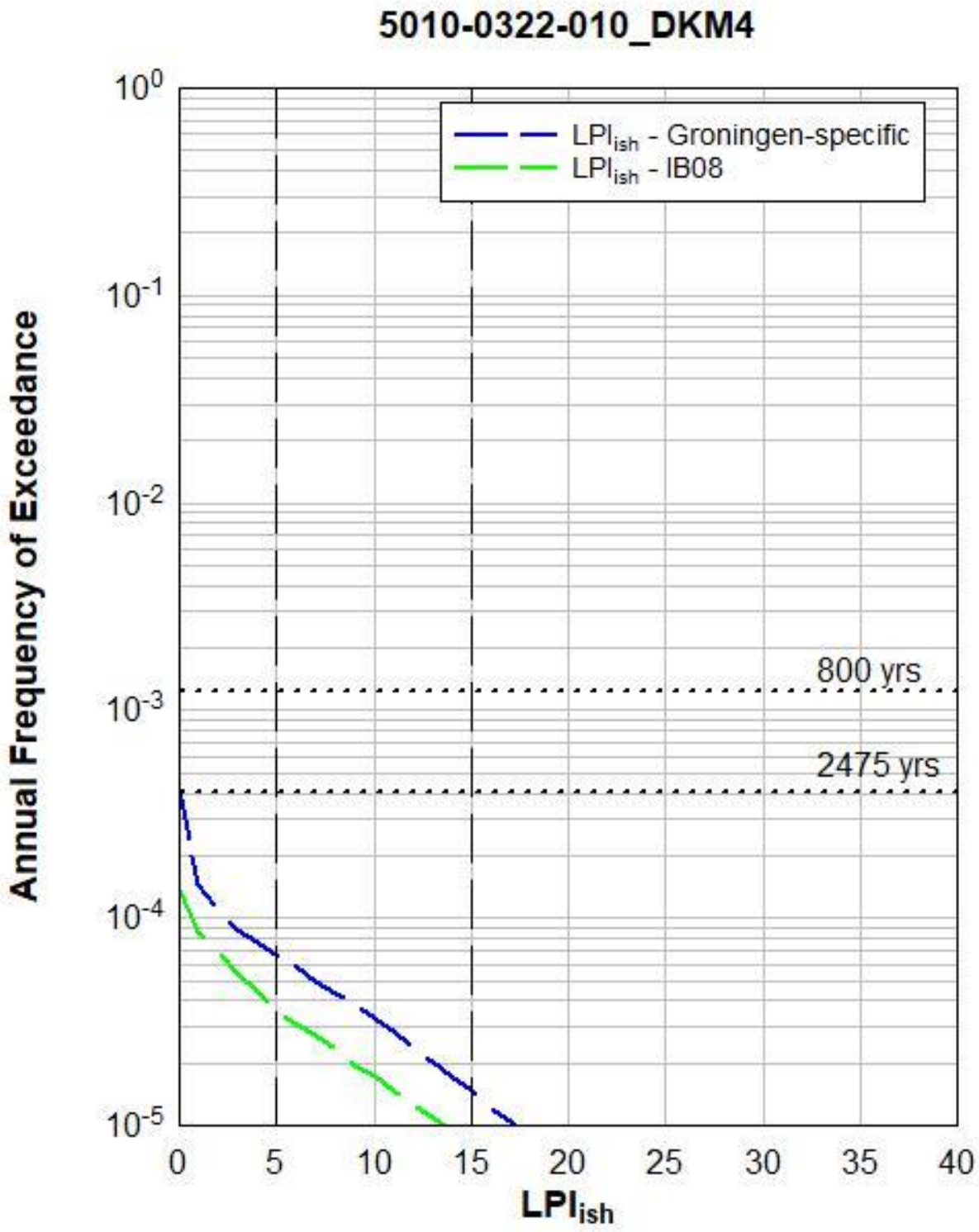
5010-0322-010_DKM4
LPIish - Groningen-specific
LPIish - IB08
800 yrs
2475 yrs
Annual Frequency of Exceedance
LPIish
10^0
10^-1
10^-2
10^-3
10^-4
10^-5
0
5
10
15
20
25
30
35
40

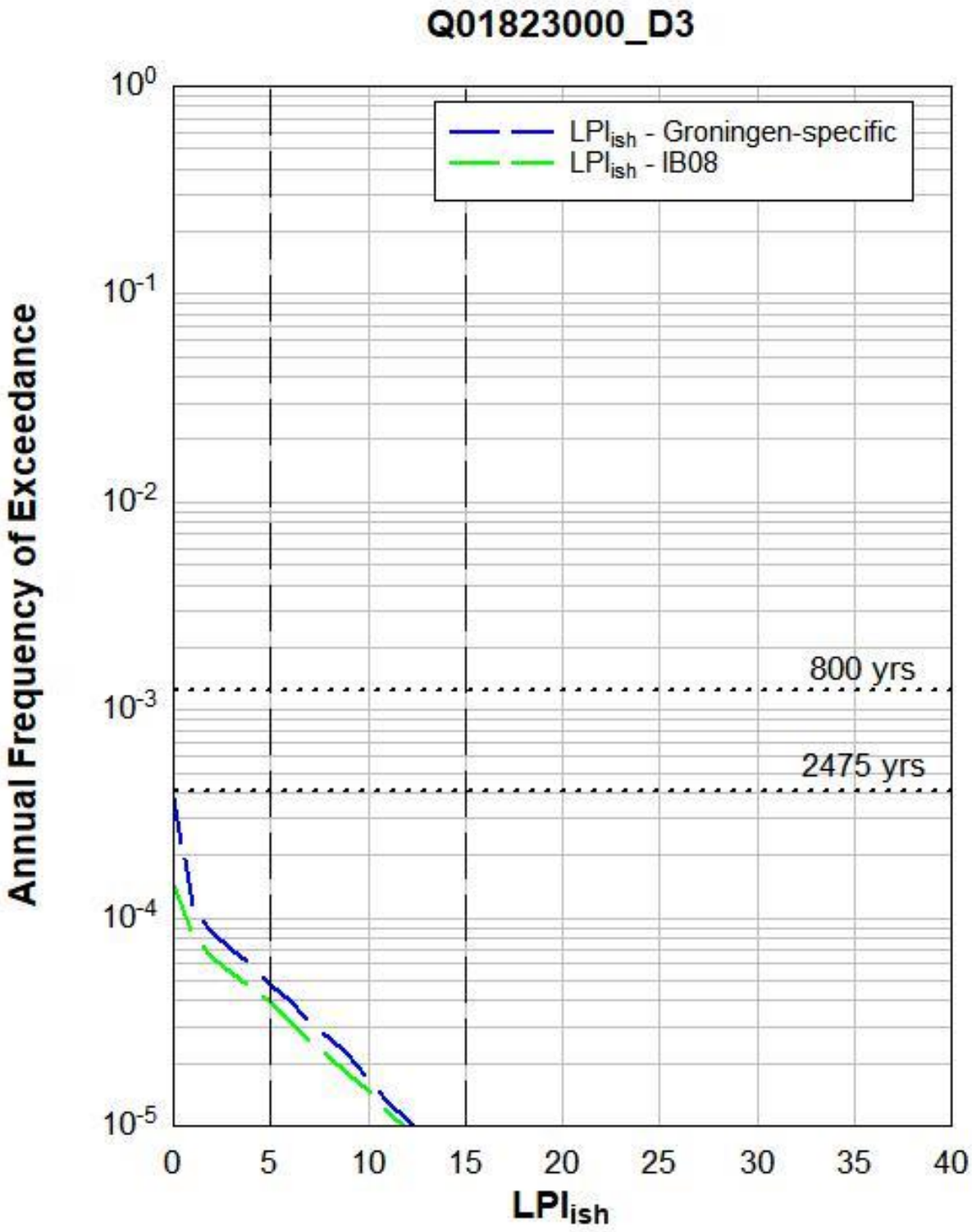
Q01823000_D3
LPIish - Groningen-specific
LPIish - IB08
800 yrs
2475 yrs
Annual Frequency of Exceedance
LPIish
10^0
10^-1
10^-2
10^-3
10^-4
10^-5
0
5
10
15
20
25
30
35
40

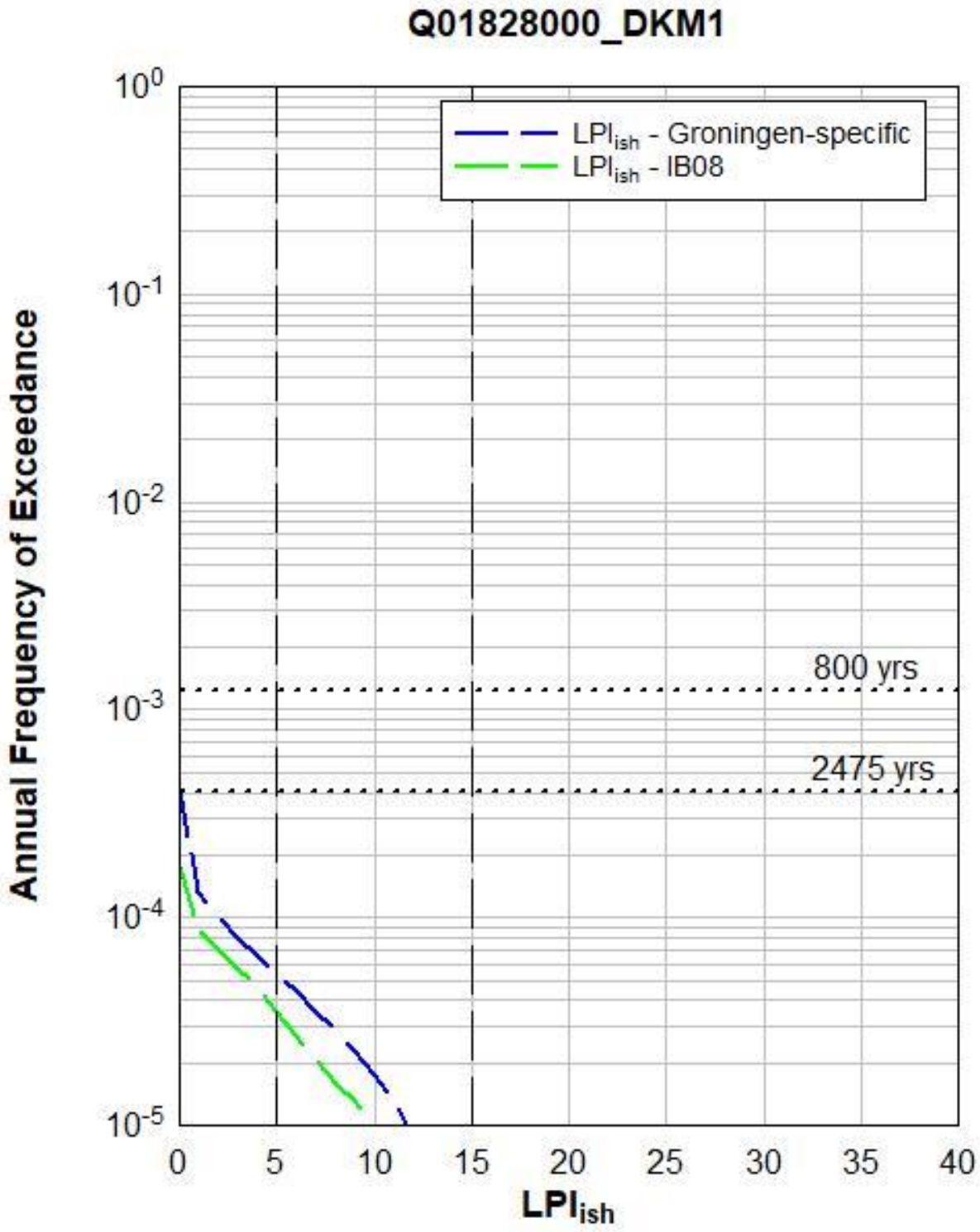
Q01828000_DKM1
LPIish - Groningen-specific
LPIish - IB08
800 yrs
2475 yrs
Annual Frequency of Exceedance
LPIish
10^0
10^-1
10^-2
10^-3
10^-4
10^-5
0
5
10
15
20
25
30
35
40

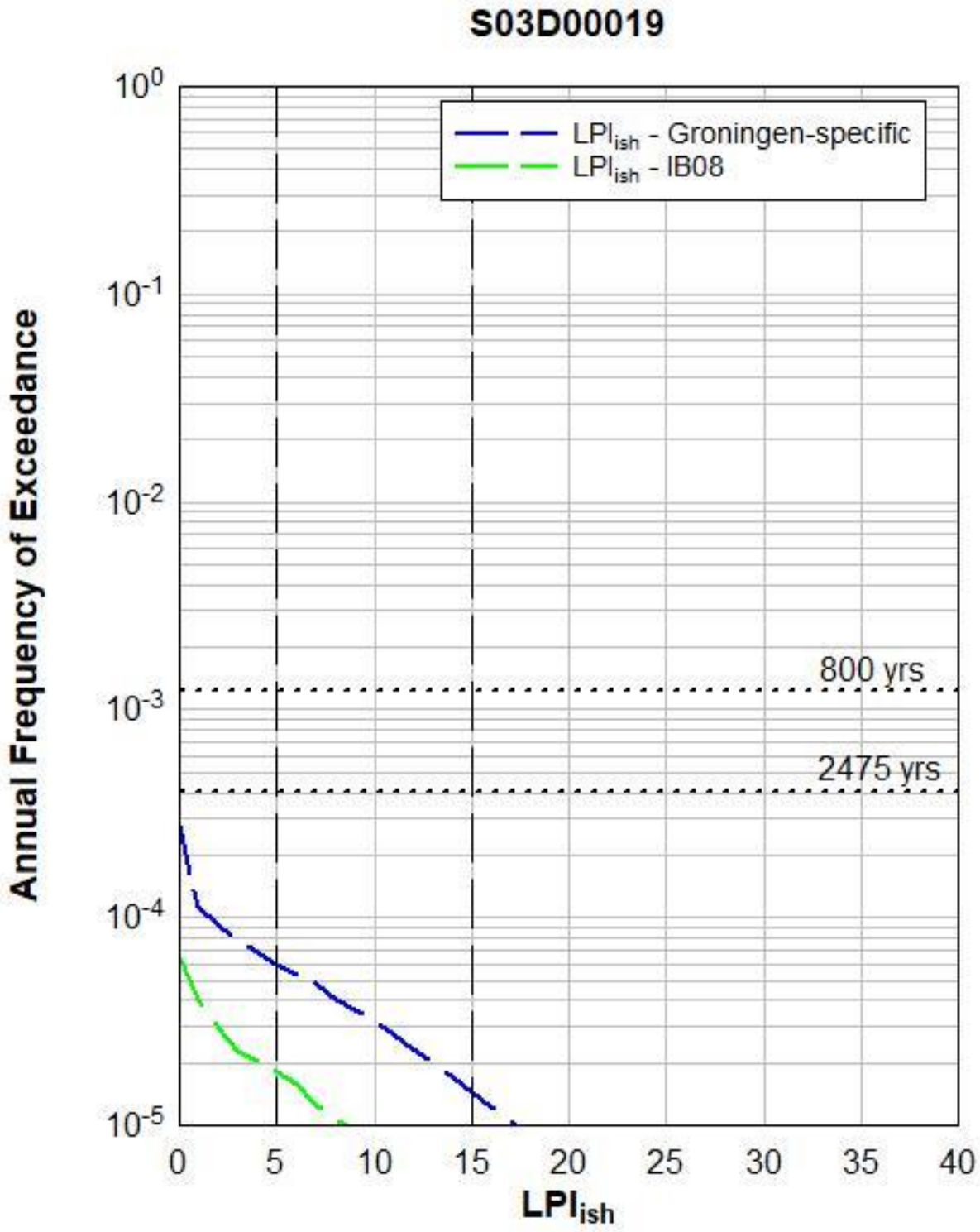
S03D00019
LPIish - Groningen-specific
LPIish - IB08
800 yrs
2475 yrs
Annual Frequency of Exceedance
LPIish
10^0
10^-1
10^-2
10^-3
10^-4
10^-5
0
5
10
15
20
25
30
35
40

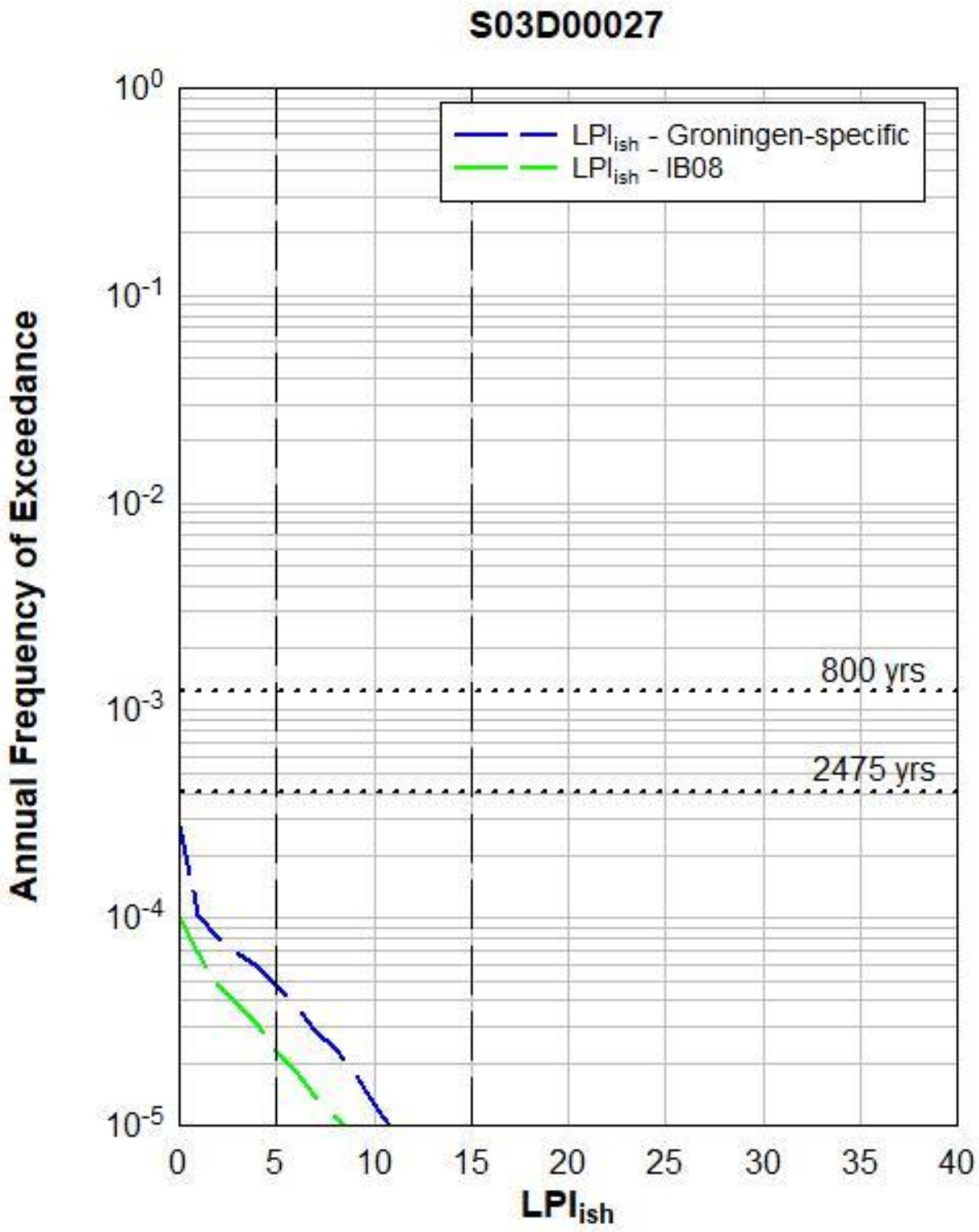
S03D00027
LPIish - Groningen-specific
LPIish - IB08
800 yrs
2475 yrs
Annual Frequency of Exceedance
LPIish
10^0
10^-1
10^-2
10^-3
10^-4
10^-5
0
5
10
15
20
25
30
35
40

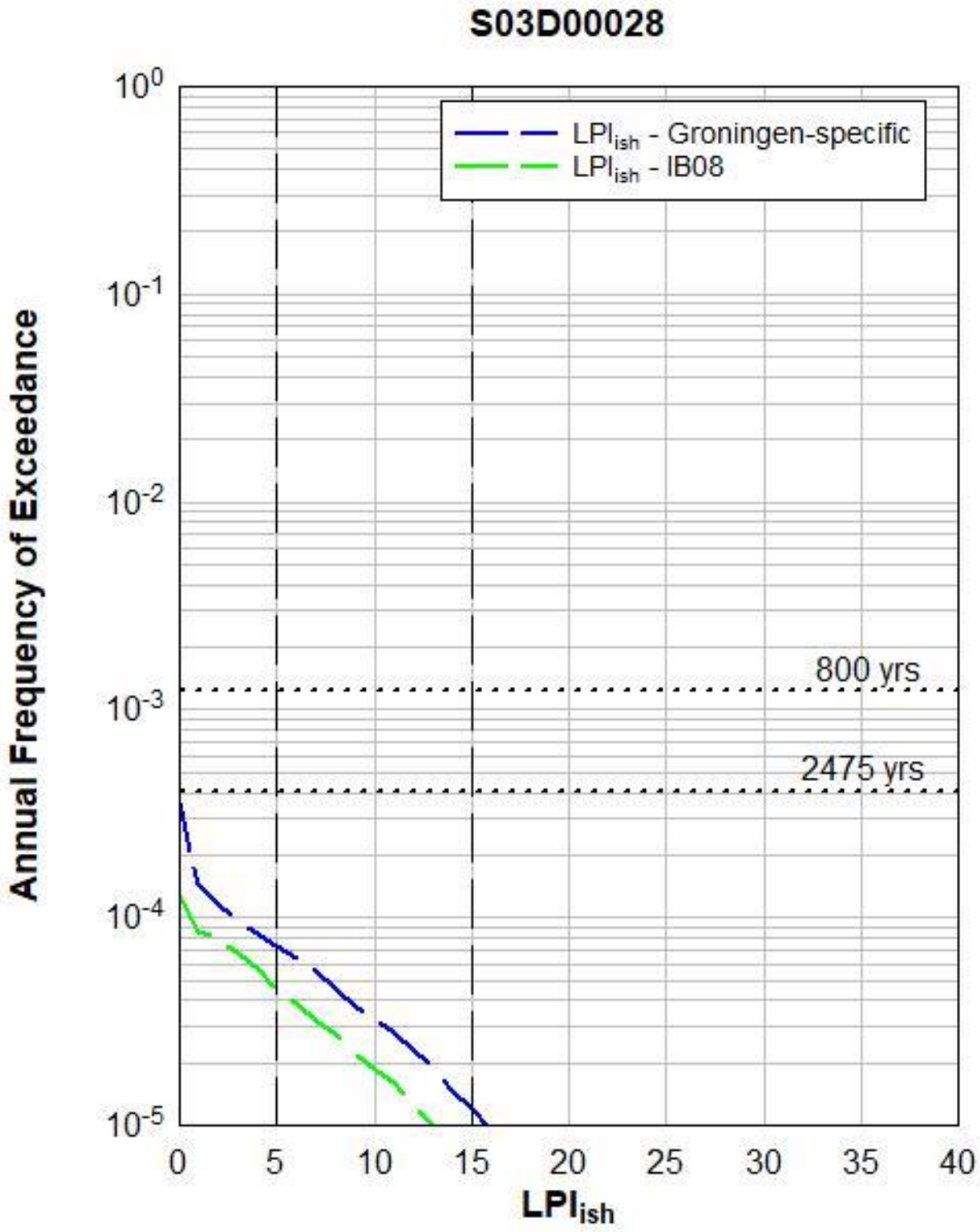
S03D00028
LPIish - Groningen-specific
LPIish - IB08
800 yrs
2475 yrs
Annual Frequency of Exceedance
LPIish
10^0
10^-1
10^-2
10^-3
10^-4
10^-5
0
5
10
15
20
25
30
35
40

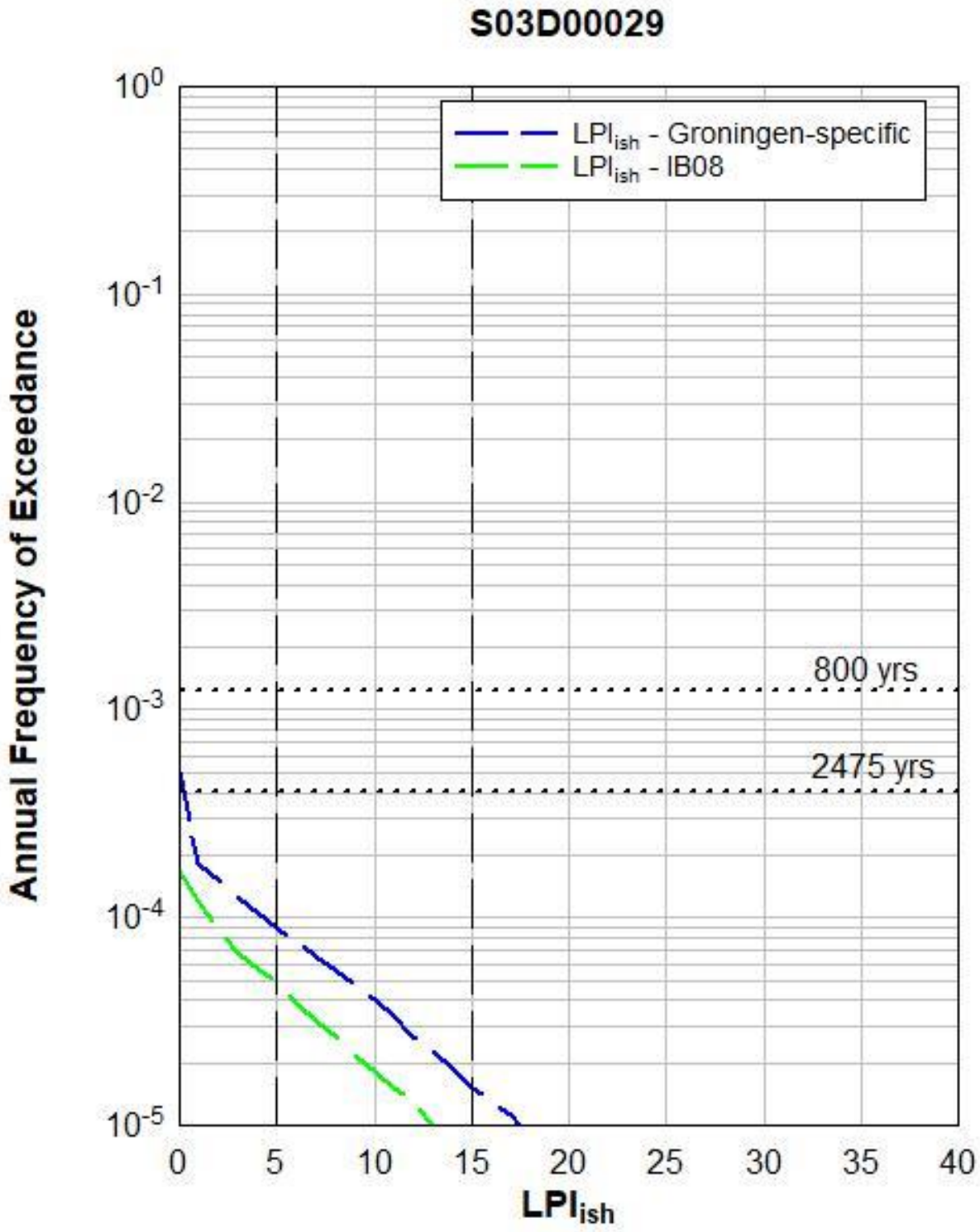
S03D00029
LPIish - Groningen-specific
LPIish - IB08
800 yrs
2475 yrs
Annual Frequency of Exceedance
LPIish
10^0
10^-1
10^-2
10^-3
10^-4
10^-5
0
5
10
15
20
25
30
35
40

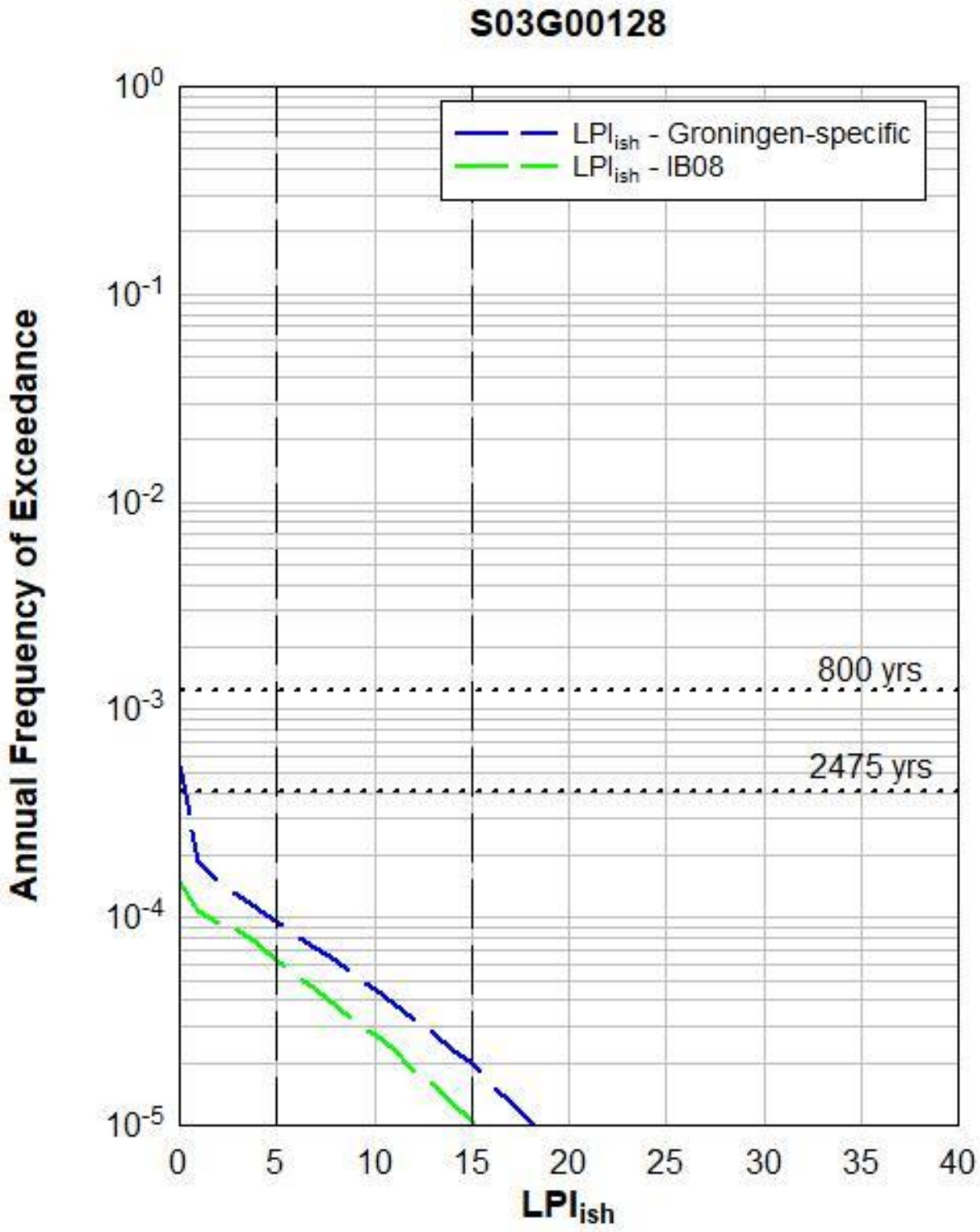
S03G00128
LPIish - Groningen-specific
LPIish - IB08
800 yrs
2475 yrs
Annual Frequency of Exceedance
LPIish
10^0
10^-1
10^-2
10^-3
10^-4
10^-5
0
5
10
15
20
25
30
35
40

Zone 603

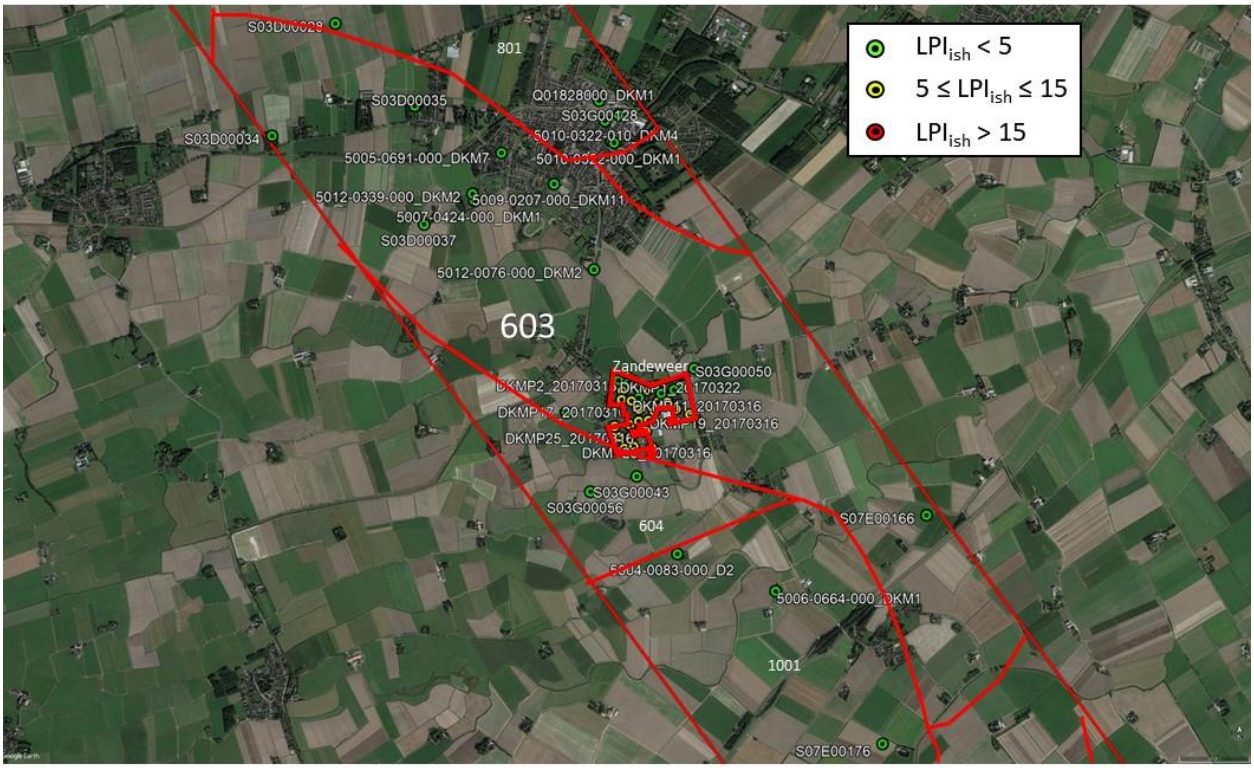
LPI$_{ish}$ < 5
5 ≤ LPI$_{ish}$ ≤ 15
LPI$_{ish}$ > 15
S03D00028
801
S03D00035
Q01828000_DKM1
S03G00128
S03D00034
5010-0322-010_DKM4
5005-0691-000_DKM7
5010-0322-000_DKM1
5012-0339-000_DKM2
5009-0207-000_DKM11
5007-0424-000_DKM1
S03D00037
5012-0076-000_DKM2
603
Zandeweer
S03G00050
DKMP2_2017031
170322
DKMP17_2017031
20170316
DKMP25_20176316
0170316
S03G00043
S03G00056
604
S07E00166
5004-0083-000_D2
5006-0664-000_DKM1
1001
S07E00176

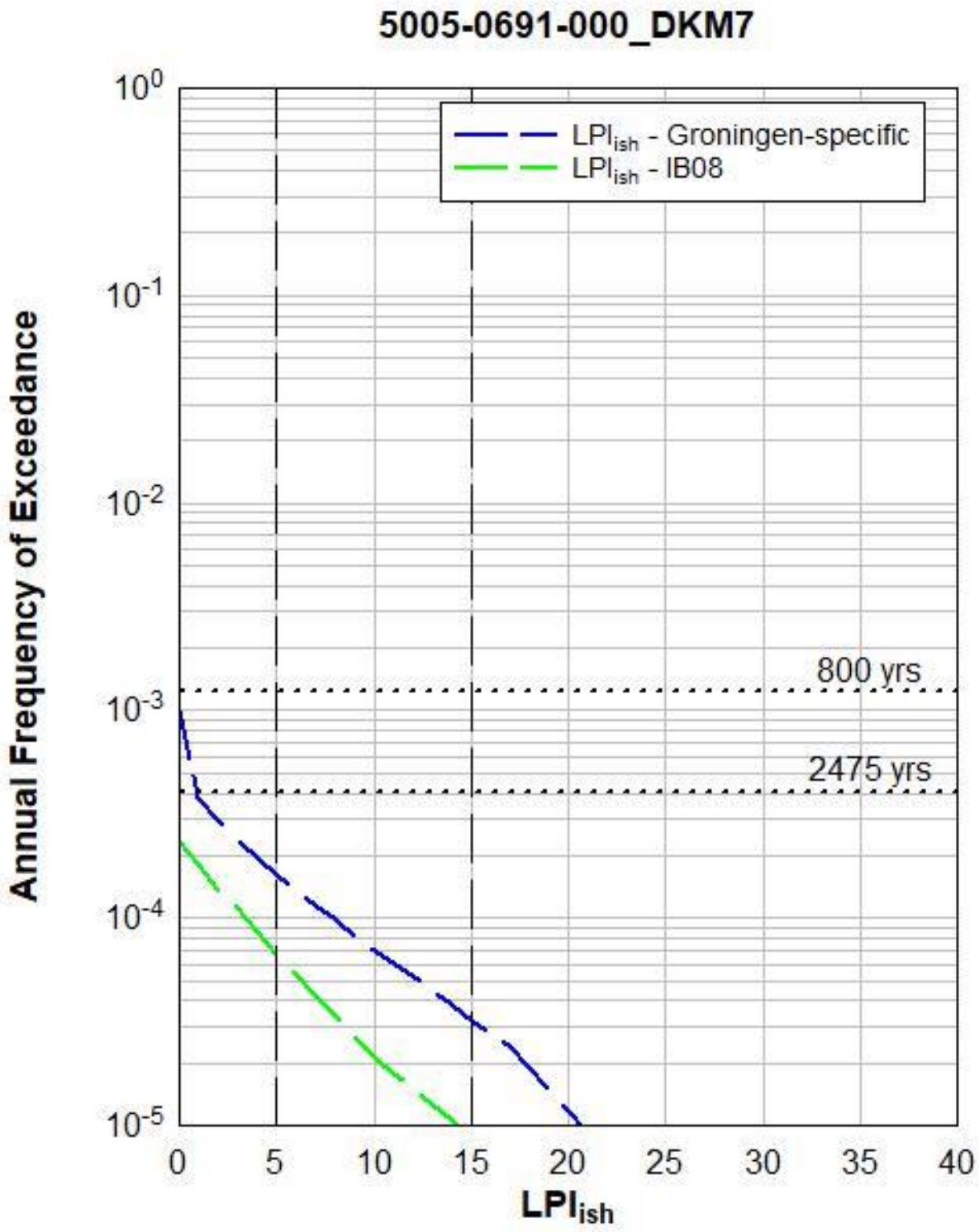
5005-0691-000_DKM7
LPIish - Groningen-specific
LPIish - IB08
800 yrs
2475 yrs
Annual Frequency of Exceedance
LPIish
10^0
10^-1
10^-2
10^-3
10^-4
10^-5
0
5
10
15
20
25
30
35
40

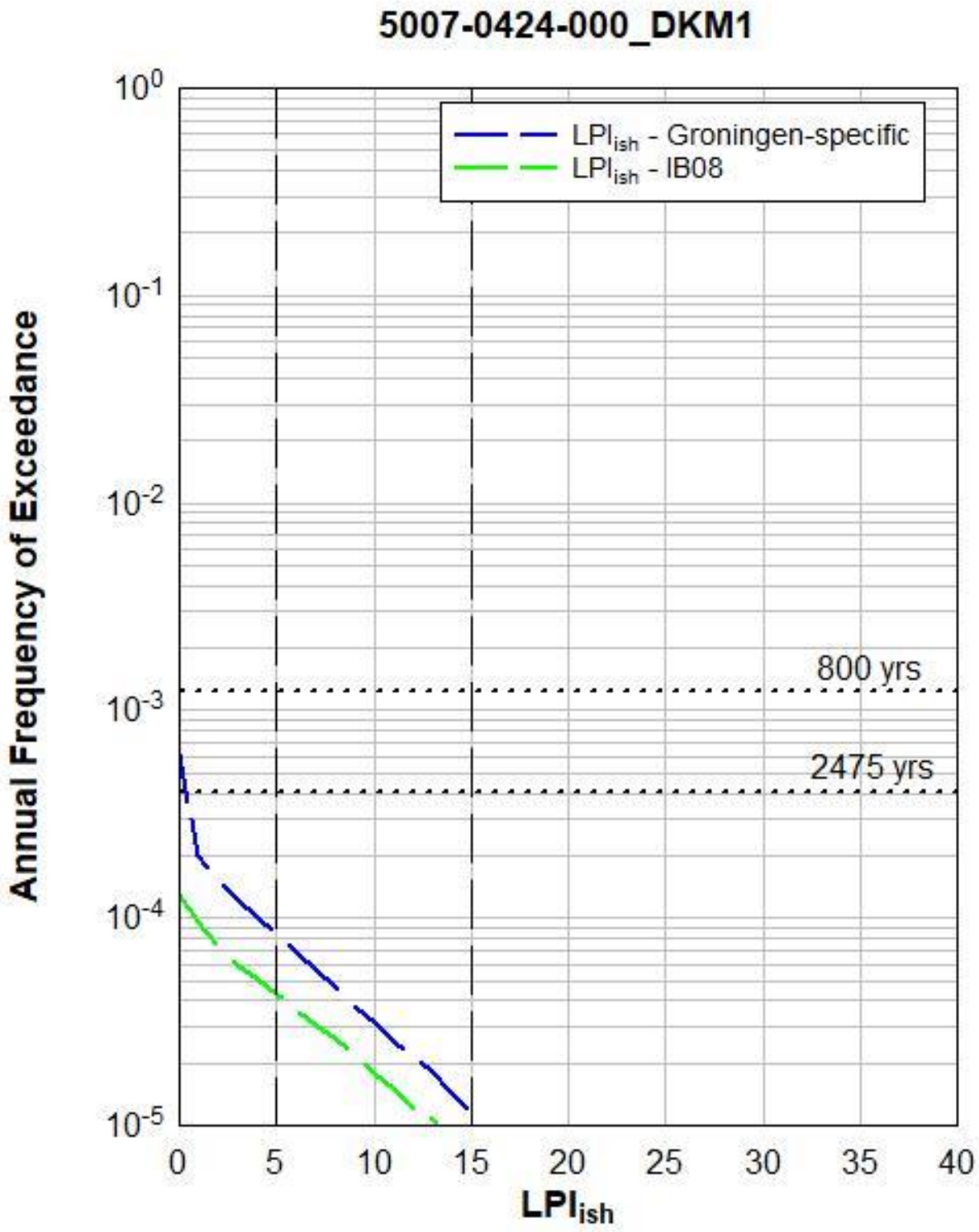
5007-0424-000_DKM1
LPIish - Groningen-specific
LPIish - IB08
800 yrs
2475 yrs
Annual Frequency of Exceedance
LPIish
10^0
10^-1
10^-2
10^-3
10^-4
10^-5
0
5
10
15
20
25
30
35
40

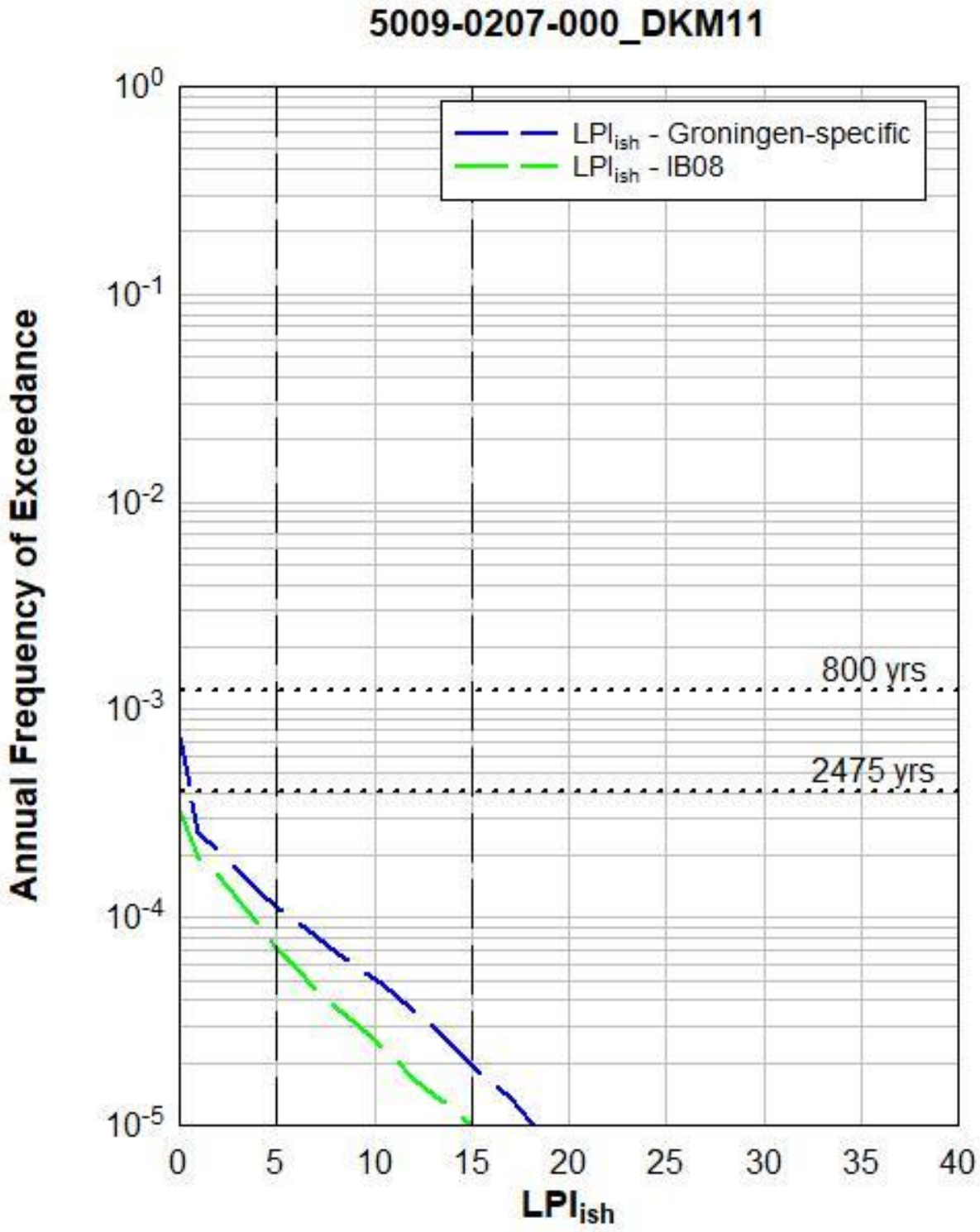
5009-0207-000_DKM11
LPIish - Groningen-specific
LPIish - IB08
800 yrs
2475 yrs
Annual Frequency of Exceedance
LPIish
10^0
10^-1
10^-2
10^-3
10^-4
10^-5
0
5
10
15
20
25
30
35
40

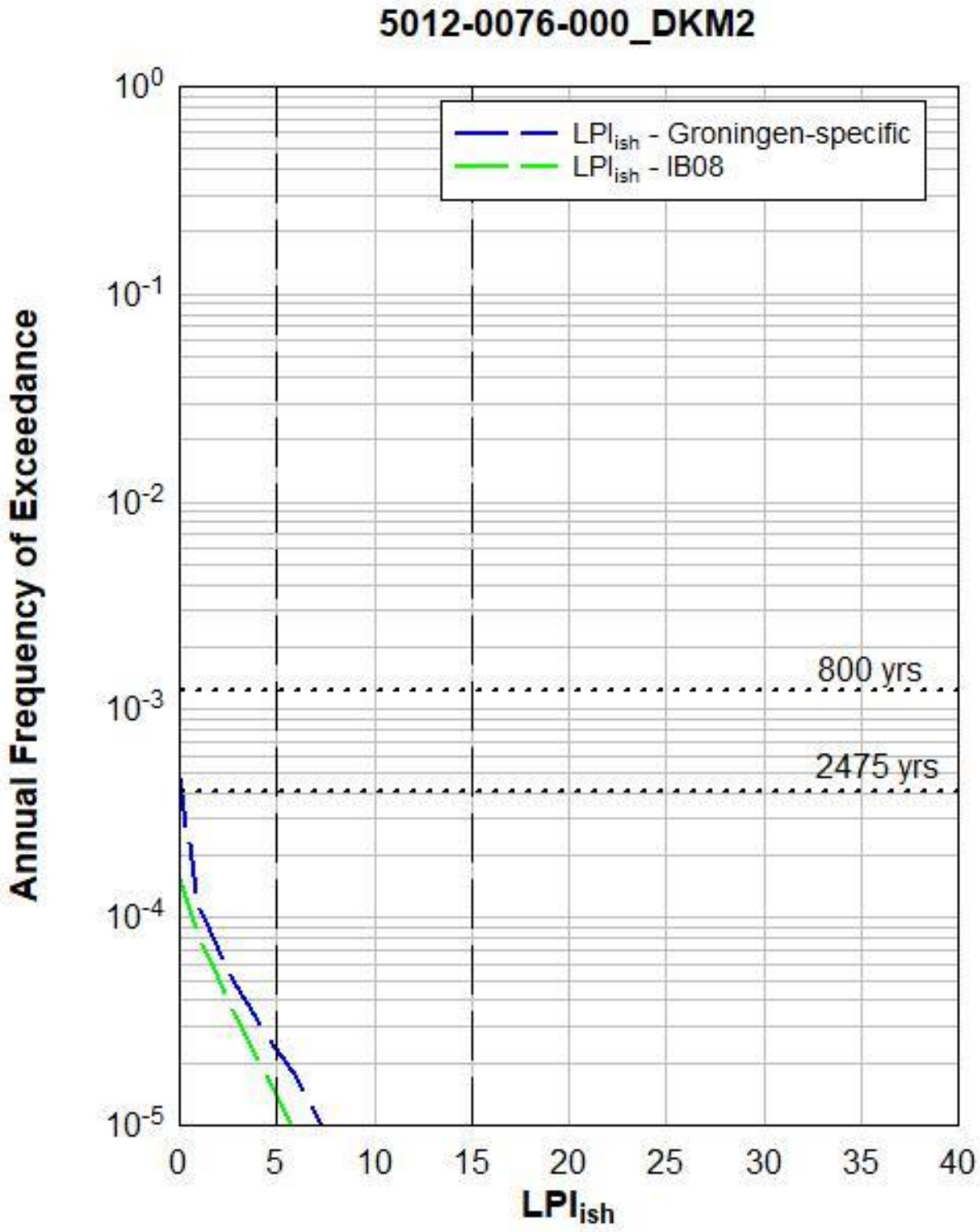
5012-0076-000_DKM2
LPIish - Groningen-specific
LPIish - IB08
800 yrs
2475 yrs
Annual Frequency of Exceedance
LPIish
10^0
10^-1
10^-2
10^-3
10^-4
10^-5
0
5
10
15
20
25
30
35
40

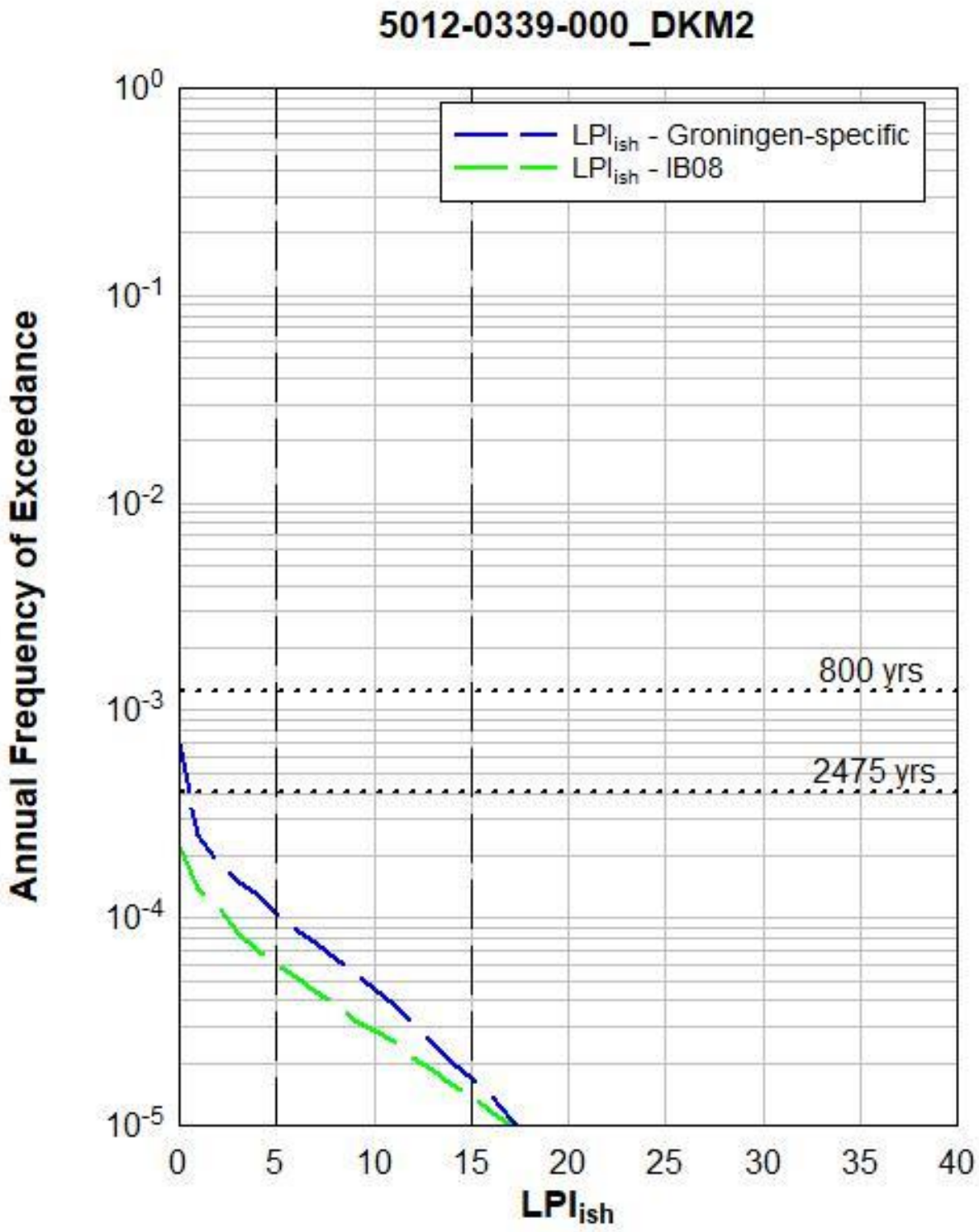
5012-0339-000_DKM2
LPIish - Groningen-specific
LPIish - IB08
800 yrs
2475 yrs
Annual Frequency of Exceedance
LPIish
10^0
10^-1
10^-2
10^-3
10^-4
10^-5
0
5
10
15
20
25
30
35
40

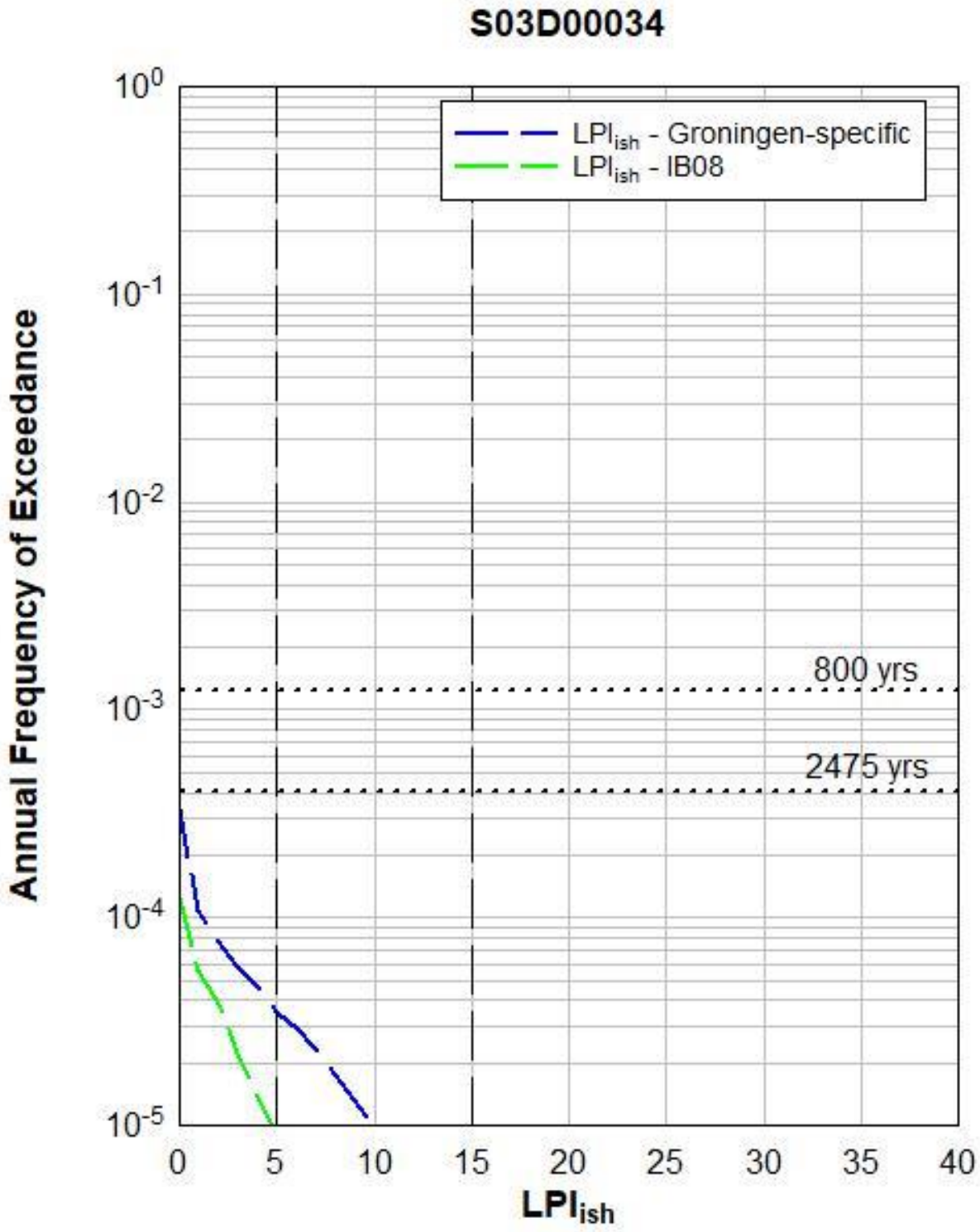
S03D00034
LPIish - Groningen-specific
LPIish - IB08
800 yrs
2475 yrs
Annual Frequency of Exceedance
LPIish
10^0
10^-1
10^-2
10^-3
10^-4
10^-5
0
5
10
15
20
25
30
35
40

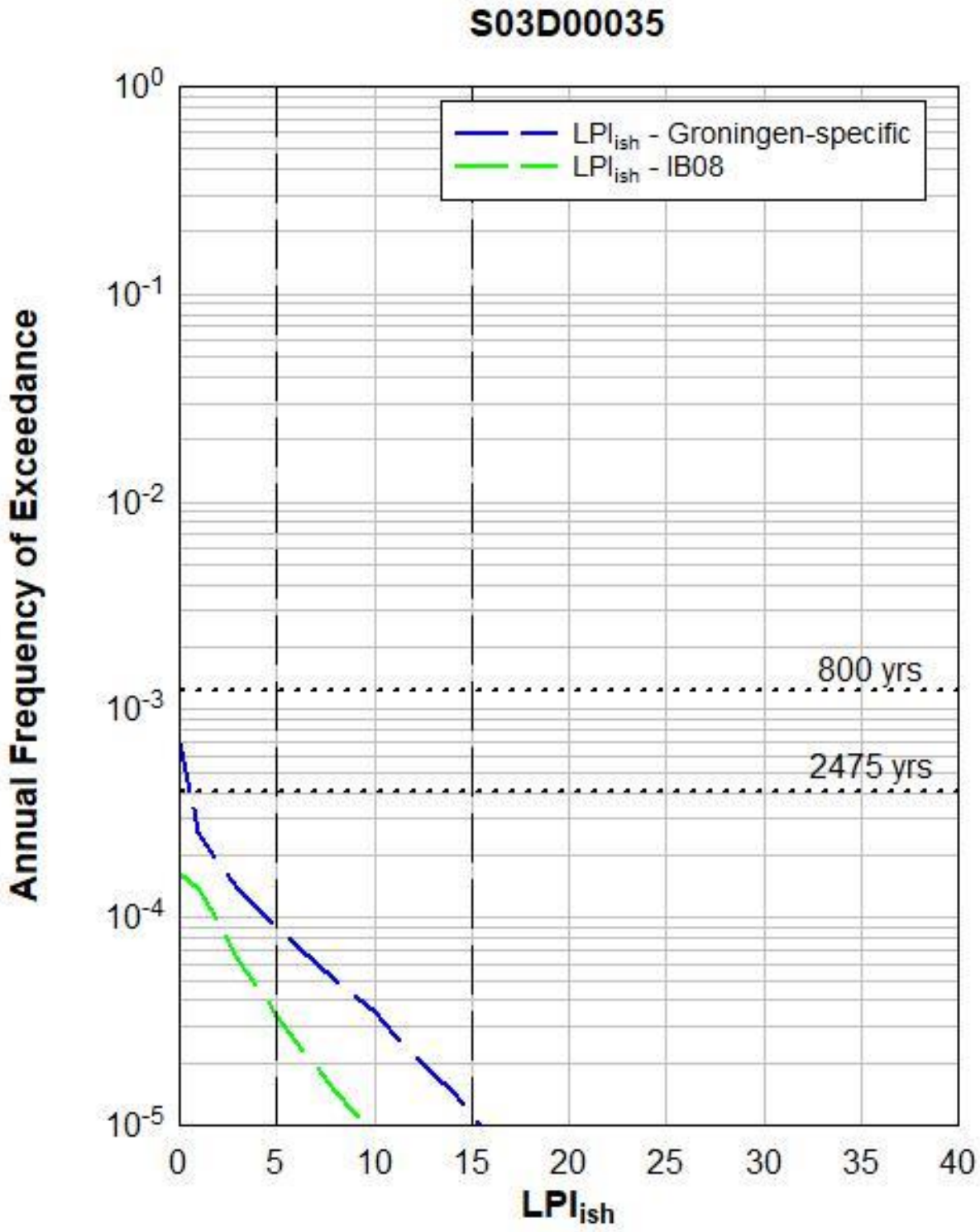
S03D00035
LPIish - Groningen-specific
LPIish - IB08
800 yrs
2475 yrs
Annual Frequency of Exceedance
LPIish
10^0
10^-1
10^-2
10^-3
10^-4
10^-5
0
5
10
15
20
25
30
35
40

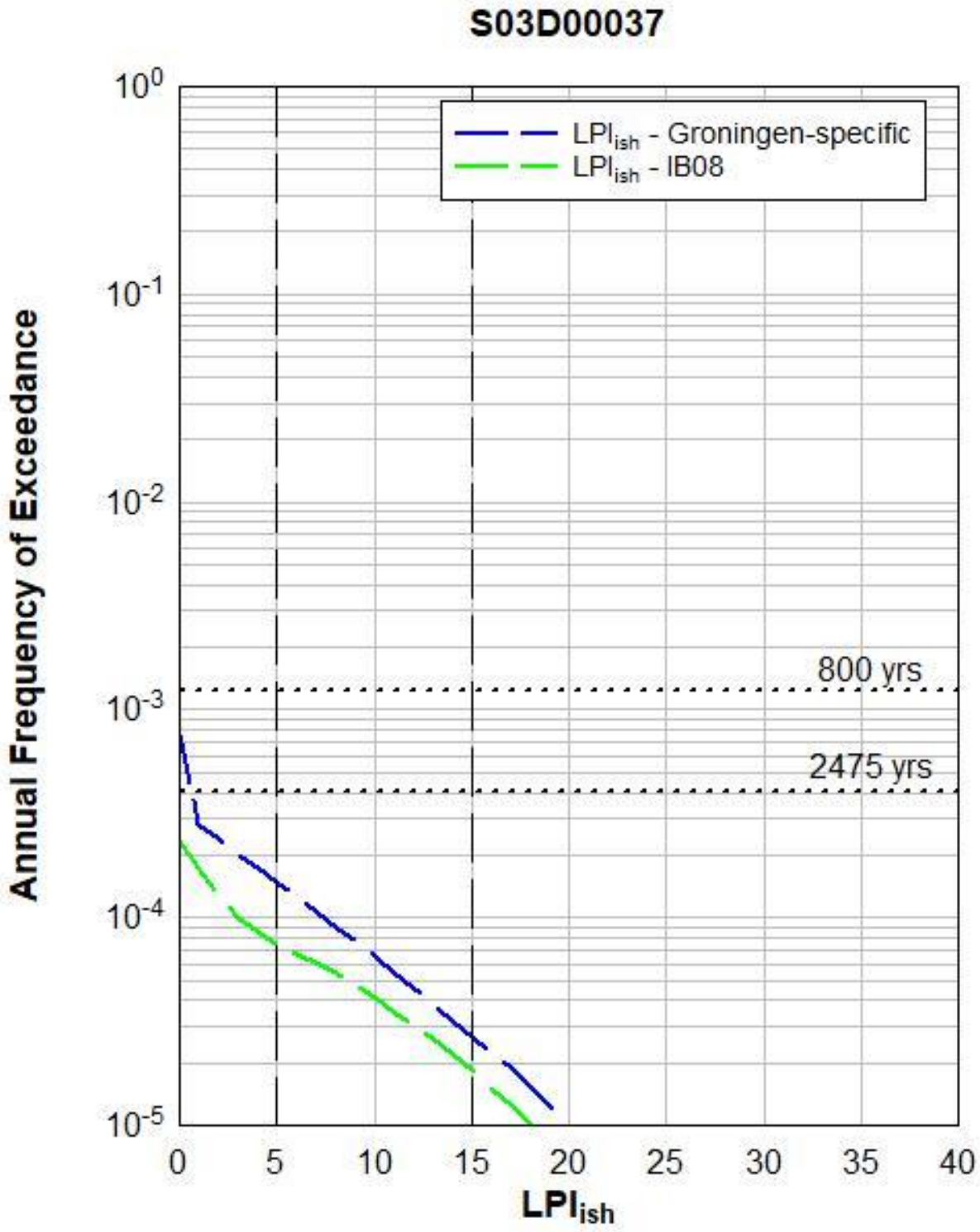
S03D00037
LPIish - Groningen-specific
LPIish - IB08
800 yrs
2475 yrs
Annual Frequency of Exceedance
LPIish
10^0
10^-1
10^-2
10^-3
10^-4
10^-5
0
5
10
15
20
25
30
35
40

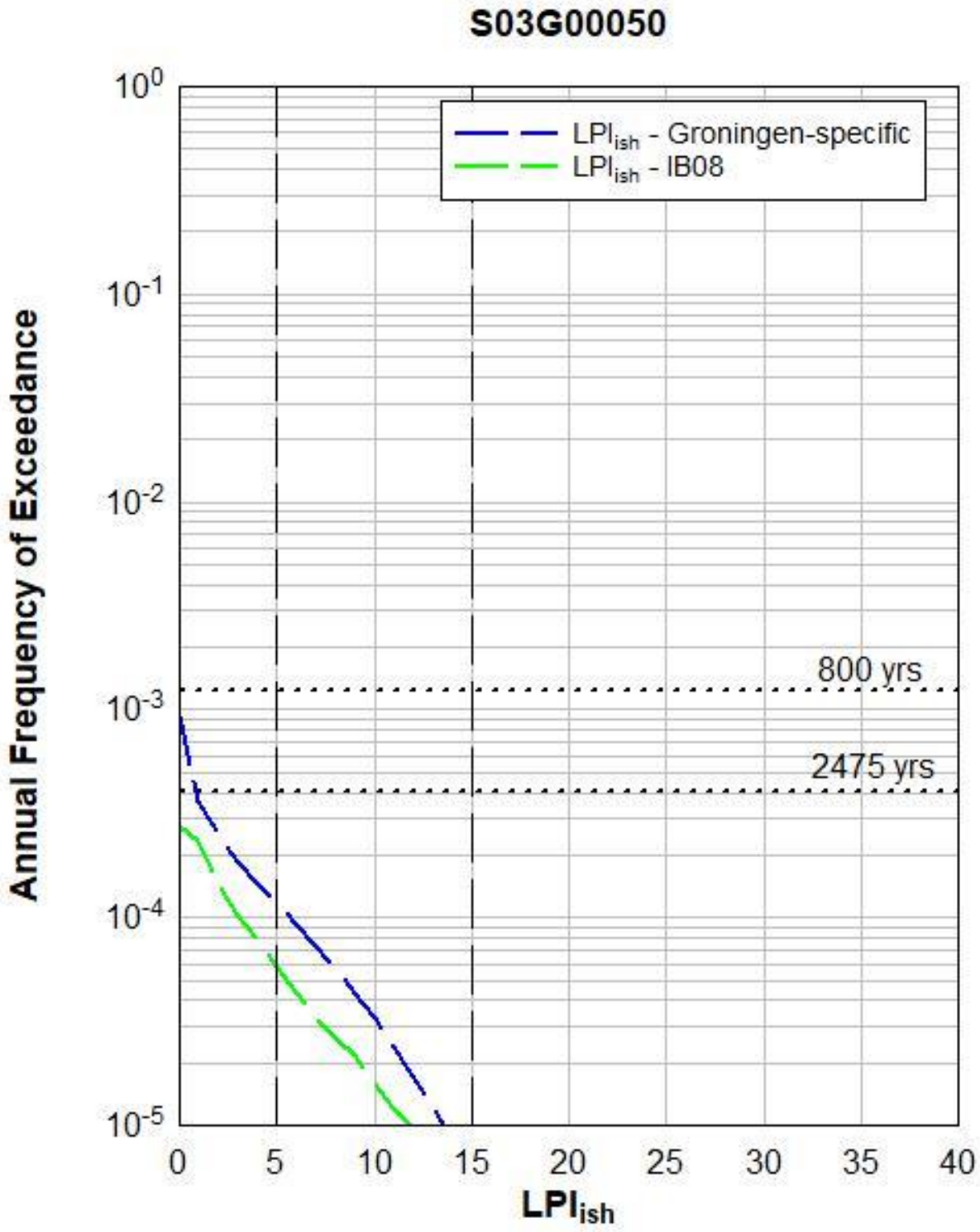
S03G00050
LPIish - Groningen-specific
LPIish - IB08
800 yrs
2475 yrs
Annual Frequency of Exceedance
LPIish
10^0
10^-1
10^-2
10^-3
10^-4
10^-5
0
5
10
15
20
25
30
35
40

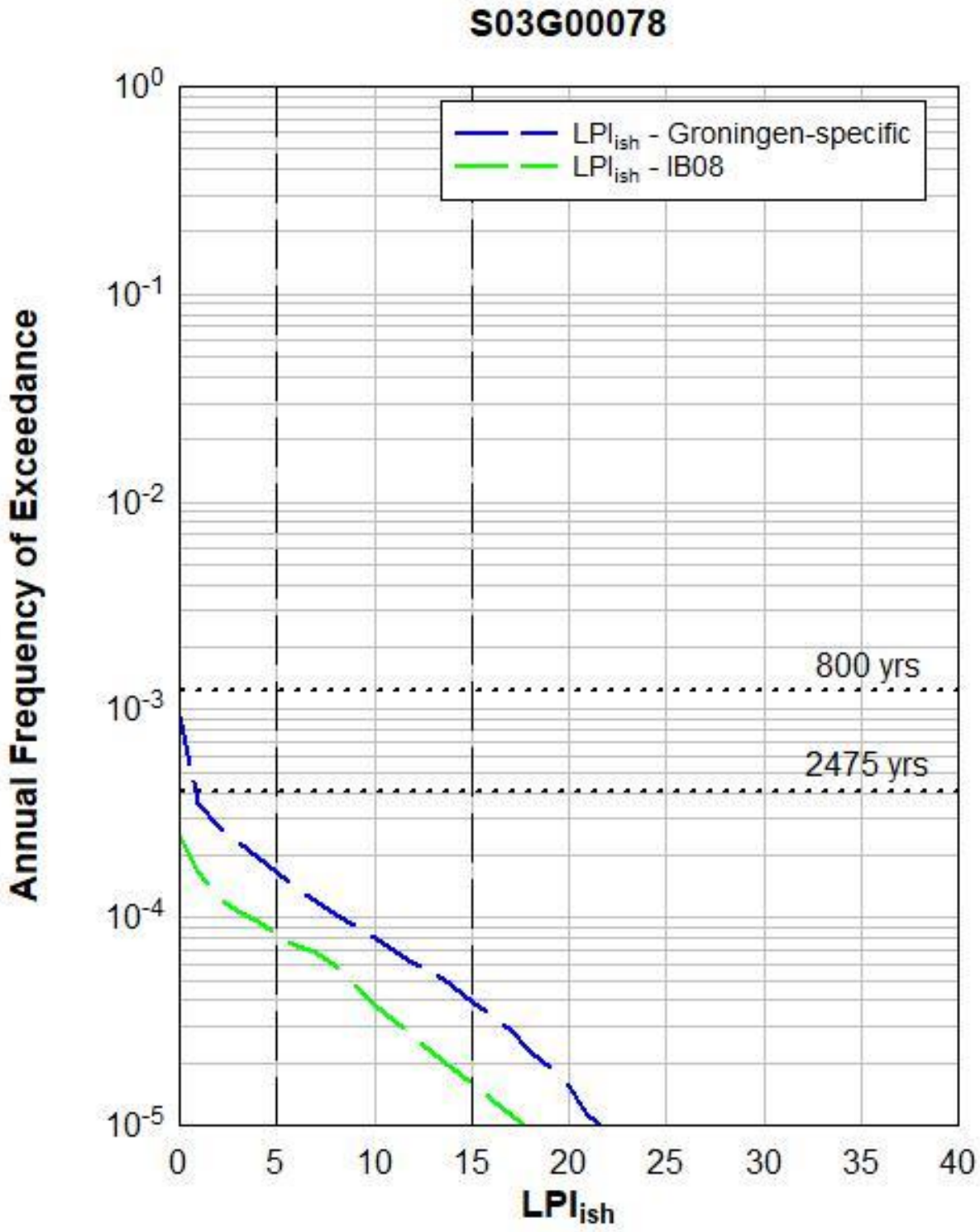
S03G00078
LPIish - Groningen-specific
LPIish - IB08
800 yrs
2475 yrs
Annual Frequency of Exceedance
LPIish
10^0
10^-1
10^-2
10^-3
10^-4
10^-5
0
5
10
15
20
25
30
35
40

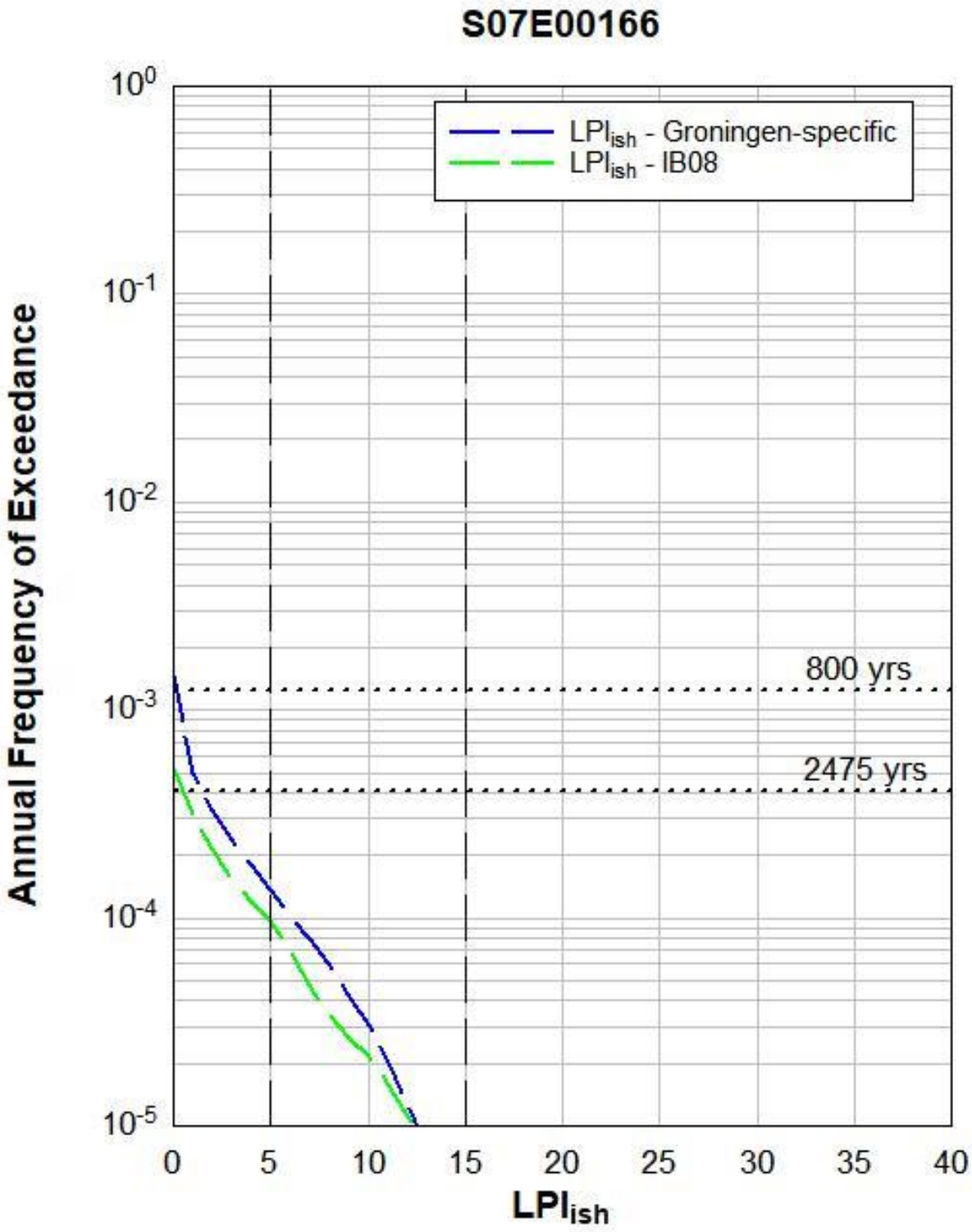
S07E00166
LPIish - Groningen-specific
LPIish - IB08
800 yrs
2475 yrs
Annual Frequency of Exceedance
LPIish
10^0
10^-1
10^-2
10^-3
10^-4
10^-5
0
5
10
15
20
25
30
35
40

Zone Zandeweer

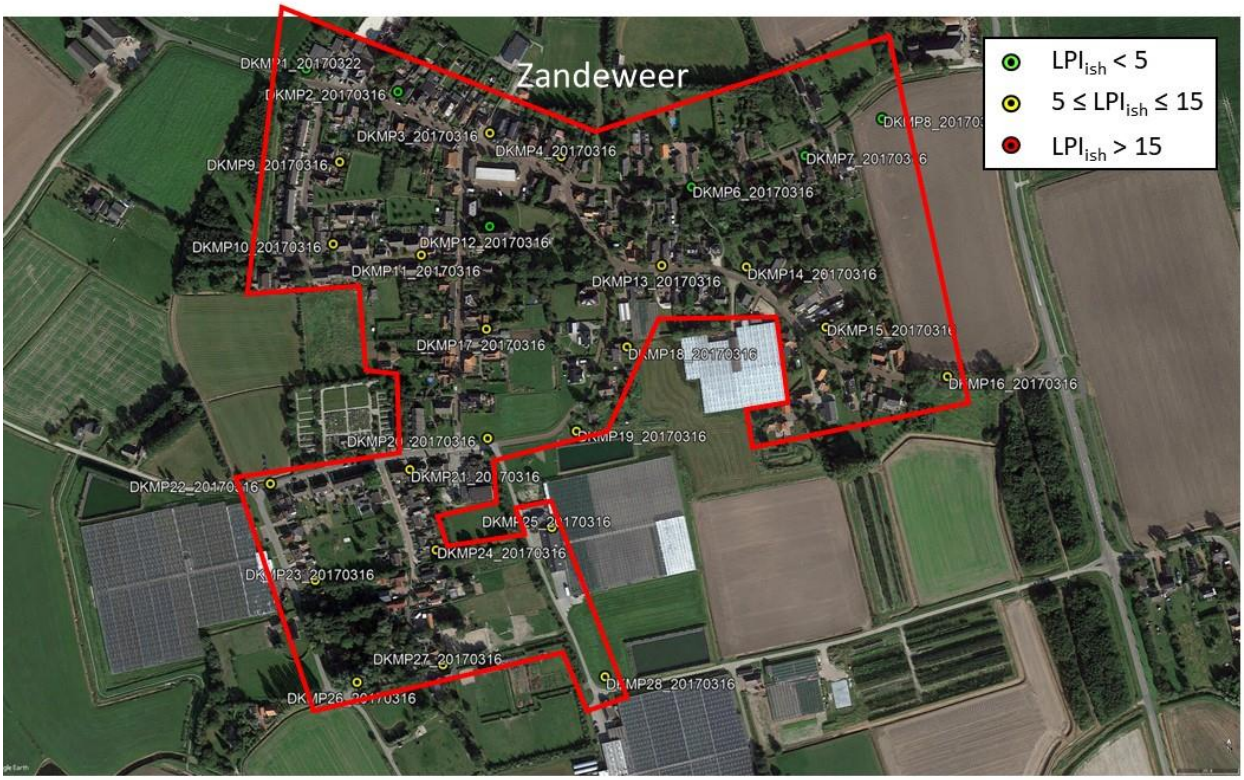

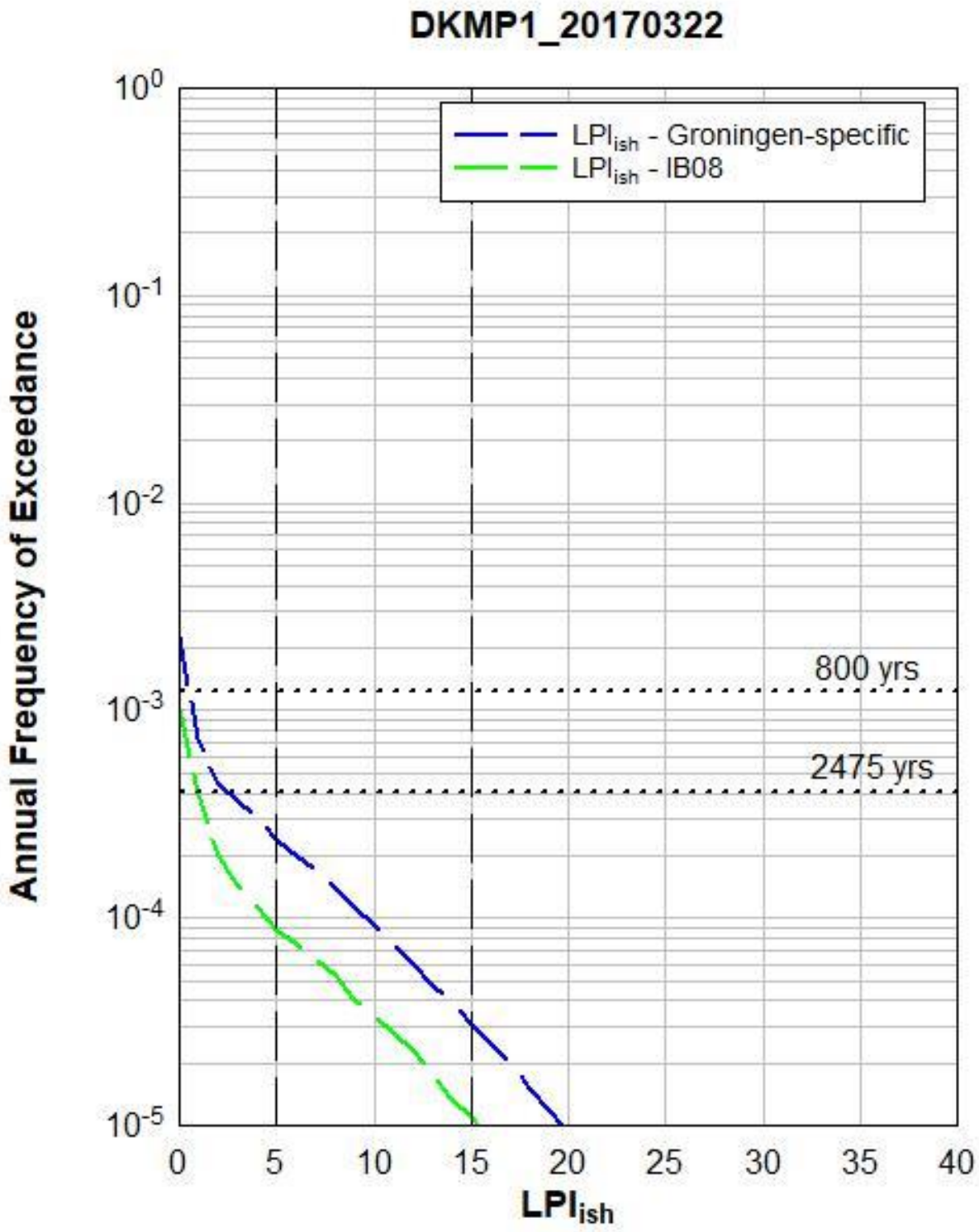
DKMP1_20170322
LPIish - Groningen-specific
LPIish - IB08
800 yrs
2475 yrs
Annual Frequency of Exceedance
LPIish
10^0
10^-1
10^-2
10^-3
10^-4
10^-5
0
5
10
15
20
25
30
35
40

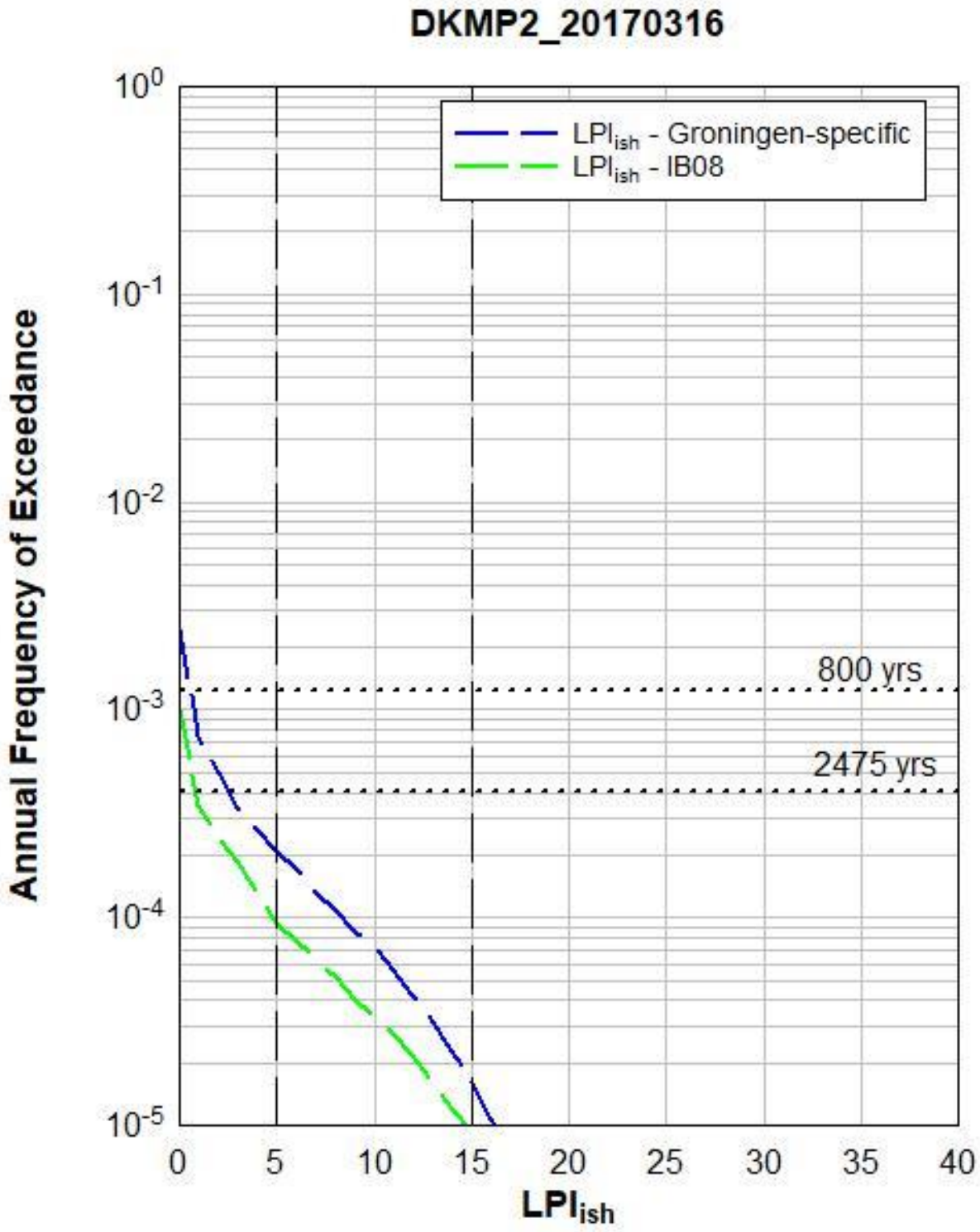
DKMP2_20170316
LPIish - Groningen-specific
LPIish - IB08
800 yrs
2475 yrs
Annual Frequency of Exceedance
LPIish
10^0
10^-1
10^-2
10^-3
10^-4
10^-5
0
5
10
15
20
25
30
35
40

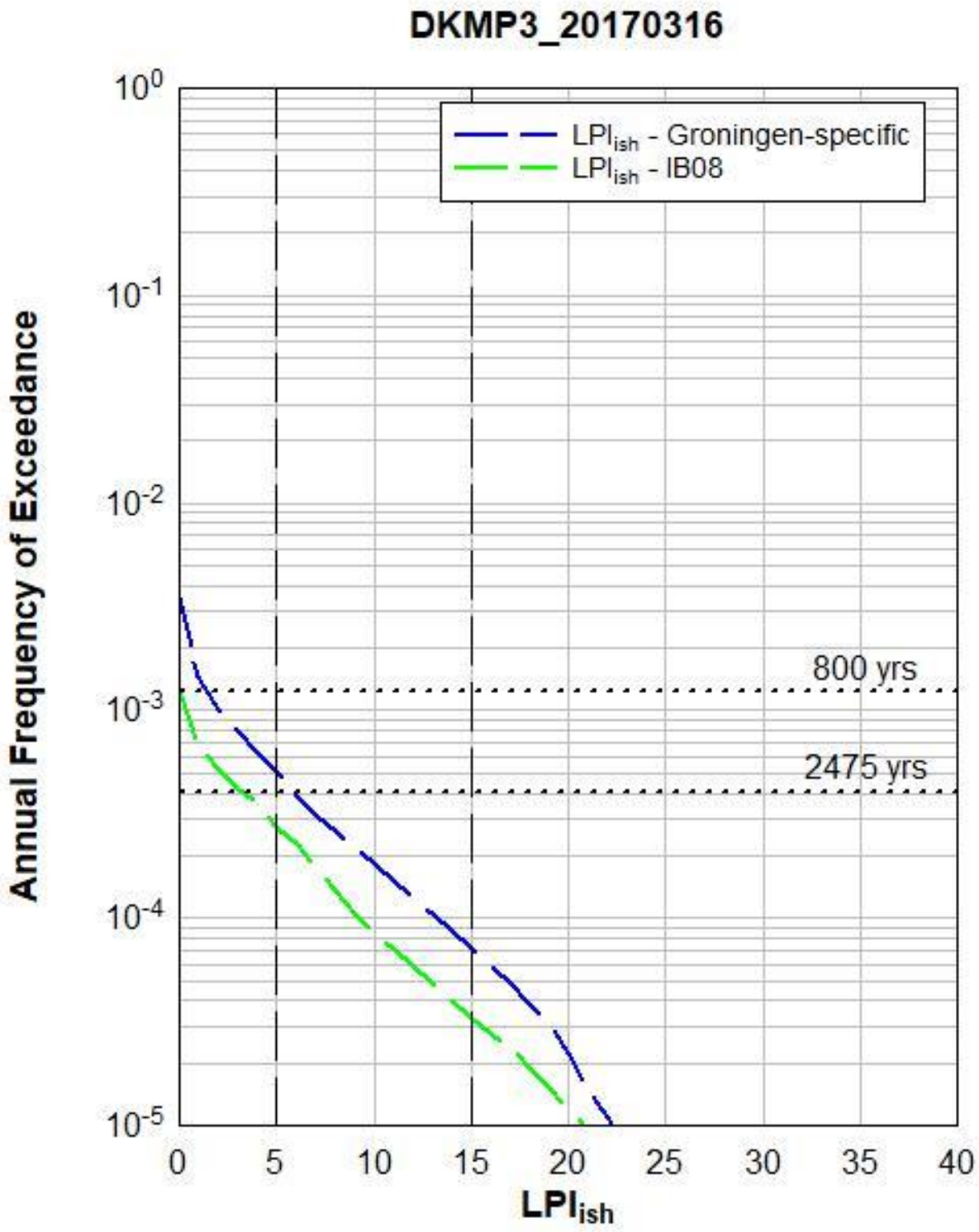
DKMP3_20170316
LPIish - Groningen-specific
LPIish - IB08
800 yrs
2475 yrs
Annual Frequency of Exceedance
LPIish
10^0
10^-1
10^-2
10^-3
10^-4
10^-5
0
5
10
15
20
25
30
35
40

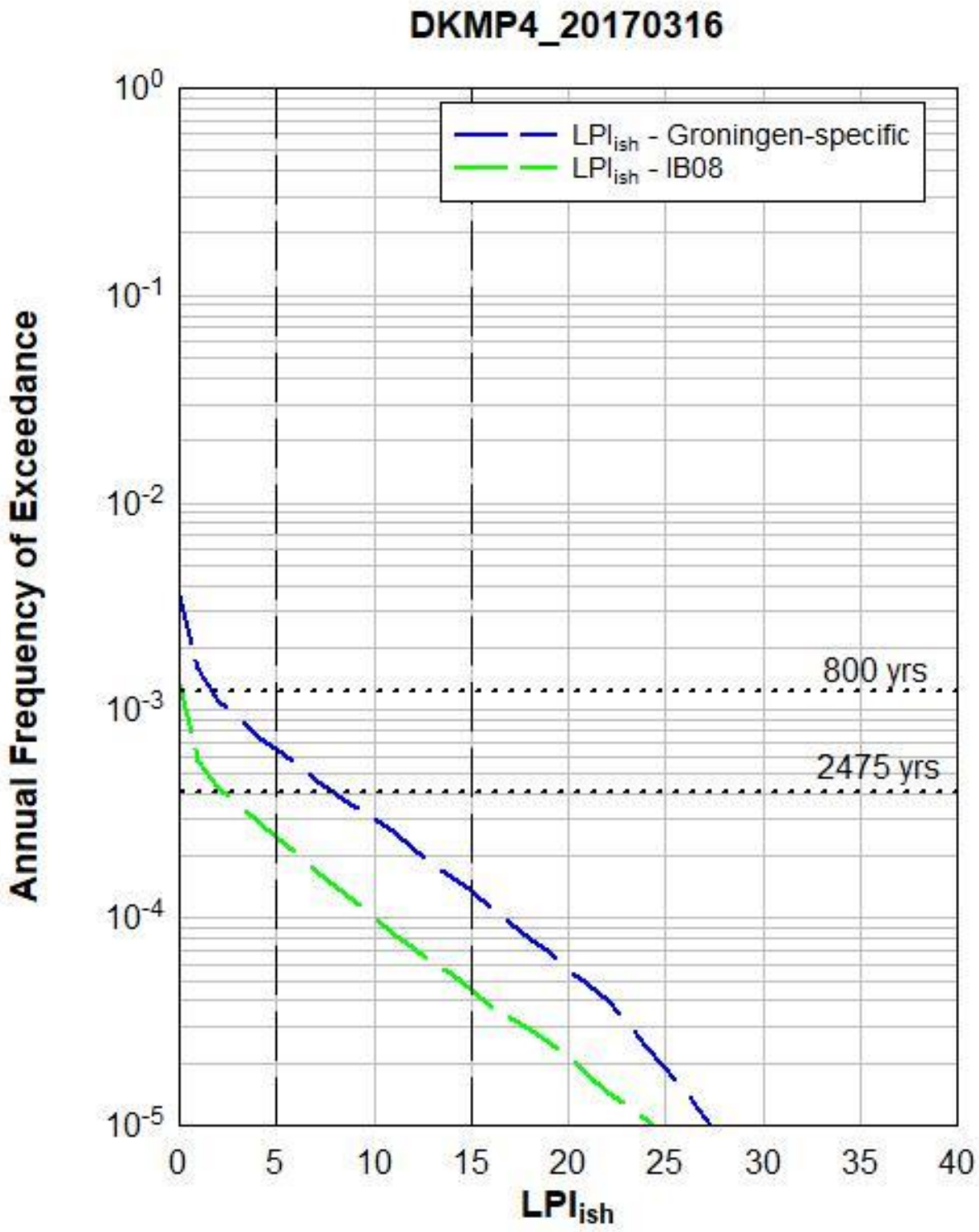
DKMP4_20170316
LPIish - Groningen-specific
LPIish - IB08
800 yrs
2475 yrs
Annual Frequency of Exceedance
LPIish
10^0
10^-1
10^-2
10^-3
10^-4
10^-5
0
5
10
15
20
25
30
35
40

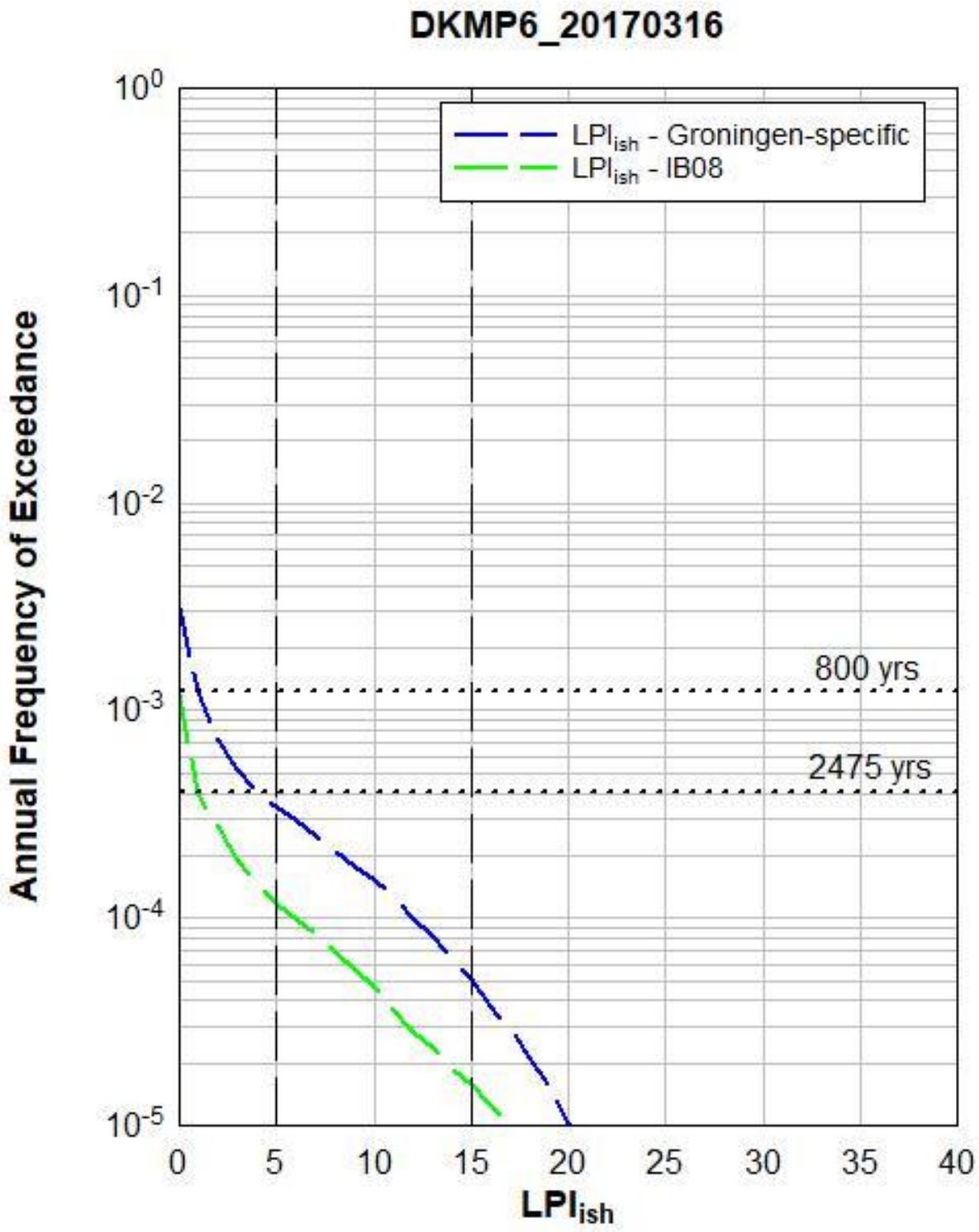
DKMP6_20170316
LPIish - Groningen-specific
LPIish - IB08
800 yrs
2475 yrs
Annual Frequency of Exceedance
LPIish
10^0
10^-1
10^-2
10^-3
10^-4
10^-5
0
5
10
15
20
25
30
35
40

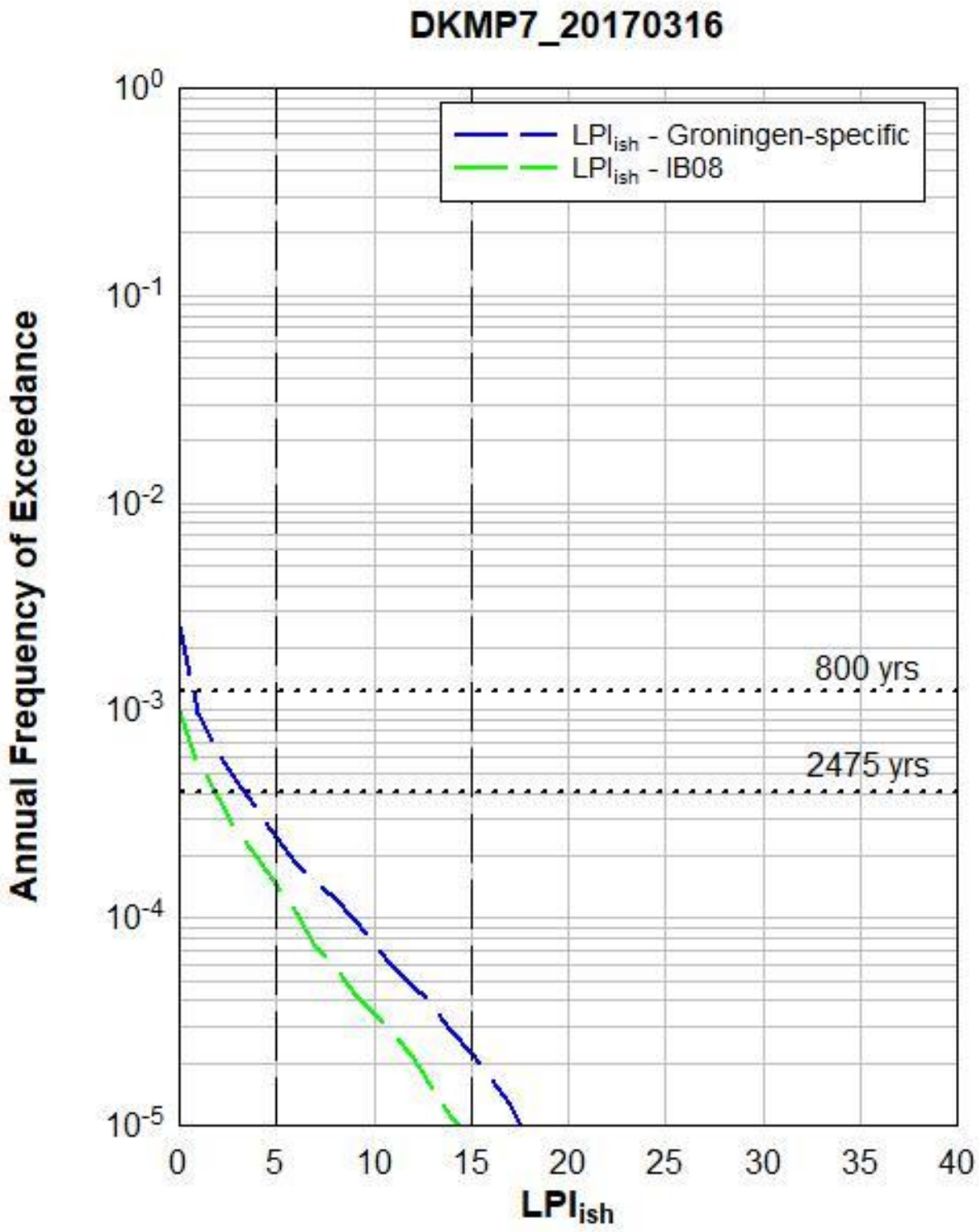
DKMP7_20170316
LPIish - Groningen-specific
LPIish - IB08
800 yrs
2475 yrs
Annual Frequency of Exceedance
LPIish
10^0
10^-1
10^-2
10^-3
10^-4
10^-5
0
5
10
15
20
25
30
35
40

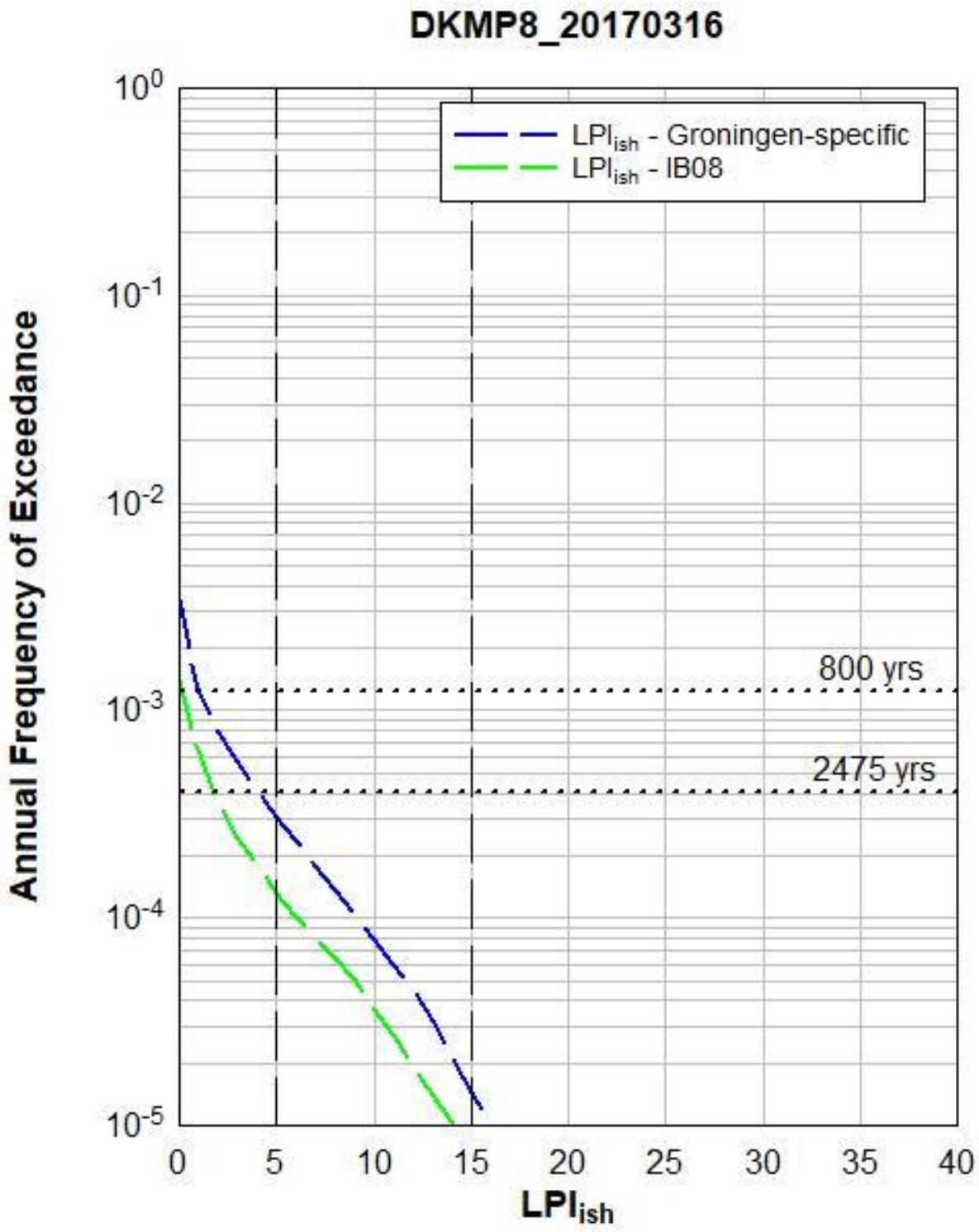
DKMP8_20170316
LPIish - Groningen-specific
LPIish - IB08
800 yrs
2475 yrs
Annual Frequency of Exceedance
LPIish
10^0
10^-1
10^-2
10^-3
10^-4
10^-5
0
5
10
15
20
25
30
35
40

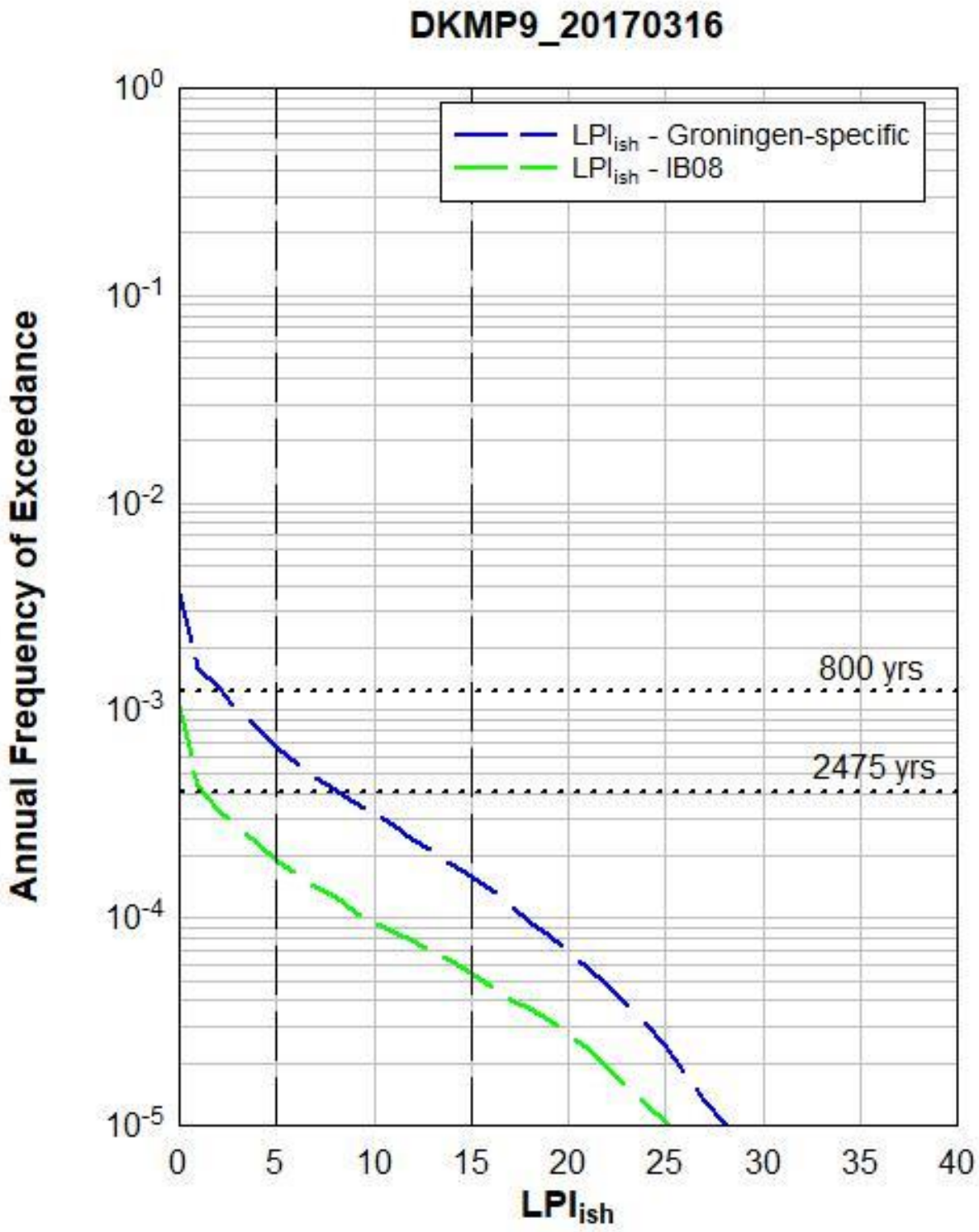
DKMP9_20170316
LPIish - Groningen-specific
LPIish - IB08
800 yrs
2475 yrs
Annual Frequency of Exceedance
LPIish
10^0
10^-1
10^-2
10^-3
10^-4
10^-5
0
5
10
15
20
25
30
35
40

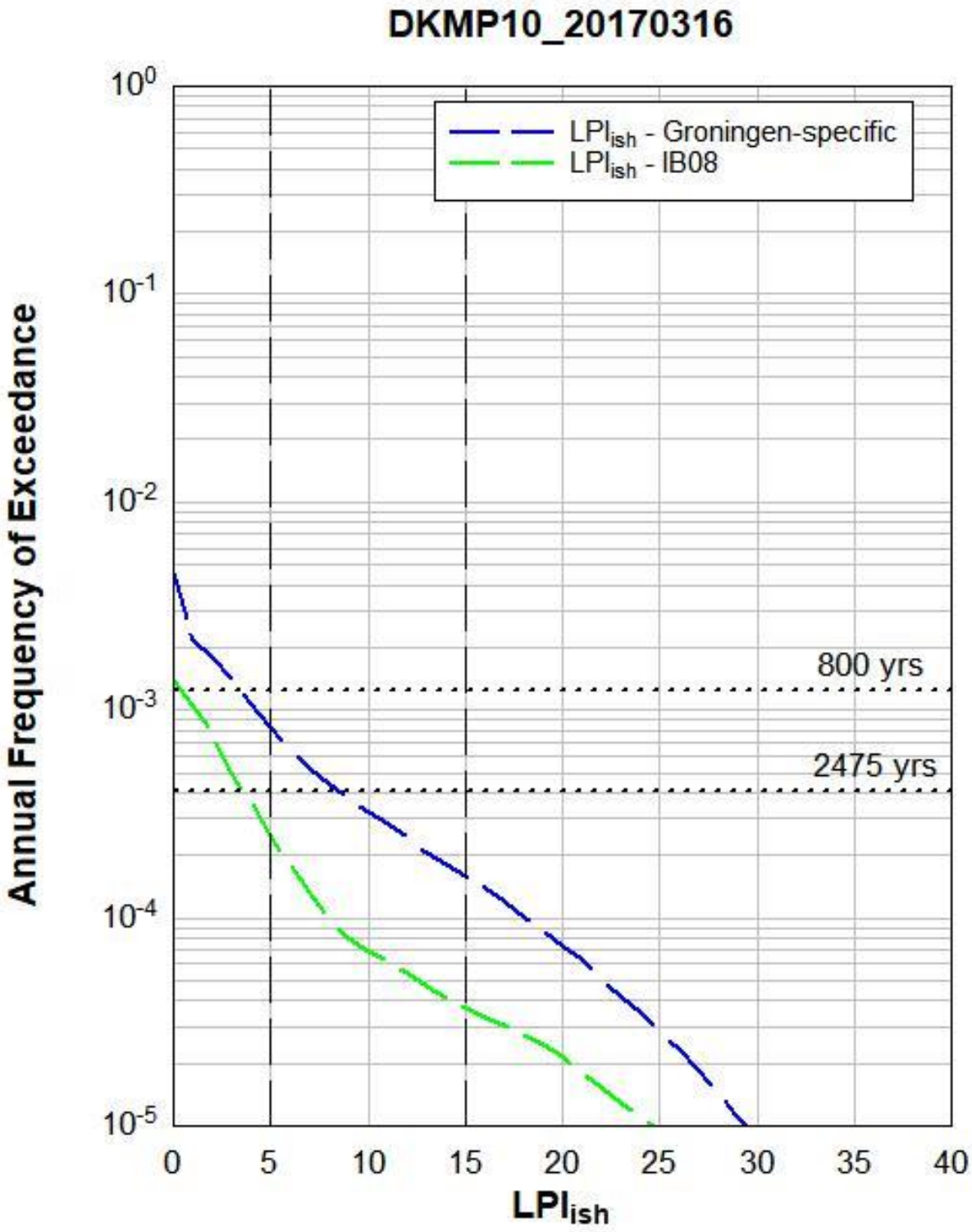
DKMP10_20170316
LPIish - Groningen-specific
LPIish - IB08
800 yrs
2475 yrs
Annual Frequency of Exceedance
LPIish
10^0
10^-1
10^-2
10^-3
10^-4
10^-5
0
5
10
15
20
25
30
35
40

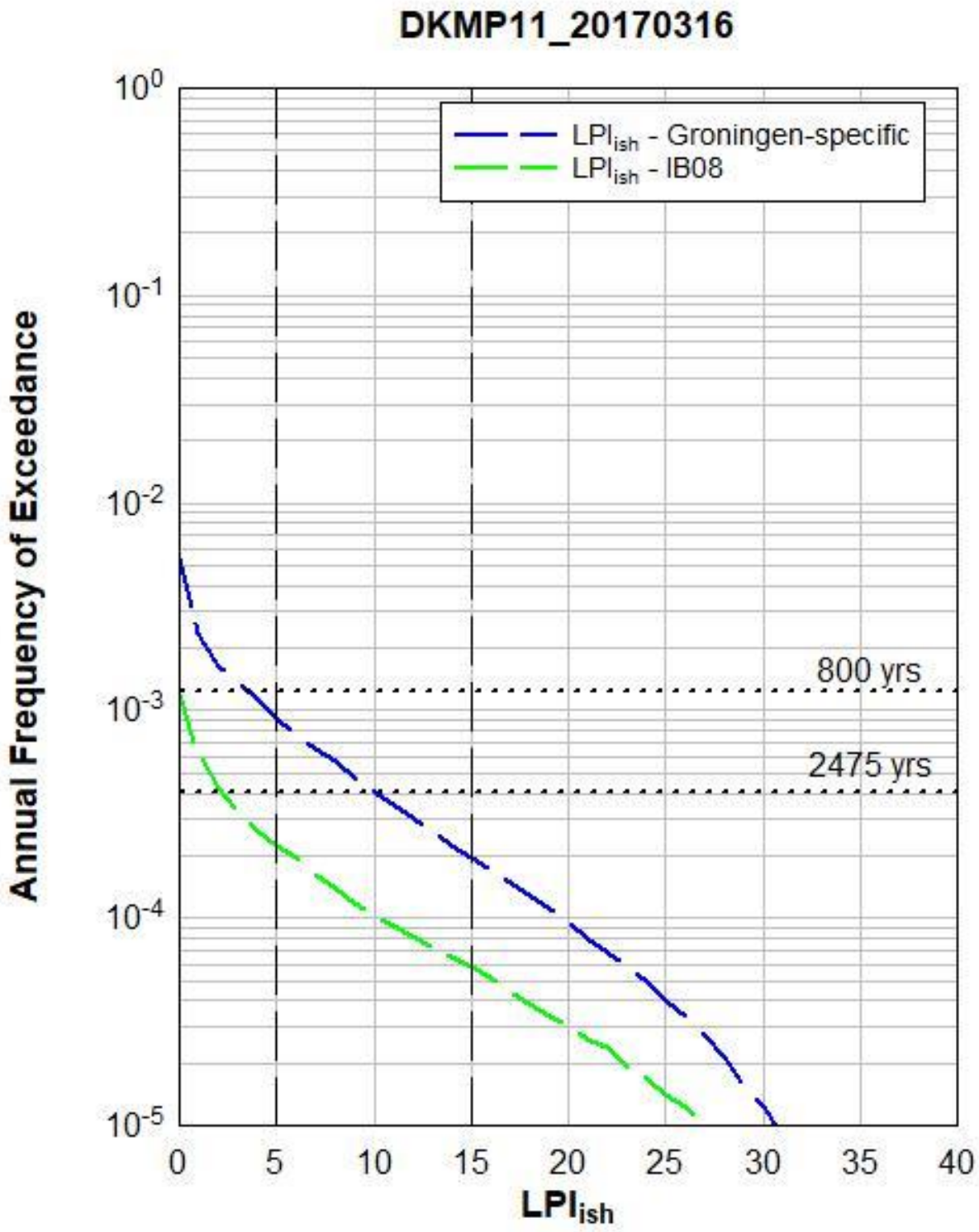
DKMP11_20170316
LPIish - Groningen-specific
LPIish - IB08
800 yrs
2475 yrs
Annual Frequency of Exceedance
LPIish
10^0
10^-1
10^-2
10^-3
10^-4
10^-5
0
5
10
15
20
25
30
35
40

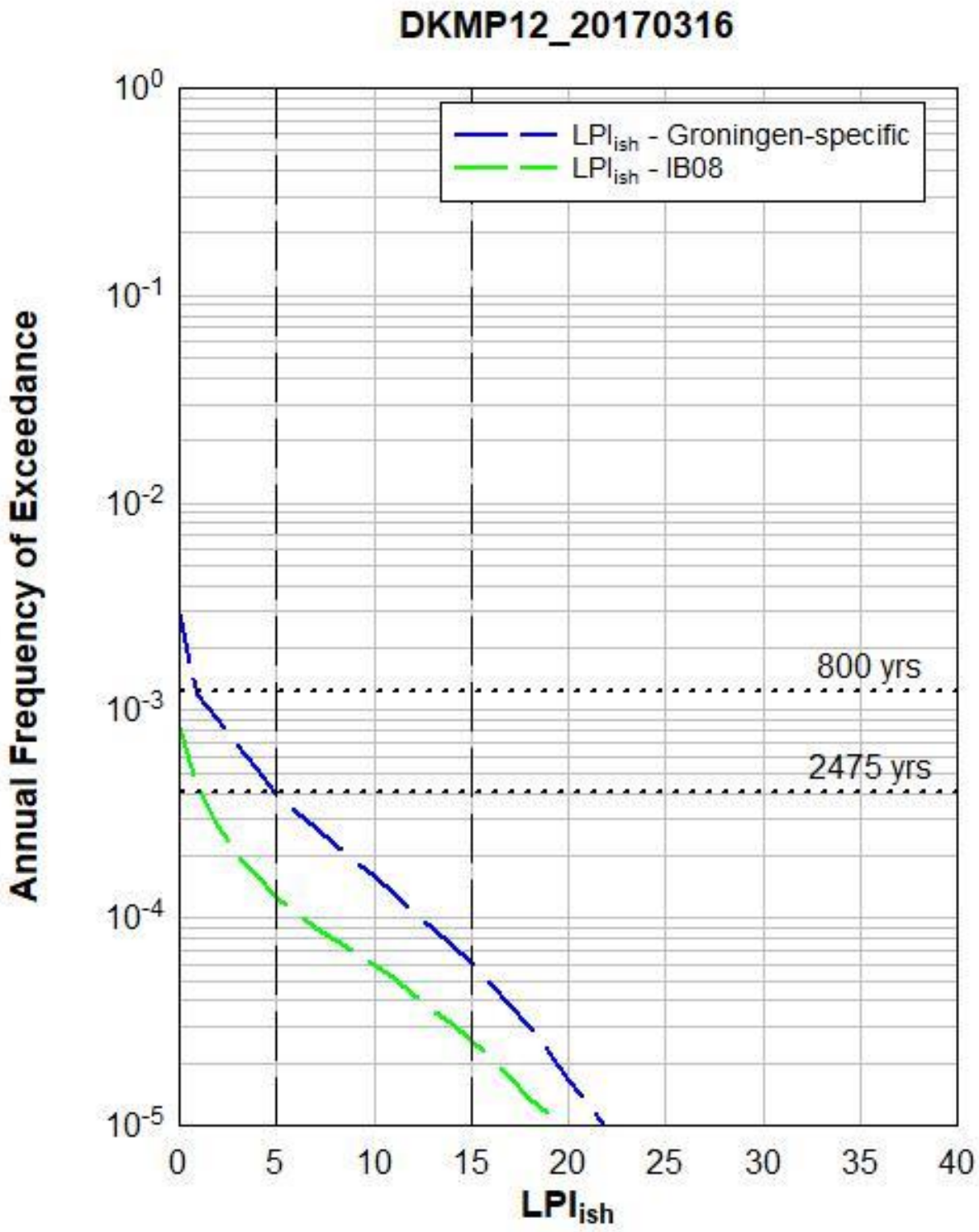
DKMP12_20170316
LPIish - Groningen-specific
LPIish - IB08
800 yrs
2475 yrs
Annual Frequency of Exceedance
LPIish
10^0
10^-1
10^-2
10^-3
10^-4
10^-5
0
5
10
15
20
25
30
35
40

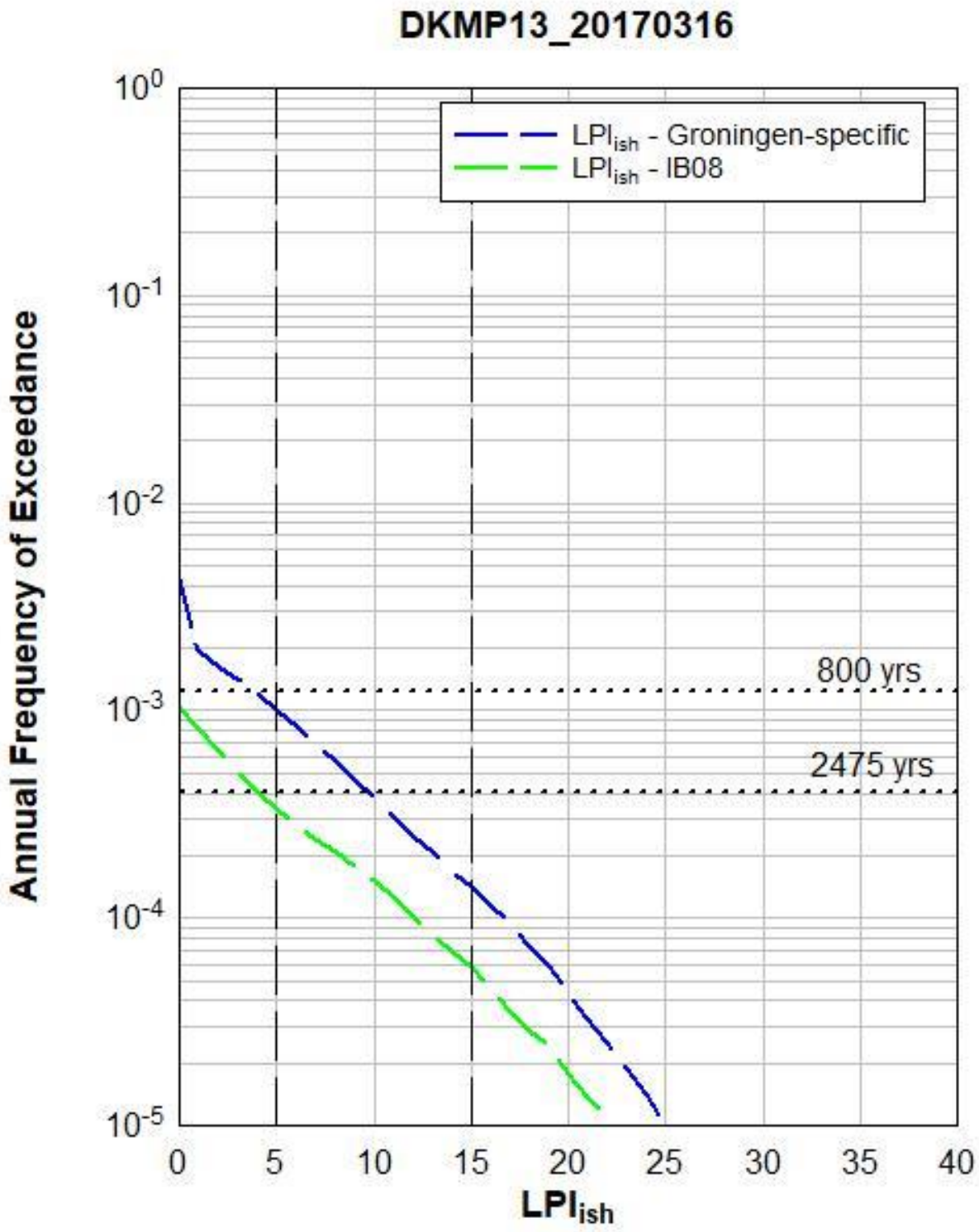
DKMP13_20170316
LPIish - Groningen-specific
LPIish - IB08
800 yrs
2475 yrs
Annual Frequency of Exceedance
LPIish
10^0
10^-1
10^-2
10^-3
10^-4
10^-5
0
5
10
15
20
25
30
35
40

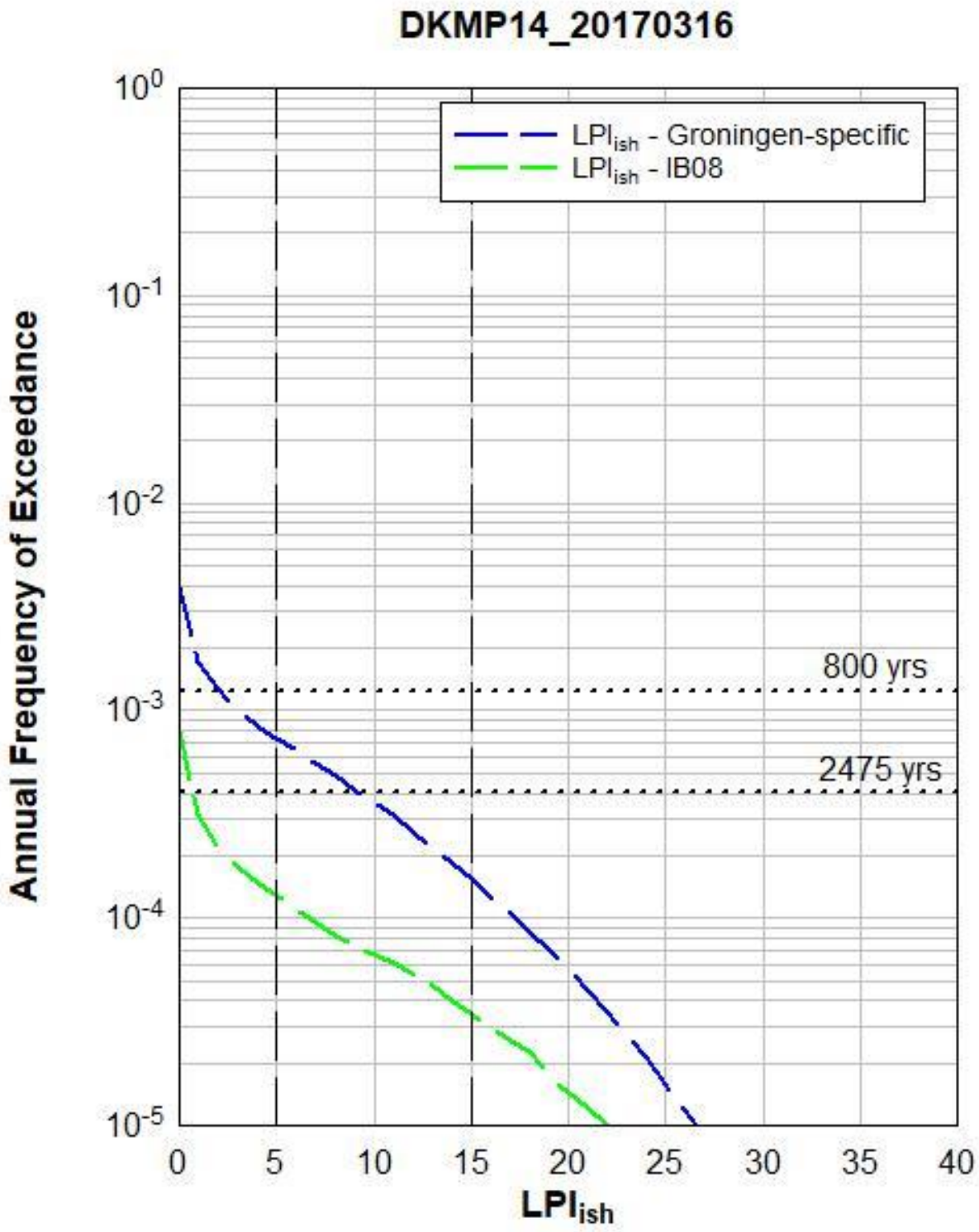
DKMP14_20170316
LPIish - Groningen-specific
LPIish - IB08
800 yrs
2475 yrs
Annual Frequency of Exceedance
LPIish
10^0
10^-1
10^-2
10^-3
10^-4
10^-5
0
5
10
15
20
25
30
35
40

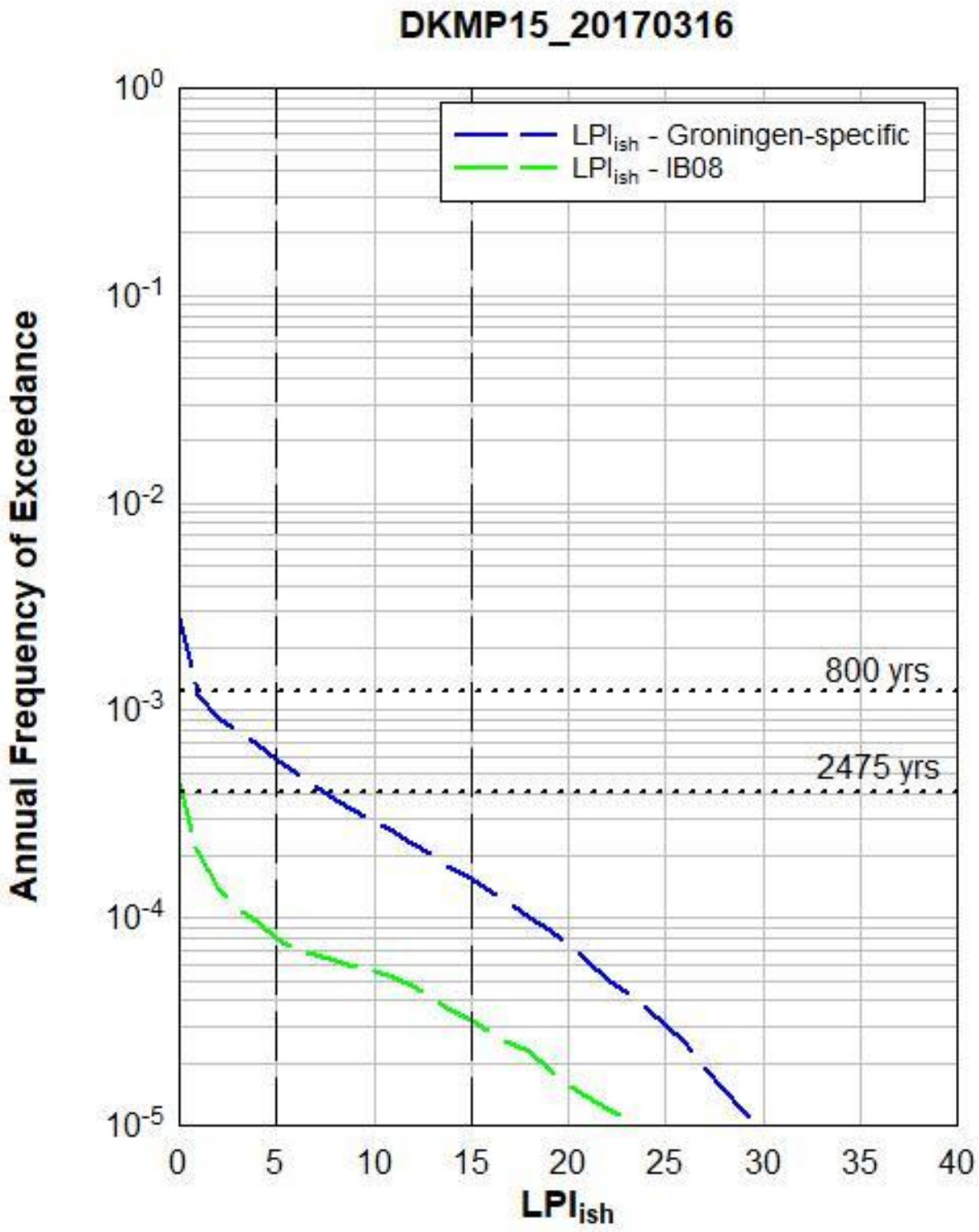
DKMP15_20170316
LPIish - Groningen-specific
LPIish - IB08
800 yrs
2475 yrs
Annual Frequency of Exceedance
LPIish
10^0
10^-1
10^-2
10^-3
10^-4
10^-5
0
5
10
15
20
25
30
35
40

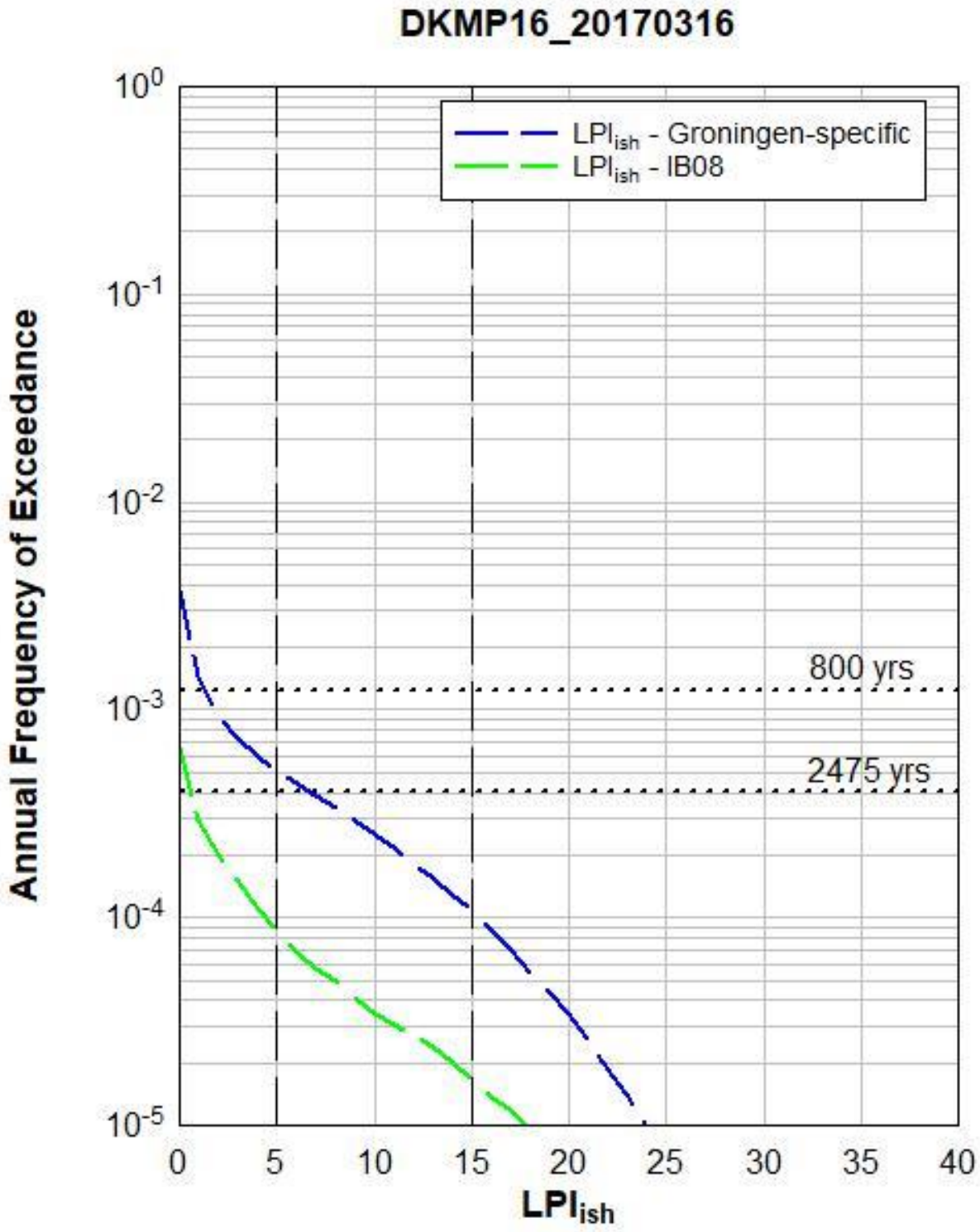
DKMP16_20170316
LPIish - Groningen-specific
LPIish - IB08
800 yrs
2475 yrs
Annual Frequency of Exceedance
LPIish
10^0
10^-1
10^-2
10^-3
10^-4
10^-5
0
5
10
15
20
25
30
35
40

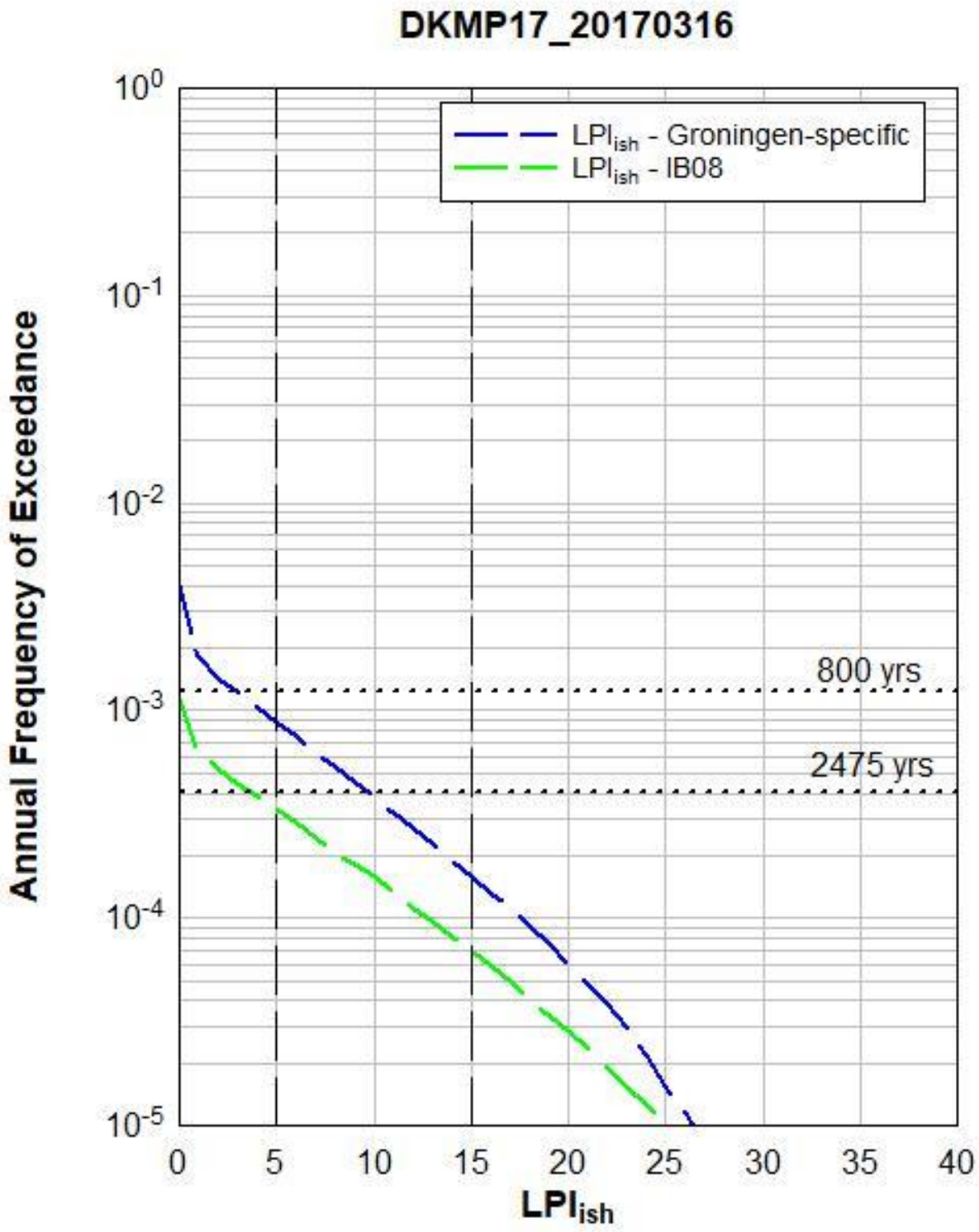
DKMP17_20170316
LPIish - Groningen-specific
LPIish - IB08
800 yrs
2475 yrs
Annual Frequency of Exceedance
LPIish
10^0
10^-1
10^-2
10^-3
10^-4
10^-5
0
5
10
15
20
25
30
35
40

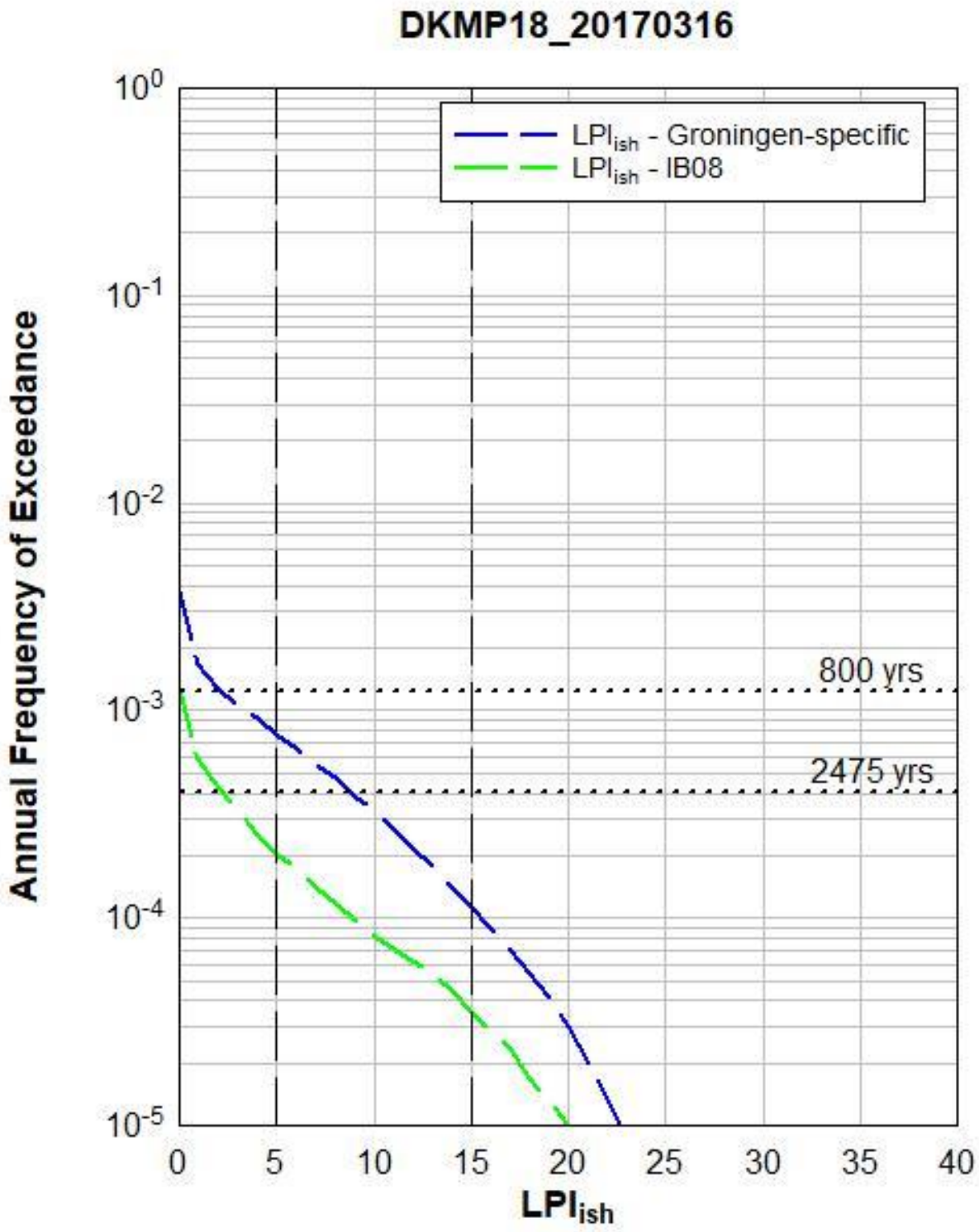
DKMP18_20170316
LPIish - Groningen-specific
LPIish - IB08
800 yrs
2475 yrs
Annual Frequency of Exceedance
LPIish
10^0
10^-1
10^-2
10^-3
10^-4
10^-5
0
5
10
15
20
25
30
35
40

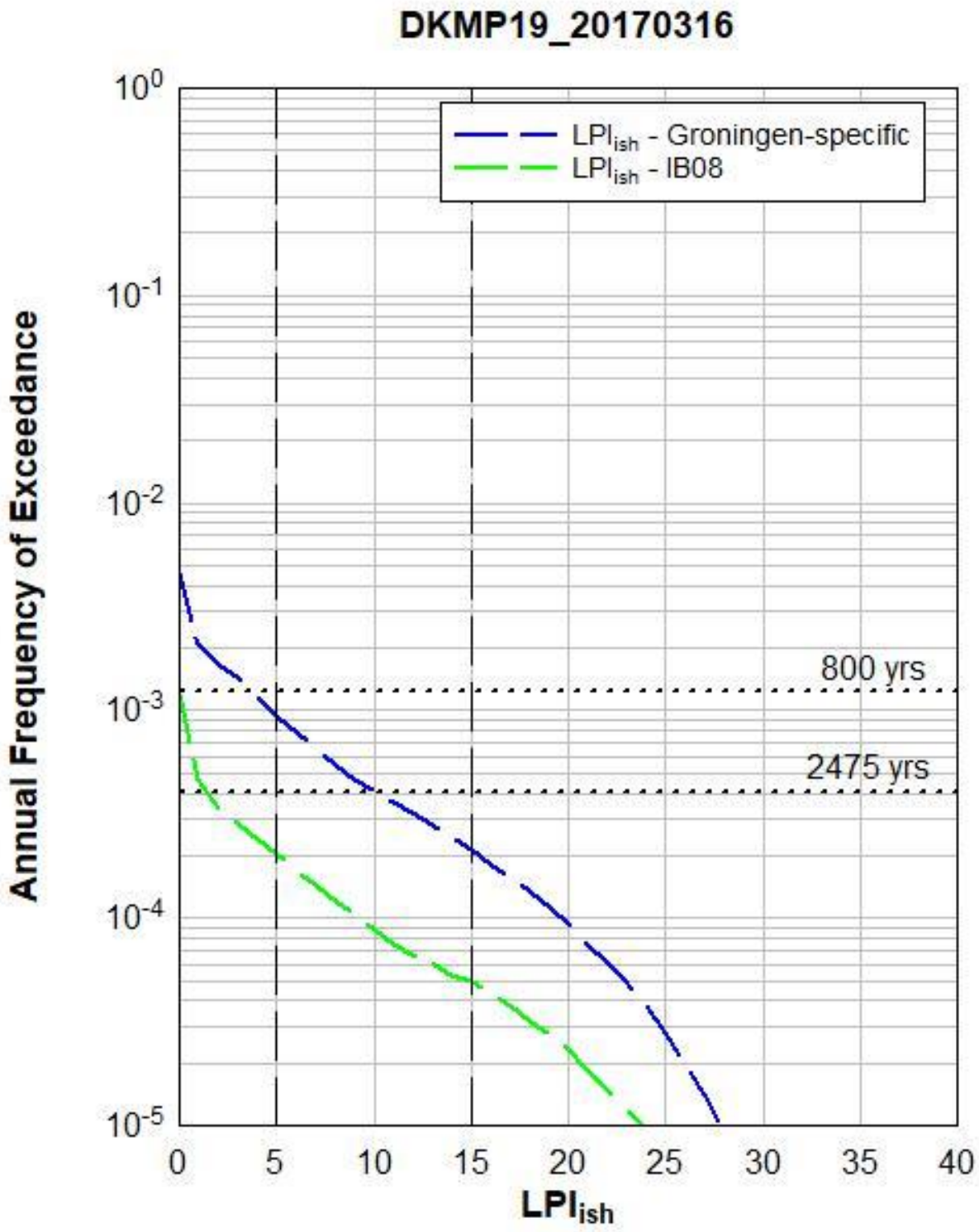
DKMP19_20170316
LPIish - Groningen-specific
LPIish - IB08
800 yrs
2475 yrs
Annual Frequency of Exceedance
LPIish
10^0
10^-1
10^-2
10^-3
10^-4
10^-5
0
5
10
15
20
25
30
35
40

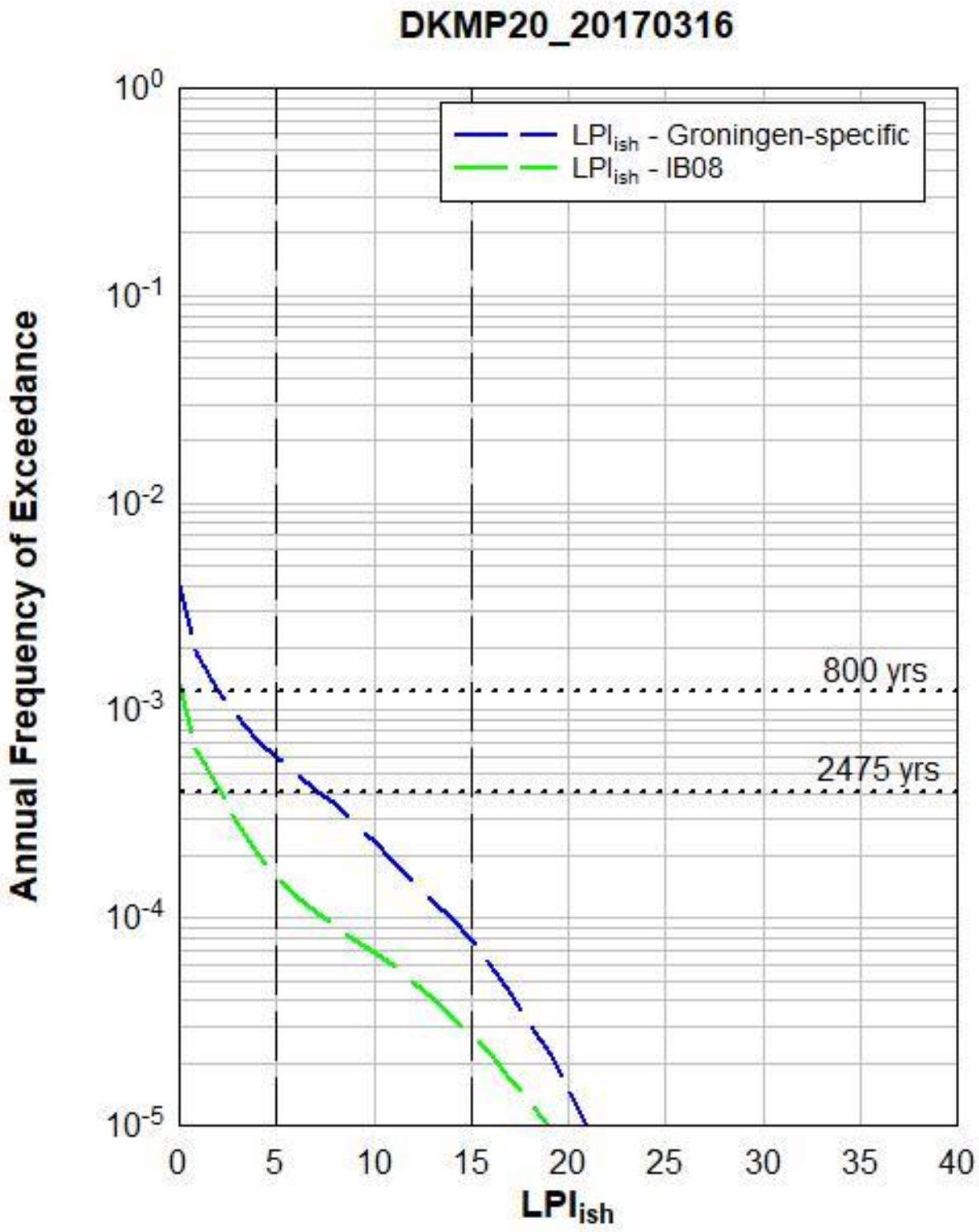
DKMP20_20170316
LPIish - Groningen-specific
LPIish - IB08
800 yrs
2475 yrs
Annual Frequency of Exceedance
LPIish
10^0
10^-1
10^-2
10^-3
10^-4
10^-5
0
5
10
15
20
25
30
35
40

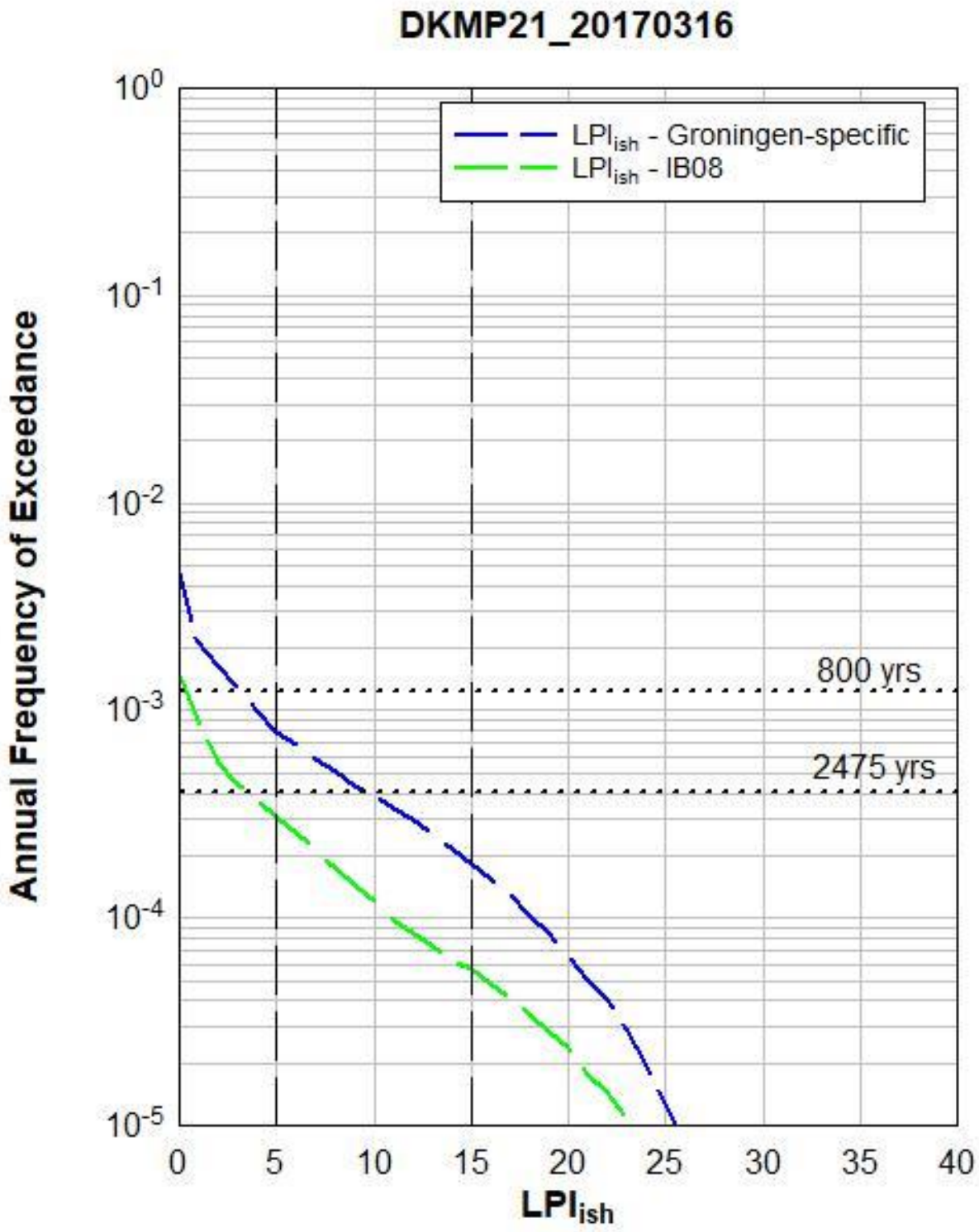
DKMP21_20170316
LPIish - Groningen-specific
LPIish - IB08
800 yrs
2475 yrs
Annual Frequency of Exceedance
LPIish
10^0
10^-1
10^-2
10^-3
10^-4
10^-5
0
5
10
15
20
25
30
35
40

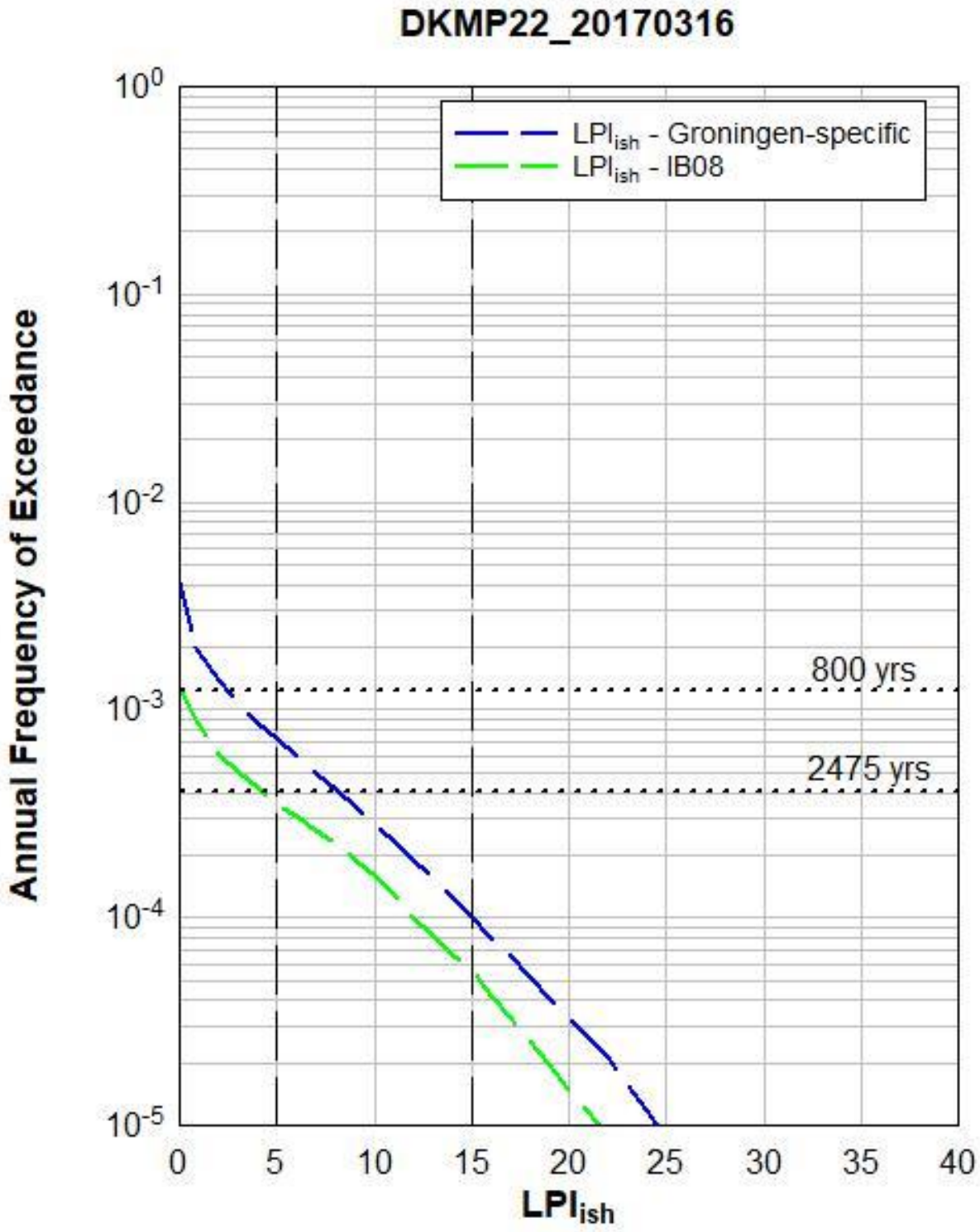
DKMP22_20170316
LPIish - Groningen-specific
LPIish - IB08
800 yrs
2475 yrs
Annual Frequency of Exceedance
LPIish
10^0
10^-1
10^-2
10^-3
10^-4
10^-5
0
5
10
15
20
25
30
35
40

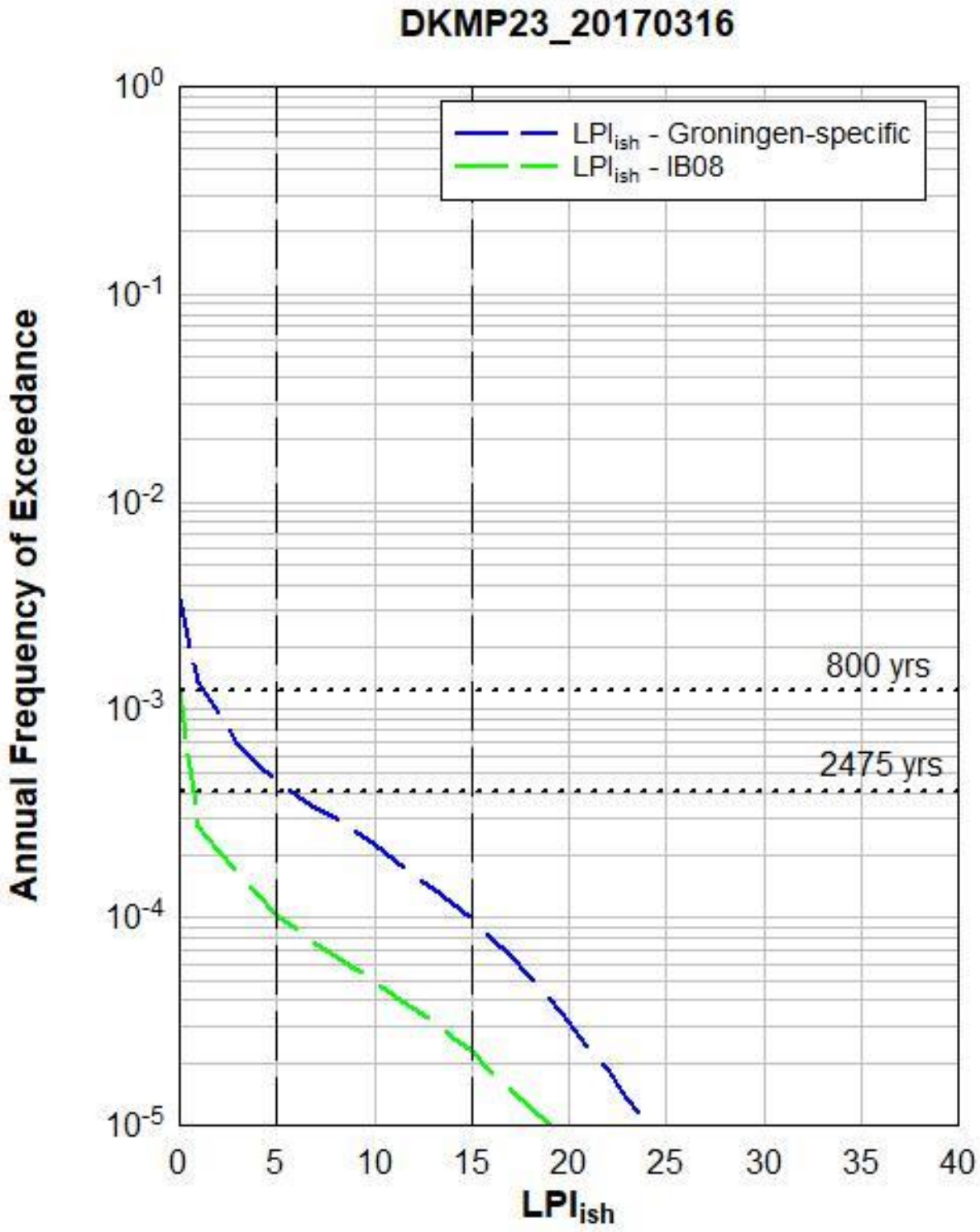
DKMP23_20170316
LPIish - Groningen-specific
LPIish - IB08
800 yrs
2475 yrs
Annual Frequency of Exceedance
LPIish
10^0
10^-1
10^-2
10^-3
10^-4
10^-5
0
5
10
15
20
25
30
35
40

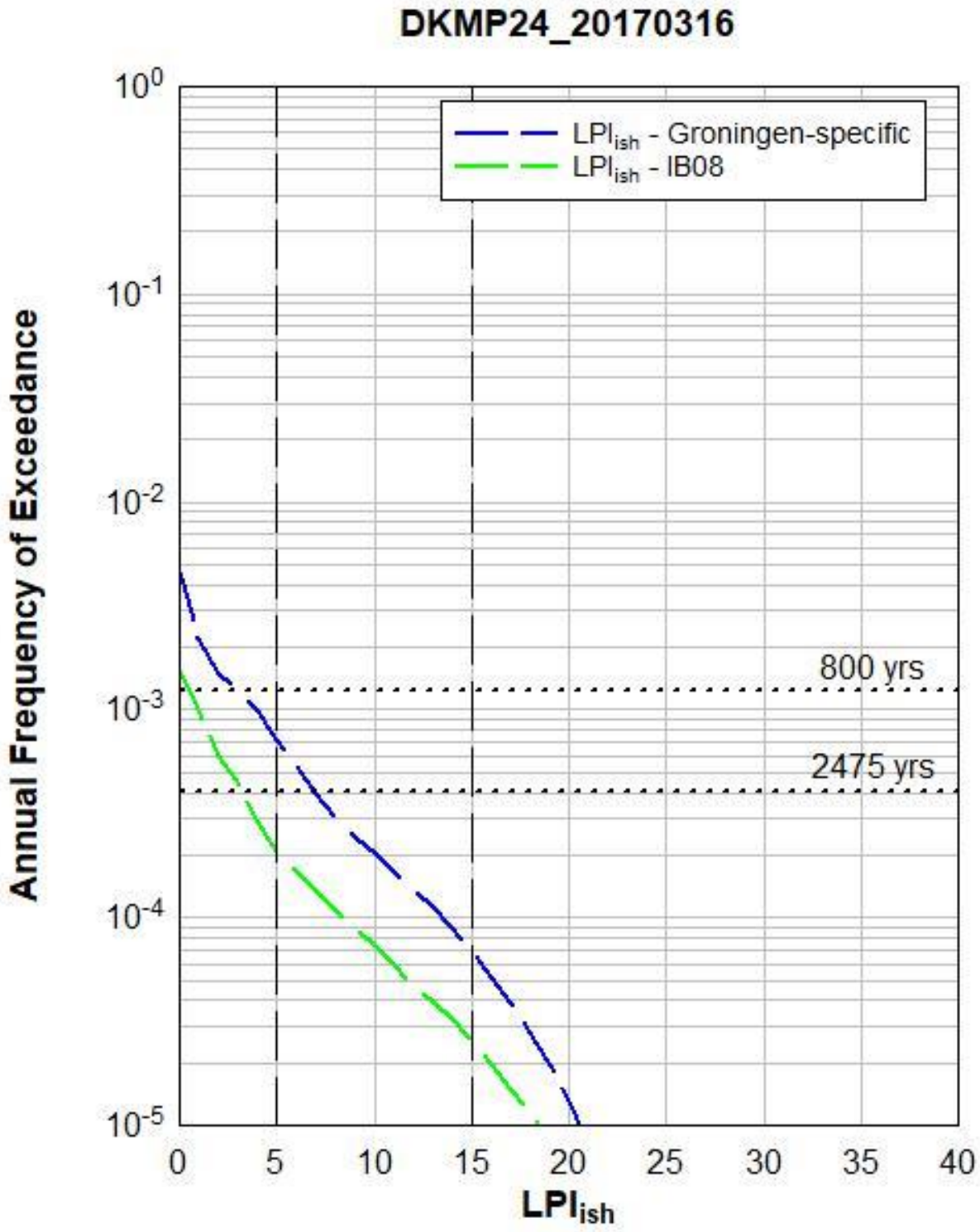
DKMP24_20170316
LPIish - Groningen-specific
LPIish - IB08
800 yrs
2475 yrs
Annual Frequency of Exceedance
LPIish
10^0
10^-1
10^-2
10^-3
10^-4
10^-5
0
5
10
15
20
25
30
35
40

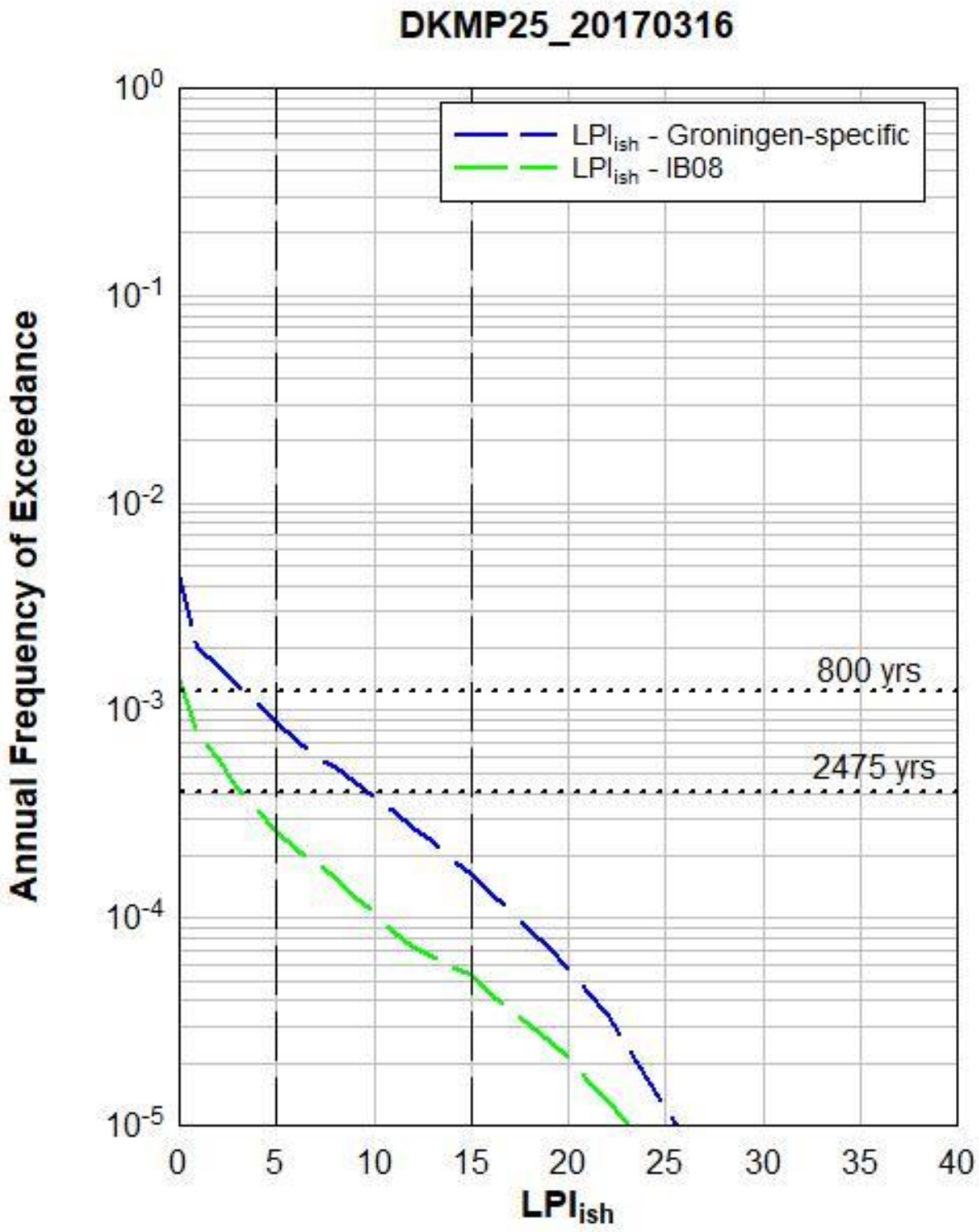
DKMP25_20170316
LPIish - Groningen-specific
LPIish - IB08
800 yrs
2475 yrs
Annual Frequency of Exceedance
LPIish
10^0
10^-1
10^-2
10^-3
10^-4
10^-5
0
5
10
15
20
25
30
35
40

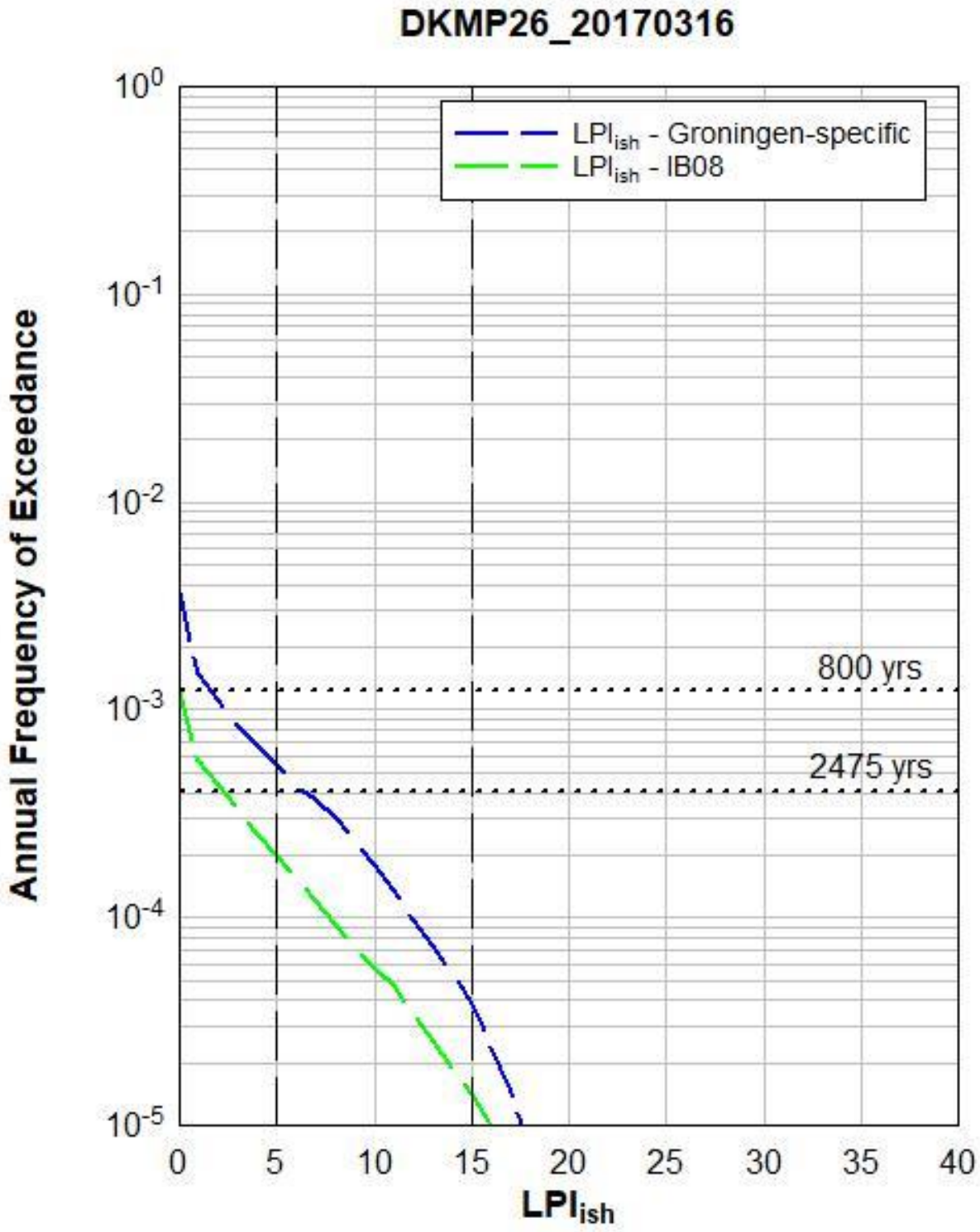
DKMP26_20170316
LPIish - Groningen-specific
LPIish - IB08
800 yrs
2475 yrs
Annual Frequency of Exceedance
LPIish
10^0
10^-1
10^-2
10^-3
10^-4
10^-5
0
5
10
15
20
25
30
35
40

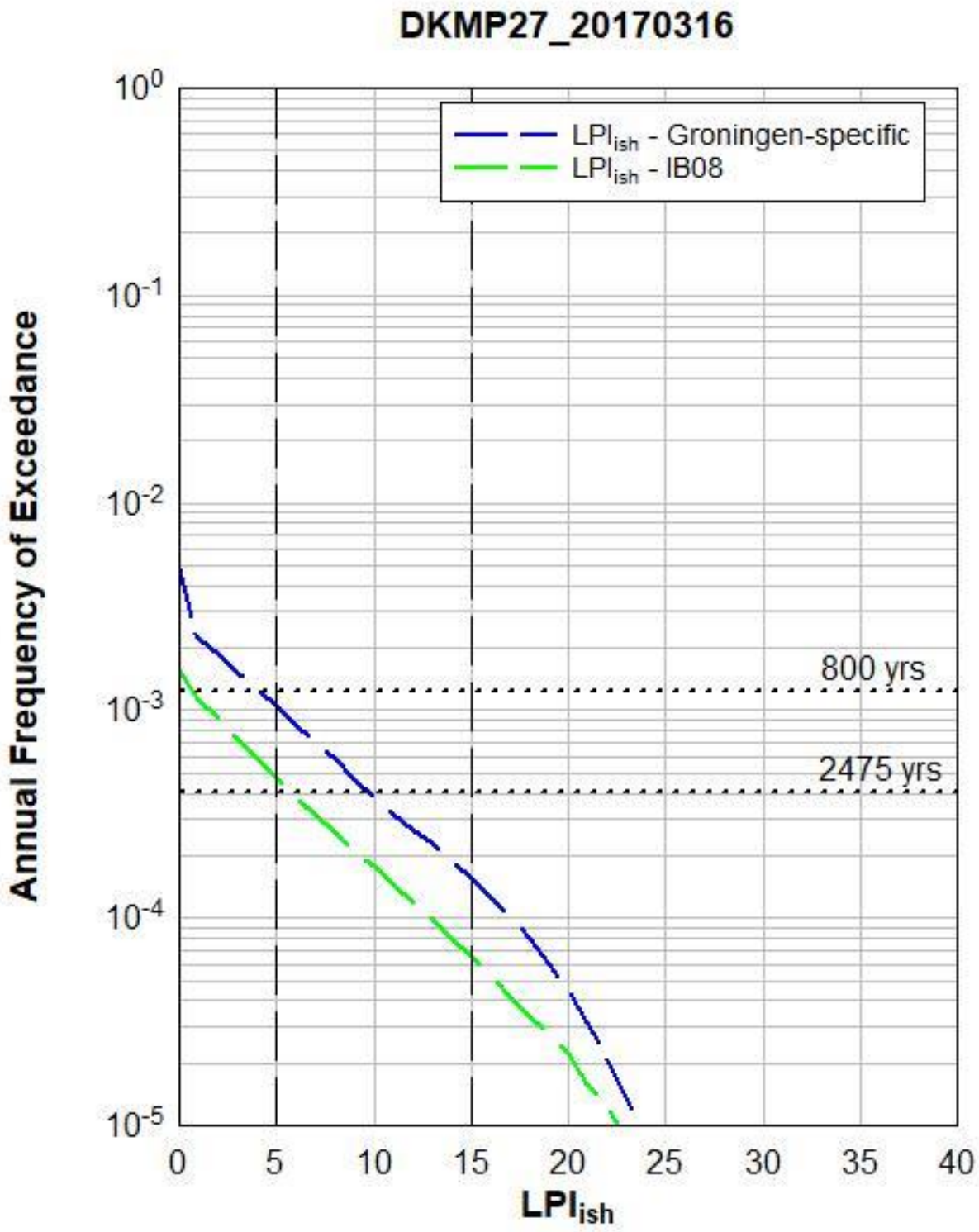
DKMP27_20170316
LPIish - Groningen-specific
LPIish - IB08
800 yrs
2475 yrs
Annual Frequency of Exceedance
LPIish
10^0
10^-1
10^-2
10^-3
10^-4
10^-5
0
5
10
15
20
25
30
35
40

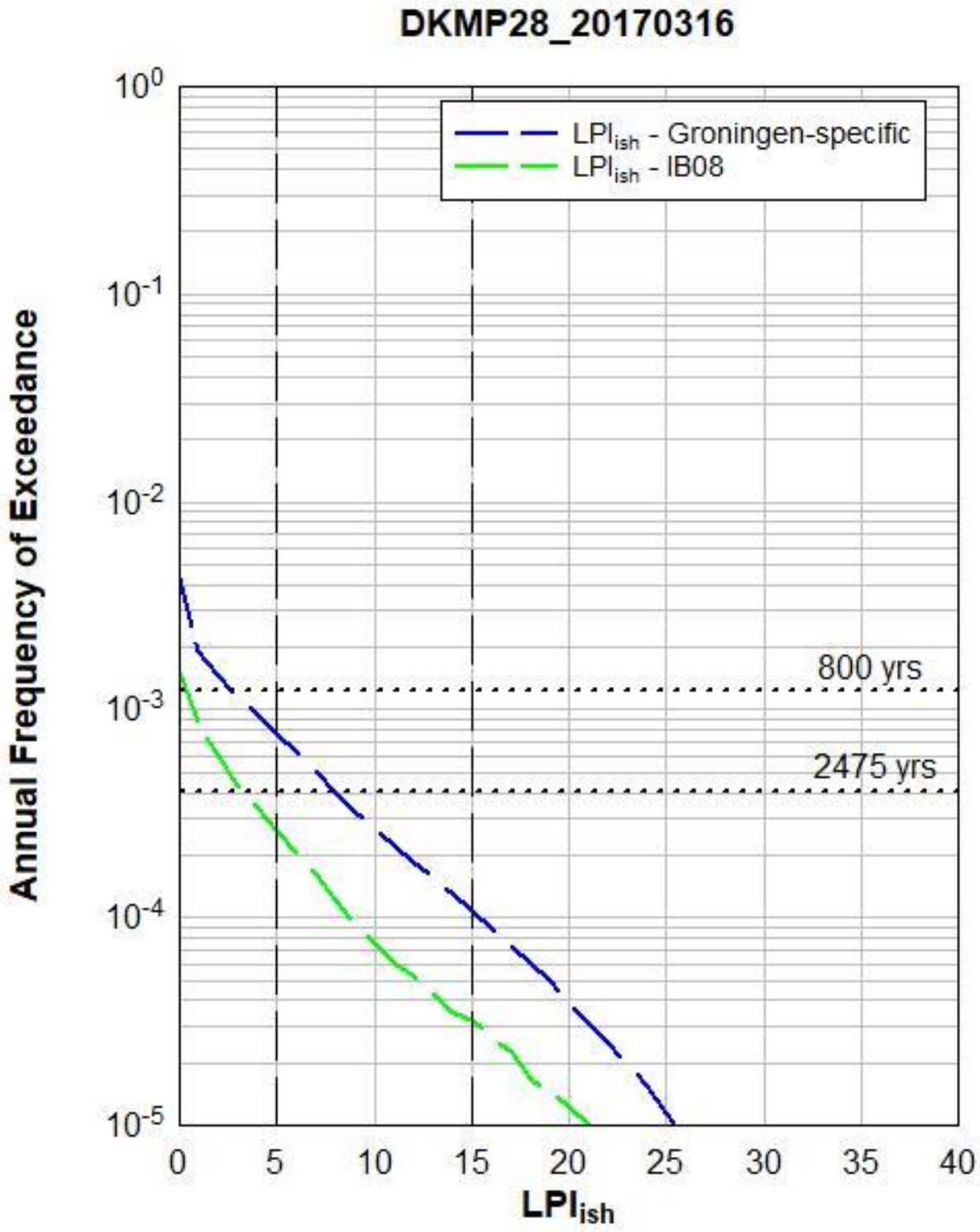
DKMP28_20170316
LPIish - Groningen-specific
LPIish - IB08
800 yrs
2475 yrs
Annual Frequency of Exceedance
LPIish
10^0
10^-1
10^-2
10^-3
10^-4
10^-5
0
5
10
15
20
25
30
35
40

Zone 604


LPI$_{ish}$ < 5
5 ≤ LPI$_{ish}$ ≤ 15
LPI$_{ish}$ > 15
5012-0076-000_DKM2
603
Zandeweer
S03G00050
DKMP2_20170316
DKMP8_20170316
DKMP7_20170316
DKMP6_20170316
DKMP12_20170316
S03G00078
S03G00043
S03G00056
604
S07E00166
1001
5004-0083-000_D2
5006-0664-000_DKM1

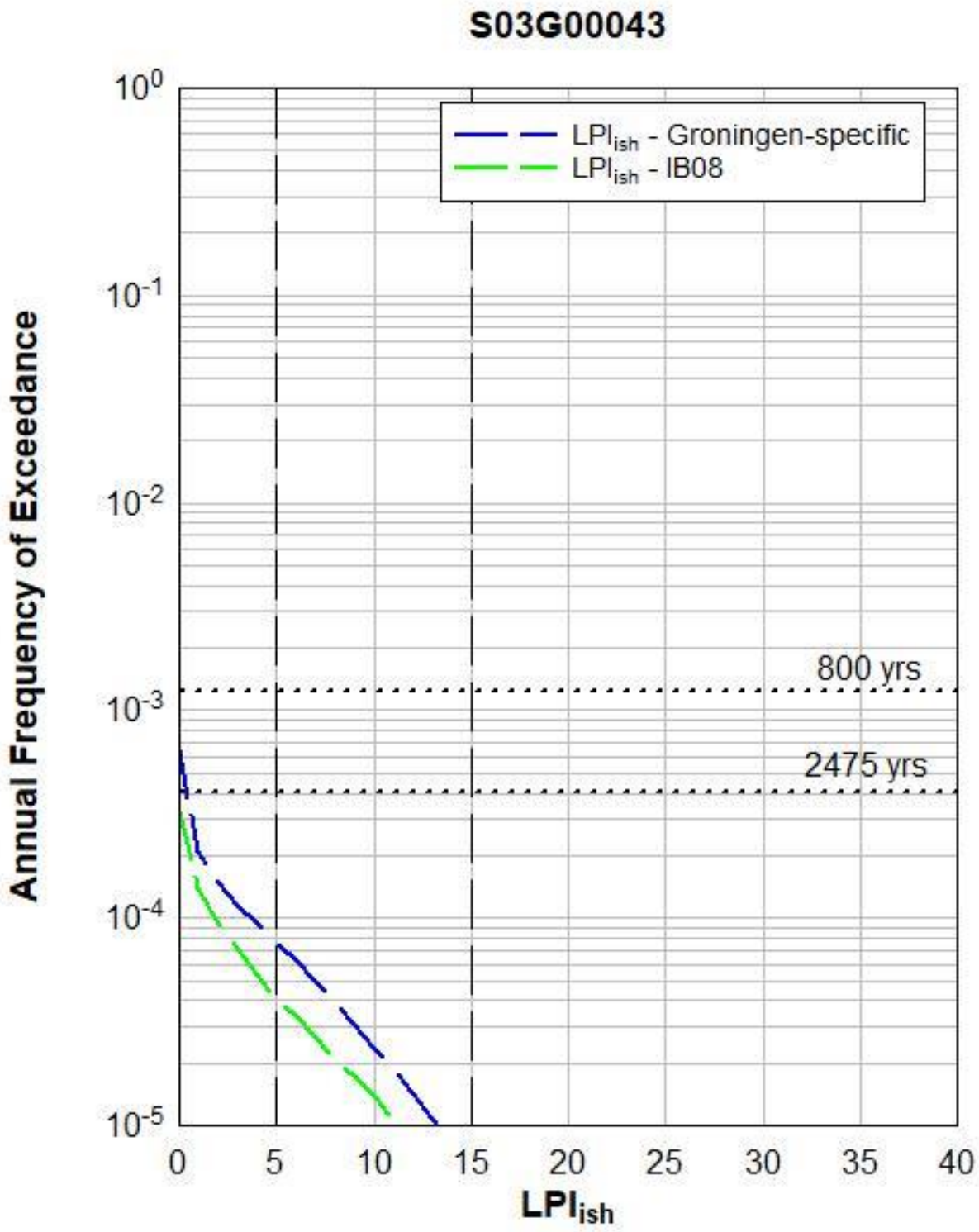
S03G00043
LPIish - Groningen-specific
LPIish - IB08
800 yrs
2475 yrs
Annual Frequency of Exceedance
LPIish
10^0
10^-1
10^-2
10^-3
10^-4
10^-5
0
5
10
15
20
25
30
35
40

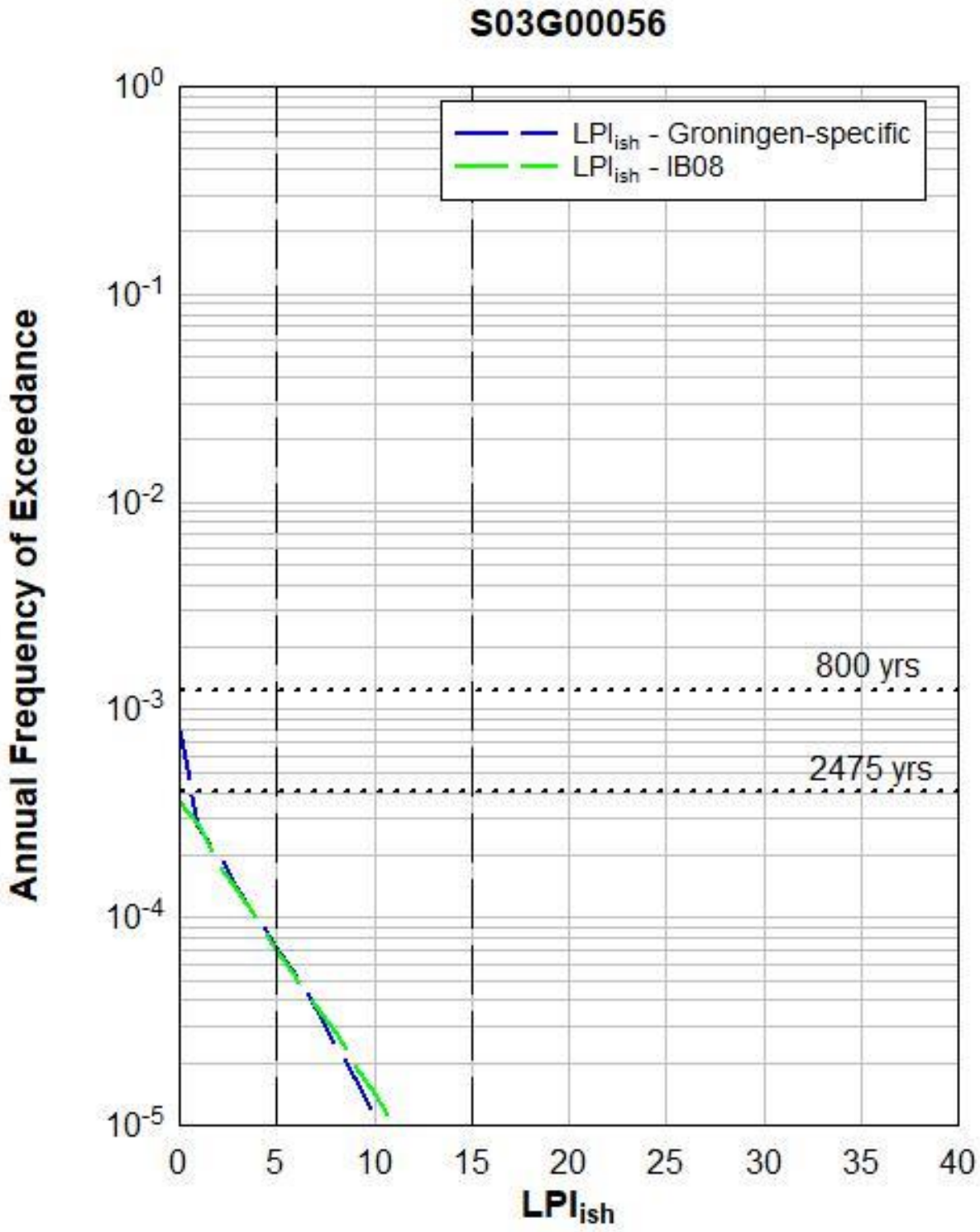
S03G00056
LPIish - Groningen-specific
LPIish - IB08
800 yrs
2475 yrs
Annual Frequency of Exceedance
LPIish
10^0
10^-1
10^-2
10^-3
10^-4
10^-5
0
5
10
15
20
25
30
35
40

Zone 1001


604
S03G00043
S03G00056
S07E00166
5004-0083-000_D2
5006-0664-000_DKM1
1001
S07E00176
602
S07E00153
6012-0102-000_DKMP733-4
S07E00151
LPI$_{ish}$ < 5
5 ≤ LPI$_{ish}$ ≤ 15
LPI$_{ish}$ > 15

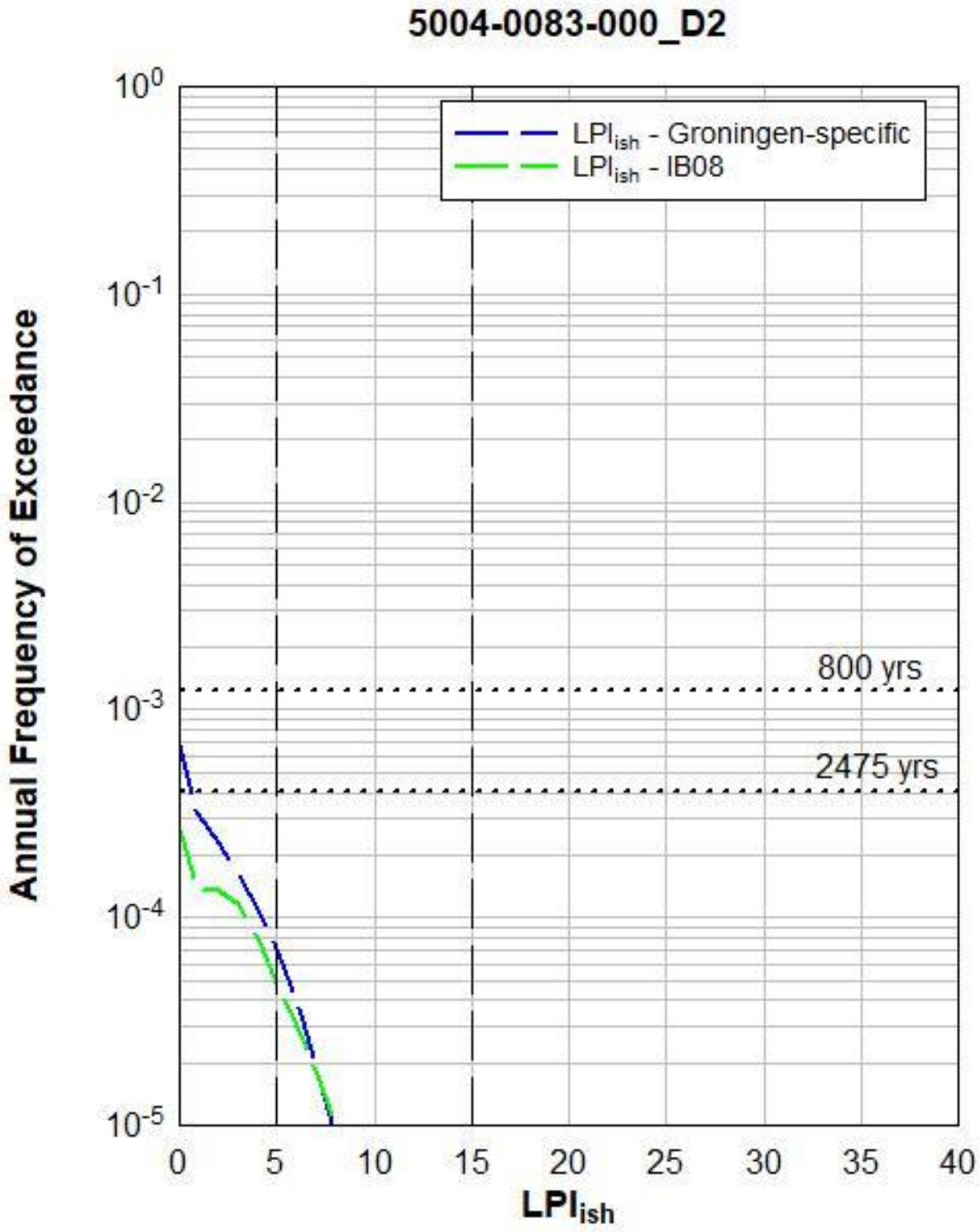
5004-0083-000_D2
LPIish - Groningen-specific
LPIish - IB08
800 yrs
2475 yrs
Annual Frequency of Exceedance
LPIish
10^0
10^-1
10^-2
10^-3
10^-4
10^-5
0
5
10
15
20
25
30
35
40

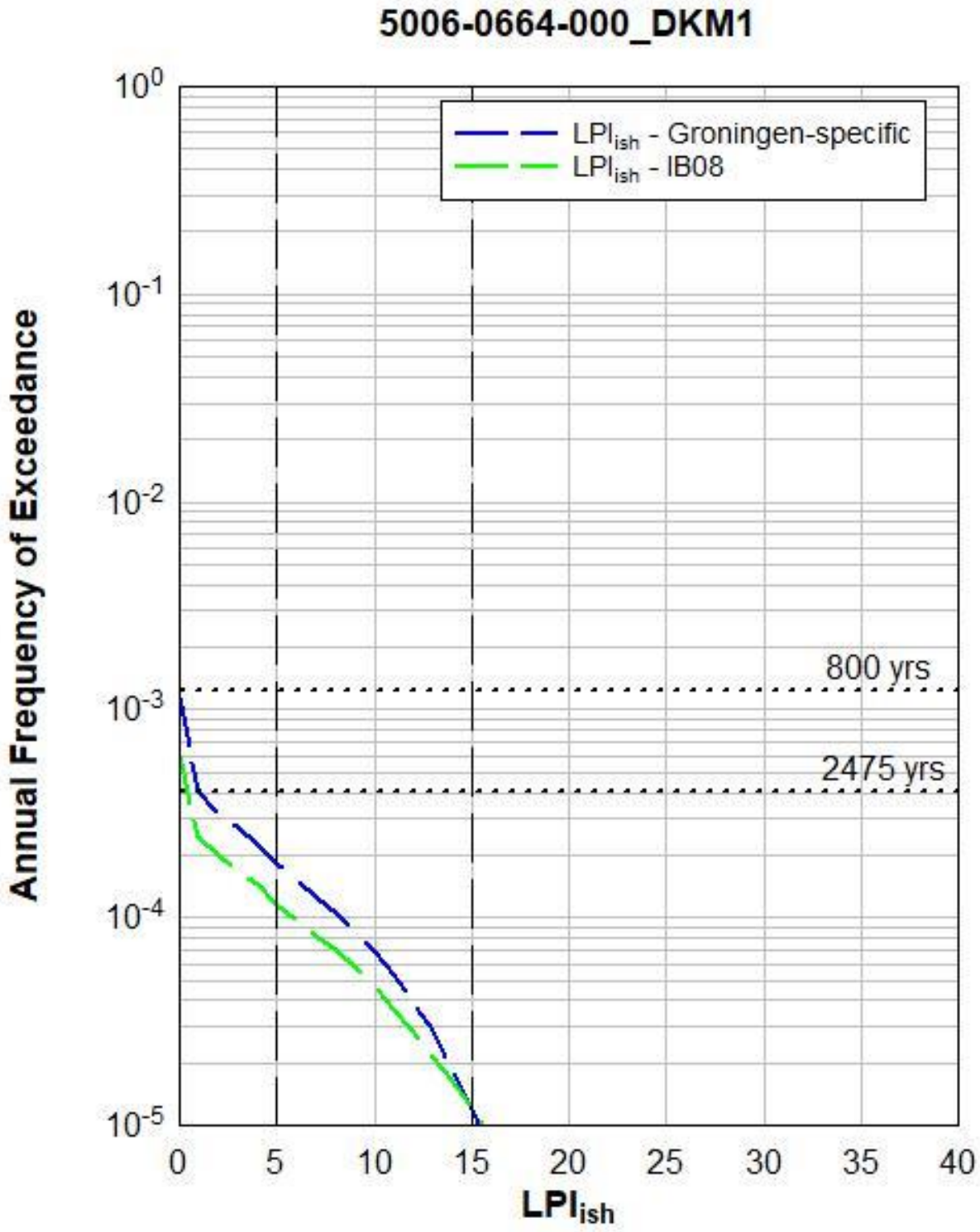
5006-0664-000_DKM1
LPIish - Groningen-specific
LPIish - IB08
800 yrs
2475 yrs
Annual Frequency of Exceedance
LPIish
10^0
10^-1
10^-2
10^-3
10^-4
10^-5
0
5
10
15
20
25
30
35
40

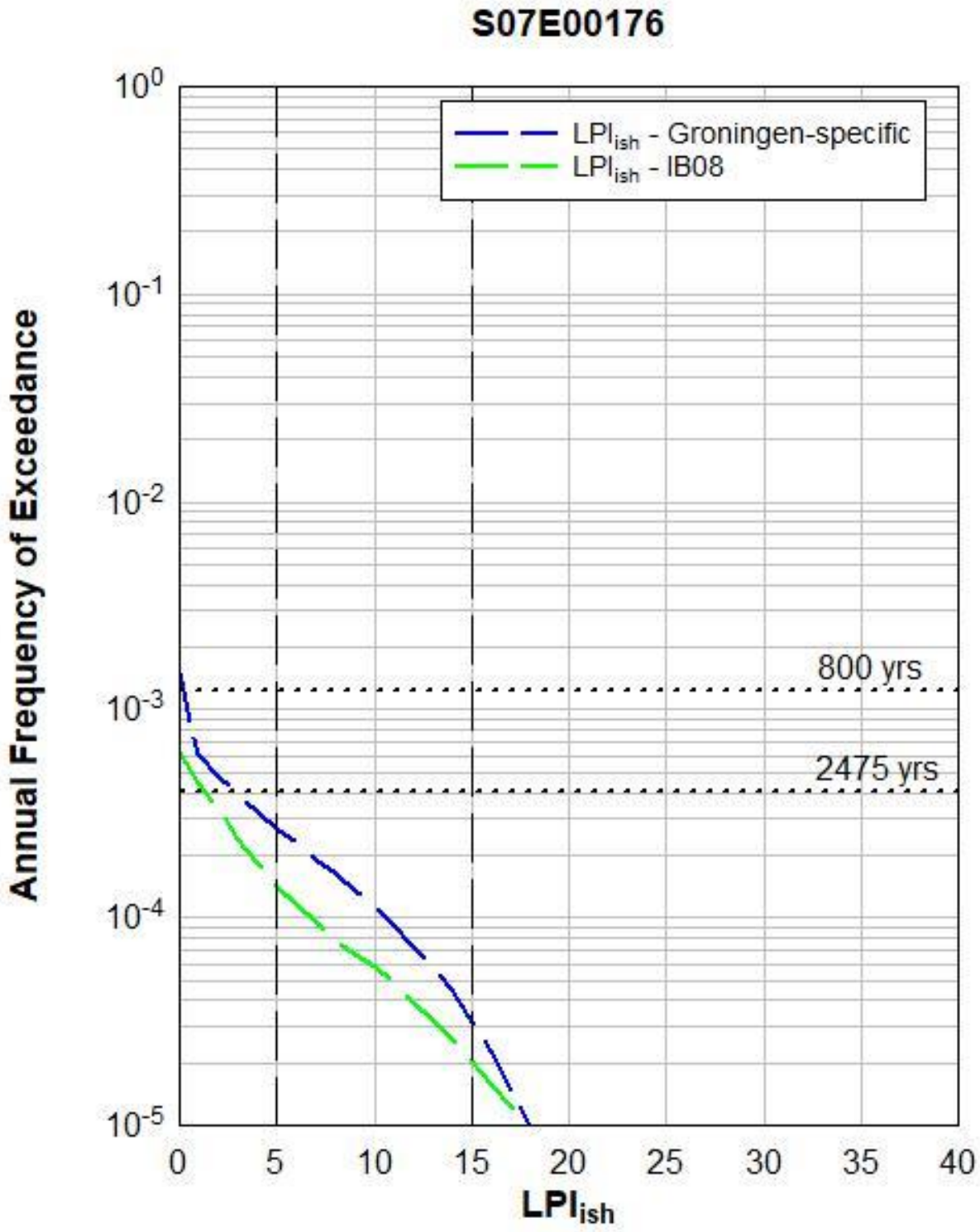
S07E00176
LPIish - Groningen-specific
LPIish - IB08
800 yrs
2475 yrs
Annual Frequency of Exceedance
LPIish
10^0
10^-1
10^-2
10^-3
10^-4
10^-5
0
5
10
15
20
25
30
35
40

Zone 602


LPIish < 5
5 ≤ LPIish ≤ 15
LPIish > 15
602
S07E00176
6012-0102-000_DKMP734-2
S07E00153
6012-0102-000_DKMP733-4
S07E00152
6012-0102-000_DKMP732-1
S07E00151
S07E00147
6012-0102-000_DKMP731-4
6012-0102-000_DKMP730-3
1032
S07E00146
6012-0102-000_DKMP729-2
S07E00145
6012-0102-000_DKMP729-1A
5007-0073-000_DKM1
6012-0102-000_DKMP728-4
5004-0308-000_DKM2
6012-0102-000_DKMP728-1A
S07E00142
6012-0102-000_DKMP727-3
S07E00036
2001
G08169000_D2
5009-0271-001_DKMP3
5009-0271-001_DKMP2
Q02332000_D1
5009-0271-001_DKMP1
G08098000_DKM1
LOPPERSUM

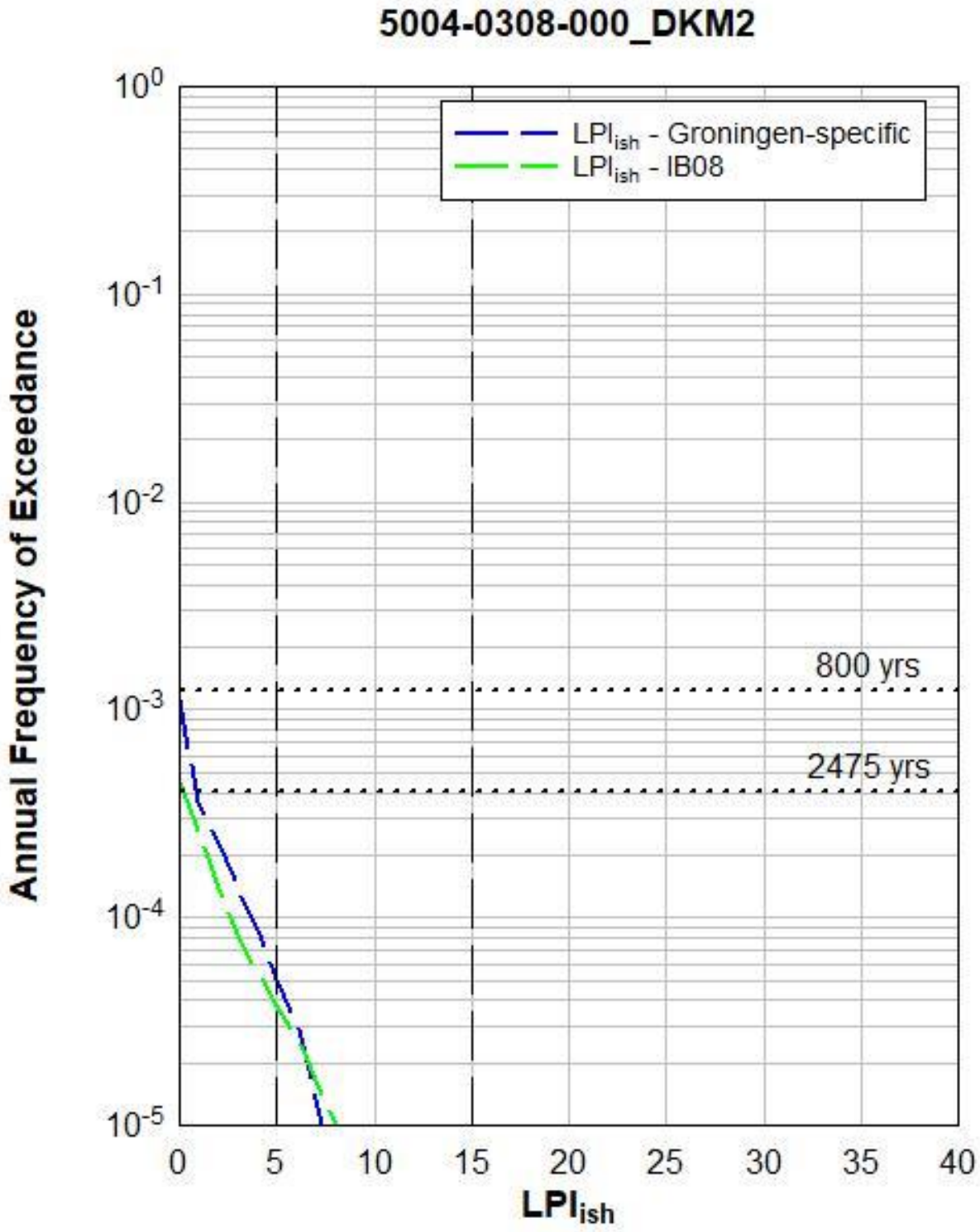
5004-0308-000_DKM2
LPIish - Groningen-specific
LPIish - IB08
800 yrs
2475 yrs
Annual Frequency of Exceedance
LPIish
10^0
10^-1
10^-2
10^-3
10^-4
10^-5
0
5
10
15
20
25
30
35
40

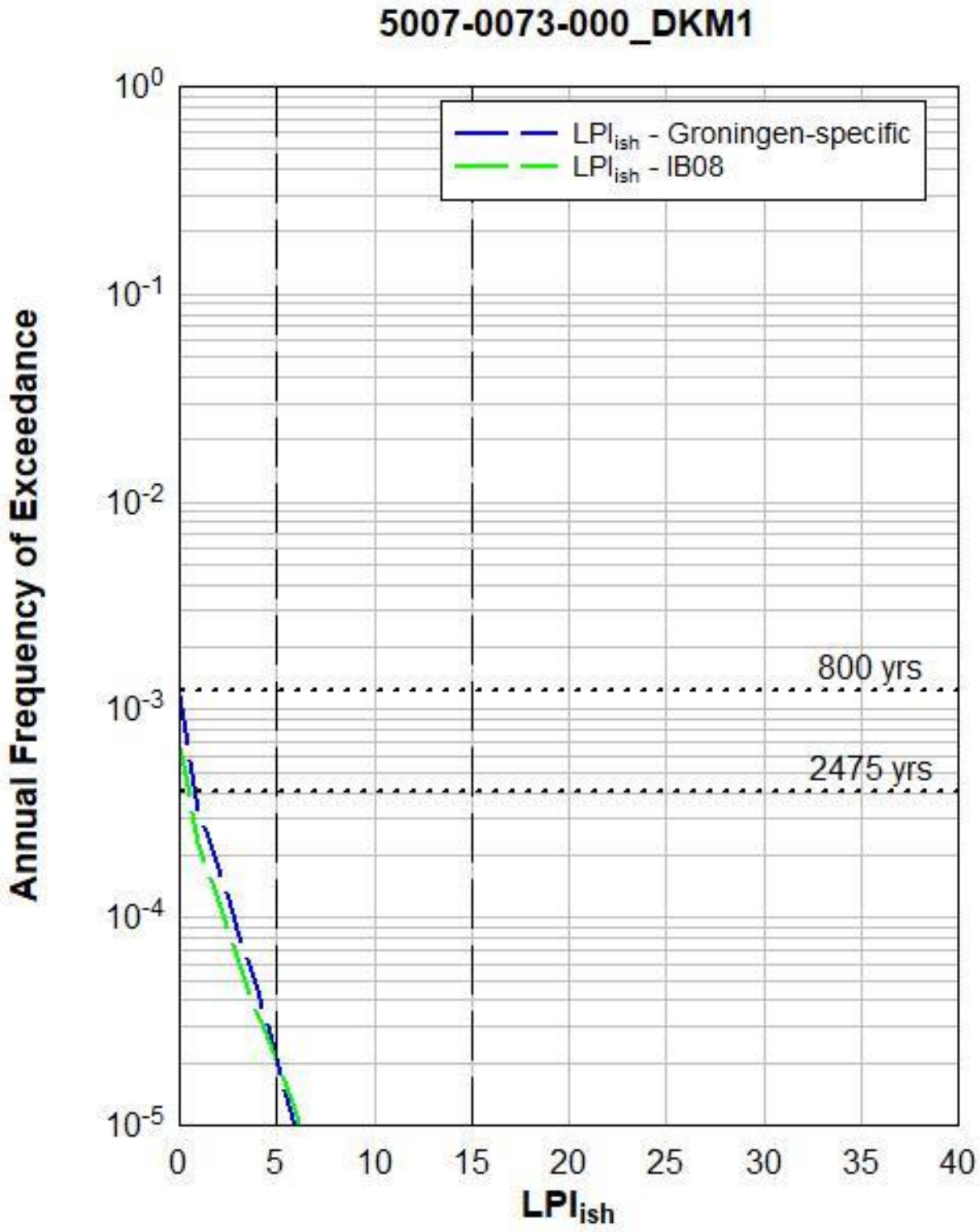
5007-0073-000_DKM1
LPIish - Groningen-specific
LPIish - IB08
800 yrs
2475 yrs
Annual Frequency of Exceedance
LPIish
10^0
10^-1
10^-2
10^-3
10^-4
10^-5
0
5
10
15
20
25
30
35
40

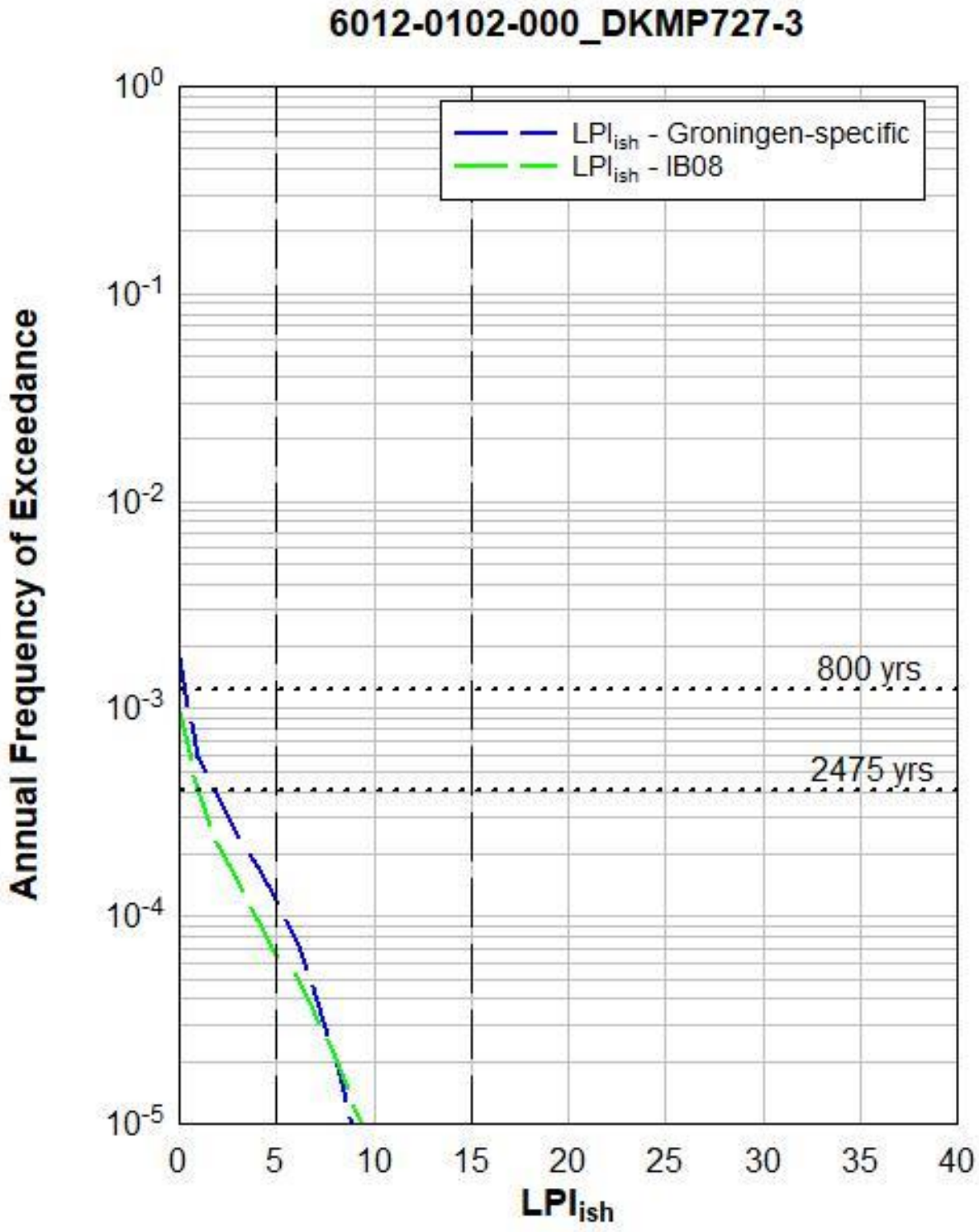
6012-0102-000_DKMP727-3
LPIish - Groningen-specific
LPIish - IB08
800 yrs
2475 yrs
Annual Frequency of Exceedance
LPIish
10^0
10^-1
10^-2
10^-3
10^-4
10^-5
0
5
10
15
20
25
30
35
40

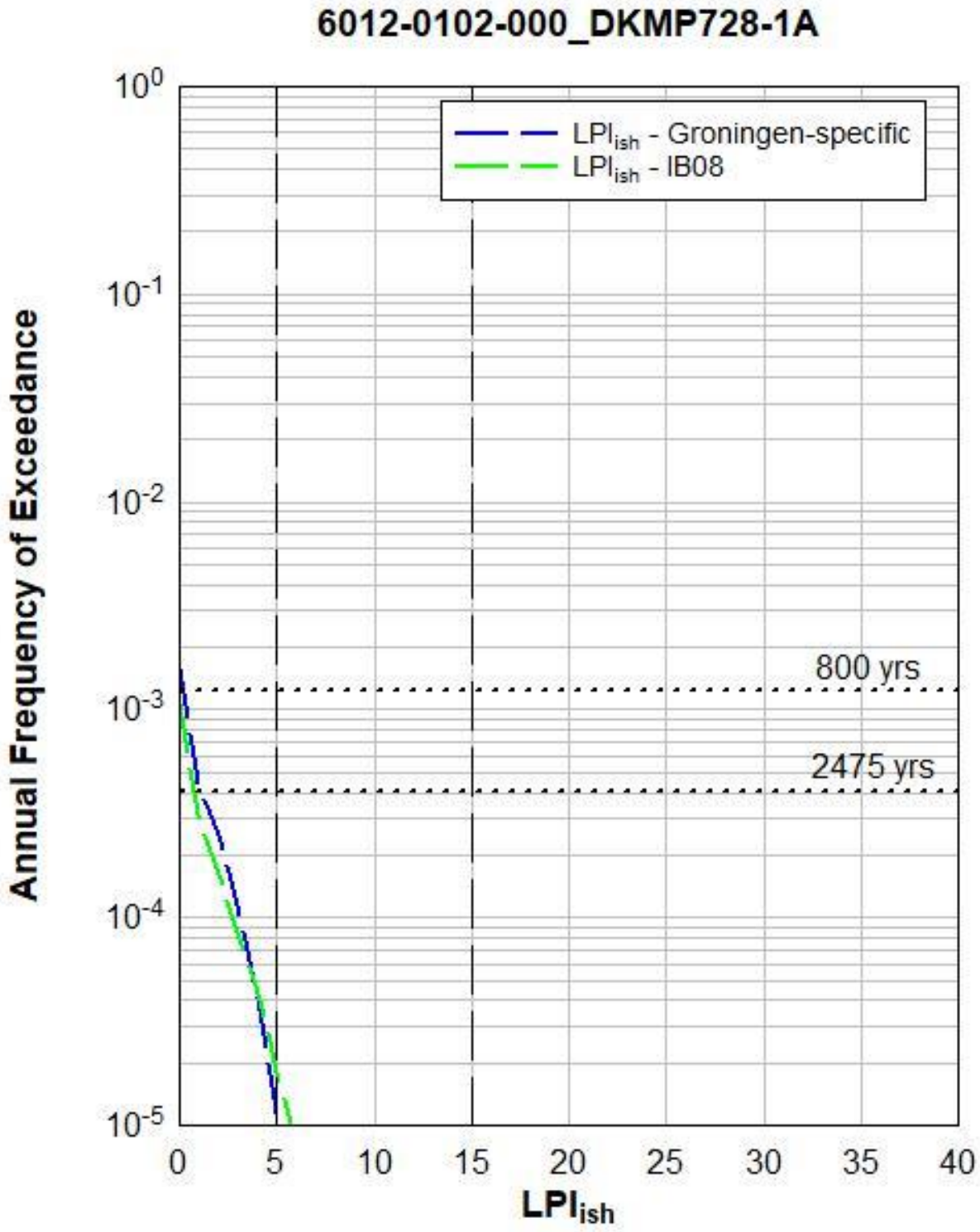
6012-0102-000_DKMP728-1A
LPIish - Groningen-specific
LPIish - IB08
800 yrs
2475 yrs
Annual Frequency of Exceedance
LPIish
10^0
10^-1
10^-2
10^-3
10^-4
10^-5
0
5
10
15
20
25
30
35
40

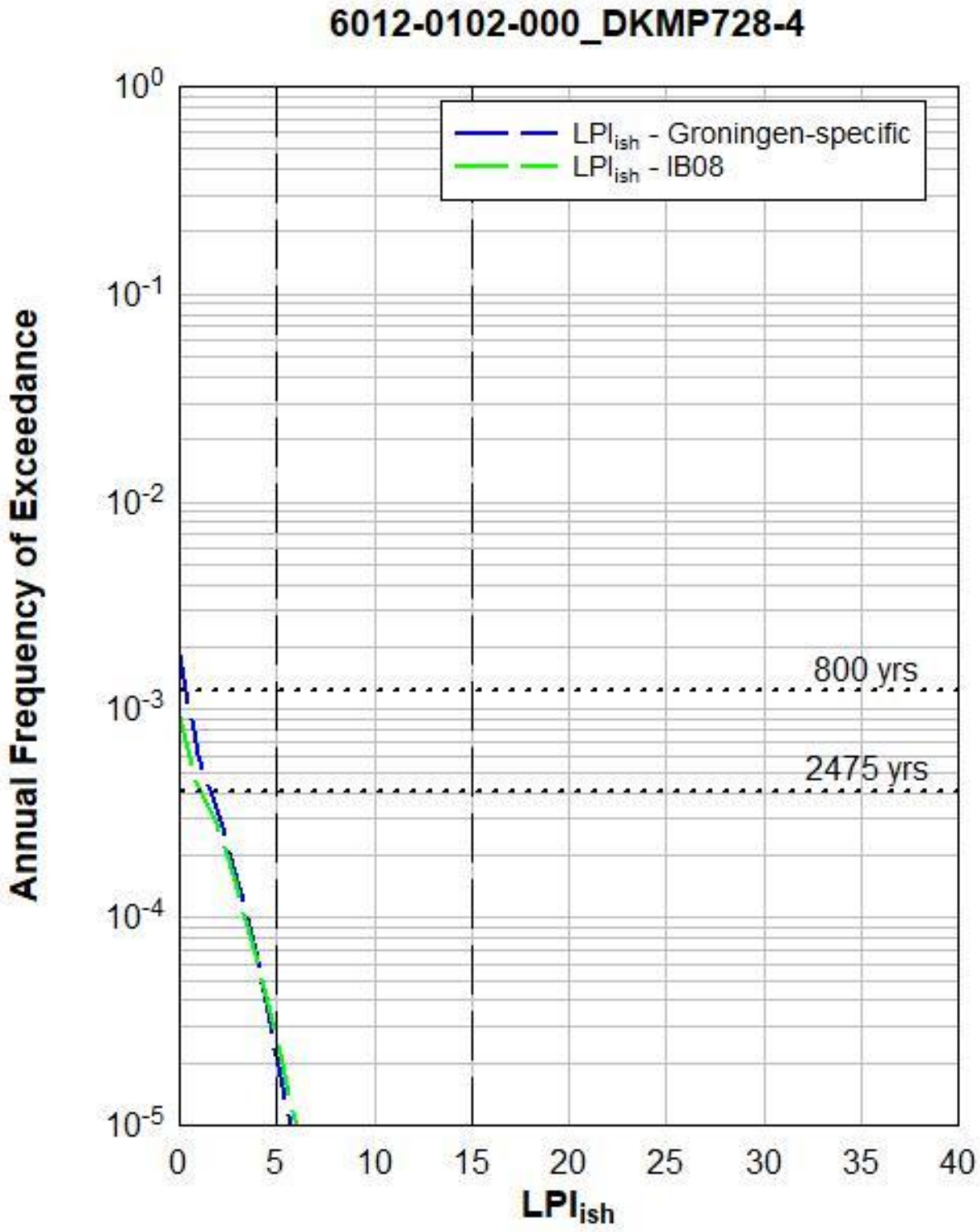
6012-0102-000_DKMP728-4
LPIish - Groningen-specific
LPIish - IB08
800 yrs
2475 yrs
Annual Frequency of Exceedance
LPIish
10^0
10^-1
10^-2
10^-3
10^-4
10^-5
0
5
10
15
20
25
30
35
40

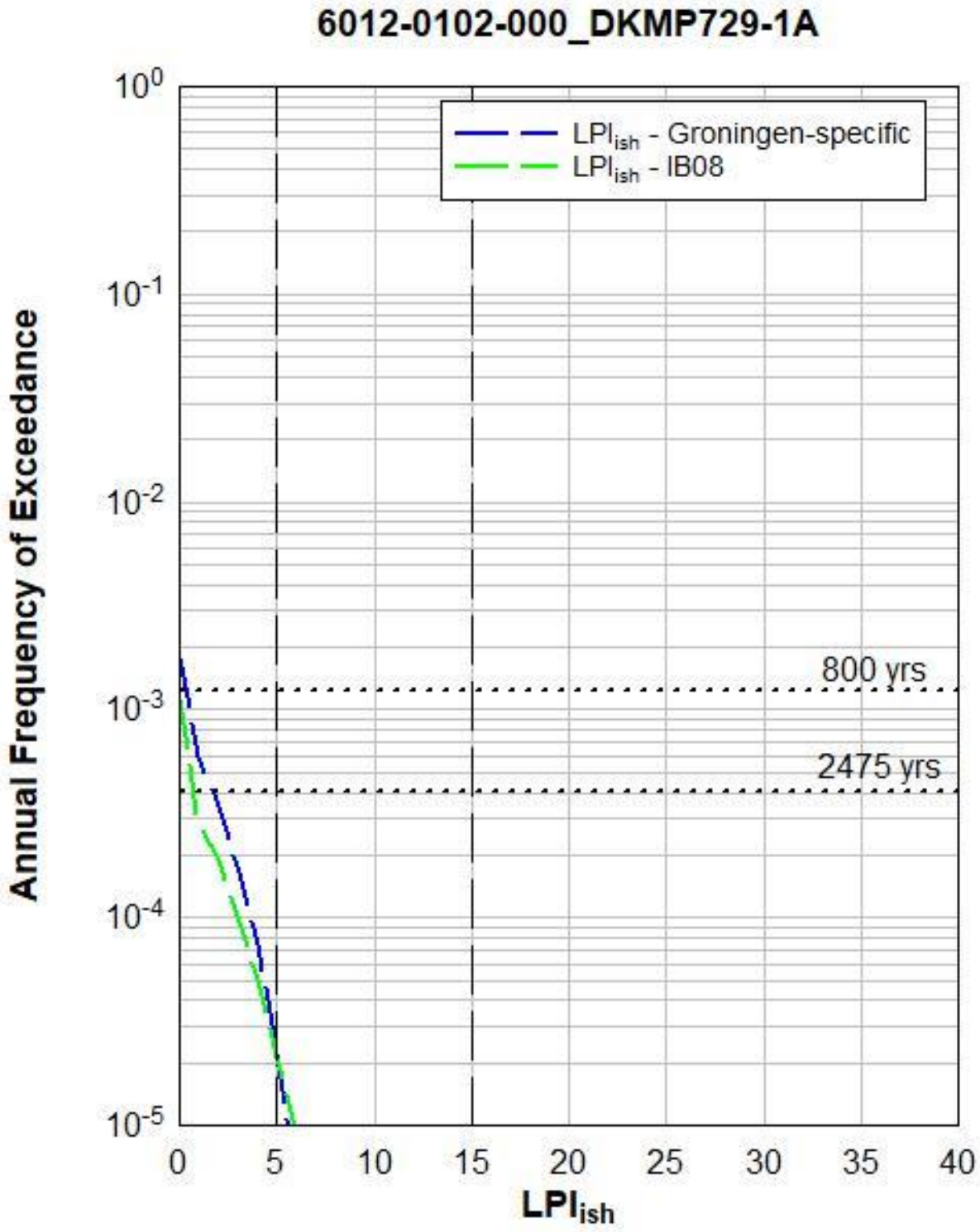
6012-0102-000_DKMP729-1A
LPIish - Groningen-specific
LPIish - IB08
800 yrs
2475 yrs
Annual Frequency of Exceedance
LPIish
10^0
10^-1
10^-2
10^-3
10^-4
10^-5
0
5
10
15
20
25
30
35
40

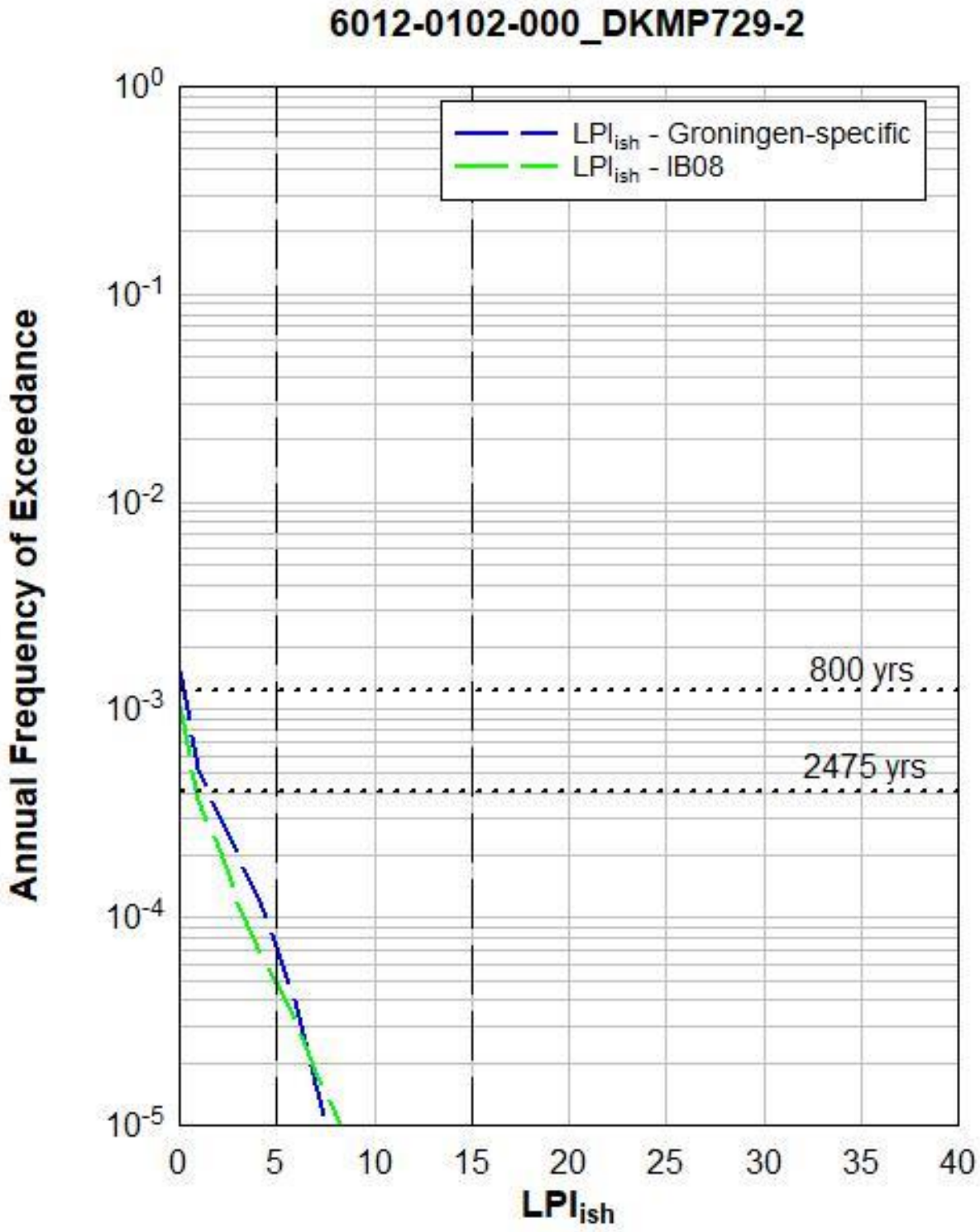
6012-0102-000_DKMP729-2
LPIish - Groningen-specific
LPIish - IB08
800 yrs
2475 yrs
Annual Frequency of Exceedance
LPIish
10^0
10^-1
10^-2
10^-3
10^-4
10^-5
0
5
10
15
20
25
30
35
40

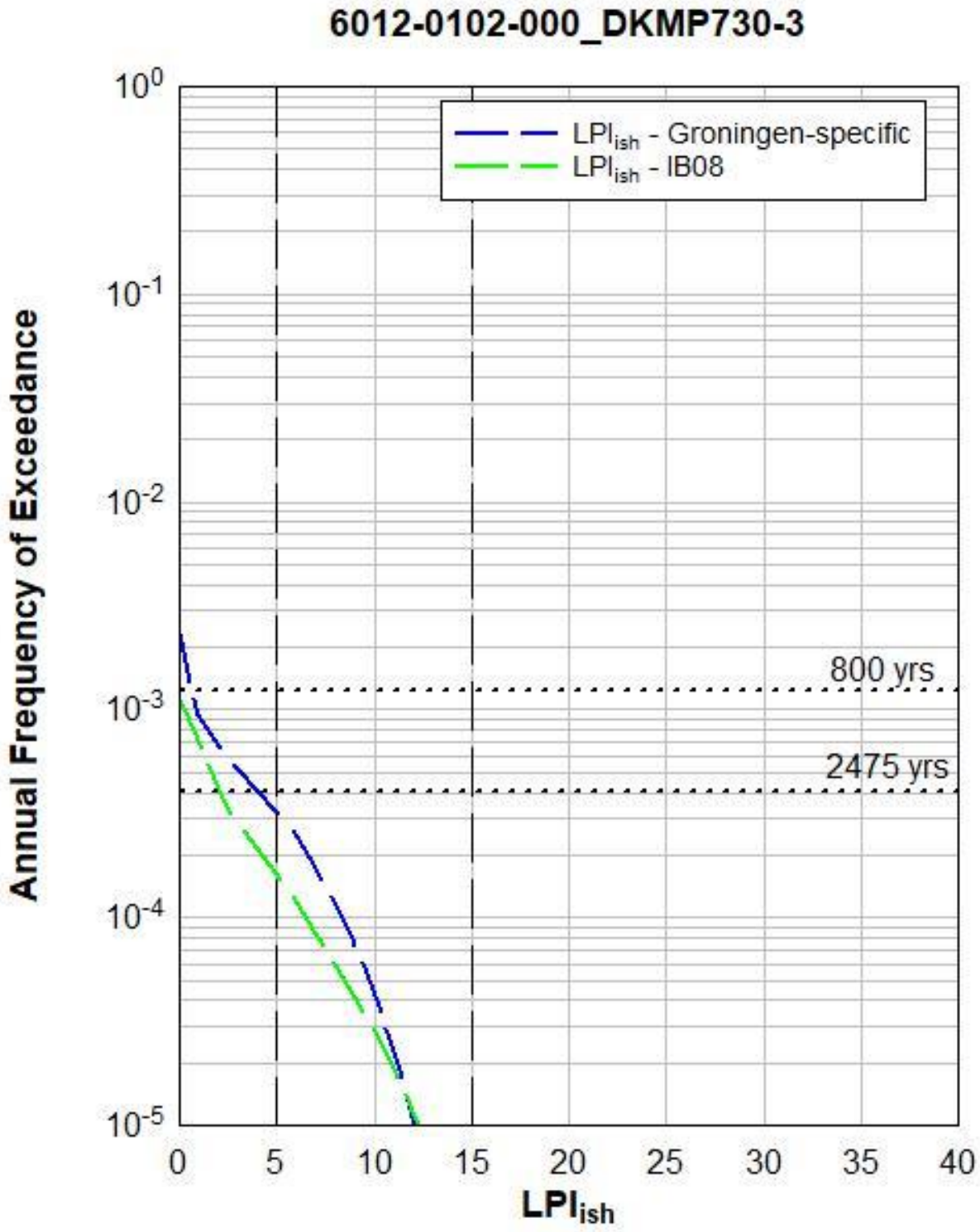
6012-0102-000_DKMP730-3
LPIish - Groningen-specific
LPIish - IB08
800 yrs
2475 yrs
Annual Frequency of Exceedance
LPIish
10^0
10^-1
10^-2
10^-3
10^-4
10^-5
0
5
10
15
20
25
30
35
40

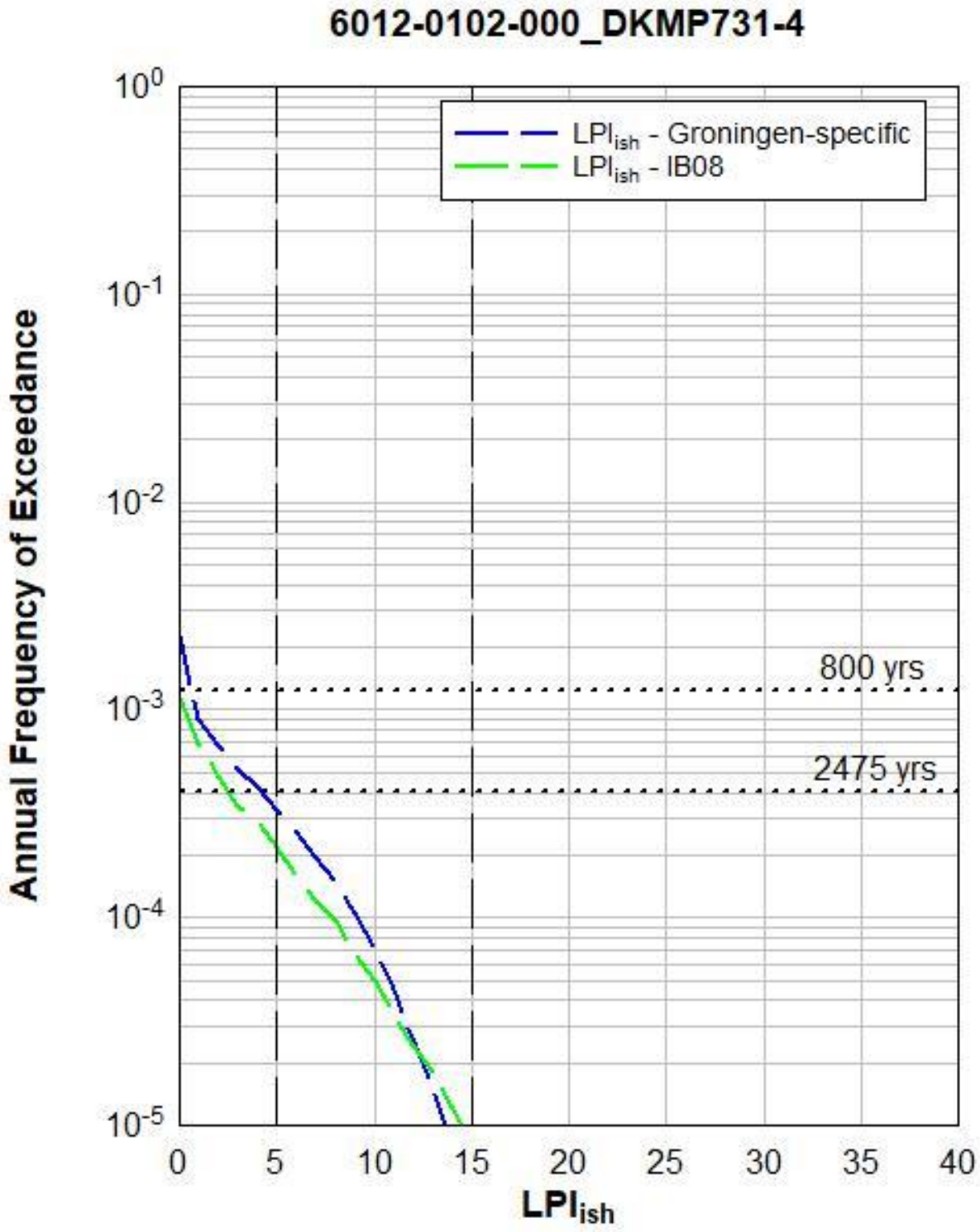
6012-0102-000_DKMP731-4
LPIish - Groningen-specific
LPIish - IB08
800 yrs
2475 yrs
Annual Frequency of Exceedance
LPIish
10^0
10^-1
10^-2
10^-3
10^-4
10^-5
0
5
10
15
20
25
30
35
40

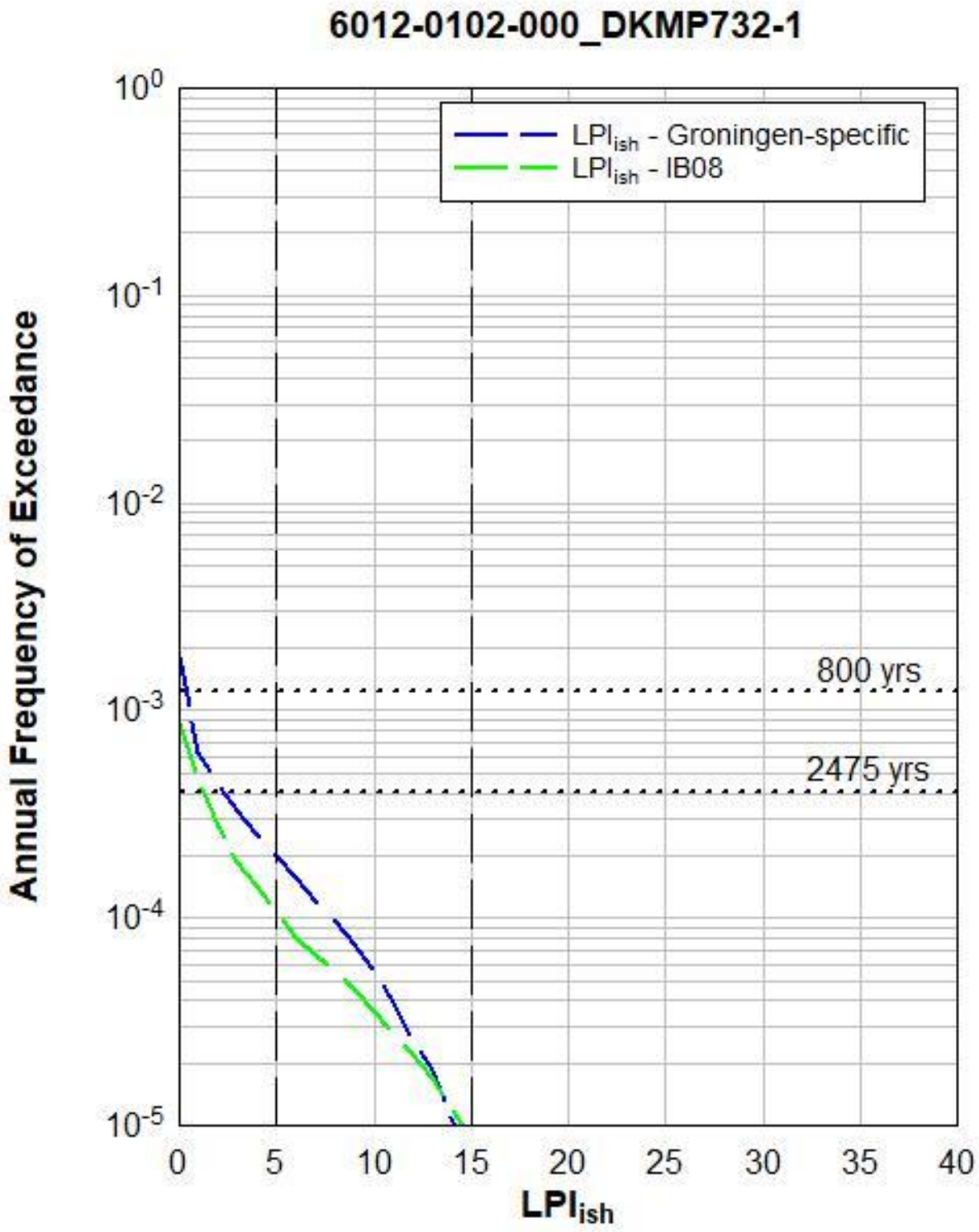
6012-0102-000_DKMP732-1
LPIish - Groningen-specific
LPIish - IB08
800 yrs
2475 yrs
Annual Frequency of Exceedance
LPIish
10^0
10^-1
10^-2
10^-3
10^-4
10^-5
0
5
10
15
20
25
30
35
40

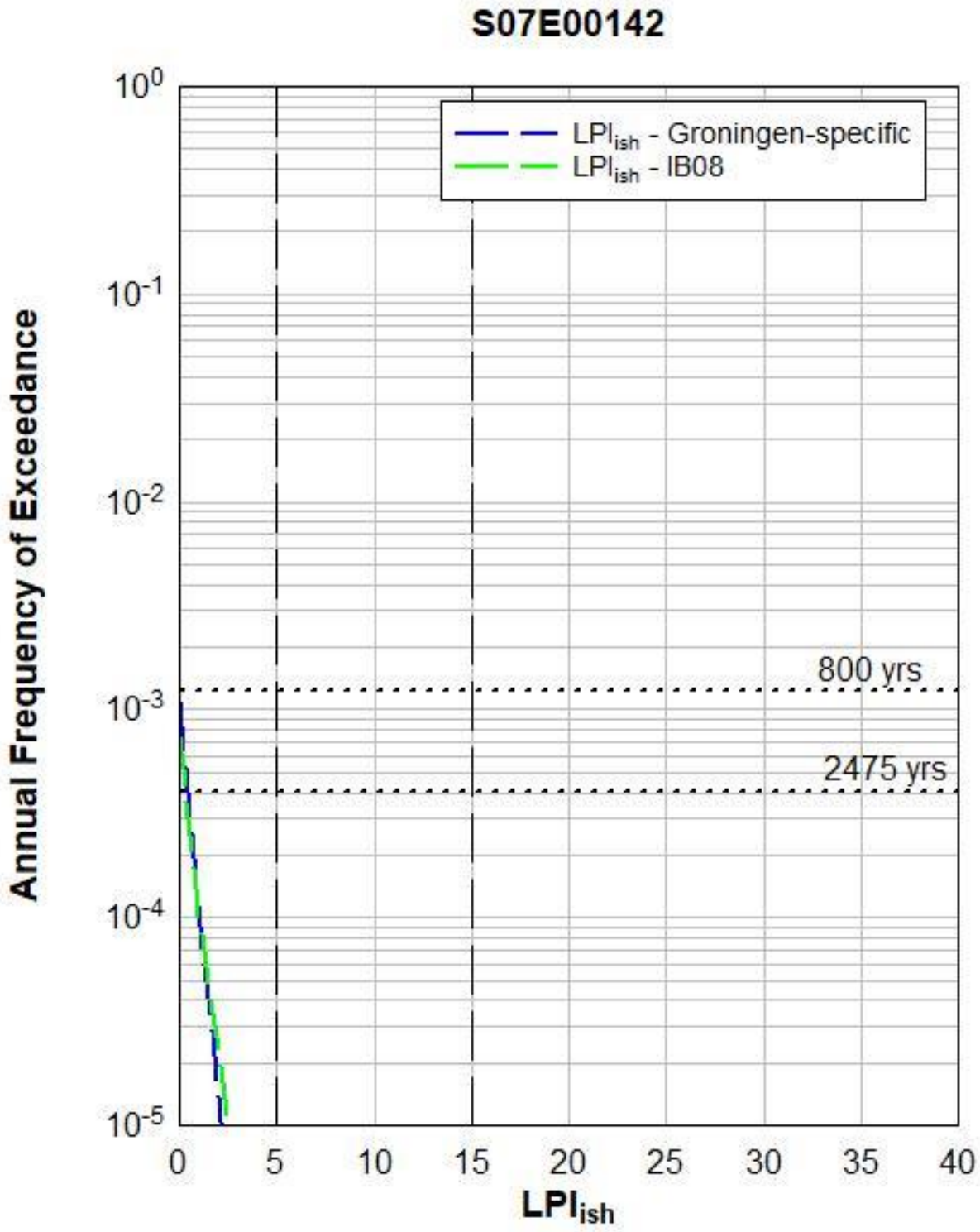
S07E00142
LPIish - Groningen-specific
LPIish - IB08
800 yrs
2475 yrs
Annual Frequency of Exceedance
LPIish
10^0
10^-1
10^-2
10^-3
10^-4
10^-5
0
5
10
15
20
25
30
35
40

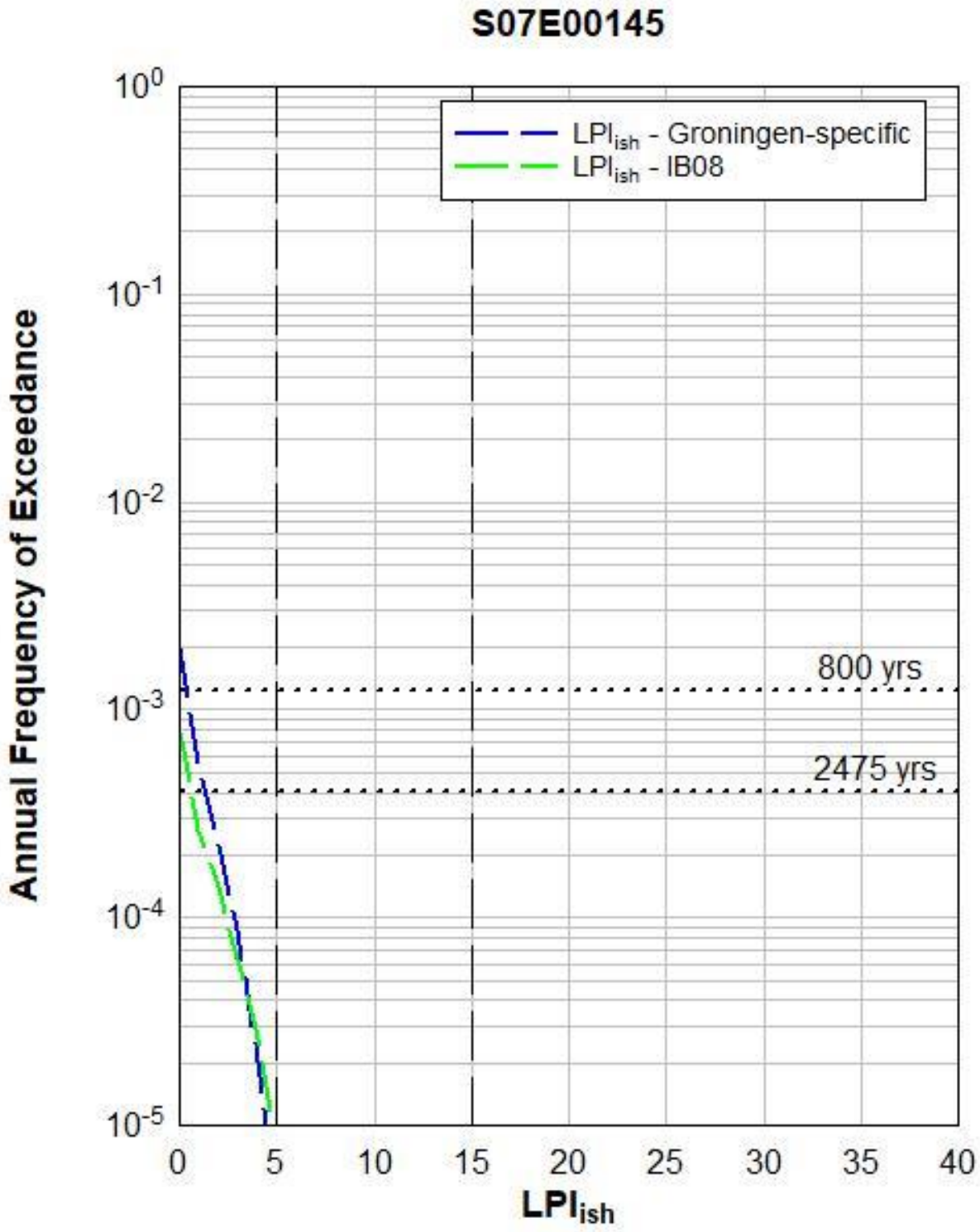
S07E00145
LPIish - Groningen-specific
LPIish - IB08
800 yrs
2475 yrs
Annual Frequency of Exceedance
LPIish
10^0
10^-1
10^-2
10^-3
10^-4
10^-5
0
5
10
15
20
25
30
35
40

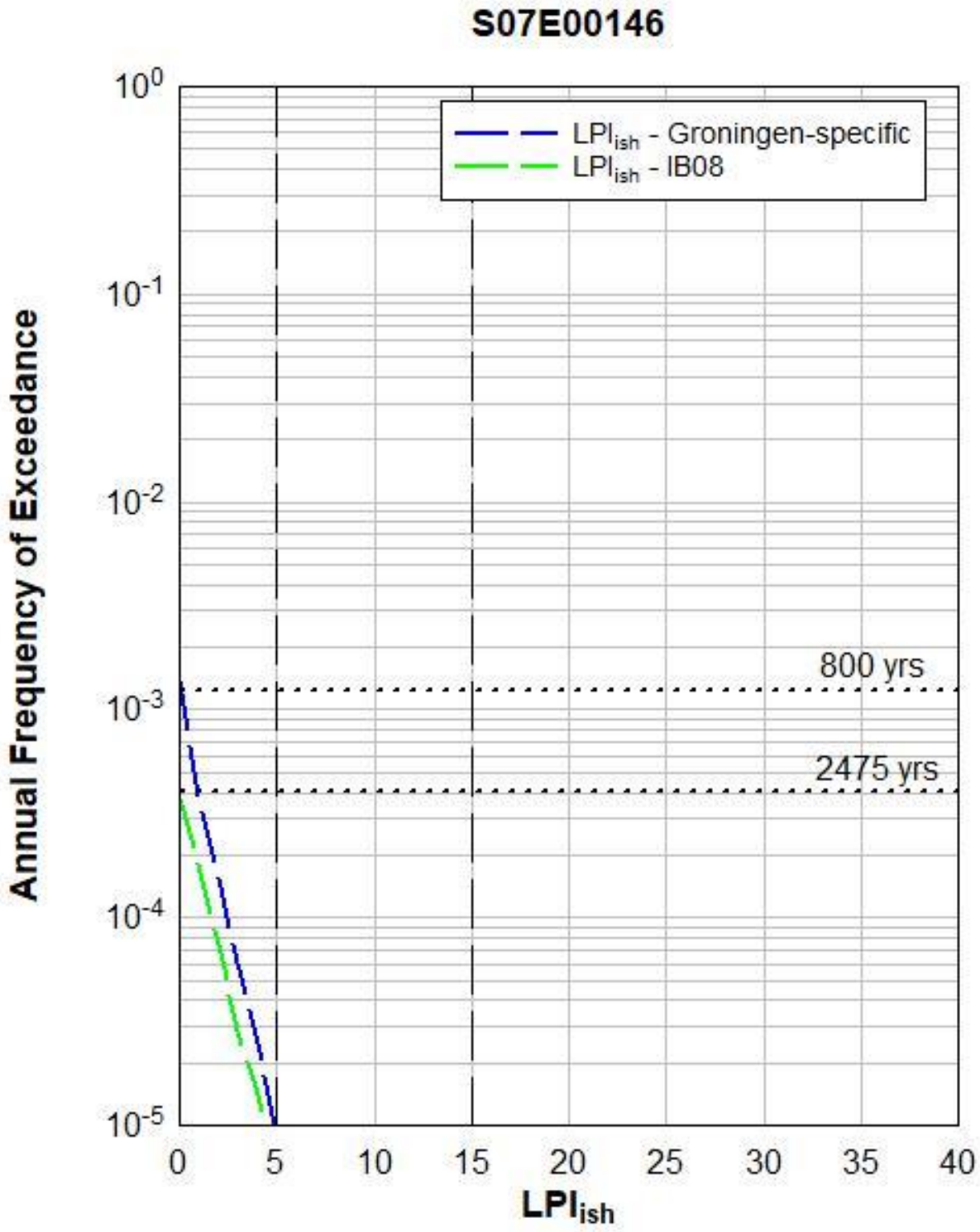
S07E00146
LPIish - Groningen-specific
LPIish - IB08
800 yrs
2475 yrs
Annual Frequency of Exceedance
LPIish
10^0
10^-1
10^-2
10^-3
10^-4
10^-5
0
5
10
15
20
25
30
35
40

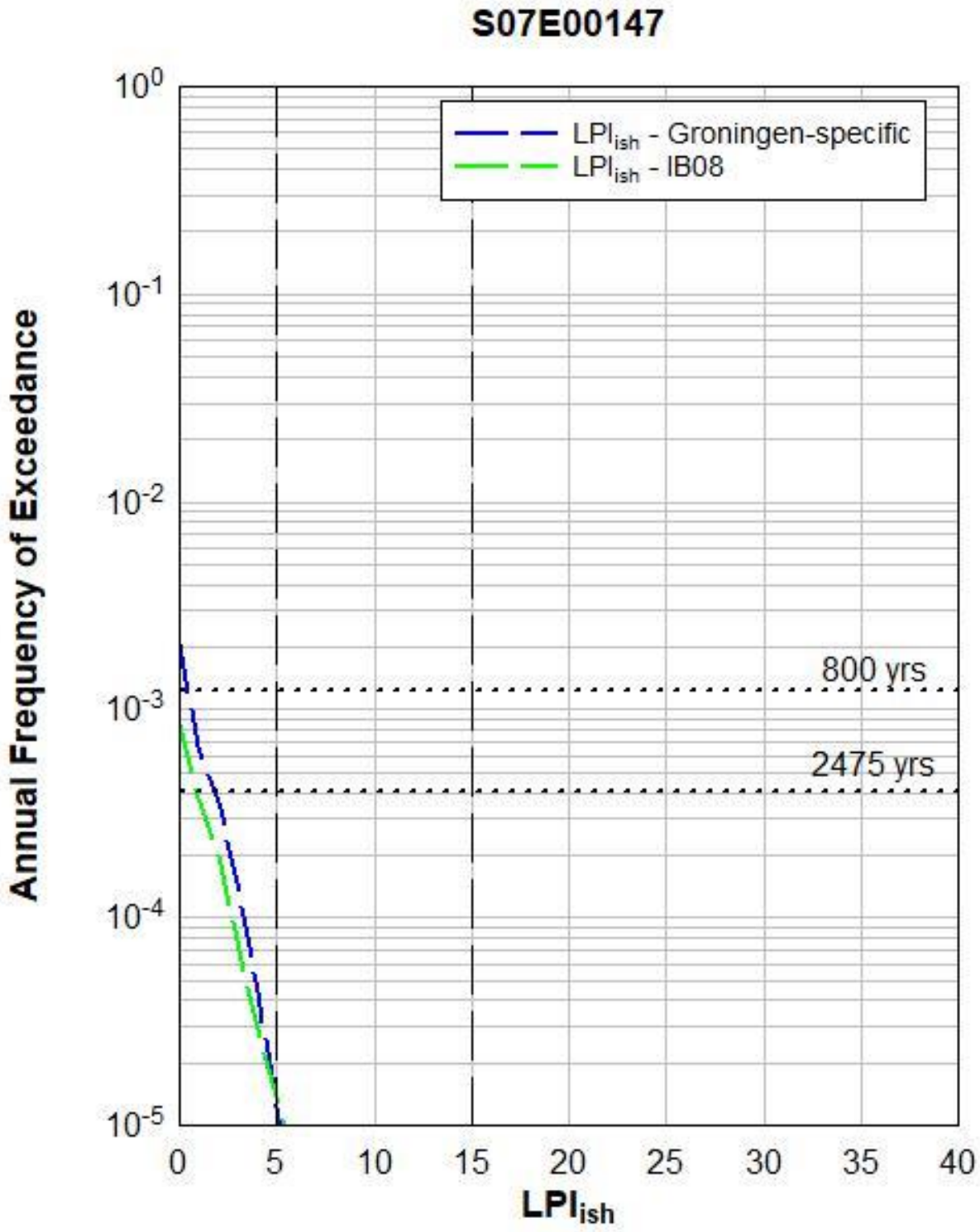
S07E00147
LPIish - Groningen-specific
LPIish - IB08
800 yrs
2475 yrs
Annual Frequency of Exceedance
LPIish
10^0
10^-1
10^-2
10^-3
10^-4
10^-5
0
5
10
15
20
25
30
35
40

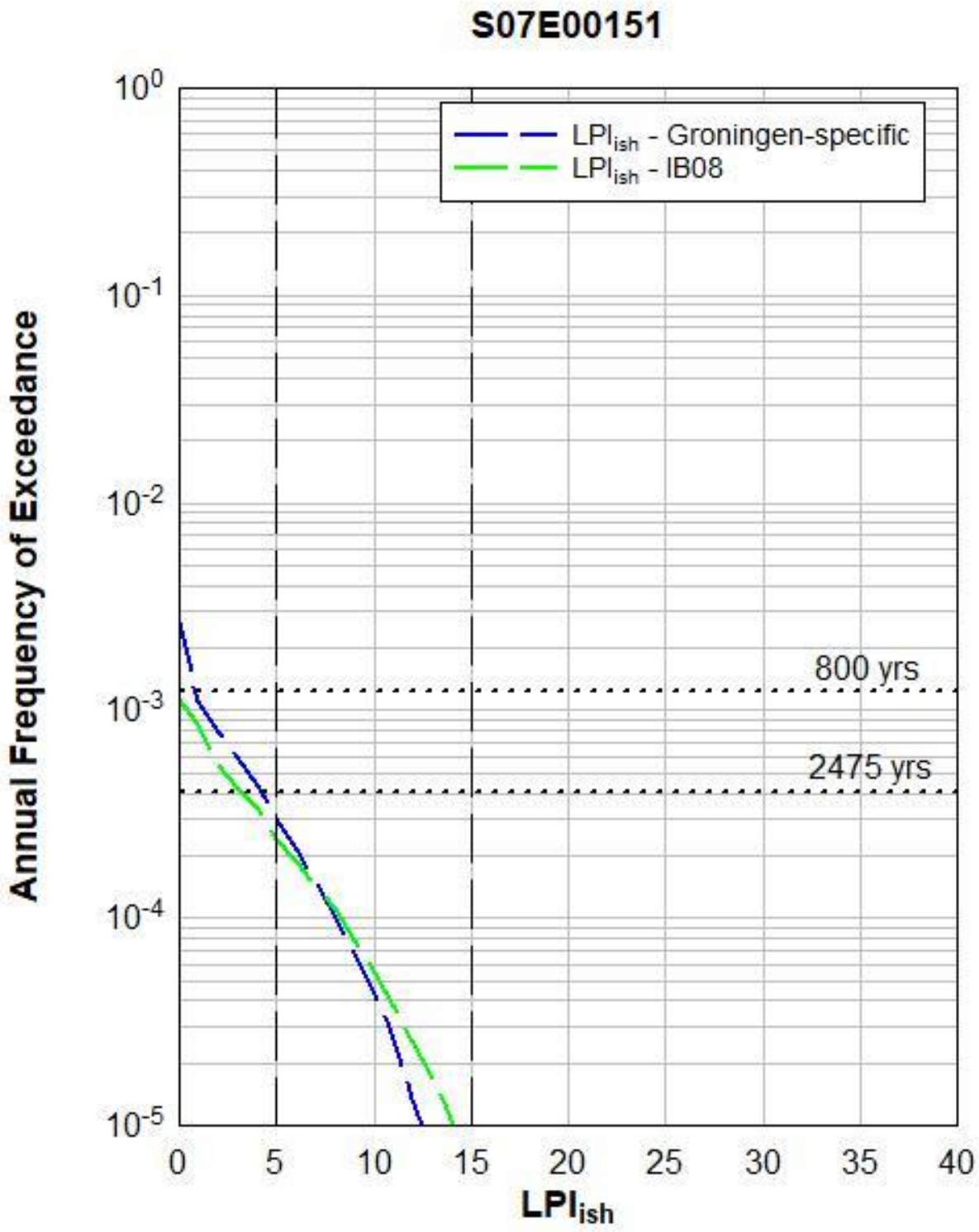
S07E00151
LPIish - Groningen-specific
LPIish - IB08
800 yrs
2475 yrs
Annual Frequency of Exceedance
LPIish
10^0
10^-1
10^-2
10^-3
10^-4
10^-5
0
5
10
15
20
25
30
35
40

Zone 1032


LPIish < 5
5 ≤ LPIish ≤ 15
LPIish > 15
S07E00176
6012-0102-000_DKMP734-2
S07E00153
6012-0102-000_DKMP733-4
S07E00152
602
6012-0102-000_DKMP732-1
S07E00151
6012-0102-000_DKMP731-4
S07E00147
6012-0102-000_DKMP730-3
S07E00146
6012-0102-000_DKMP729-2
S07E00145
6012-0102-000_DKMP729-1A
5007-0073-000_DKM1
6012-0102-000_DKMP728-4
G07044000_D4
5004-0308-000_DKM2
6012-0102-000_DKMP728-1A
S07E00142
6012-0102-000_DKMP727-3
1032
S07E00036
G08169000_D2
5009-0271-001_DKMP3
5009-0271-001_DKMP2
G02332000_D1
5009-0271-001_DKMP1
G08098000_DKM1
LOPPERSUM
2001

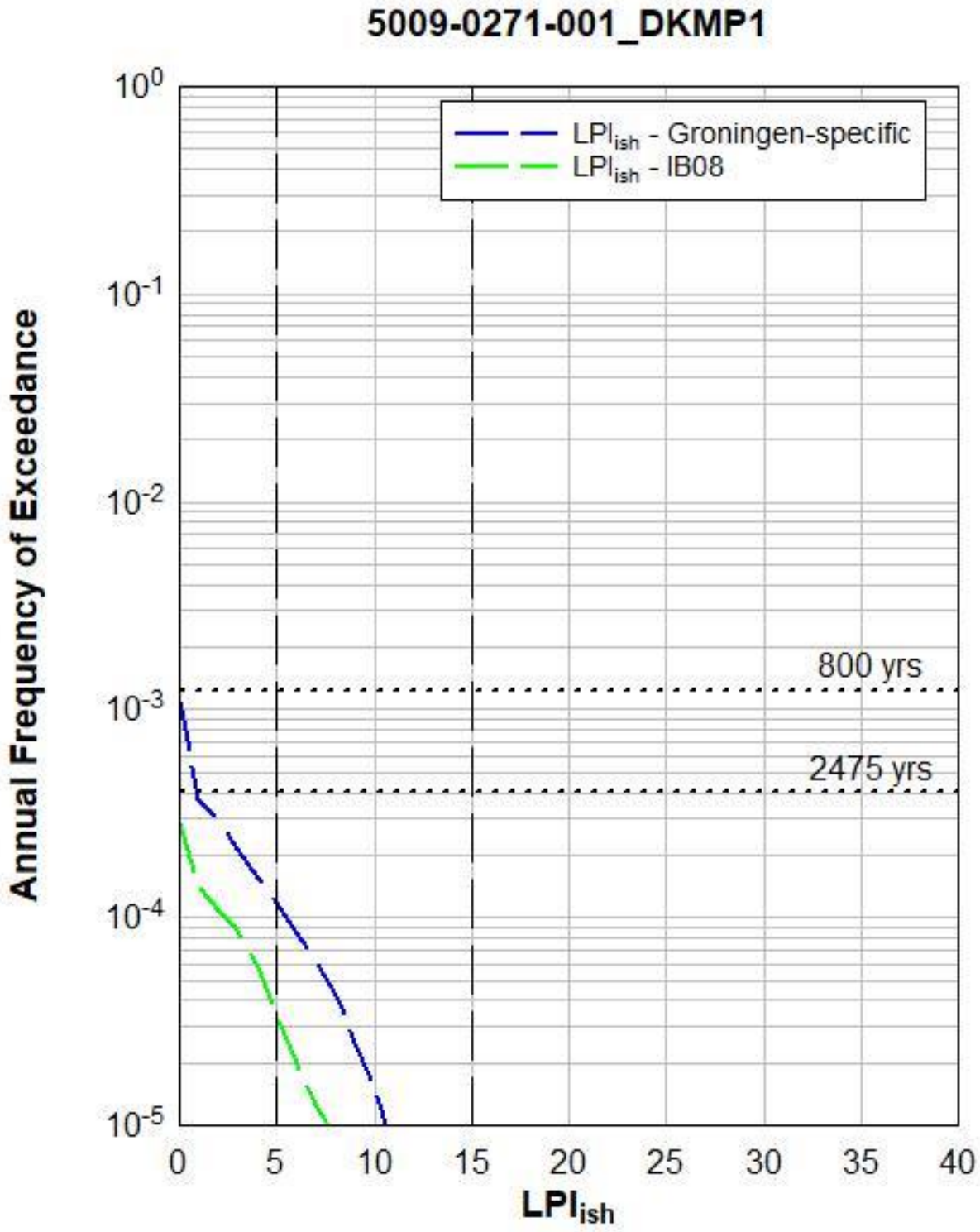
5009-0271-001_DKMP1
LPIish - Groningen-specific
LPIish - IB08
800 yrs
2475 yrs
Annual Frequency of Exceedance
LPIish
10^0
10^-1
10^-2
10^-3
10^-4
10^-5
0
5
10
15
20
25
30
35
40

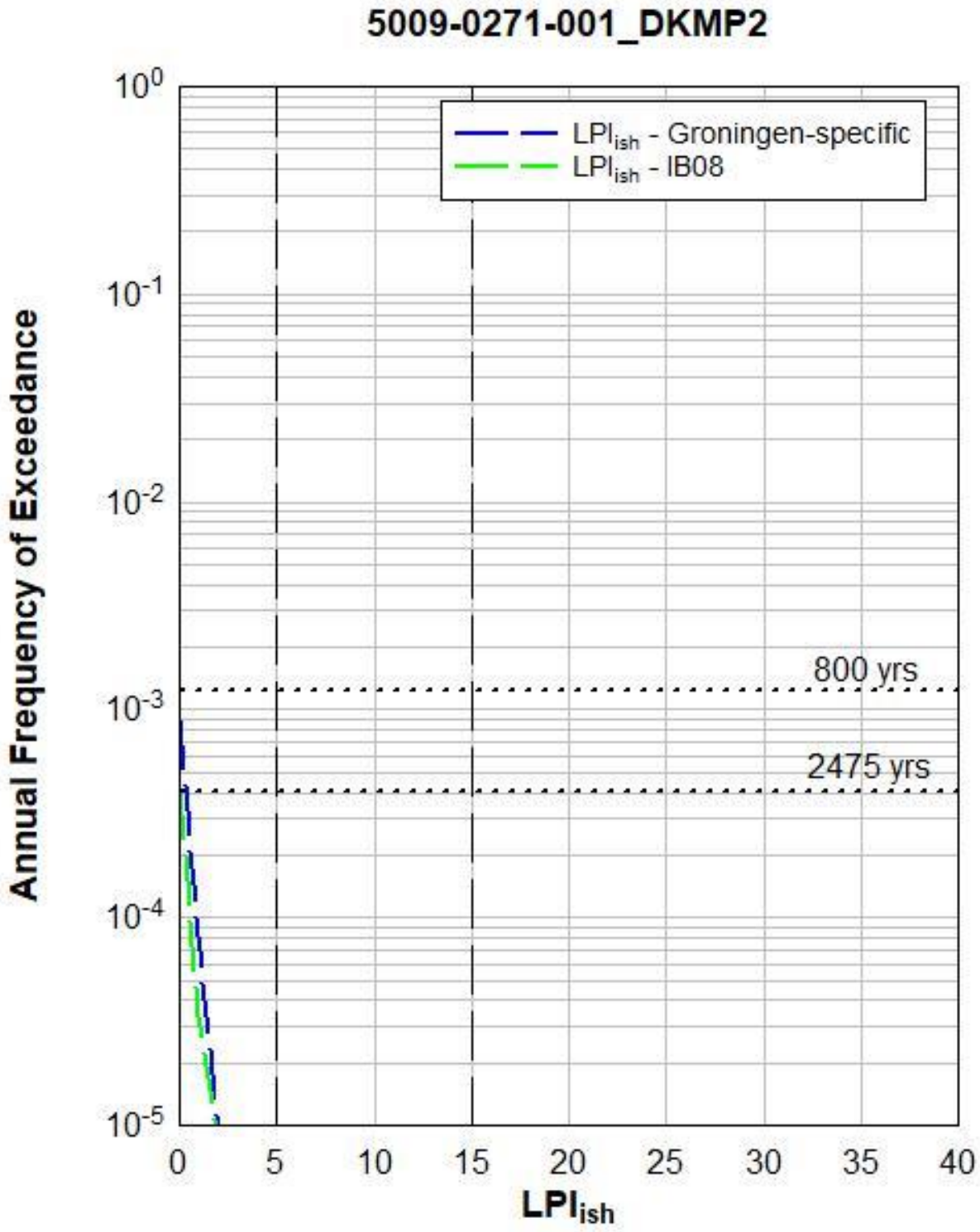
5009-0271-001_DKMP2
LPIish - Groningen-specific
LPIish - IB08
800 yrs
2475 yrs
Annual Frequency of Exceedance
LPIish
10^0
10^-1
10^-2
10^-3
10^-4
10^-5
0
5
10
15
20
25
30
35
40

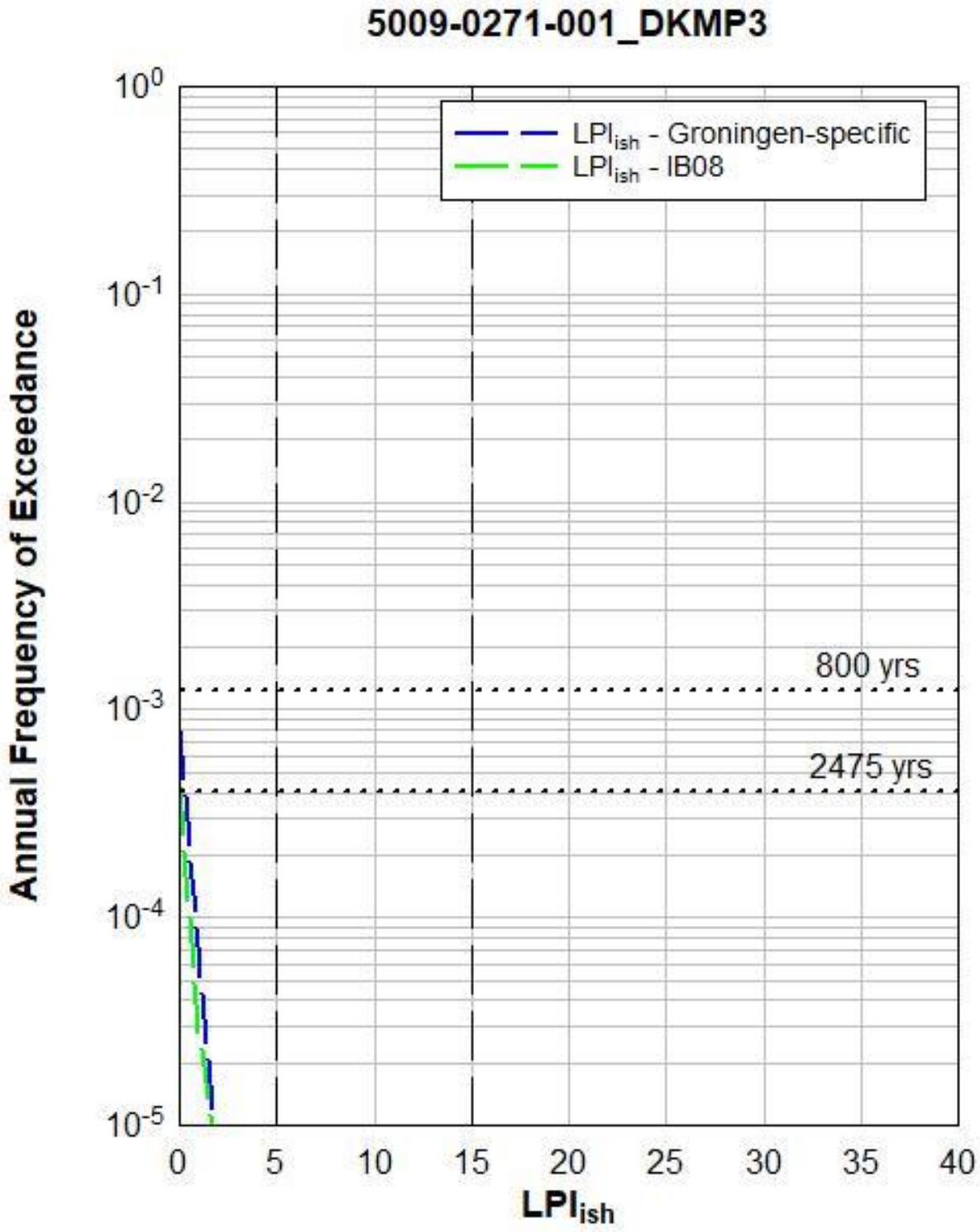
5009-0271-001_DKMP3
LPIish - Groningen-specific
LPIish - IB08
800 yrs
2475 yrs
Annual Frequency of Exceedance
LPIish
10^0
10^-1
10^-2
10^-3
10^-4
10^-5
0
5
10
15
20
25
30
35
40

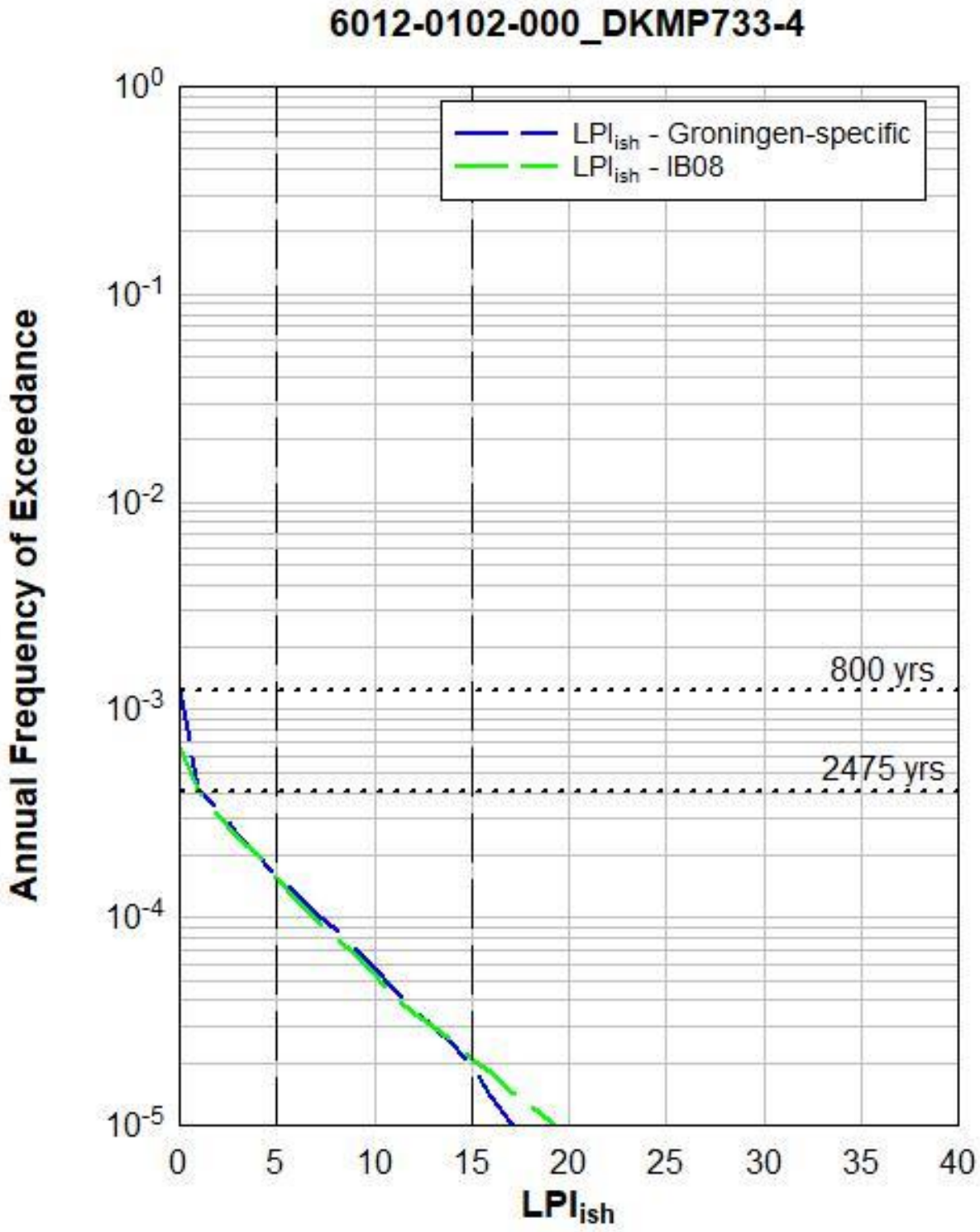
6012-0102-000_DKMP733-4
LPIish - Groningen-specific
LPIish - IB08
800 yrs
2475 yrs
Annual Frequency of Exceedance
LPIish
10^0
10^-1
10^-2
10^-3
10^-4
10^-5
0
5
10
15
20
25
30
35
40

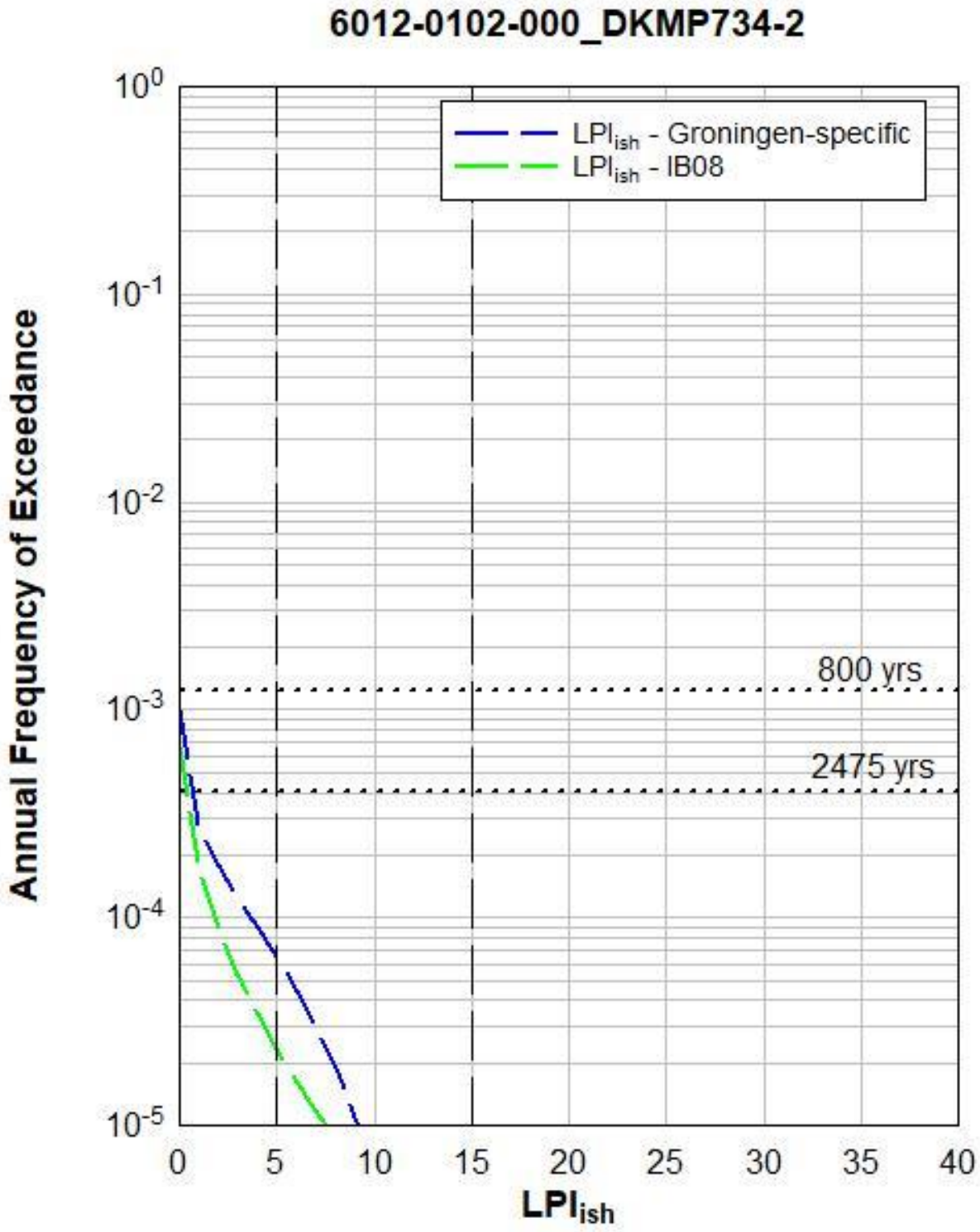
6012-0102-000_DKMP734-2
LPIish - Groningen-specific
LPIish - IB08
800 yrs
2475 yrs
Annual Frequency of Exceedance
LPIish
10^0
10^-1
10^-2
10^-3
10^-4
10^-5
0
5
10
15
20
25
30
35
40

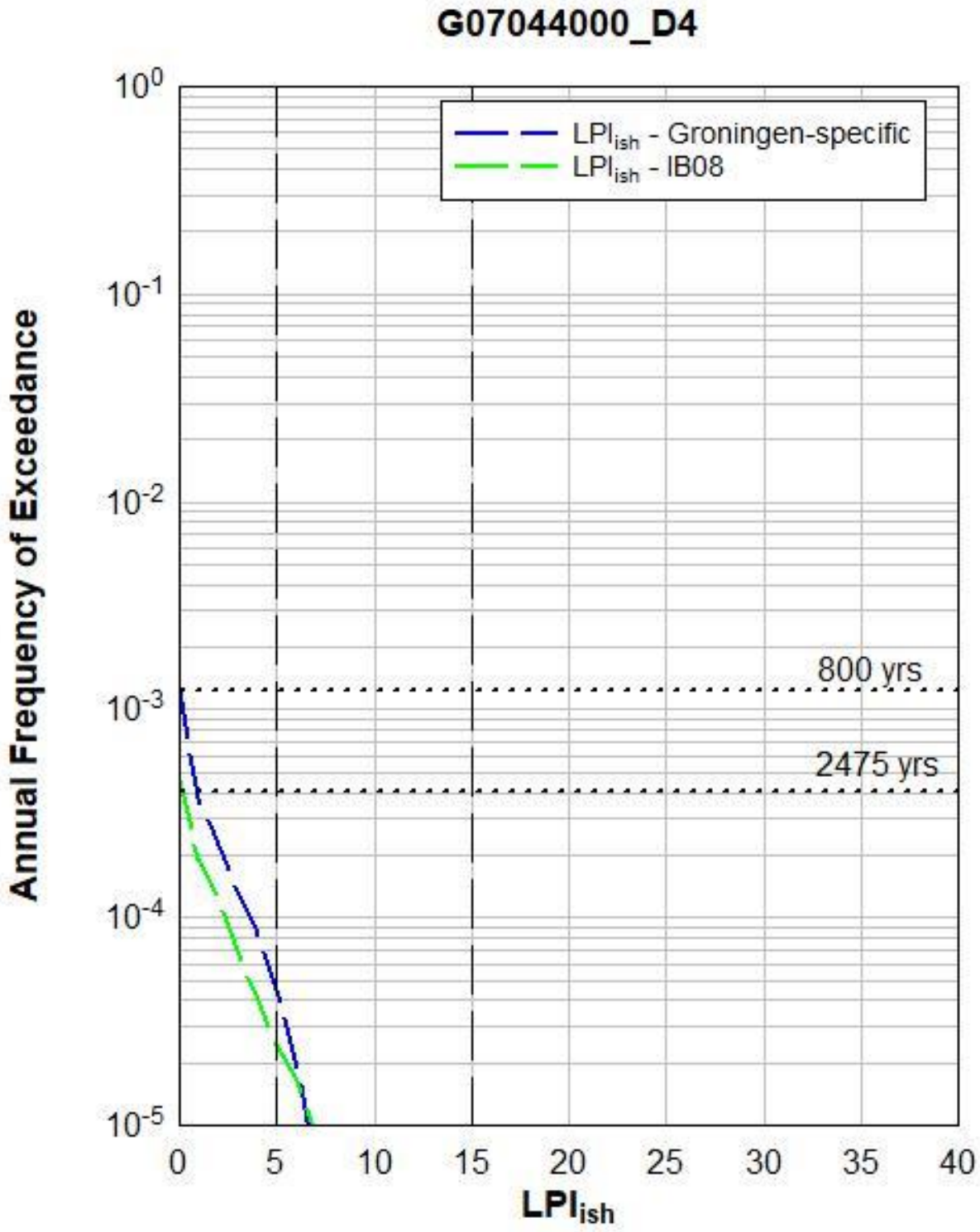
G07044000_D4
LPIish - Groningen-specific
LPIish - IB08
800 yrs
2475 yrs
Annual Frequency of Exceedance
LPIish
10^0
10^-1
10^-2
10^-3
10^-4
10^-5
0
5
10
15
20
25
30
35
40

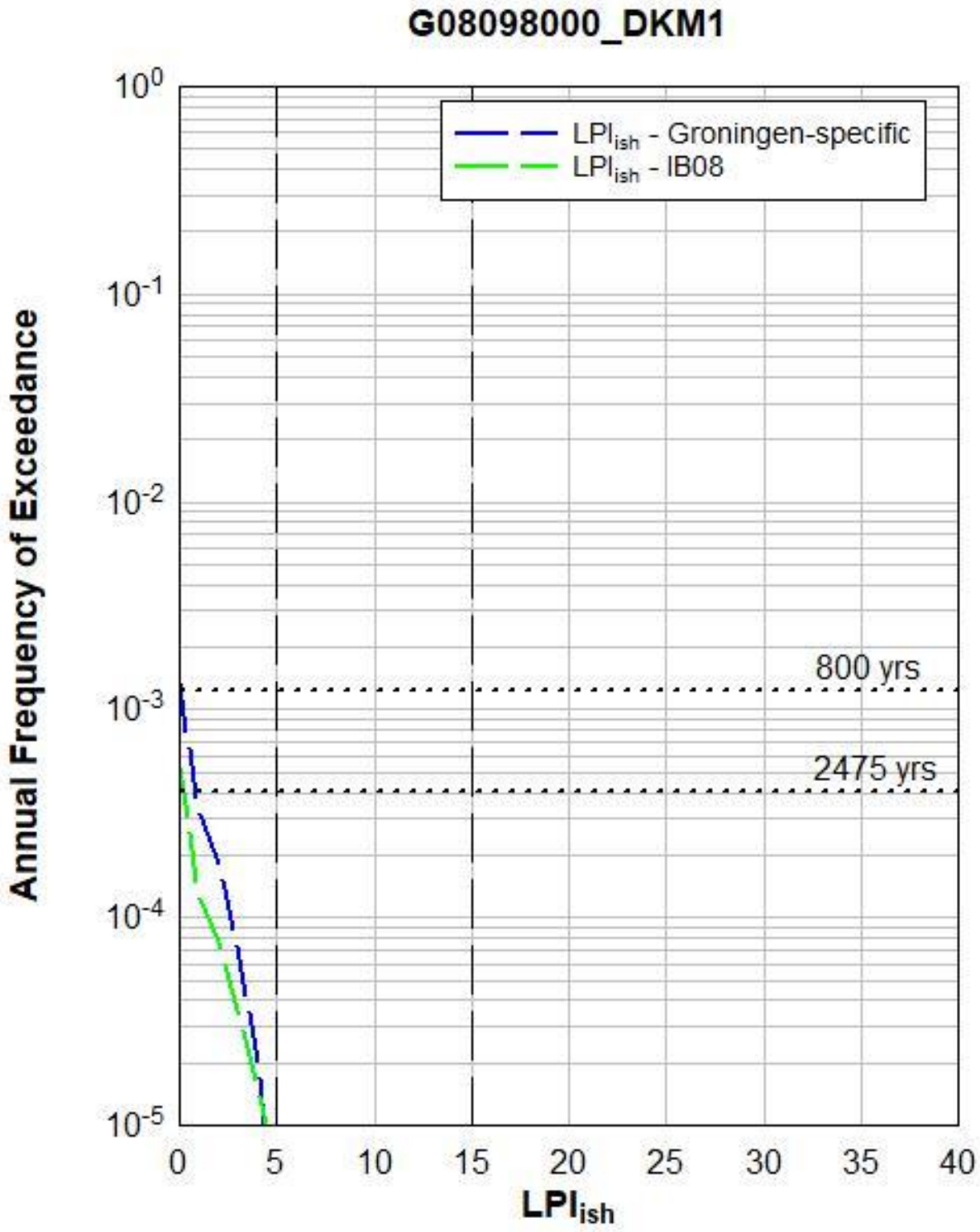
G08098000_DKM1
LPIish - Groningen-specific
LPIish - IB08
800 yrs
2475 yrs
Annual Frequency of Exceedance
LPIish
10^0
10^-1
10^-2
10^-3
10^-4
10^-5
0
5
10
15
20
25
30
35
40

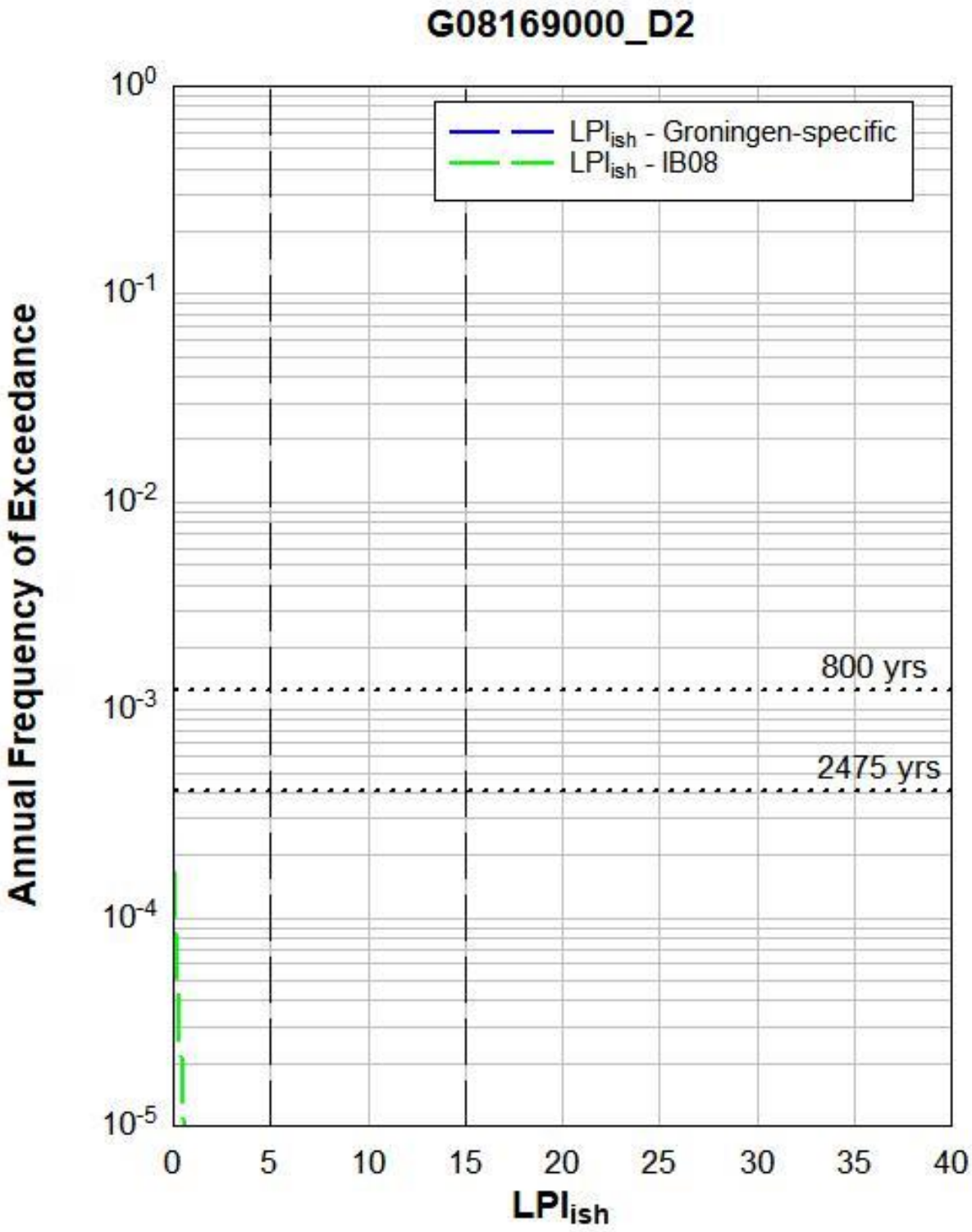
G08169000_D2
Annual Frequency of Exceedance
10^{0}
10^{-1}
10^{-2}
10^{-3}
10^{-4}
10^{-5}
LPI_{ish} - Groningen-specific
LPI_{ish} - IB08
800 yrs
2475 yrs
0
5
10
15
20
25
30
35
40
LPI_{ish}

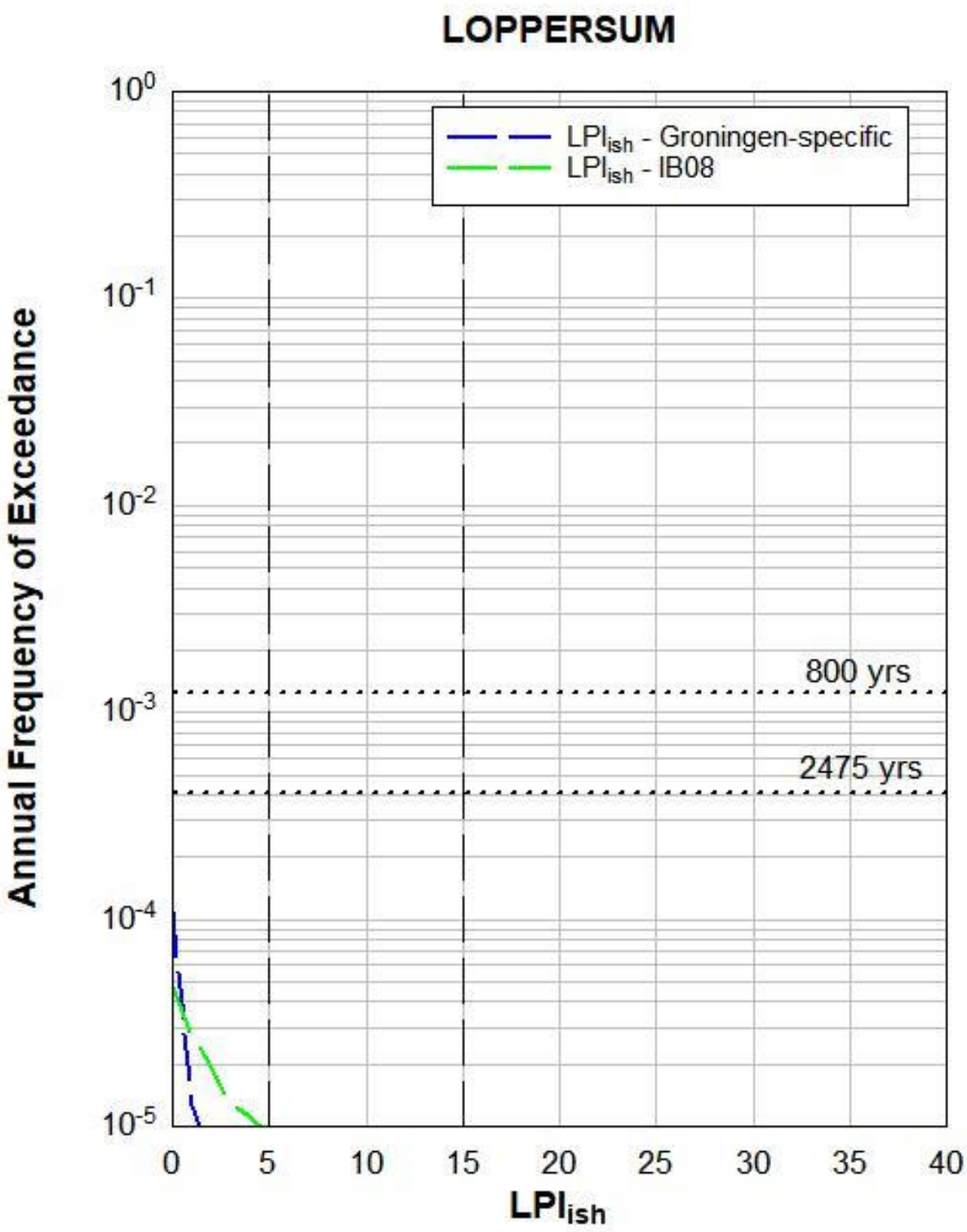
LOPPERSUM
Annual Frequency of Exceedance
10^{0}
10^{-1}
10^{-2}
10^{-3}
10^{-4}
10^{-5}
LPI_{ish} - Groningen-specific
LPI_{ish} - IB08
800 yrs
2475 yrs
0
5
10
15
20
25
30
35
40
LPI_{ish}

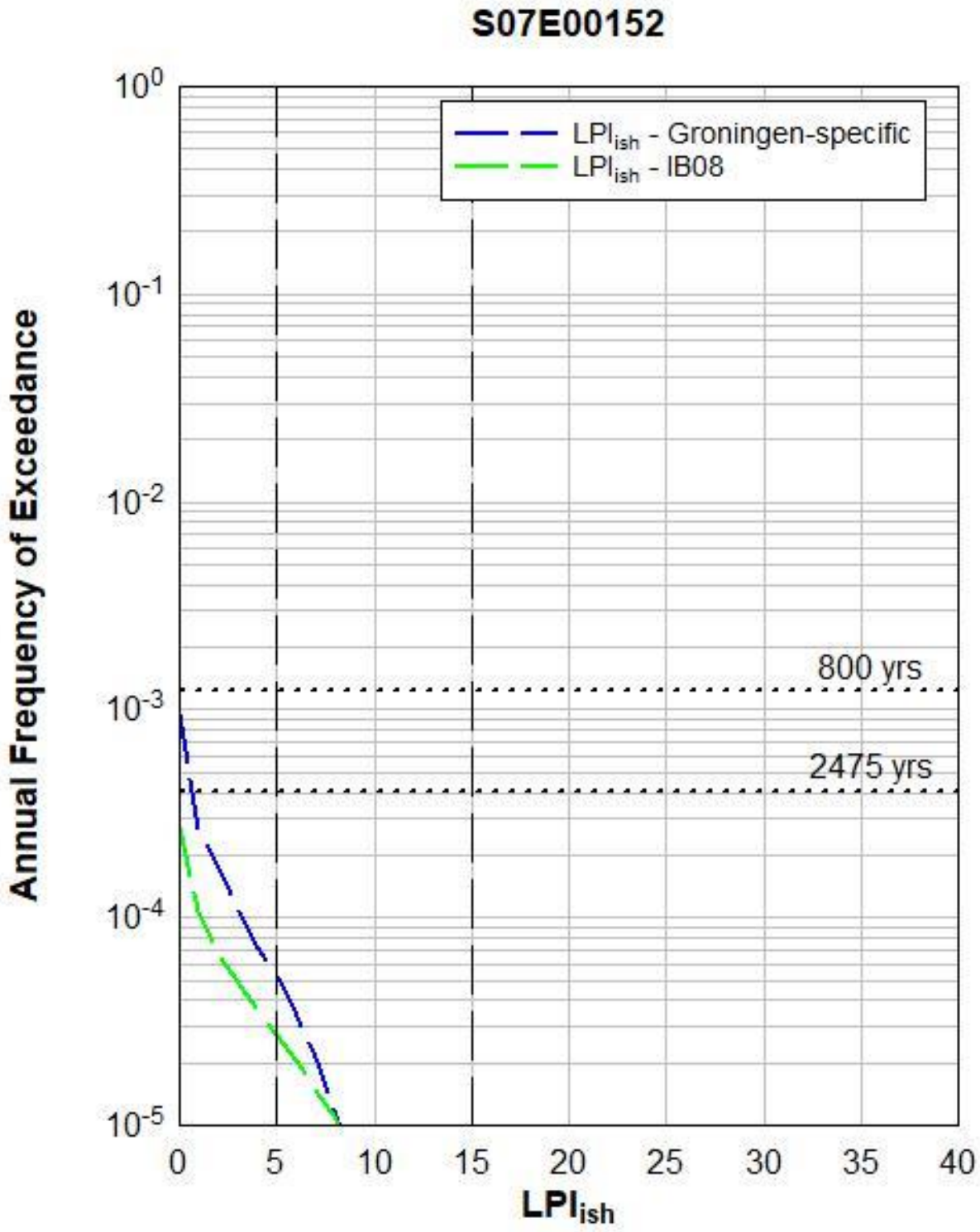
S07E00152
LPIish - Groningen-specific
LPIish - IB08
800 yrs
2475 yrs
Annual Frequency of Exceedance
LPIish
10^0
10^-1
10^-2
10^-3
10^-4
10^-5
0
5
10
15
20
25
30
35
40

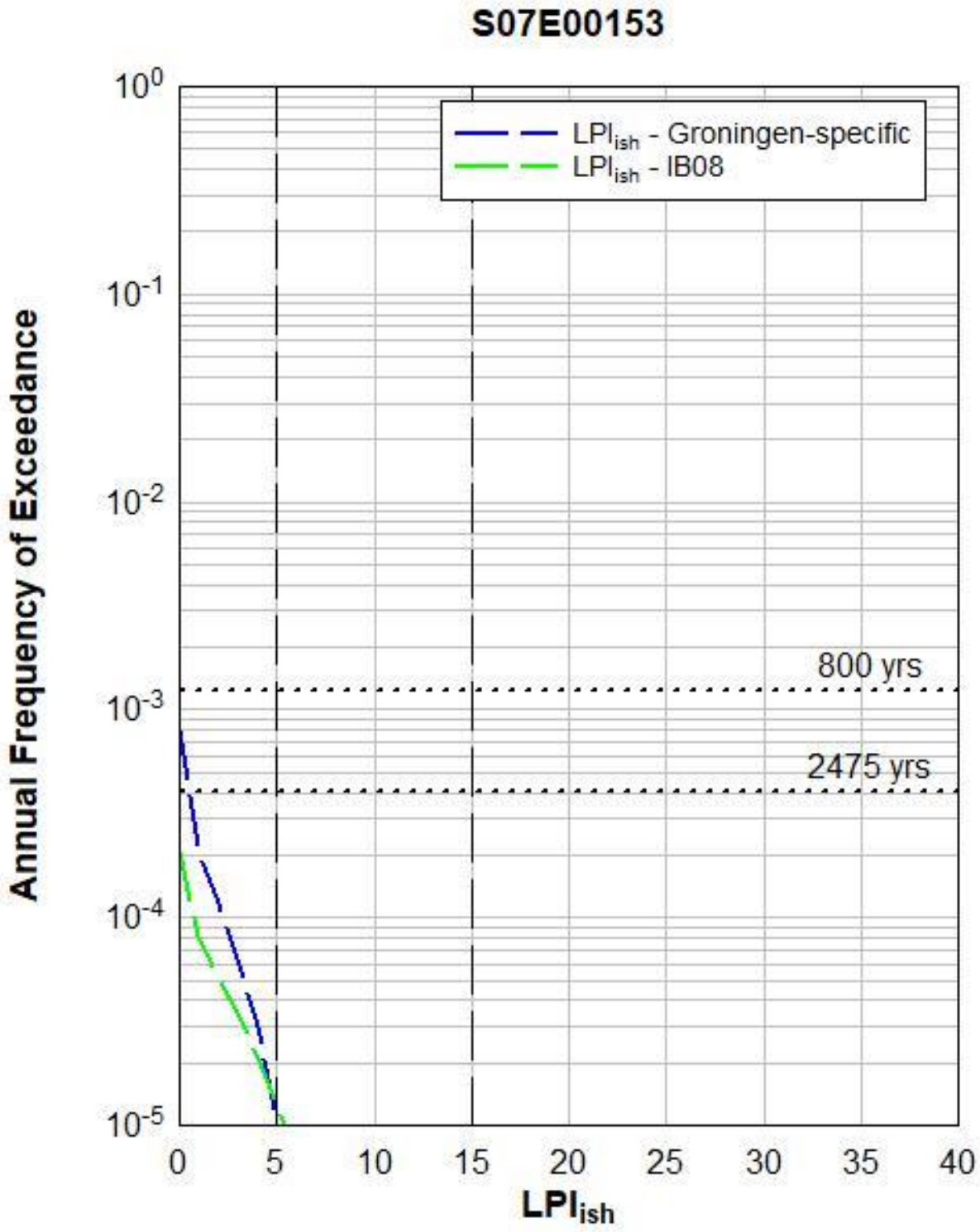
S07E00153
LPIish - Groningen-specific
LPIish - IB08
800 yrs
2475 yrs
Annual Frequency of Exceedance
LPIish
10^0
10^-1
10^-2
10^-3
10^-4
10^-5
0
5
10
15
20
25
30
35
40

Zone 2001

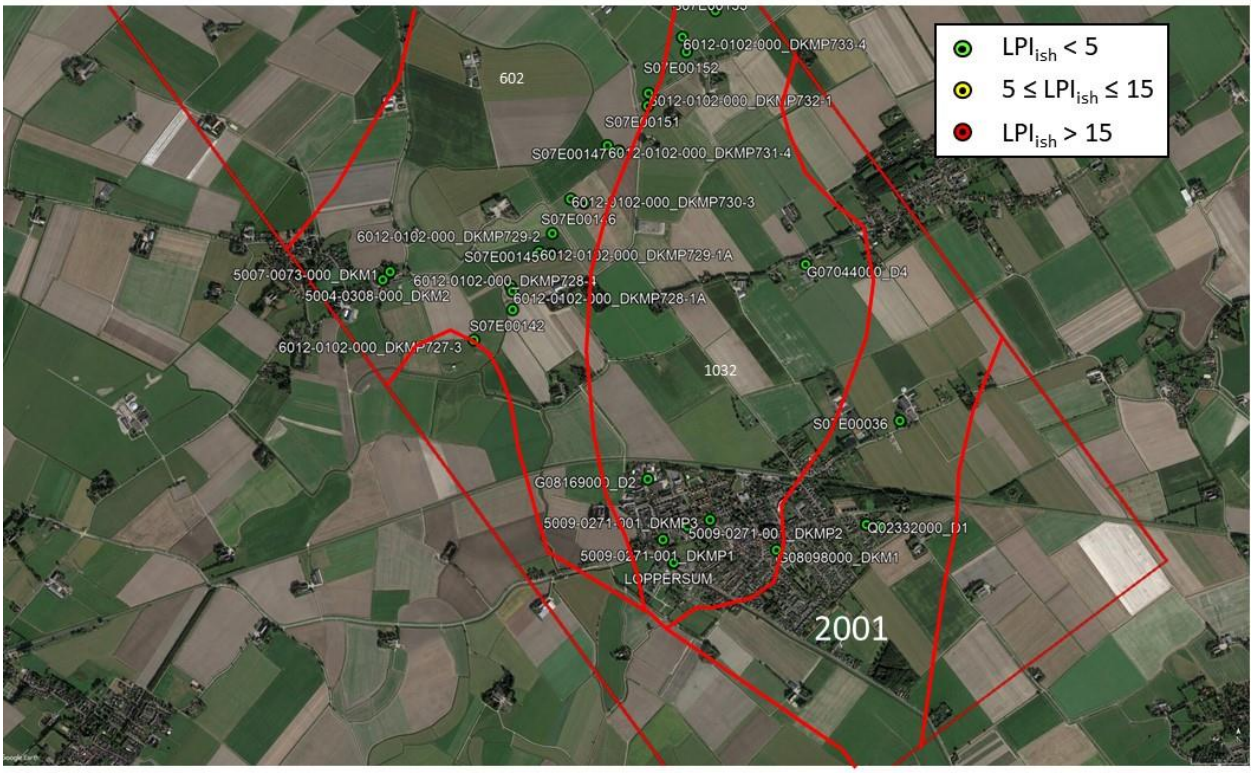
LPI$_{ish}$ < 5
5 ≤ LPI$_{ish}$ ≤ 15
LPI$_{ish}$ > 15
602
6012-0102-000_DKMP733-4
S07E00152
6012-0102-000_DKMP732-1
S07E00151
S07E00147
6012-0102-000_DKMP731-4
6012-0102-000_DKMP730-3
S07E00146
6012-0102-000_DKMP729-2
S07E00145
6012-0102-000_DKMP729-1A
5007-0073-000_DKM1
6012-0102-000_DKMP728-1
5004-0308-000_DKM2
6012-0102-000_DKMP728-1A
S07E00142
6012-0102-000_DKMP727-3
1032
S07E00036
G08169000_D2
5009-0271-001_DKMP3
5009-0271-001_DKMP2
5009-0271-001_DKMP1
LOPPERSUM
2001

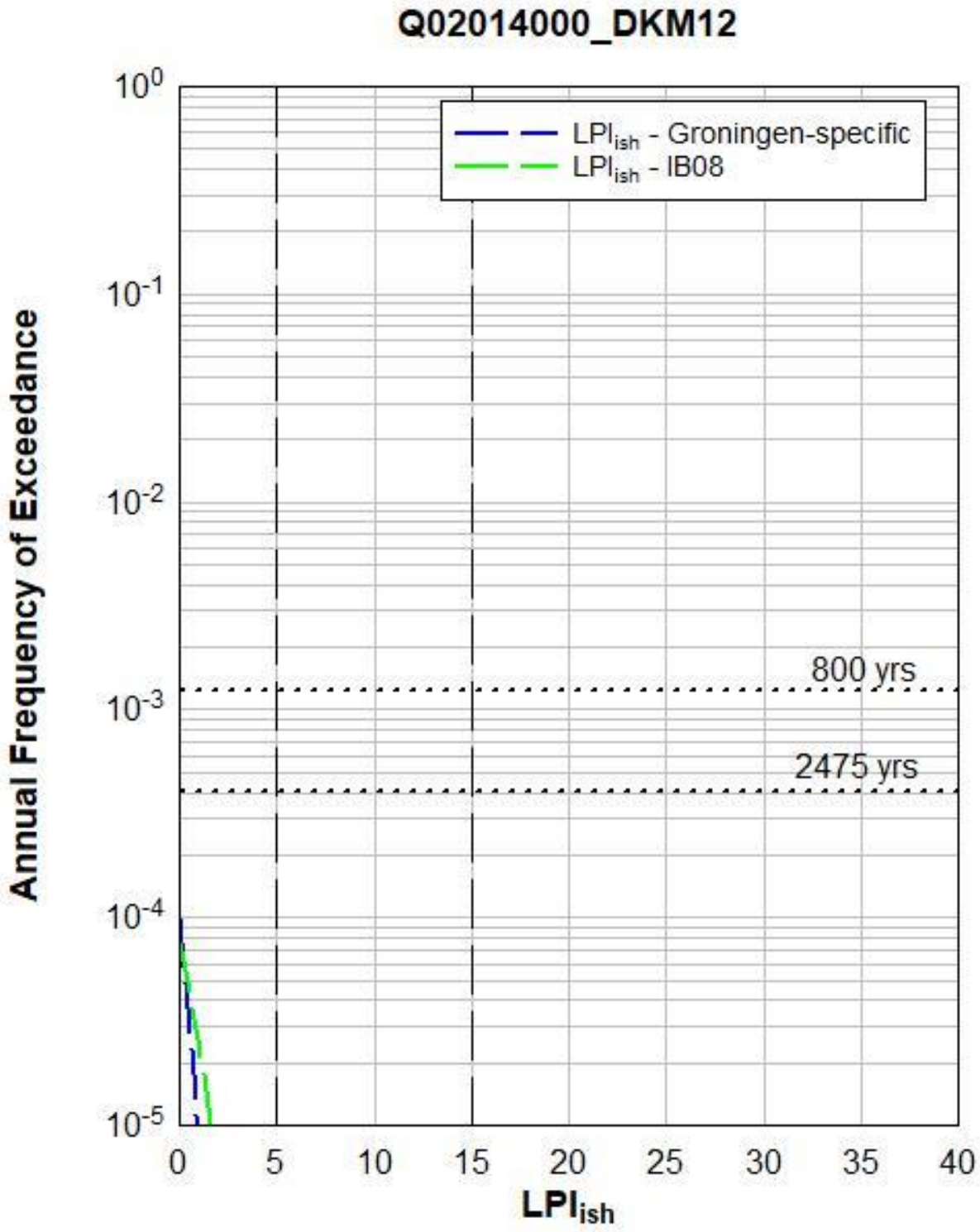
Q02014000_DKM12
LPIish - Groningen-specific
LPIish - IB08
800 yrs
2475 yrs
Annual Frequency of Exceedance
LPIish
10^0
10^-1
10^-2
10^-3
10^-4
10^-5
0
5
10
15
20
25
30
35
40

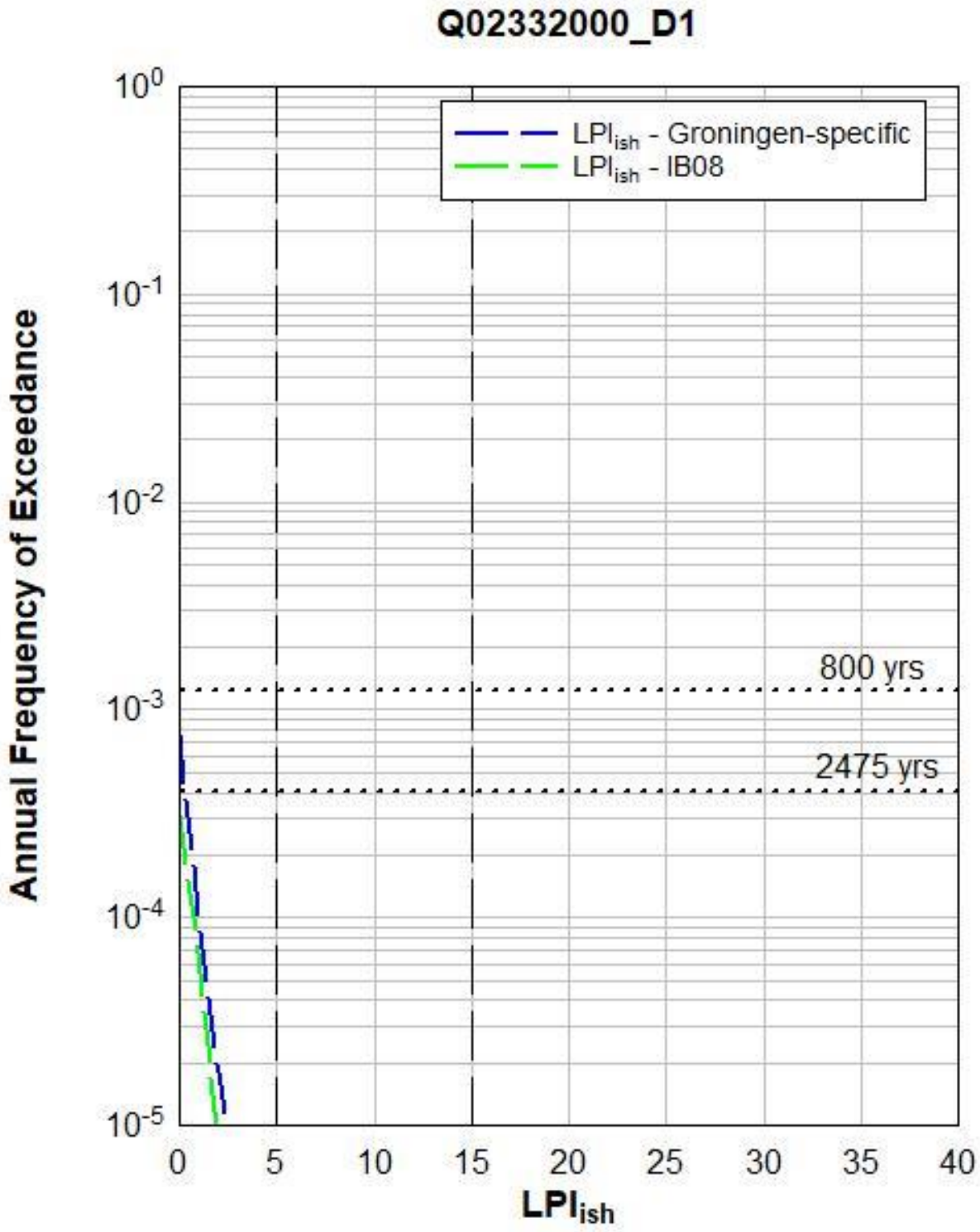
Q02332000_D1
LPIish - Groningen-specific
LPIish - IB08
800 yrs
2475 yrs
Annual Frequency of Exceedance
LPIish
10^0
10^-1
10^-2
10^-3
10^-4
10^-5
0
5
10
15
20
25
30
35
40

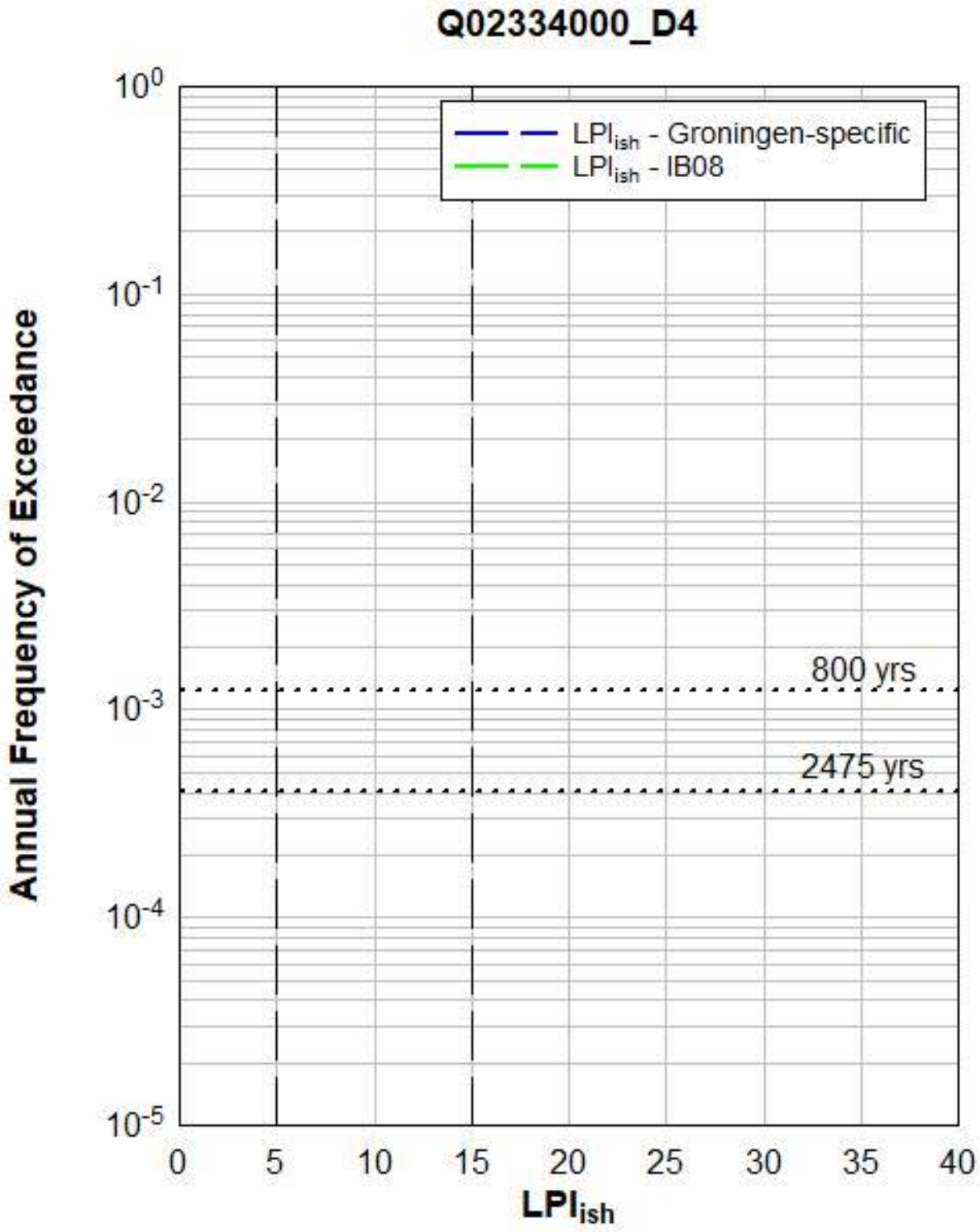
Q02334000_D4
LPIish - Groningen-specific
LPIish - IB08
800 yrs
2475 yrs
Annual Frequency of Exceedance
LPIish
10^0
10^-1
10^-2
10^-3
10^-4
10^-5
0
5
10
15
20
25
30
35
40

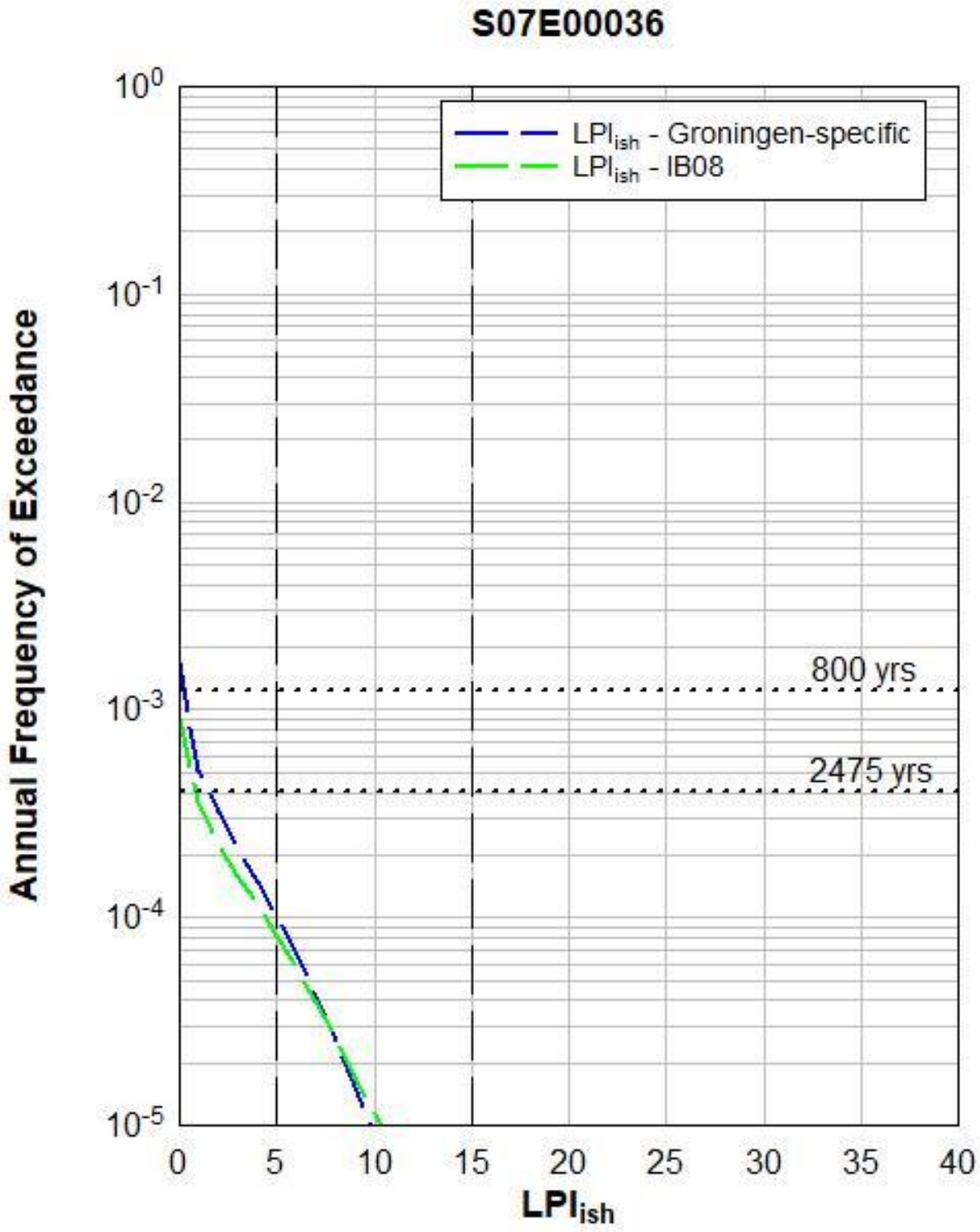
S07E00036
LPIish - Groningen-specific
LPIish - IB08
800 yrs
2475 yrs
Annual Frequency of Exceedance
LPIish
10^0
10^-1
10^-2
10^-3
10^-4
10^-5
0
5
10
15
20
25
30
35
40